NASA TECHNICAL NOTE

NASA TN D-6239

c. 1

NASA TN D-6239

LONGITUDINAL STABILITY CHARACTERISTICS OF PRELIMINARY CONFIGURATIONS FOR SCOUT D AT MACH NUMBERS 0.20 TO 4.63

by Robert J. Keynton

Langley Research Center
Hampton, Va. 23365

NATIONAL AERONAUTICS AND SPACE ADMINISTRATION • WASHINGTON, D. C. • MAY 1971

1. Report No.	2. Government Accession No.	3. Recipient's Catalog No.
NASA TN D-6239		

4. Title and Subtitle
LONGITUDINAL STABILITY CHARACTERISTICS OF PRELIMINARY CONFIGURATIONS FOR SCOUT D AT MACH NUMBERS 0.20 TO 4.63

5. Report Date
May 1971

6. Performing Organization Code

7. Author(s)
Robert J. Keynton

8. Performing Organization Report No.
L-7538

9. Performing Organization Name and Address
NASA Langley Research Center
Hampton, Va. 23365

10. Work Unit No.
490-00-00-00

11. Contract or Grant No.

12. Sponsoring Agency Name and Address
National Aeronautics and Space Administration
Washington, D.C. 20546

13. Type of Report and Period Covered
Technical Note

14. Sponsoring Agency Code

15. Supplementary Notes

16. Abstract

Results have been obtained in the Langley 8-foot transonic pressure tunnel and the Langley Unitary Plan wind tunnel at Mach numbers from 0.20 to 4.63 for several variations of a 1/15-scale model of the NASA Scout D launch vehicle and with two heat-shield configurations. The investigation extended over an angle-of-attack range of $\pm 10^{\circ}$ and selected roll angles from 0° to 180°. The Reynolds number was 13.1×10^6 per meter (4×10^6 per foot) for the 8-foot transonic pressure tunnel and 9.8×10^6 per meter (3×10^6 per foot) for the Unitary Plan wind tunnel (except at Mach numbers 0.20 and 0.40, which had Reynolds numbers of 6.6×10^6 and 9.8×10^6 per meter (2×10^6 and 3×10^6 per foot), respectively). With the currently estimated center-of-gravity Mach number history, both heat-shield configurations were statically unstable through portions of the supersonic Mach number region. The effect of protuberances (wiring tunnels, antennas, etc.) on the center of pressure was negligible with the exception of the wiring tunnels, which produced a small change in static margin.

17. Key Words (Suggested by Author(s))	18. Distribution Statement
Scout Longitudinal stability Launch vehicles	Unclassified – Unlimited

19. Security Classif. (of this report)	20. Security Classif. (of this page)	21. No. of Pages	22. Price*
Unclassified	Unclassified	130	$3.00

*For sale by the National Technical Information Service, Springfield, Virginia 22151

LONGITUDINAL STABILITY CHARACTERISTICS OF PRELIMINARY CONFIGURATIONS FOR SCOUT D AT MACH NUMBERS 0.20 TO 4.63

By Robert J. Keynton
Langley Research Center

SUMMARY

Results have been obtained in the Langley 8-foot transonic pressure tunnel and the Langley Unitary Plan wind tunnel at Mach numbers from 0.20 to 4.63 for several variations of a 1/15-scale model of the NASA Scout D launch vehicle and with two heat-shield configurations. The investigation extended over an angle-of-attack range of $\pm 10^{\circ}$ and selected roll angles from 0° to 180°. The Reynolds number was 13.1×10^6 per meter (4×10^6 per foot) for the 8-foot transonic pressure tunnel and 9.8×10^6 per meter (3×10^6 per foot) for the Unitary Plan wind tunnel (except at Mach numbers 0.20 and 0.40, which had Reynolds numbers of 6.6×10^6 and 9.8×10^6 per meter (2×10^6 and 3×10^6 per foot), respectively). With the currently estimated center-of-gravity Mach number history, both heat-shield configurations were statically unstable through portions of the supersonic Mach number region. The effect of protuberances (wiring tunnels, antennas, etc.) on the center of pressure was negligible with the exception of the wiring tunnels, which produced a small change in static margin.

INTRODUCTION

A 114.3-cm-diameter (45-in.) first-stage motor is under development for the NASA Scout launch vehicle. The new configuration will be known as Scout D. The development concept is that the new stage, Algol-III, will be mechanically interchangeable with the existing first stage Algol-IIB. As part of the development program a wind-tunnel program was initiated to determine the stability characteristics of the proposed configuration with the extended-length Scout heat shield and a second configuration with a proposed 106.7-cm-diameter (42-in.) heat shield. Other configurations tested were used to determine the effect of the various protuberances, telemetry antenna, launch fittings, etc., which are mounted to the external surface of the Scout launch vehicle. The tests were conducted in the Langley 8-foot transonic pressure tunnel and the Langley Unitary Plan wind tunnel at Mach numbers from 0.20 to 4.63 through an angle-of-attack range of $\pm 10^{\circ}$.

SYMBOLS

Aerodynamic force and moment data are referred to the body system of axes (fig. 1) with coefficients based on an area of 0.00216 m^2 (0.0233 ft^2) and a length of 5.26 cm (2.07 in.) which correspond to the model second-stage cross-sectional area and diameter, respectively. Moments were measured about model station 93.98 cm (37.0 in.). The data are given in both SI and U.S. Customary Units. The measurements and calculations were made in U.S. Customary Units.

A	second-stage reference cross-sectional area, m^2 (ft^2)
C_A	axial-force coefficient, $\frac{\text{Axial force}}{qA}$
C_l	rolling-moment coefficient, $\frac{\text{Rolling moment}}{qAd}$
C_m	pitching-moment coefficient, $\frac{\text{Pitching moment}}{qAd}$
C_N	normal-force coefficient, $\frac{\text{Normal force}}{qA}$
C_n	yawing-moment coefficient, $\frac{\text{Yawing moment}}{qAd}$
C_Y	side-force coefficient, $\frac{\text{Side force}}{qA}$
d	second-stage reference cylindrical diameter, cm (in.)
q	free-stream dynamic pressure, N/m^2 (lb/ft^2)
X,Y,Z	body system of axes (see fig. 1)
α	angle of attack of body center line, deg
β	angle of sideslip of body center line, deg
ϕ	roll angle, deg

Subscript:

o	condition at $\alpha = 0^o$

APPARATUS AND TESTS

Model

Details and design dimensions for the 1/15-scale model of Scout D are shown in figure 2. Figure 2(a) shows the body dimensions, figure 2(b) shows the protuberance arrangement, and figure 2(c) shows the larger diameter heat-shield configuration. The cruciform fins had a leading-edge-sweep angle of 45° and a single-wedge airfoil section having a streamwise included-wedge angle of 8°. The fin leading edges were blunted and had a radius of curvature (measured normal to the leading edge) of 0.043 cm (0.017 in.). Figure 3 is a photograph of the overall model, rolled 45° counterclockwise from the top, to provide a view of the wiring tunnels. Closeup photographs of the other protuberances are shown in figure 4.

The model was tested first with the large heat shield and all protuberances. Then the large heat shield was exchanged for one of smaller diameter and the protuberances were successively removed. Thus seven configurations were tested as follows:

Configuration	Description
1	Large heat shield, protuberances, fins
2	Small heat shield, protuberances, fins
3	Removed base "A" launch fittings from configuration 2
4	Removed transition "B" launch fitting from configuration 3
5	Removed telemetry and radar antenna from configuration 4
6	Removed wiring tunnels from configuration 5
7	Removed fins from configuration 6

Test Conditions

The tests were conducted in both the Langley 8-foot transonic pressure tunnel (8' TT) and in the Langley Unitary Plan wind tunnel (UPWT) through an overall Mach number range of 0.20 to 4.63. The following table gives the test conditions:

Mach number	Angle-of-attack range, deg	Reynolds number		Stagnation temperature	
		per meter	per foot	K	$^{\circ}$F
0.20	±10	6.6×10^6	2.0×10^6	322	120
0.40	±10	9.8	3.0	322	120
0.60, 0.70, 0.80, 0.90, 1.00, 1.05	±6	13.1	4.0	322	120
2.30, 2.96, 3.95, 4.63	±6	9.8	3.0	---	---

The tests in the Unitary Plan wind tunnel were performed at stagnation temperatures of 339 K (150° F) for Mach numbers of 2.30 and 2.96 and at 353 K (175° F) for Mach numbers of 3.95 and 4.63. The dewpoint was maintained below 239 K (-30° F) to prevent adverse condensation effects.

Transition strips, consisting of carborundum granules, were used to insure proper flow conditions over the model. The size and the location of these strips were a function of the test conditions of the particular wind tunnel. The distance from the stagnation point for the nose cone is measured longitudinally along the body center line. For the fin, it is measured perpendicular to the leading edge. Relevant transition information for nose and fin is as follows:

Tunnel	Component	Distance from stagnation point		Width		Diameter of particles	
		cm	in.	cm	in.	cm	in.
8' TT	Nose	4.95	1.95	0.2540	0.10	0.0124	0.0049
	Fin	---	---	-----	-----	-----	-----
UPWT	Nose	3.05	1.2	.0386	.0152	.0386	.0152
	Fin	.51	.2				

Corrections and Accuracy

At high transonic and low supersonic speeds, the data were generally affected by boundary-reflected disturbances. For the present tests the model length and/or tunnel power restrictions precluded the attainment of reflection-free data for the model over the entire Mach number range. Therefore, no results are presented between the Mach numbers of 1.05 and 2.30. All test data have been corrected for inclination of the air flow in the tunnel test section.

8-foot transonic pressure tunnel.- Effects of subsonic boundary interference in the slotted test section of the 8-foot transonic pressure tunnel are considered negligible and no corrections for these effects have been applied. Local variations in the nominal Mach number did not exceed ±0.003 over the Mach number range from 0.20 to 1.05.

Unitary Plan wind tunnel.- In the Unitary Plan wind tunnel the data for Mach numbers from 2.30 to 4.63 were adjusted so that the pitching-moment curve for a known symmetric configuration (configuration 6) passed through zero at $\alpha = 0^{\circ}$. This increment then was applied to the remaining configurations. The maximum deviation of the local Mach number near the model did not exceed ±0.15 over the Mach number range from 2.30 to 4.63.

Data accuracy.- Estimated accuracies of the force and moment coefficients and angle of attack and roll, based on instrument calibration and data repeatability for the two tunnels are presented in terms of absolute values as follows:

	8' TT	UPWT
C_N	±0.03	±0.01
C_Y	±0.04	±0.01
C_A	±0.02	±0.01
C_m	±0.10	±0.08
C_n	±0.05	±0.01
C_l	±0.03	±0.01
α, deg	±0.1	±0.1
ϕ and β, deg	±0.1	±0.1

PRESENTATION OF RESULTS

The data obtained from the tests are presented as a function of angle of attack and Mach number as follows:

DISCUSSION OF RESULTS

A 1/15-scale model of Scout D was tested in the Langley Unitary Plan wind tunnel and in the Langley 8-foot transonic tunnel at Mach numbers from 0.20 to 4.63. This model utilizes a larger first-stage motor, Algol-III in place of the Algol-IIB now used in Scout. Scout D as currently conceived for flight is represented by configuration 2. Flight data of Scout B have indicated via deterministic analysis several aerodynamic curiosities generally not associated with what may be considered a symmetric body, namely the presence of a $C_{m,o}$, $C_{N,o}$, $C_{Y,o}$, and $C_{n,o}$. Configurations 3 to 7 were tested in an attempt to induce experimentally the trim aerodynamics which were deduced from the flight data of two studies, the results of which have not been published. However, wind-tunnel measurement and/or flight-measurement uncertainties generally prohibited meaningful correlation with flight data under trim conditions.

By observing figure 16 one may see that the presence of the wiring tunnels (compare curves for configurations 6 and 5) causes a slight but distinctive shift in the center of pressure. The presence of the other protuberances, configurations 2 to 5, had no measurable effect on the center of pressure. Axial-force coefficients (fig. 15), showed a characteristic increase in the transonic region as components were removed; but the effect in the supersonic region was minimal.

Scout D offers greater payload capability than existing Scout vehicles and, consequently, heat shields (shrouds) of greater internal volume are required. Configuration 1 represents Scout D with a preliminary design of a larger heat shield which would yield greater payload volume. Figure 16 shows this configuration to be statically unstable between Mach numbers 2.00 and 4.63, based on the center-of-gravity Mach number history taken from an unpublished heat-shield study. At Mach number 2.70, which represents the Mach number at maximum dynamic pressure, a critical design condition for the flight vehicle, the center of pressure was shifted forward approximately 0.967 body diameter by changing the heat-shield configuration. The axial-force coefficient was increased by 32 percent at the same conditions. (See fig. 19.)

CONCLUSIONS

Results have been obtained in the Langley 8-foot transonic pressure tunnel and the Langley Unitary Plan wind tunnel at Mach numbers from 0.20 to 4.63 for several variations of a 1/15-scale model of the NASA Scout D launch vehicle and with two heat-shield configurations. The investigation extended over an angle-of-attack range of $\pm 10^{\circ}$ and selected roll angles from 0° to 180°. The Reynolds number was 13.1×10^6 per meter (4×10^6 per foot) for the 8-foot transonic pressure tunnel and 9.8×10^6 per meter (3×10^6 per foot) for the Unitary Plan wind tunnel (except at Mach numbers 0.20 and

0.40, which had Reynolds numbers of 6.6×10^6 and 9.8×10^6 per meter (2×10^6 and 3×10^6 per foot), respectively). The results of the investigation indicate the following:

1. With the currently estimated center-of-gravity Mach number history, both heat-shield configurations were statically unstable through portions of the supersonic Mach number region.

2. The effect of protuberances (wiring tunnels, antennas, etc.) on the center of pressure was negligible with the exception of the wiring tunnels, which produced a small change in static margin.

Langley Research Center,
National Aeronautics and Space Administration,
Hampton, Va., March 31, 1971.

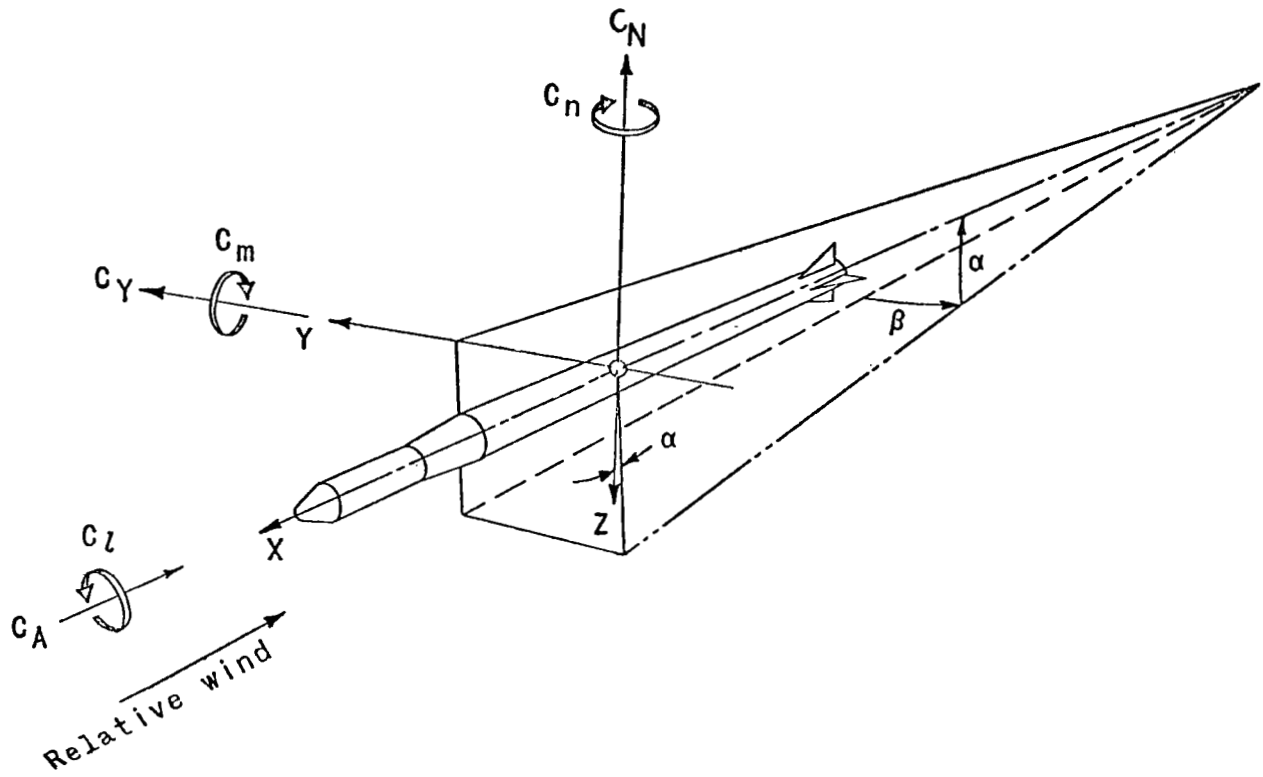

Figure 1.- System of axes. Arrows indicate positive direction.

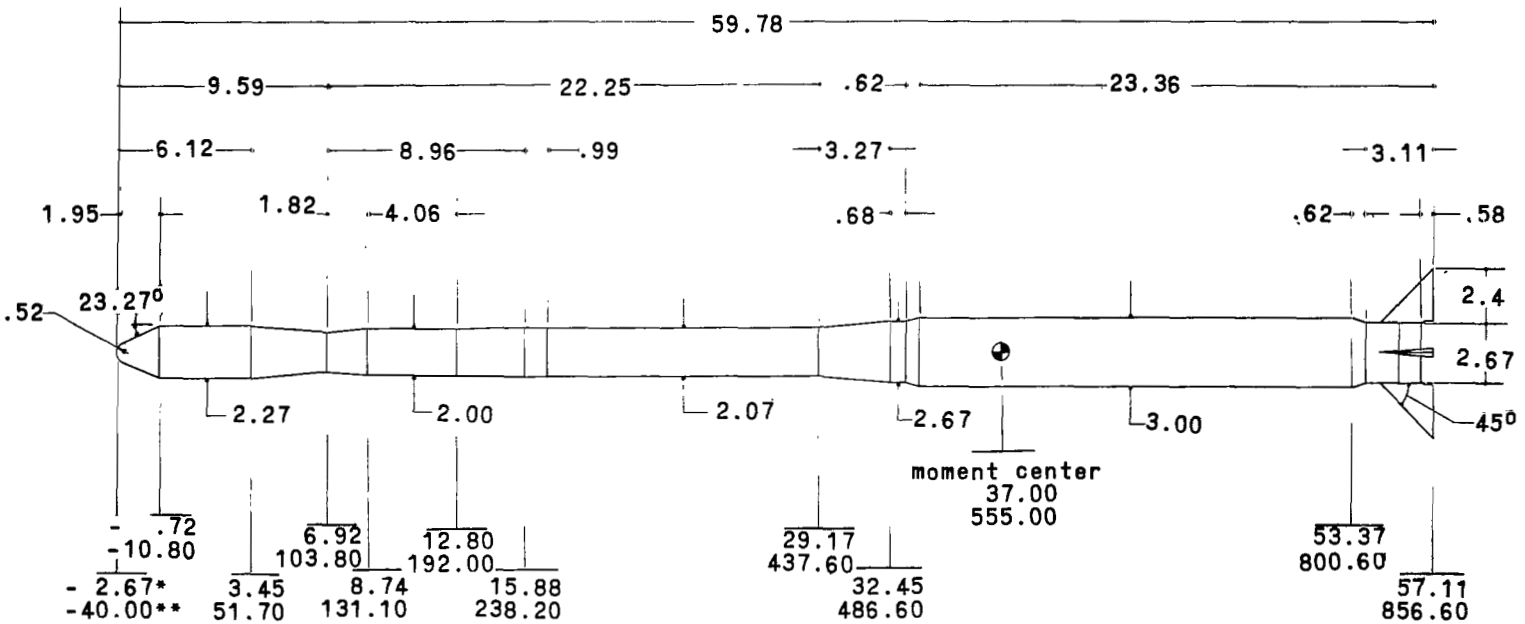

* Model Stations

** Actual Full-Scale Stations

(a) Body dimensions.

Figure 2.- Drawings of 1/15-scale model of Scout D with 114.3-cm-diameter (45-in.) first stage. (Model dimensions and model stations given in inches (1 in. = 2.54 cm).)

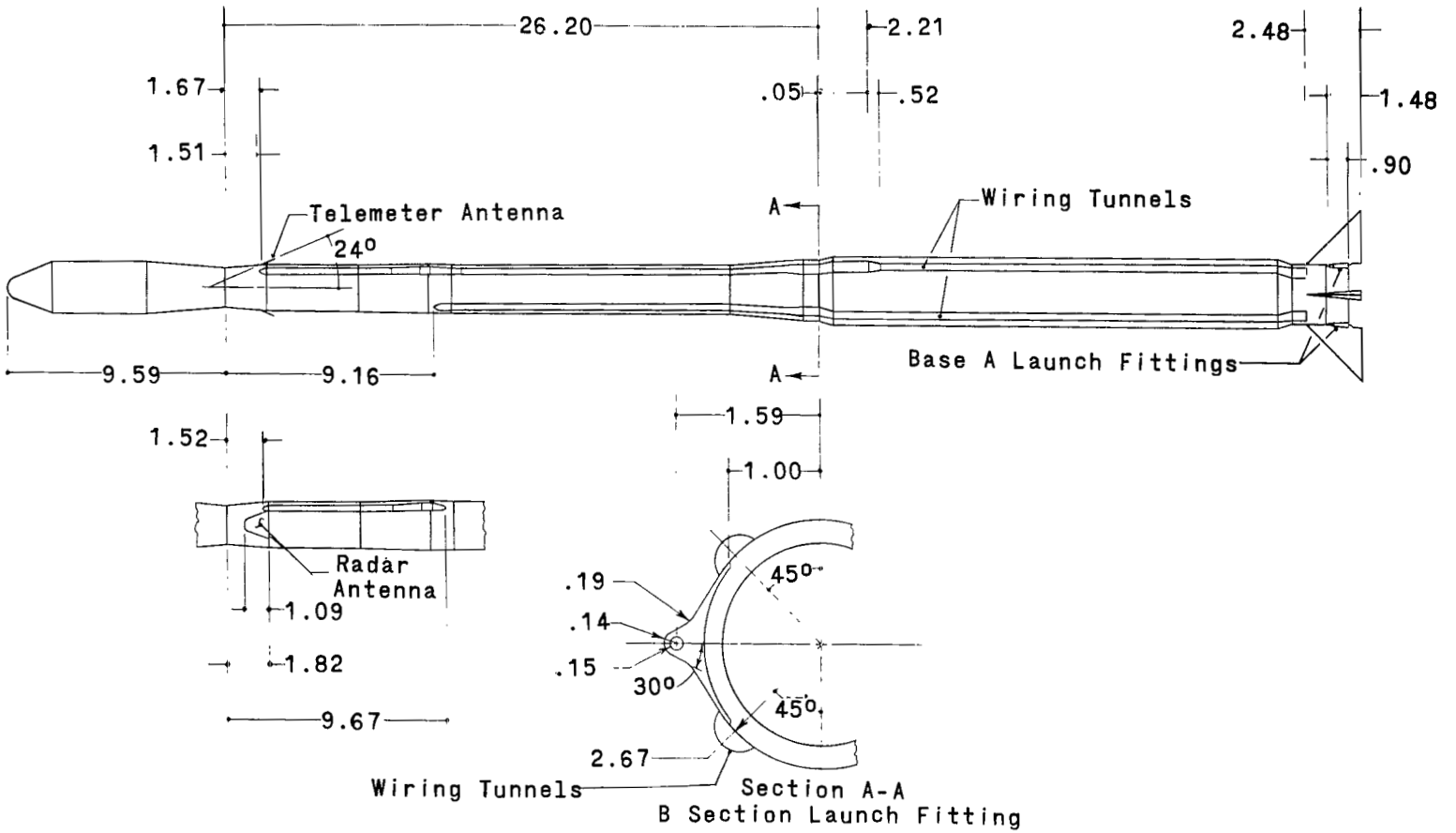

(b) Protuberance dimensions.

Figure 2.- Continued.

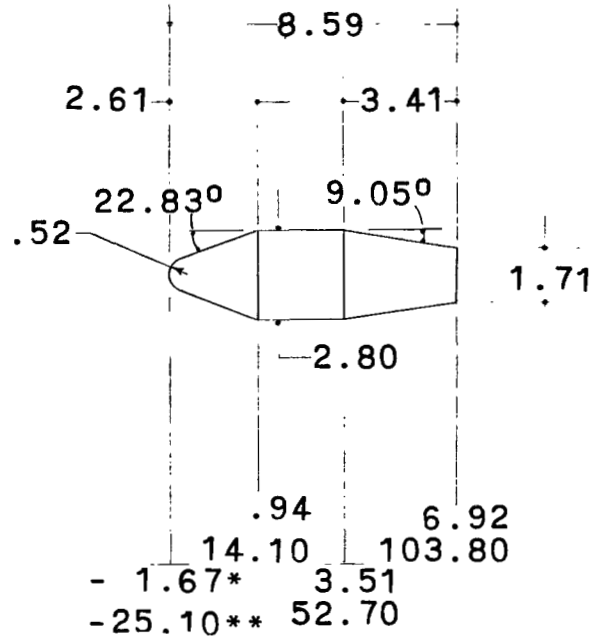

(c) Preliminary increased volume heat shield.

Figure 2.- Concluded.

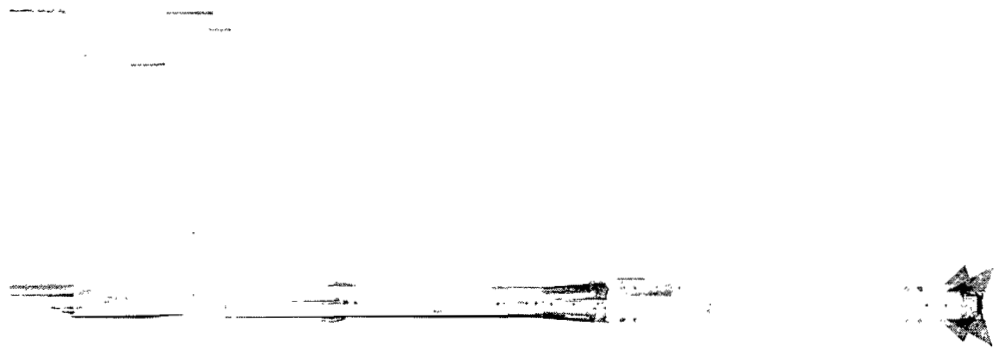

L-69-1410

Figure 3.- Photograph of model with 86.4-cm-diameter (34-in.) heat shield and all protuberances.

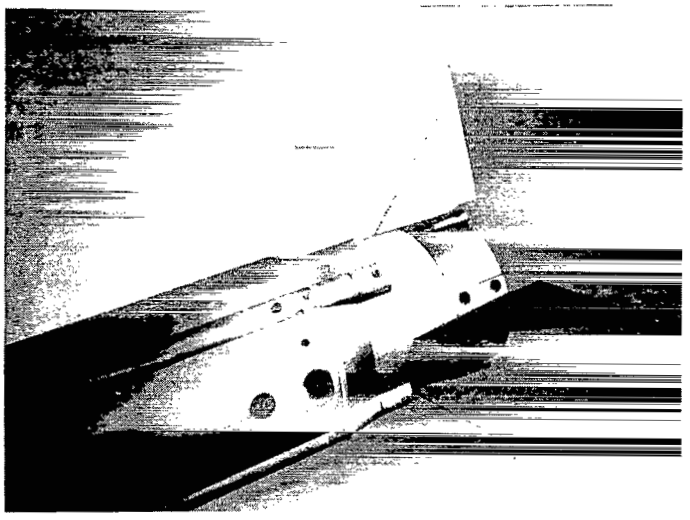

(a) Base "A" launch fitting.

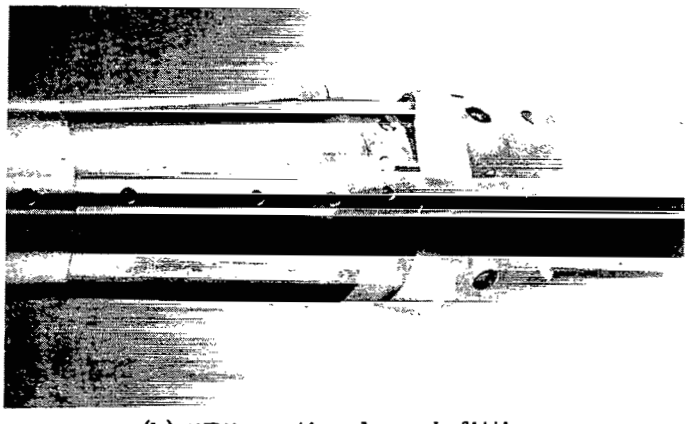

(b) "B" section launch fitting.

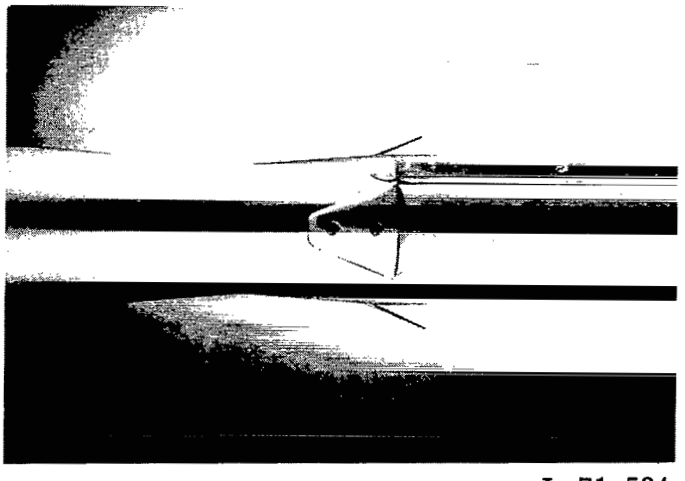

L-71-534

(c) Radar and telemetry antennas.

Figure 4.- Detail photographs of protuberances.

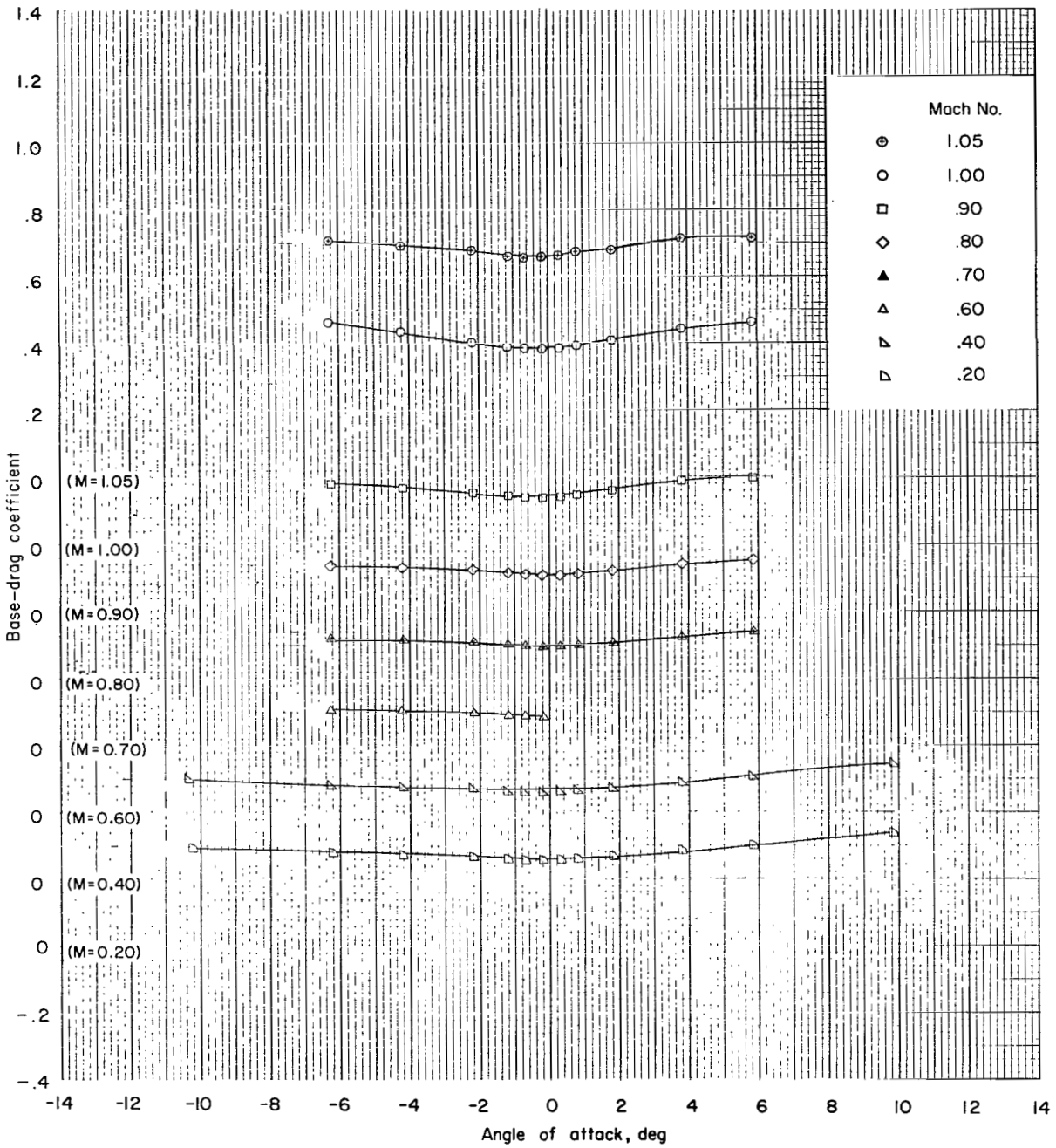

(a) Subsonic.

Figure 5.- Typical base drag as a function of angle of attack and Mach number.

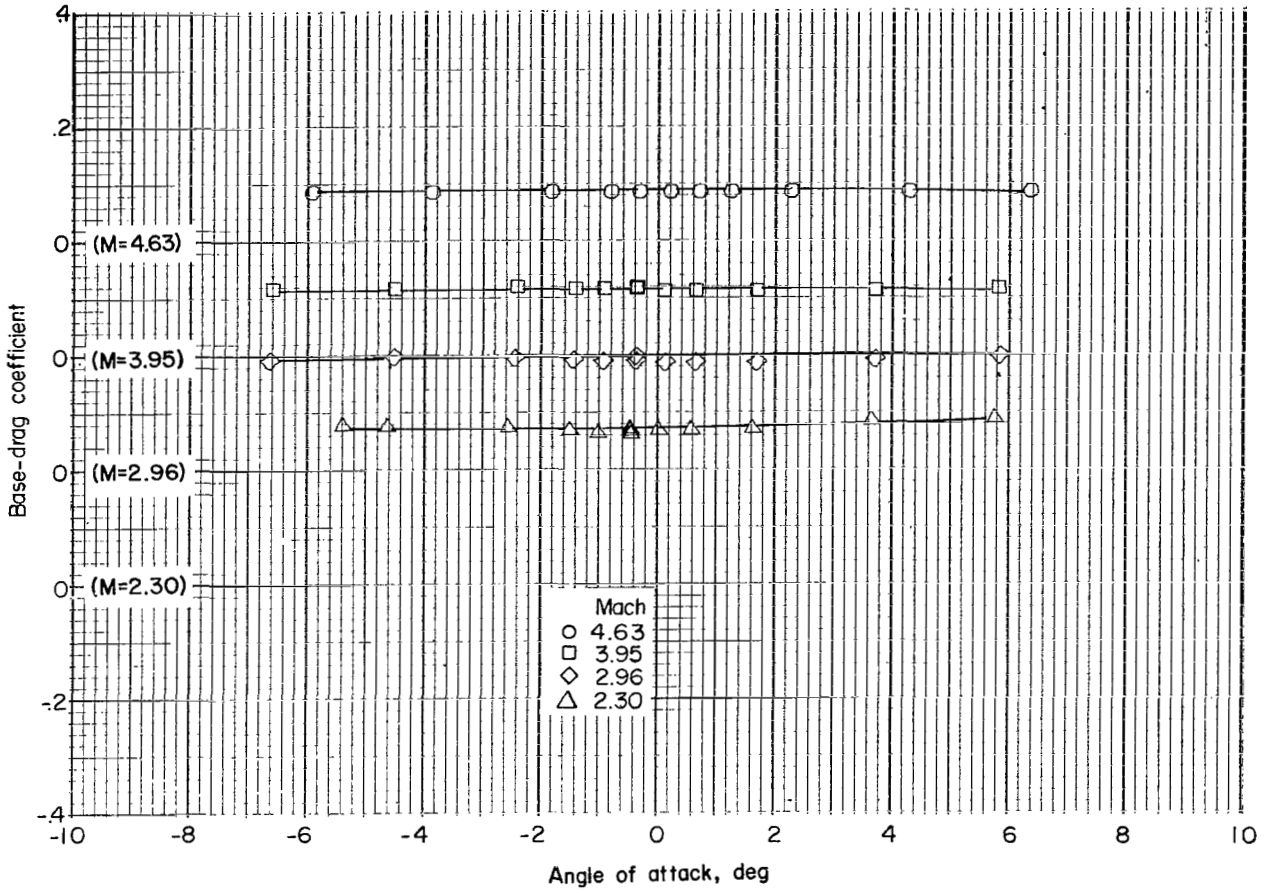

(b) Supersonic.

Figure 5.- Concluded.

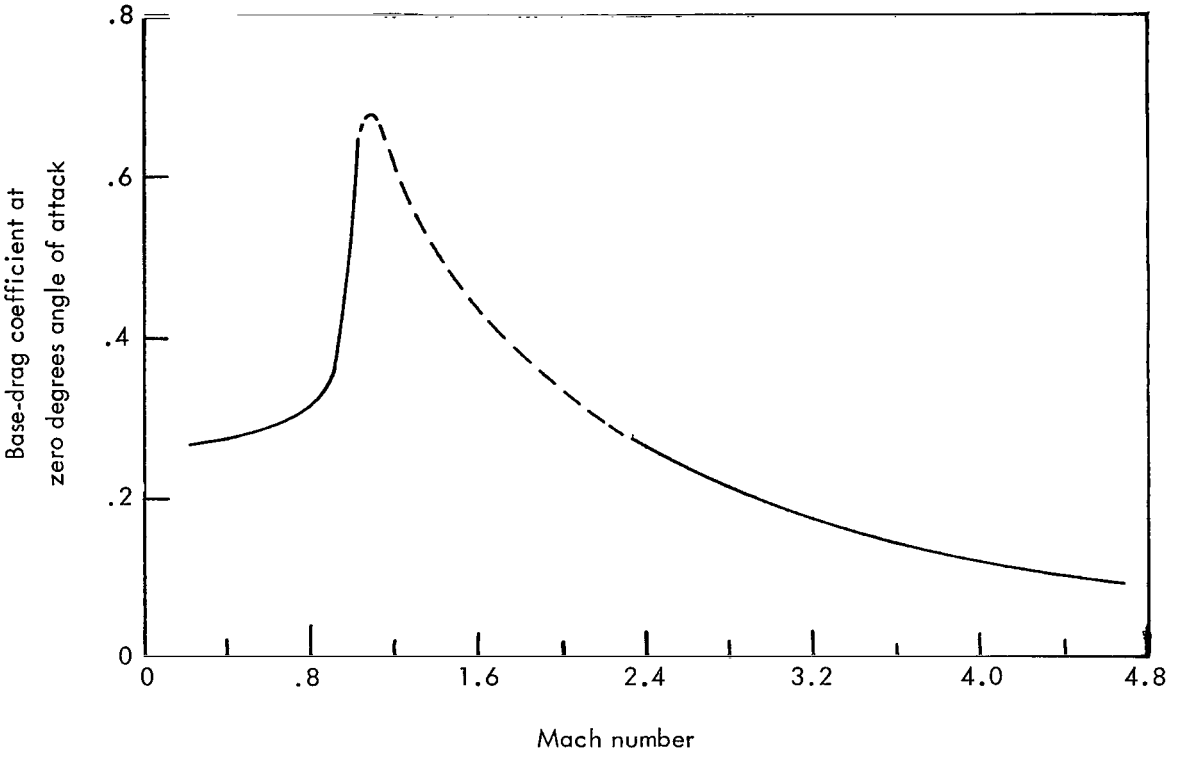

Figure 6.- Typical base-drag coefficient as function of Mach number.

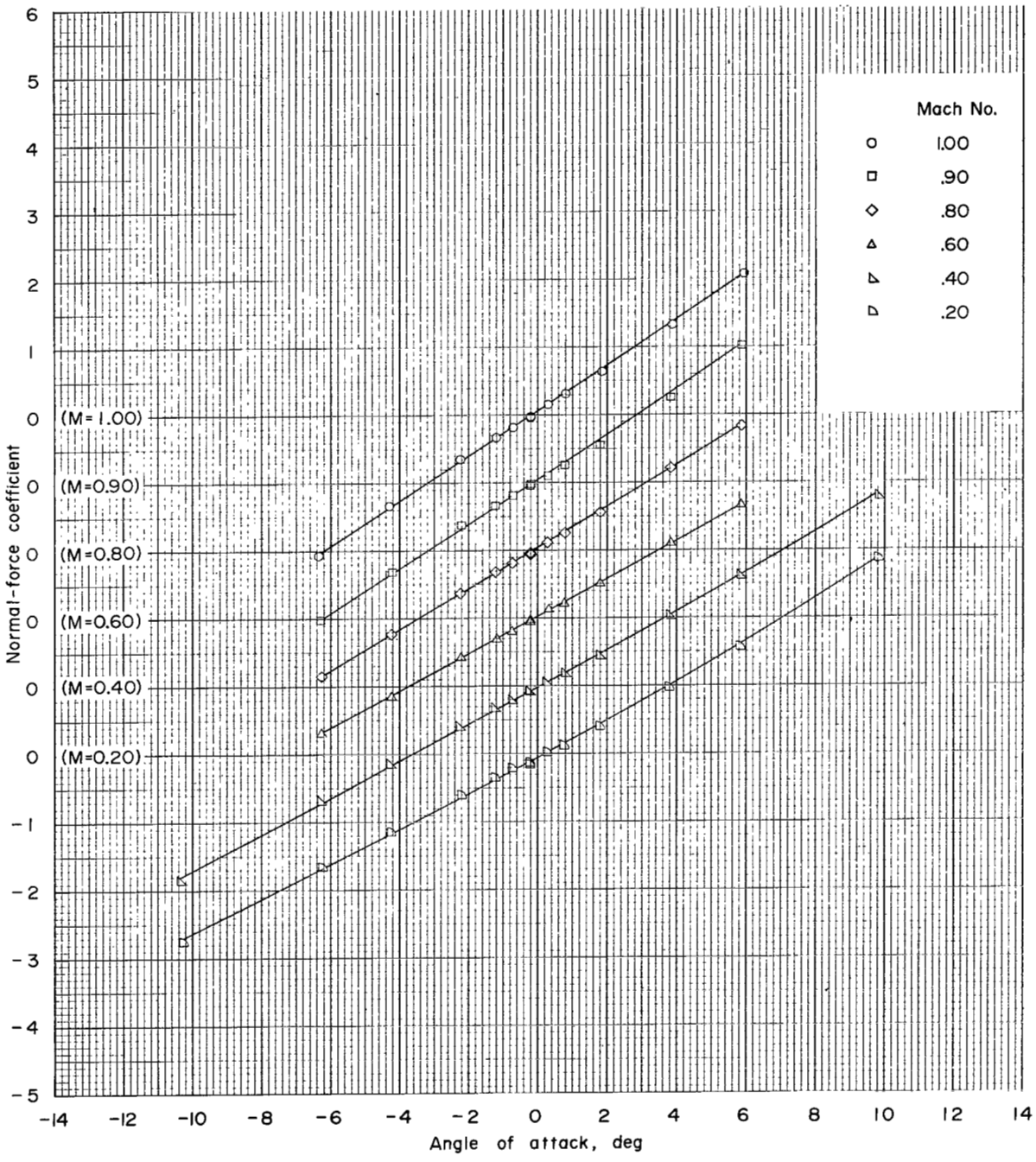

(a-1) Subsonic Mach numbers; configuration 1; $\phi = 0^{o}$.

Figure 7.- Normal-force coefficient as function of angle of attack, roll angle, and Mach number.

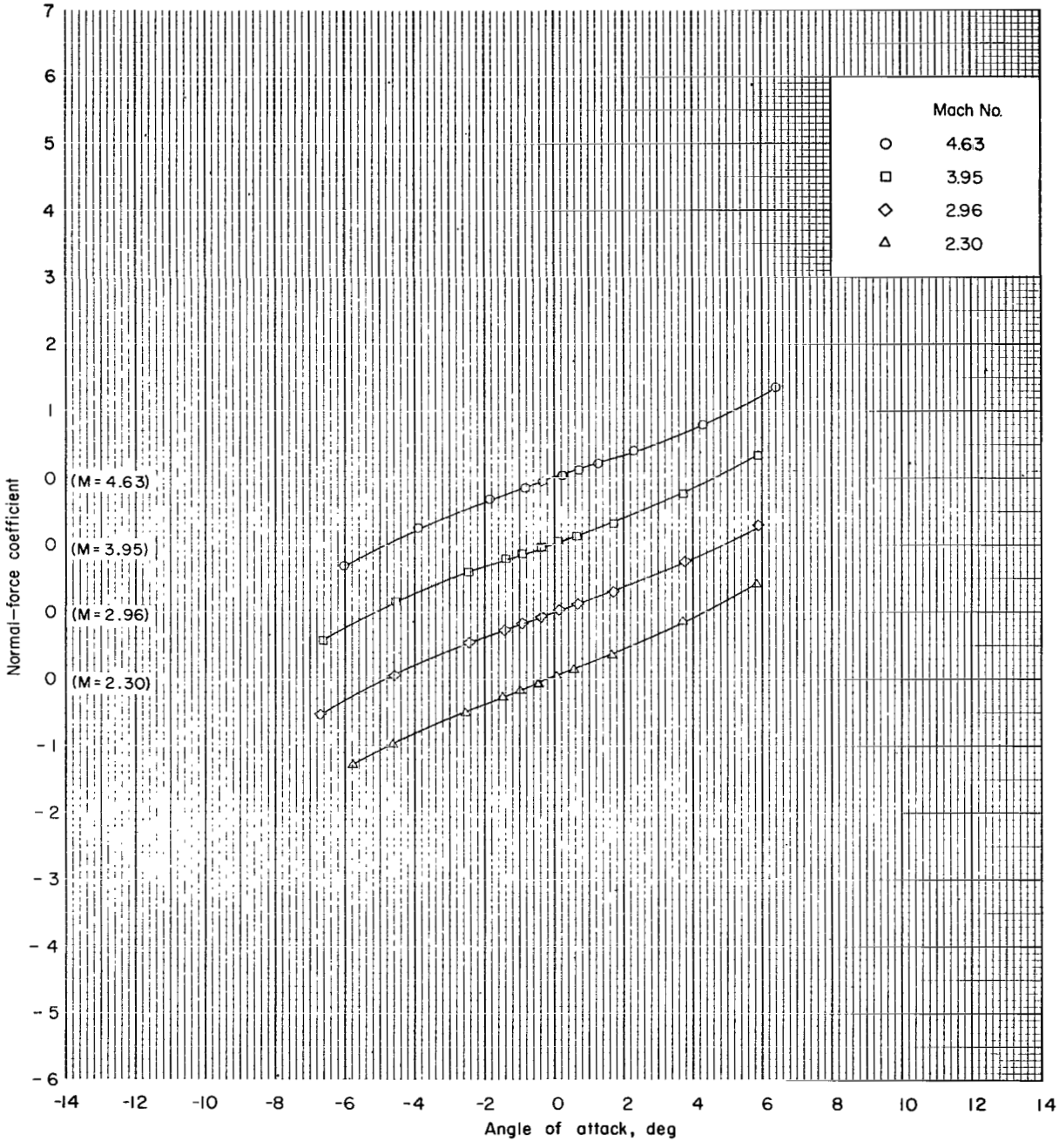

(a-2) Supersonic Mach numbers; configuration 1; $\phi = 0^{o}$.

Figure 7.- Continued.

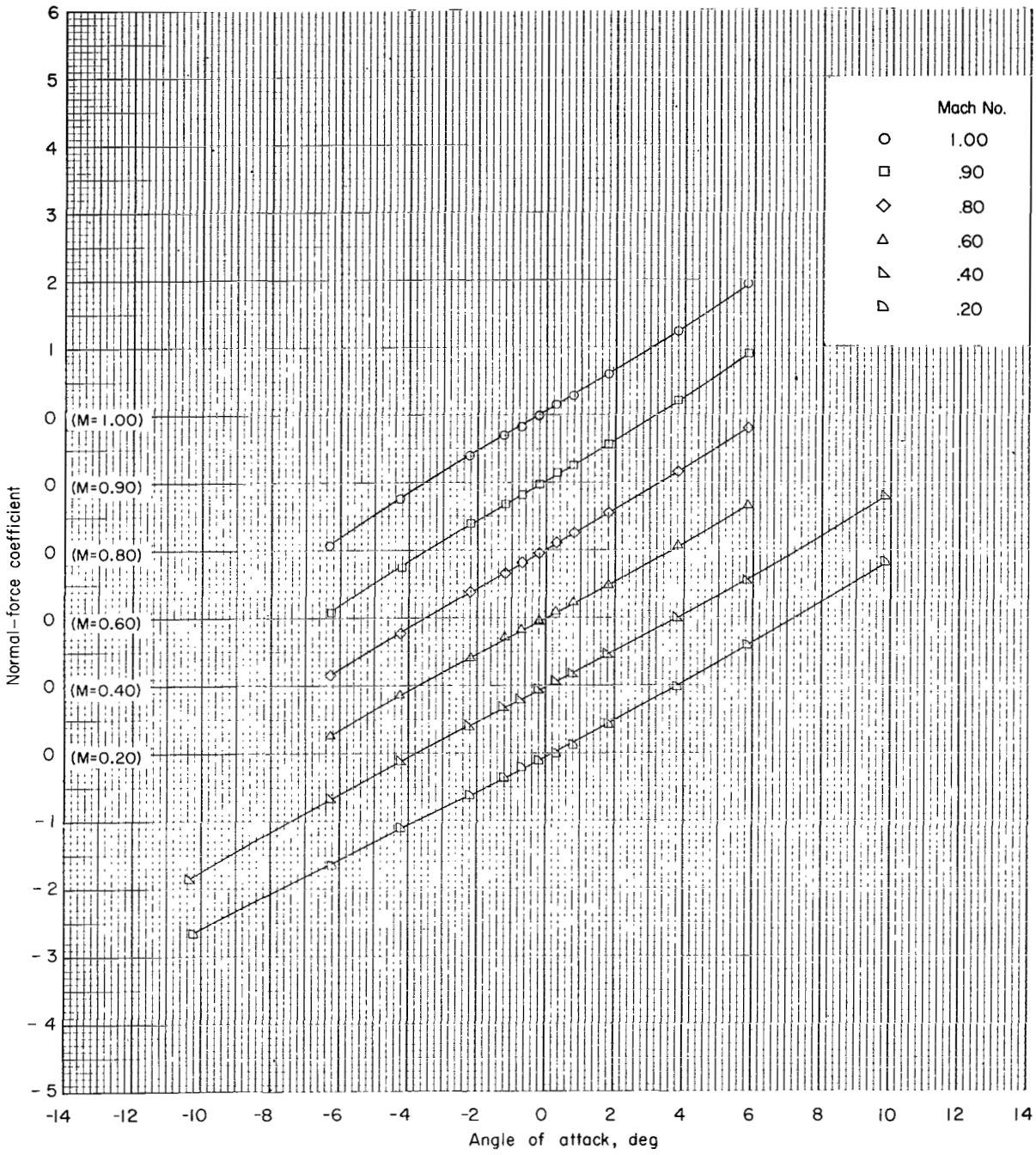

(b-1) Subsonic Mach numbers; configuration 2; $\phi = 0^{o}$.

Figure 7.- Continued.

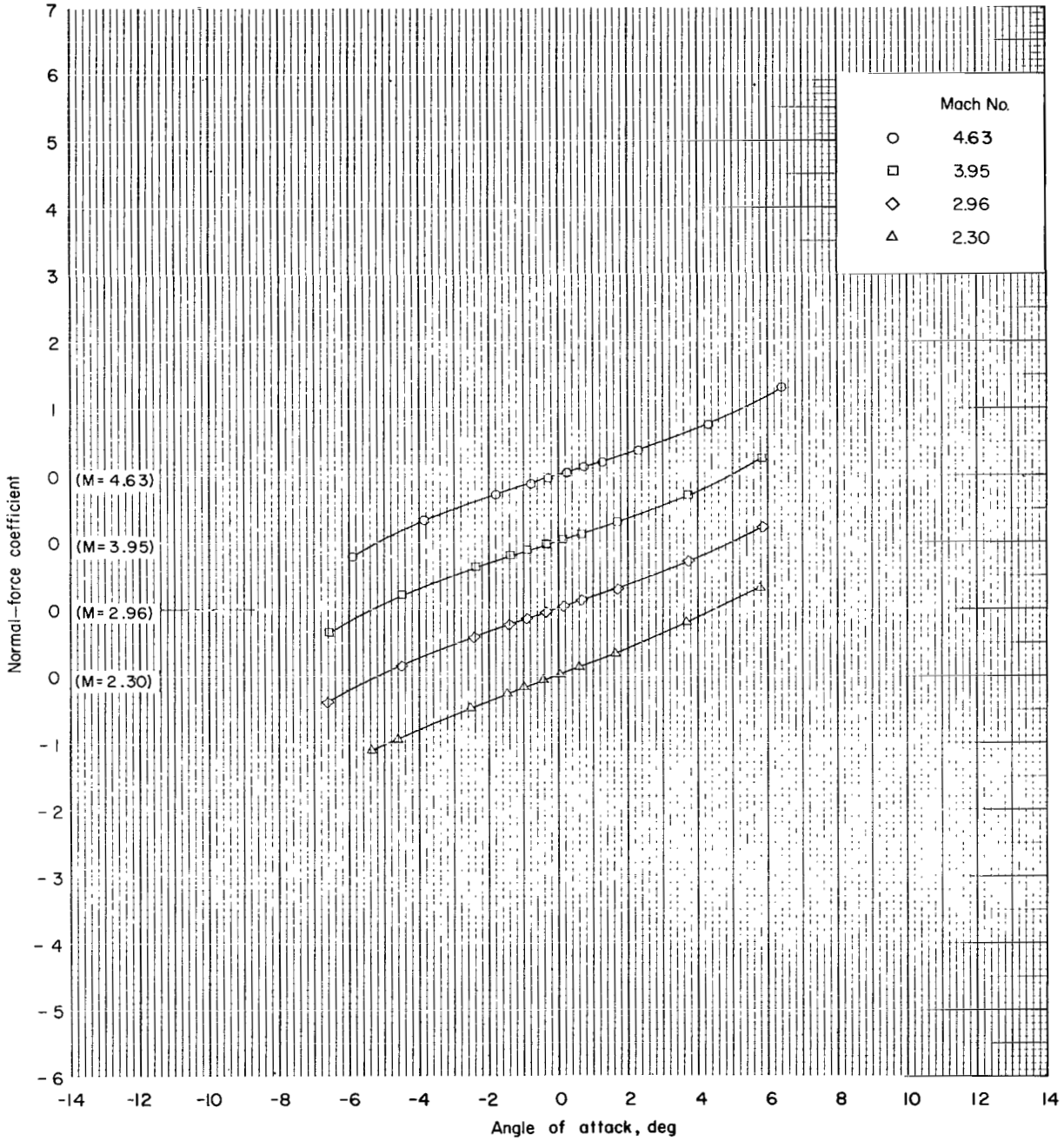

(b-2) Supersonic Mach numbers; configuration 2; $\phi = 0^{o}$.

Figure 7.- Continued.

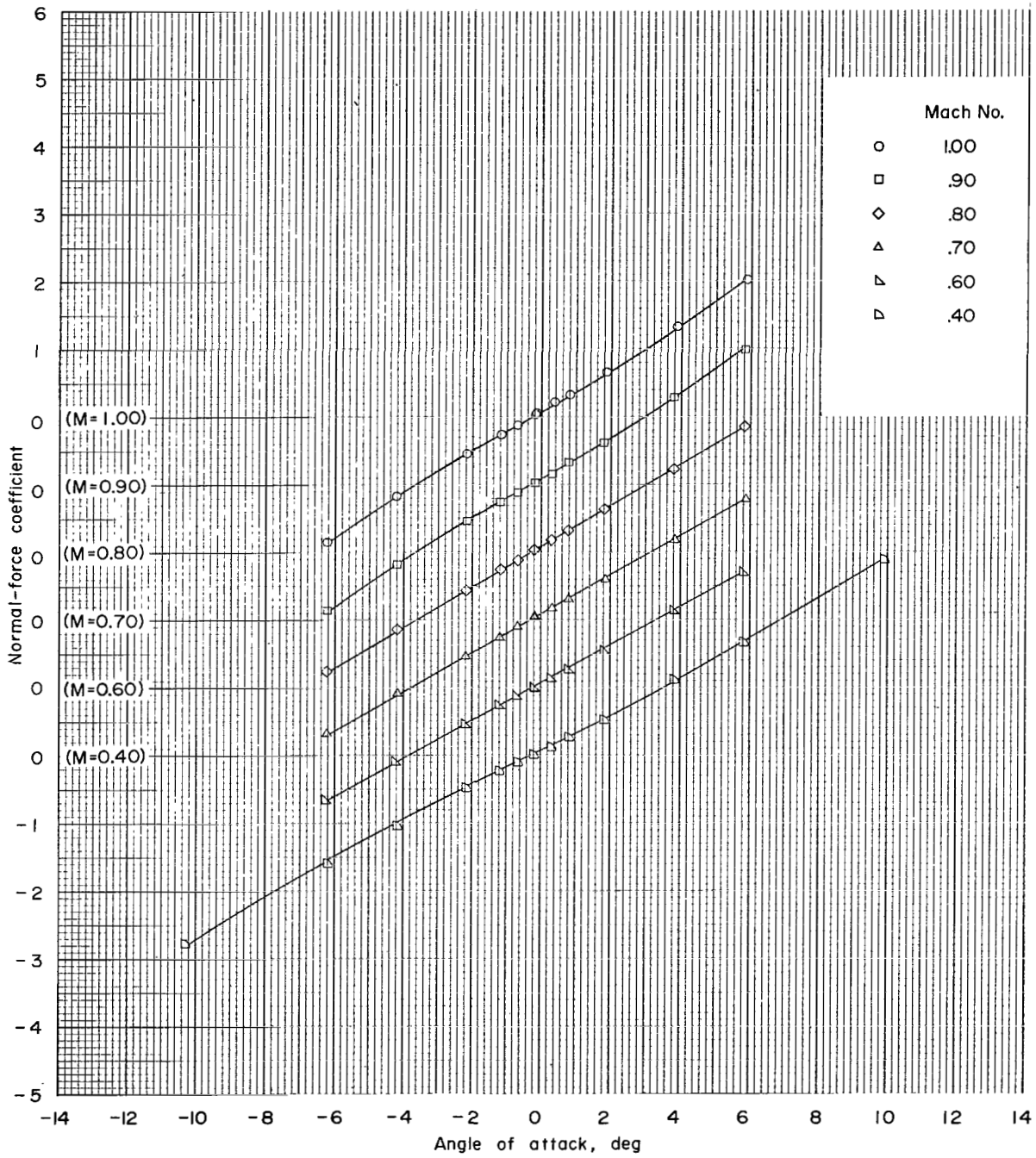

(c-1) Subsonic Mach numbers; configuration 3; $\phi = 0^{o}$.

Figure 7.- Continued.

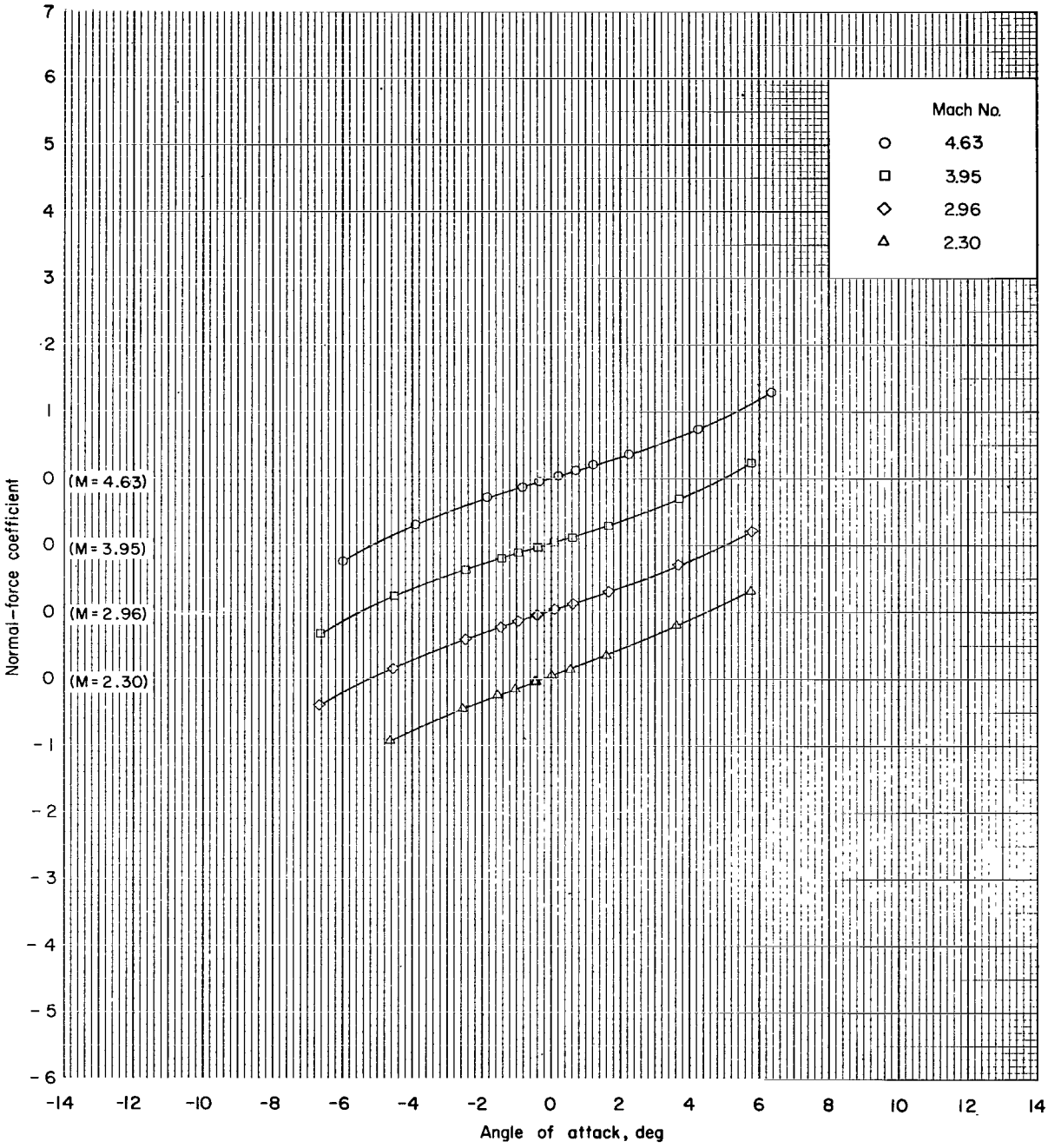

(c-2) Supersonic Mach numbers; configuration 3; $\phi = 0^{o}$.

Figure 7.- Continued.

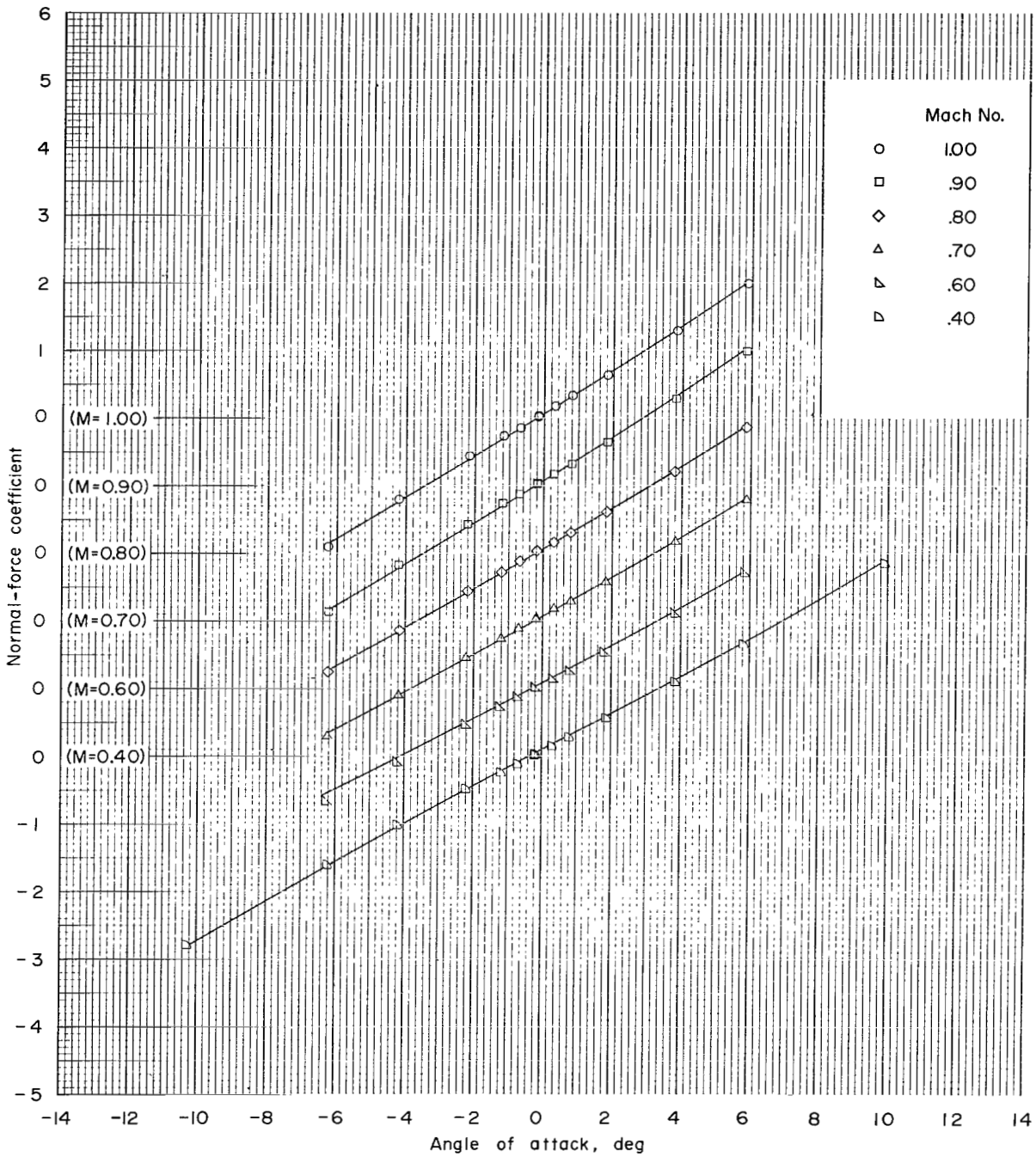

(d-1) Subsonic Mach numbers; configuration 4; $\phi = 0^{o}$.

Figure 7.- Continued.

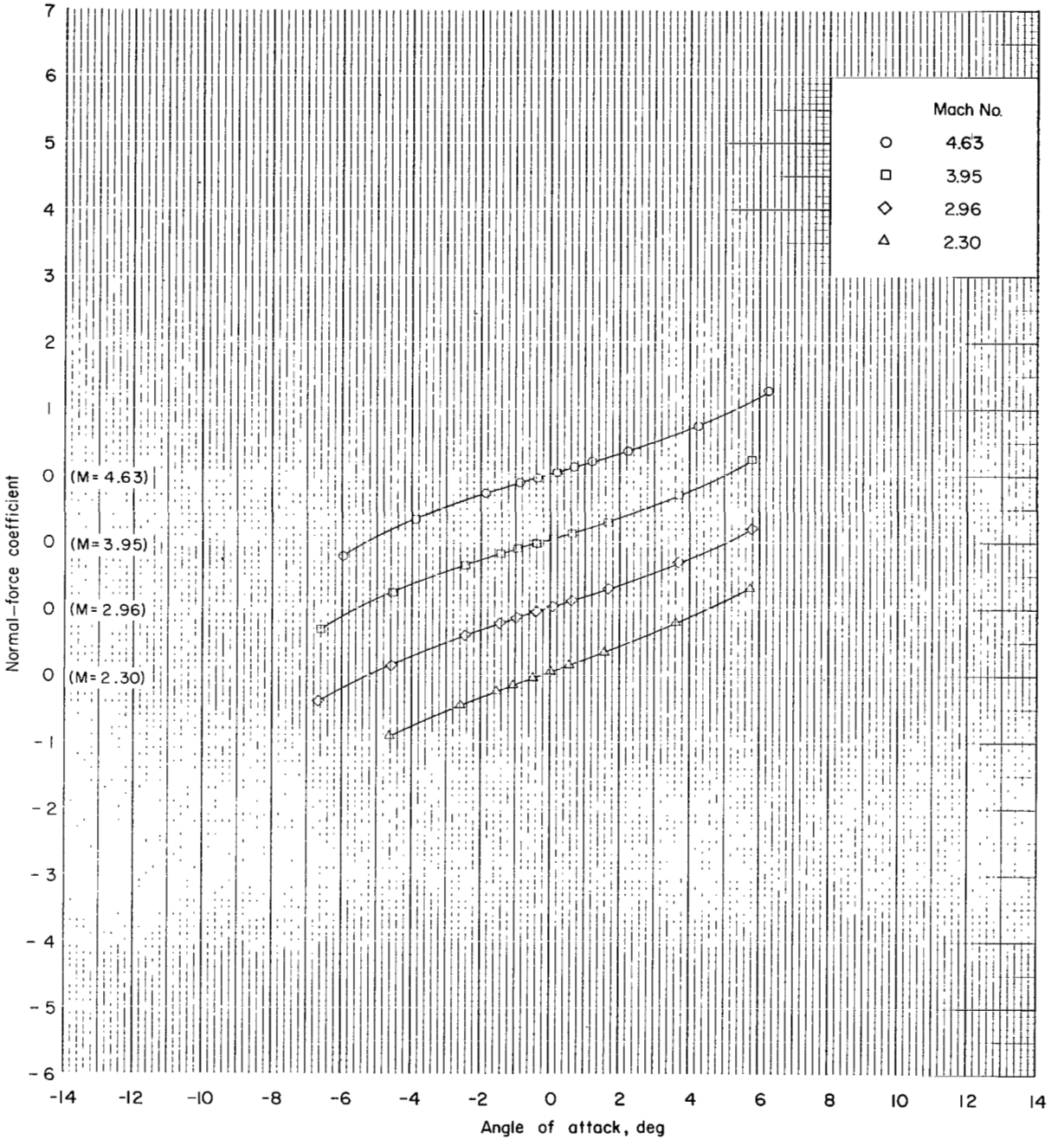

(d-2) Supersonic Mach numbers; configuration 4; $\phi = 0^{o}$.

Figure 7.- Continued.

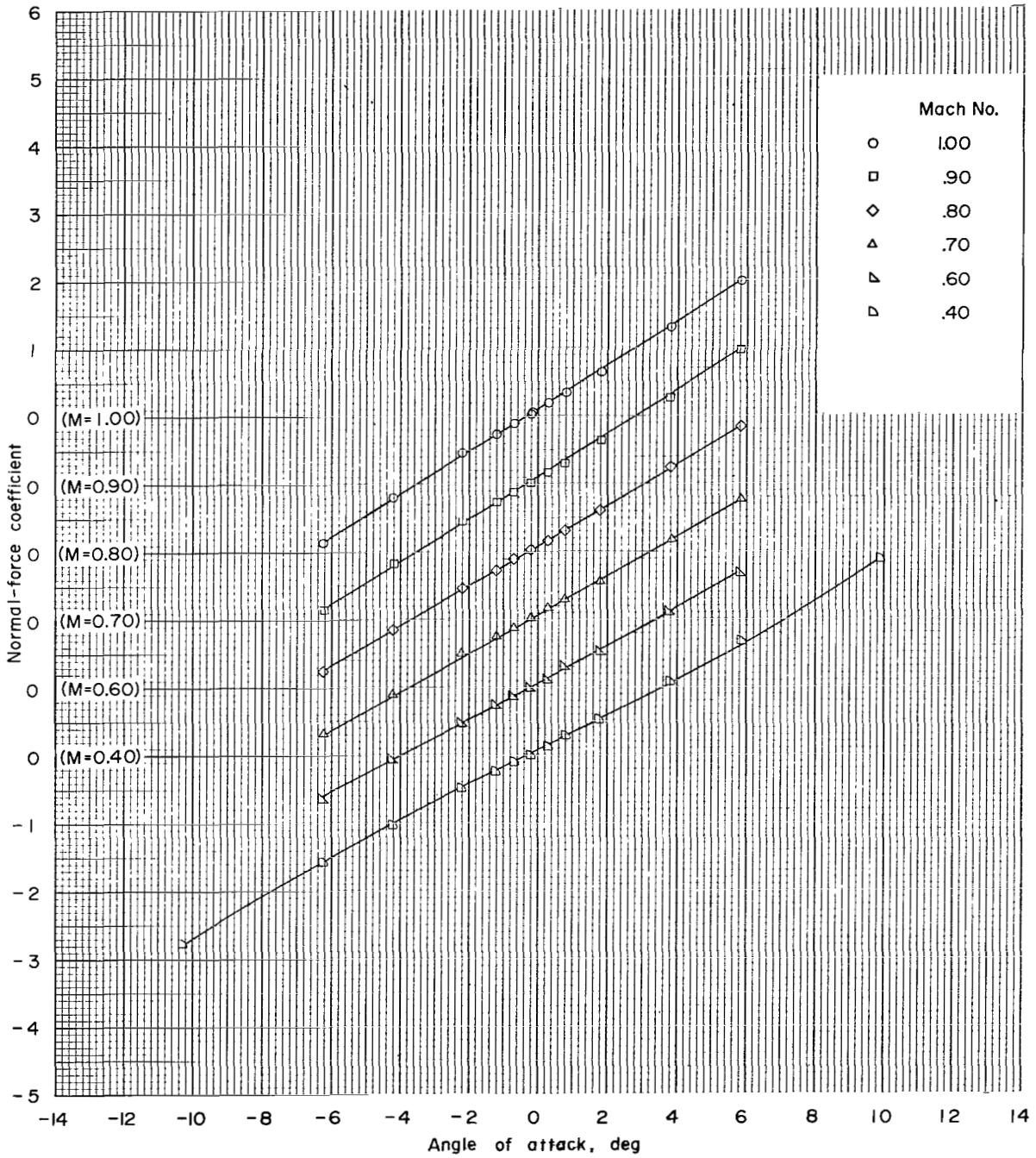

(e-1) Subsonic Mach numbers; configuration 5; $\phi = 0^{o}$.

Figure 7.- Continued.

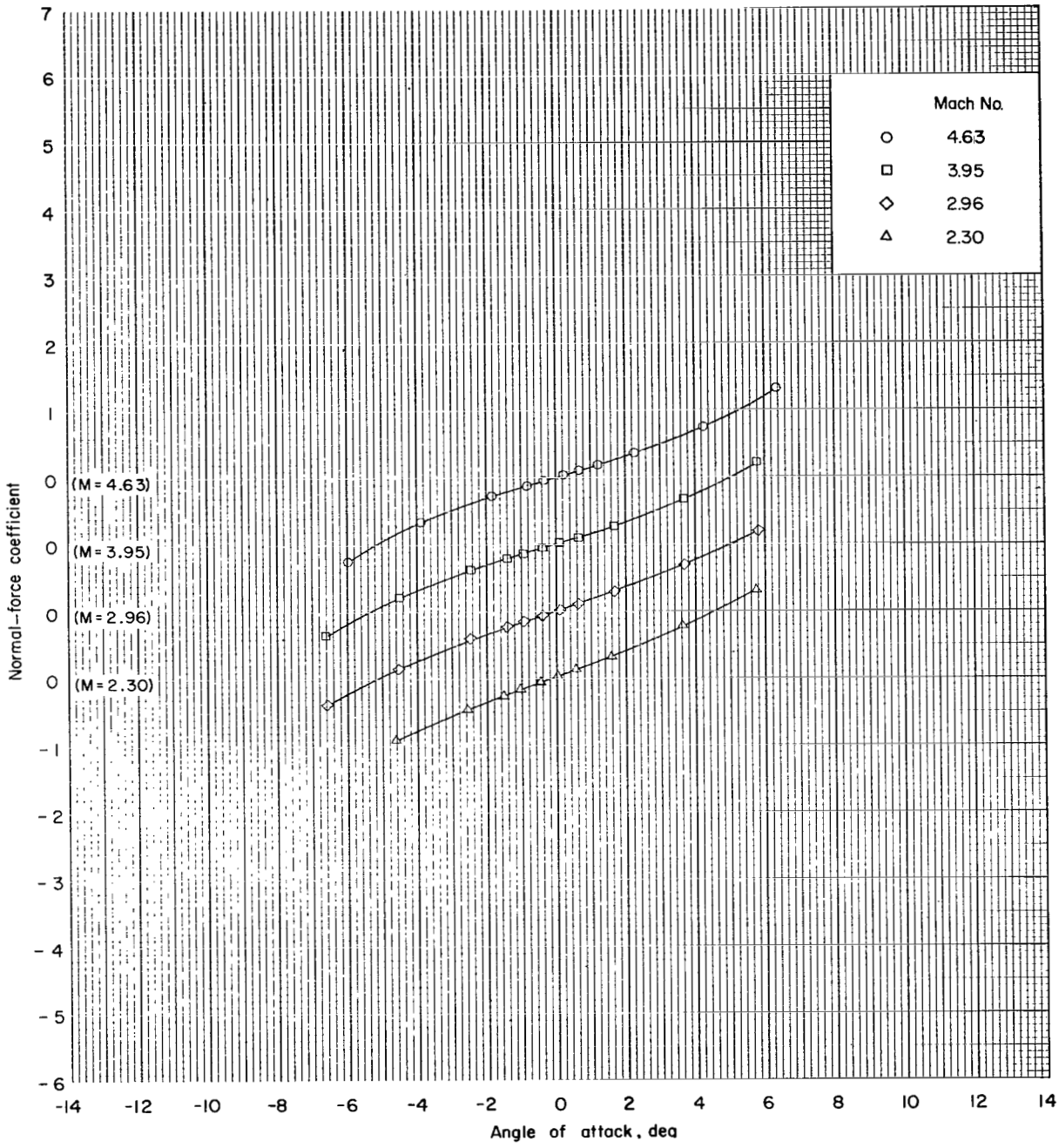

(e-2) Supersonic Mach numbers; configuration 5; $\phi = 0^{o}$.

Figure 7.- Continued.

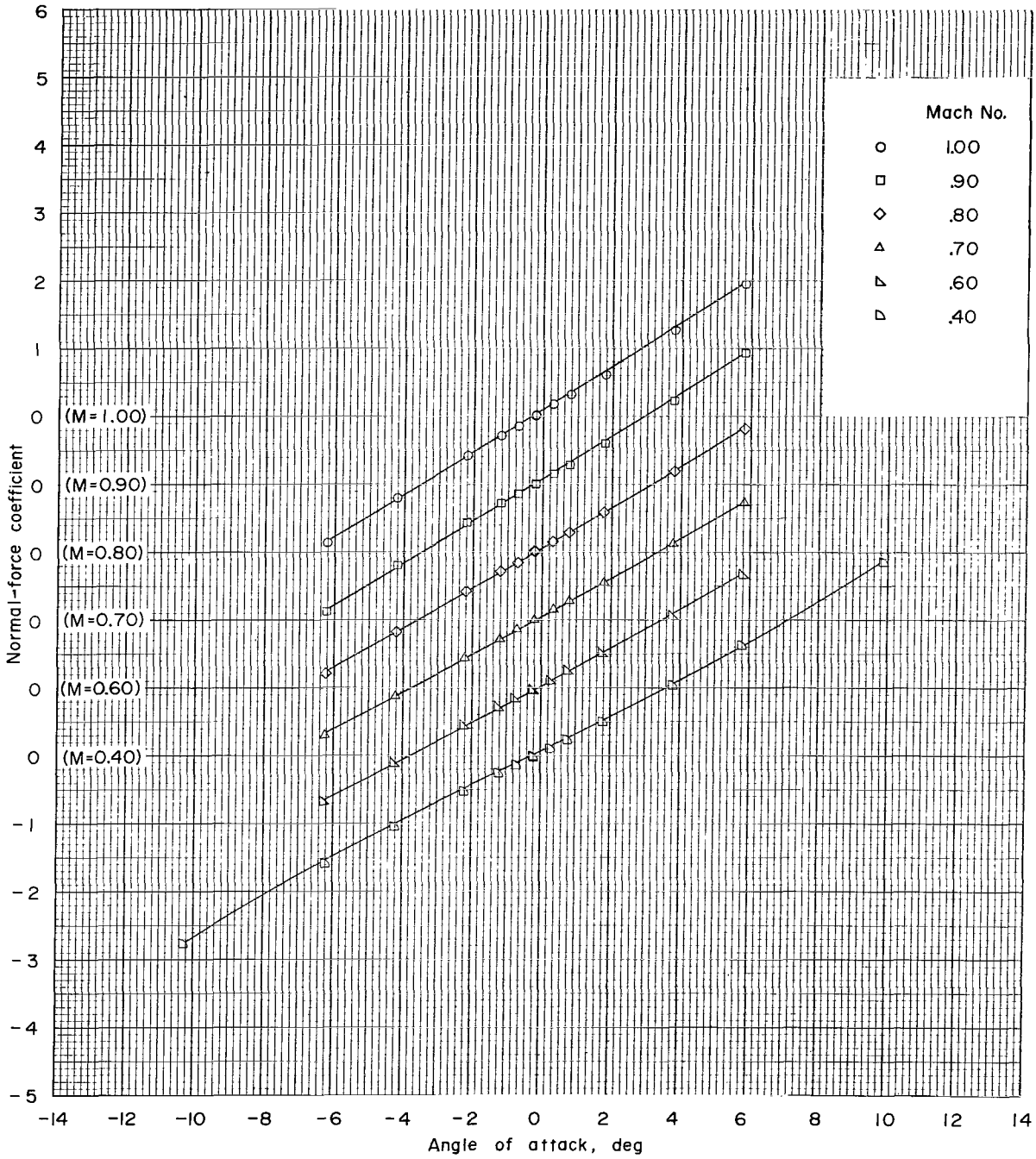

(f-1) Subsonic Mach numbers; configuration 6; $\phi = 0^{o}$.

Figure 7.- Continued.

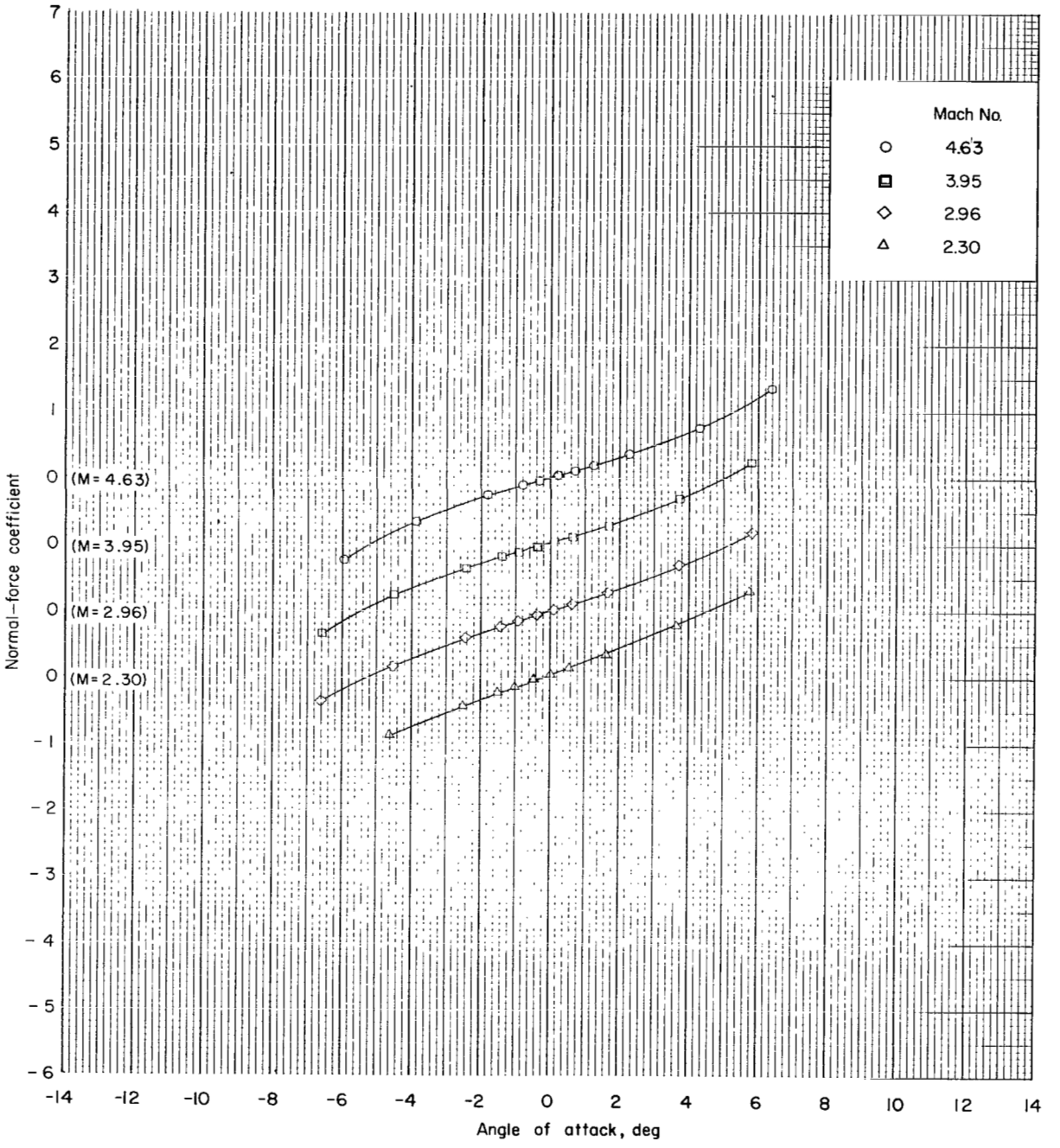

(f-2) Supersonic Mach numbers; configuration 6; $\phi = 0^{o}$.

Figure 7.- Continued.

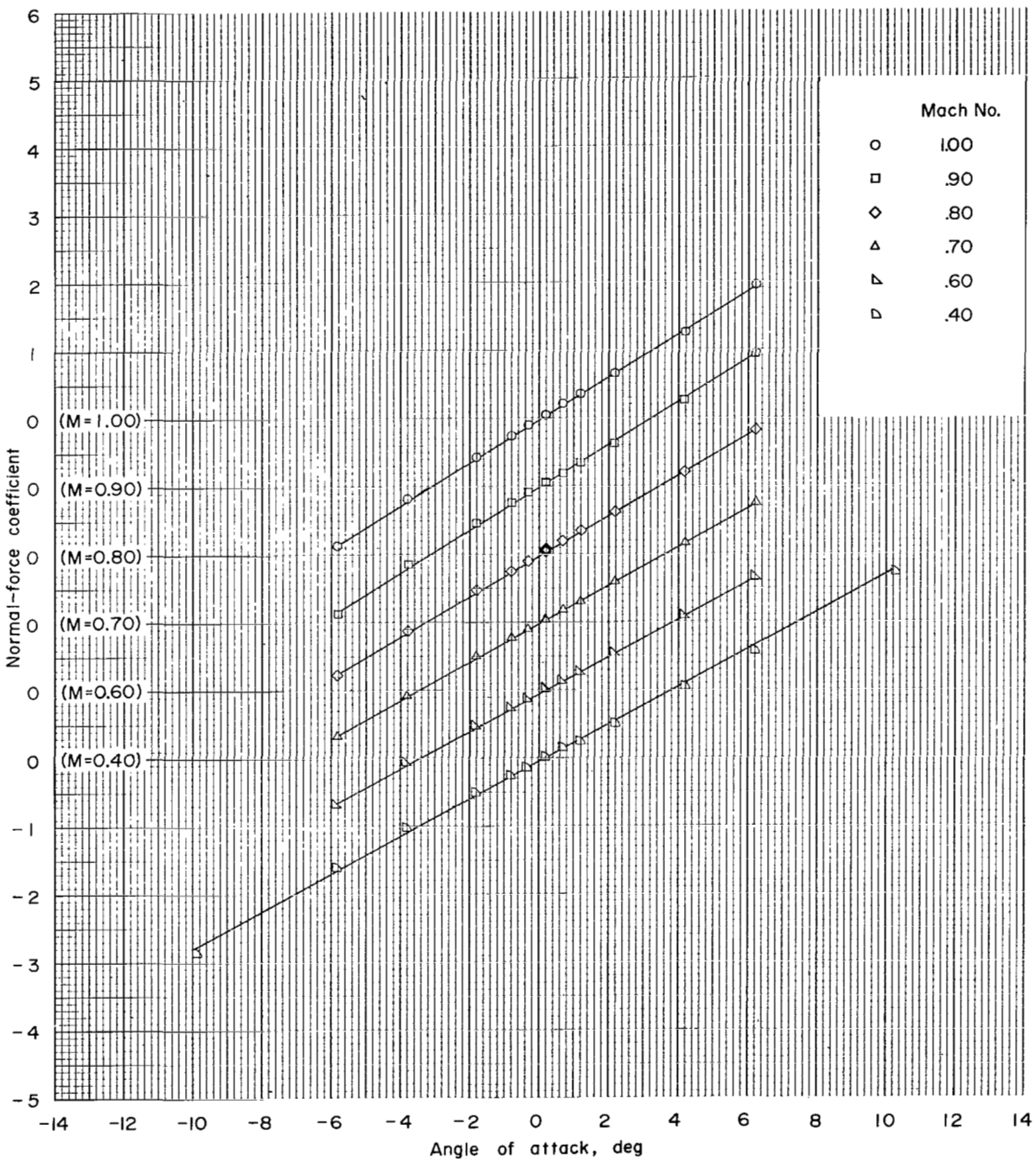

(g-1) Subsonic Mach numbers; configuration 6; $\phi = 180^{o}$.

Figure 7.- Continued.

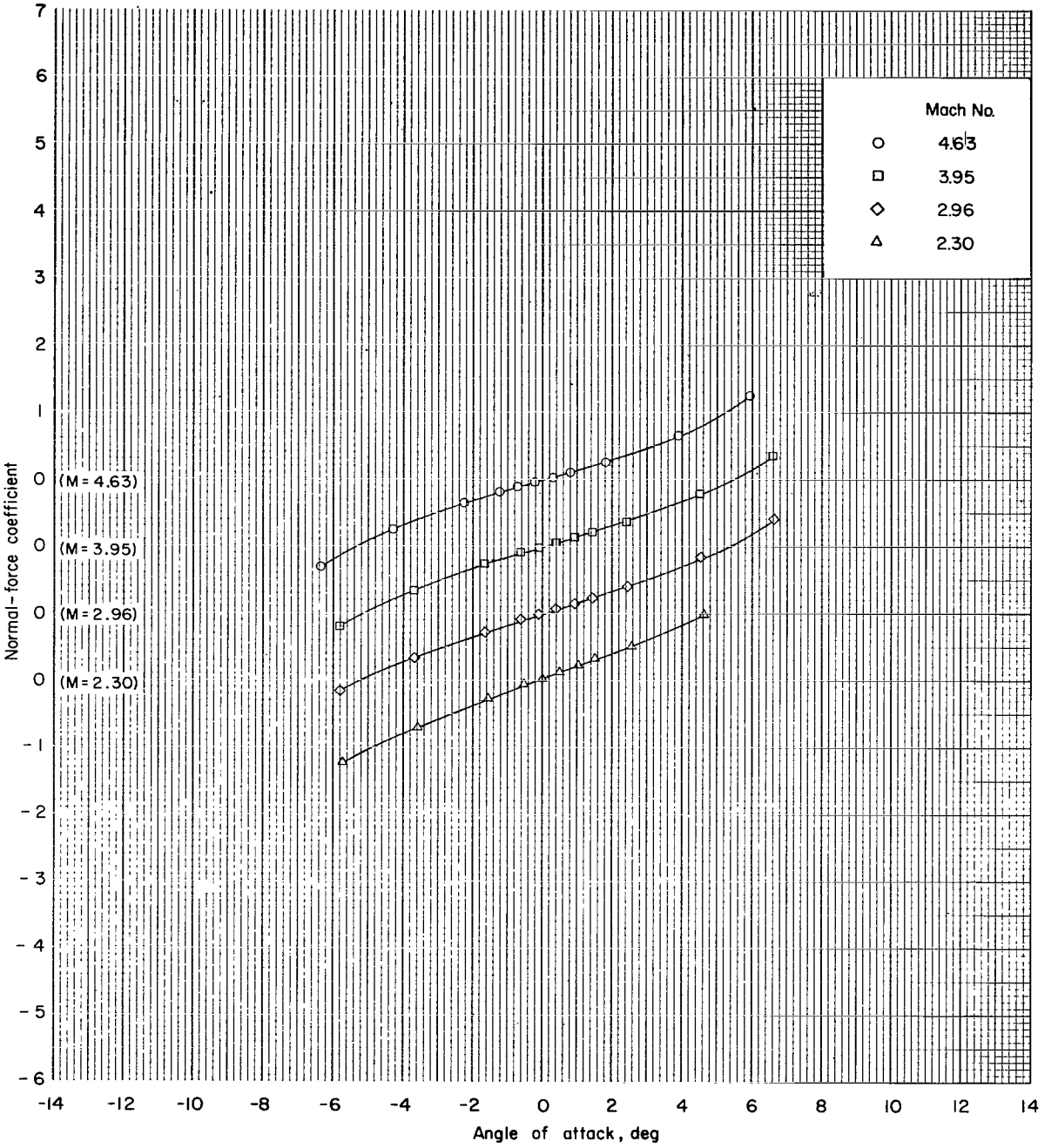

(g-2) Supersonic Mach numbers; configuration 6; $\phi = 180^{o}$.

Figure 7.- Continued.

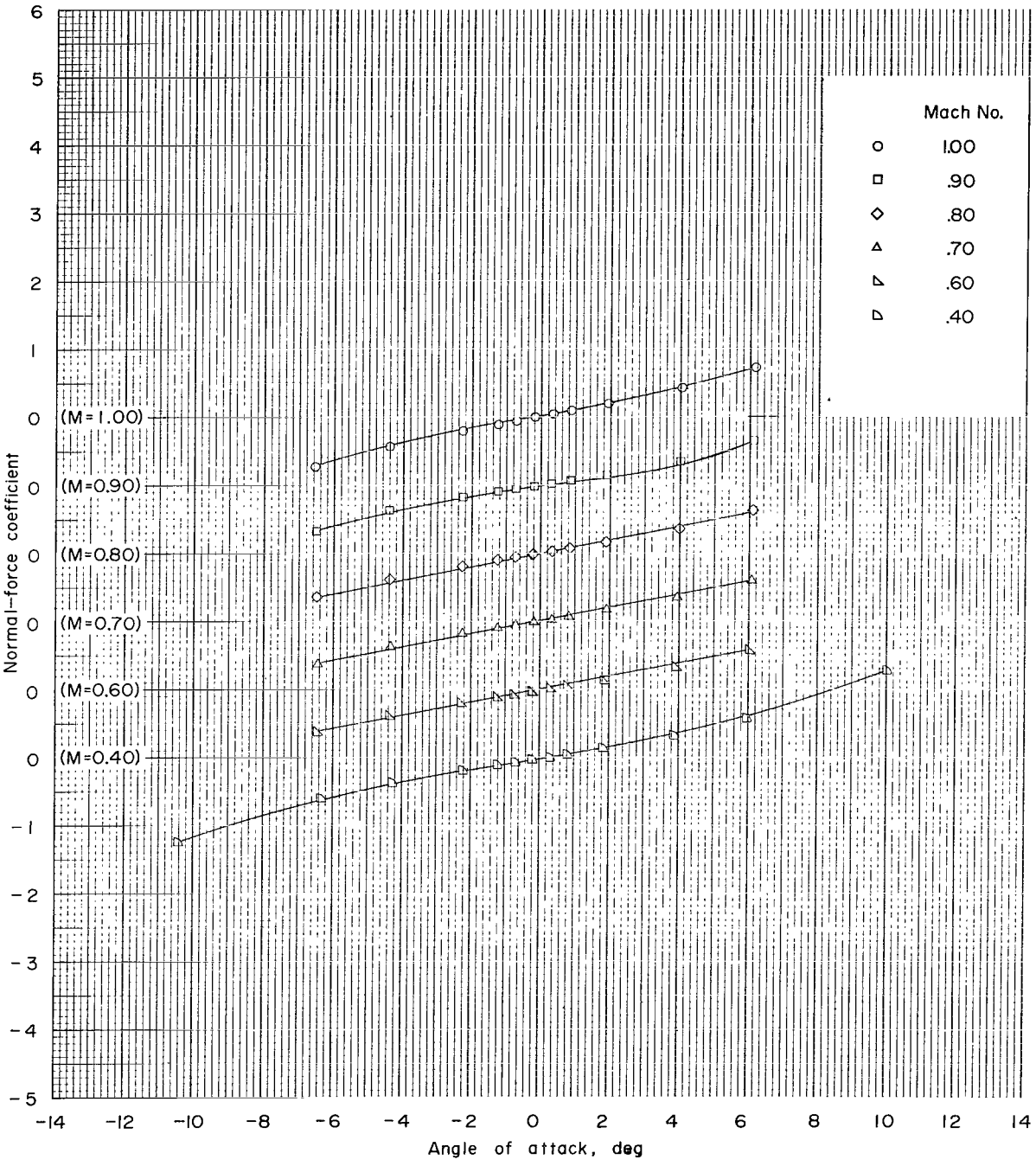

(h-1) Subsonic Mach numbers; configuration 7; $\phi = 0^{o}$.

Figure 7.- Continued.

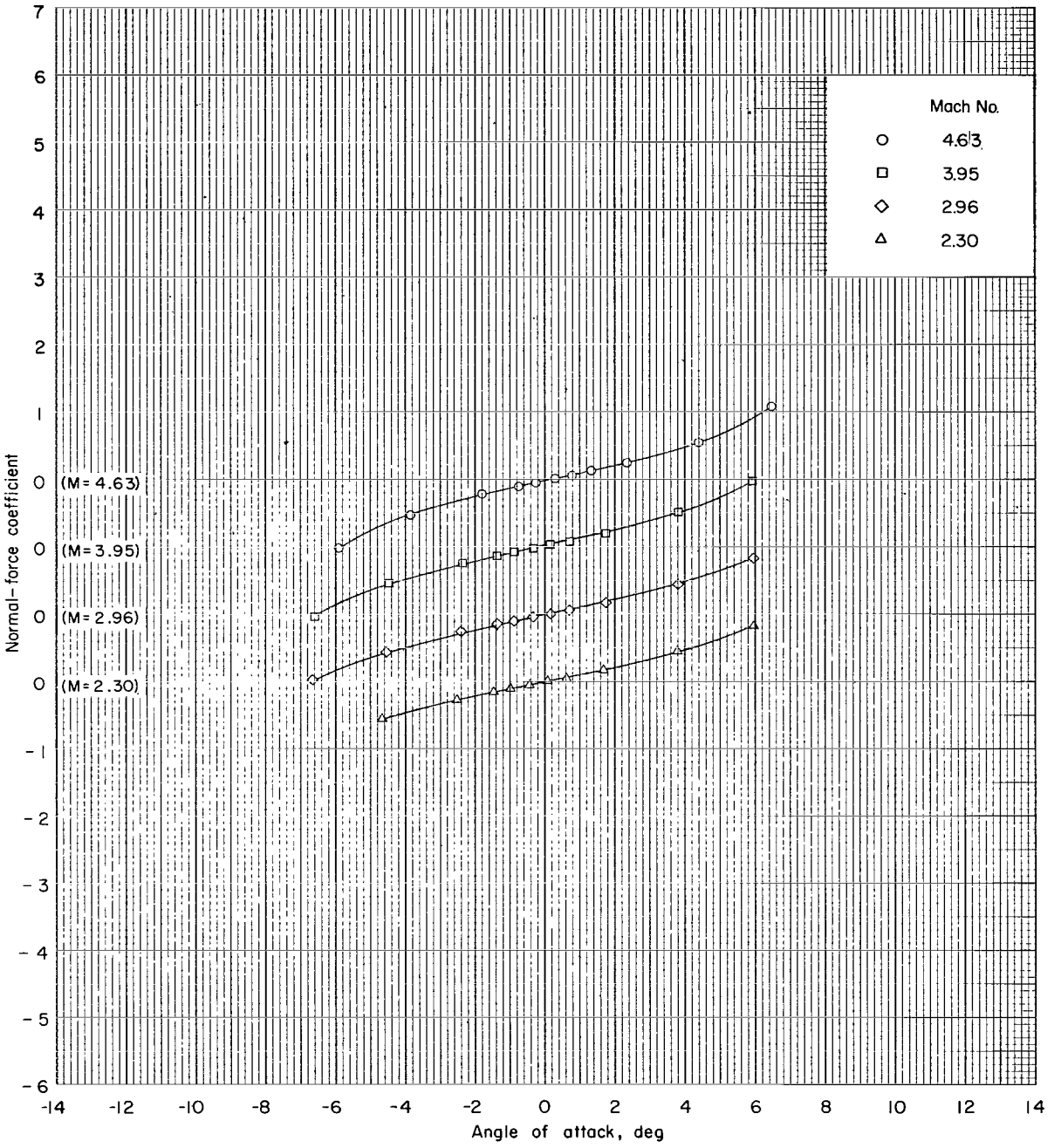

(h-2) Supersonic Mach numbers; configuration 7; $\phi = 0^{o}$.

Figure 7.- Continued.

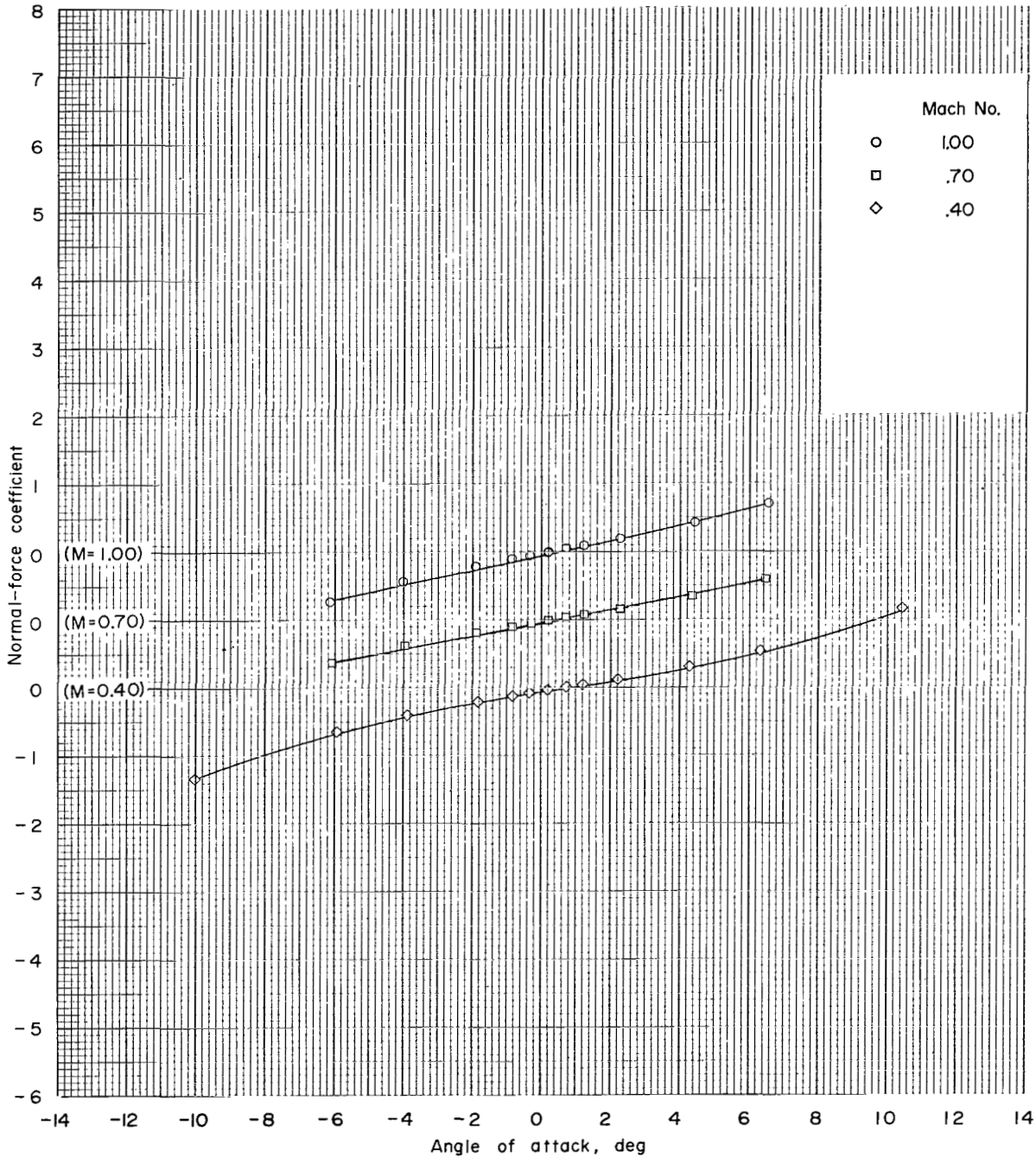

(i-1) Subsonic Mach number; configuration 7; $\phi = 180^{o}$.

Figure 7.- Continued.

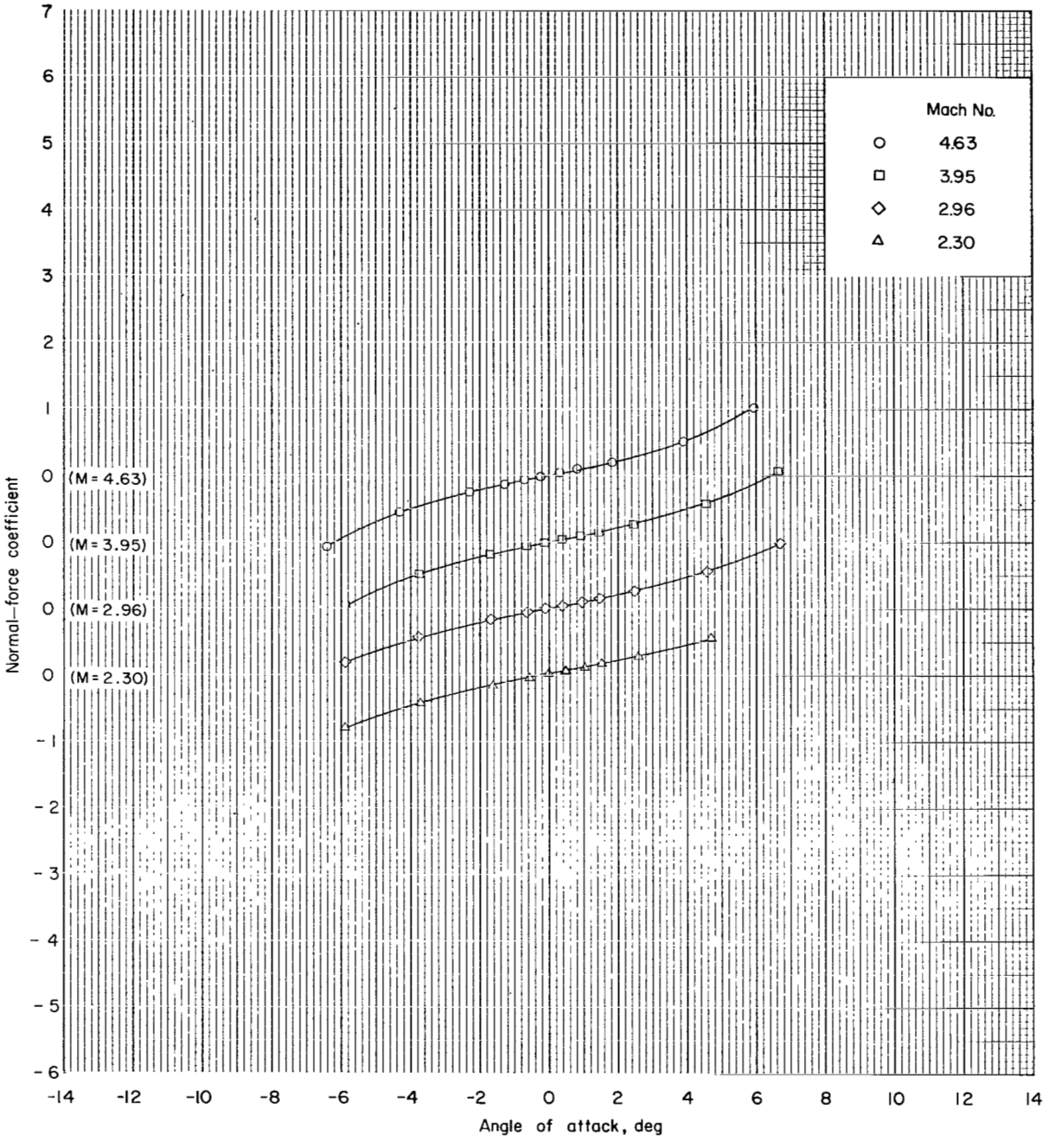

(i-2) Supersonic Mach numbers; configuration 7; $\phi = 180^{o}$.

Figure 7.- Concluded.

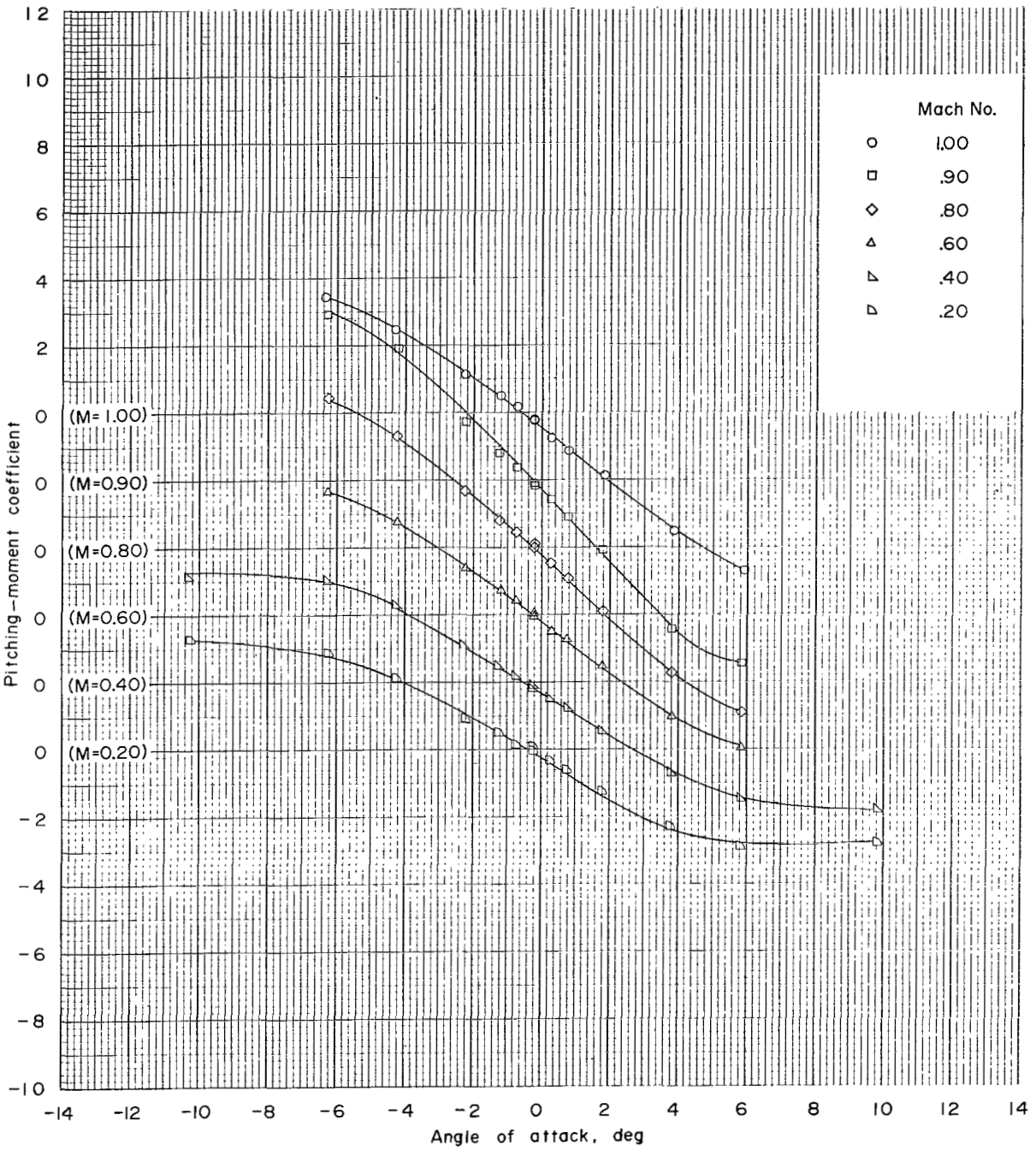

(a-1) Subsonic Mach numbers; configuration 1; $\phi = 0^{o}$.

Figure 8.- Pitching-moment coefficient as function of angle of attack, roll angle, and Mach number.

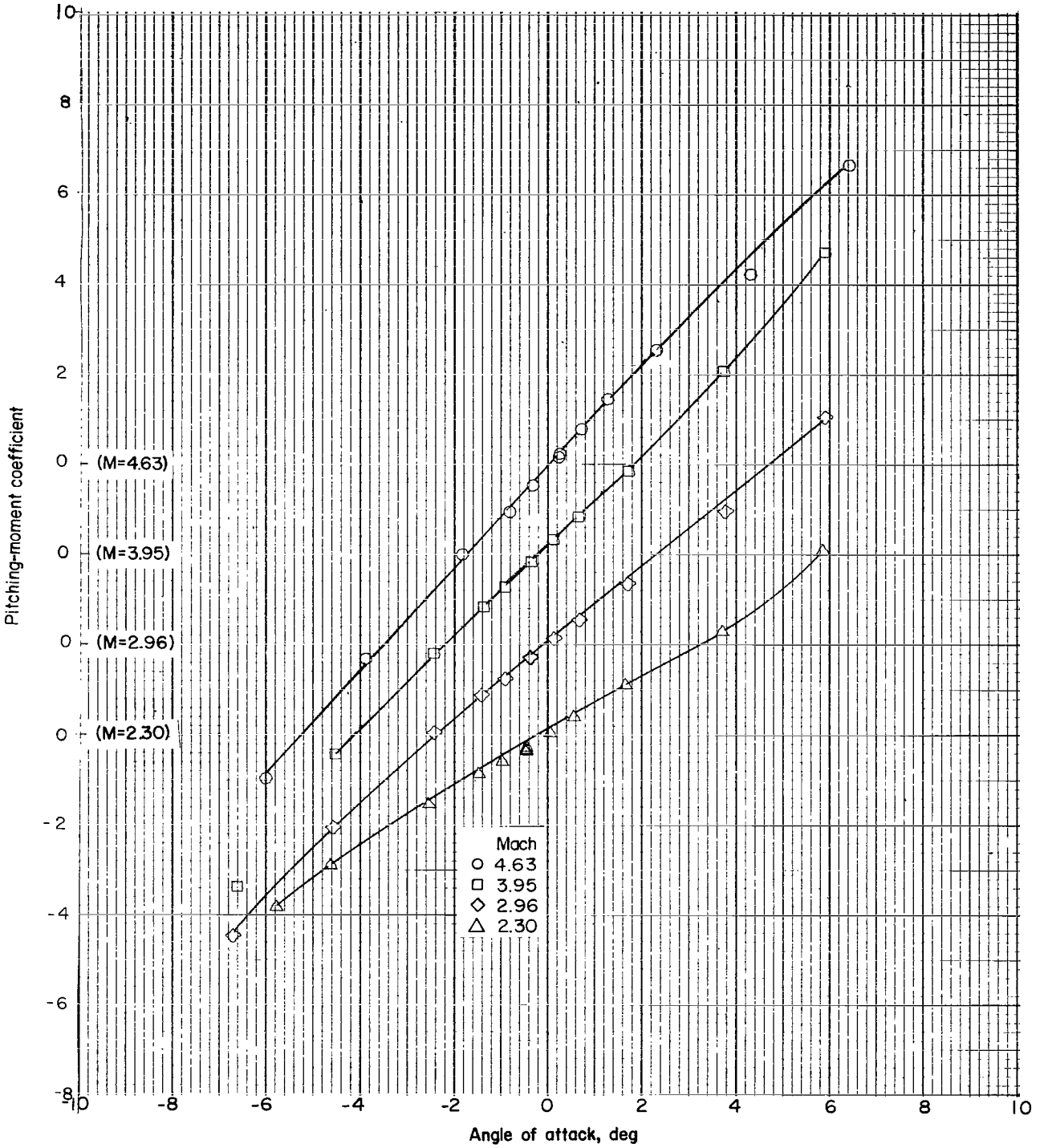

(a-2) Supersonic Mach numbers; configuration 1; $\phi = 0^{o}$.

Figure 8.- Continued.

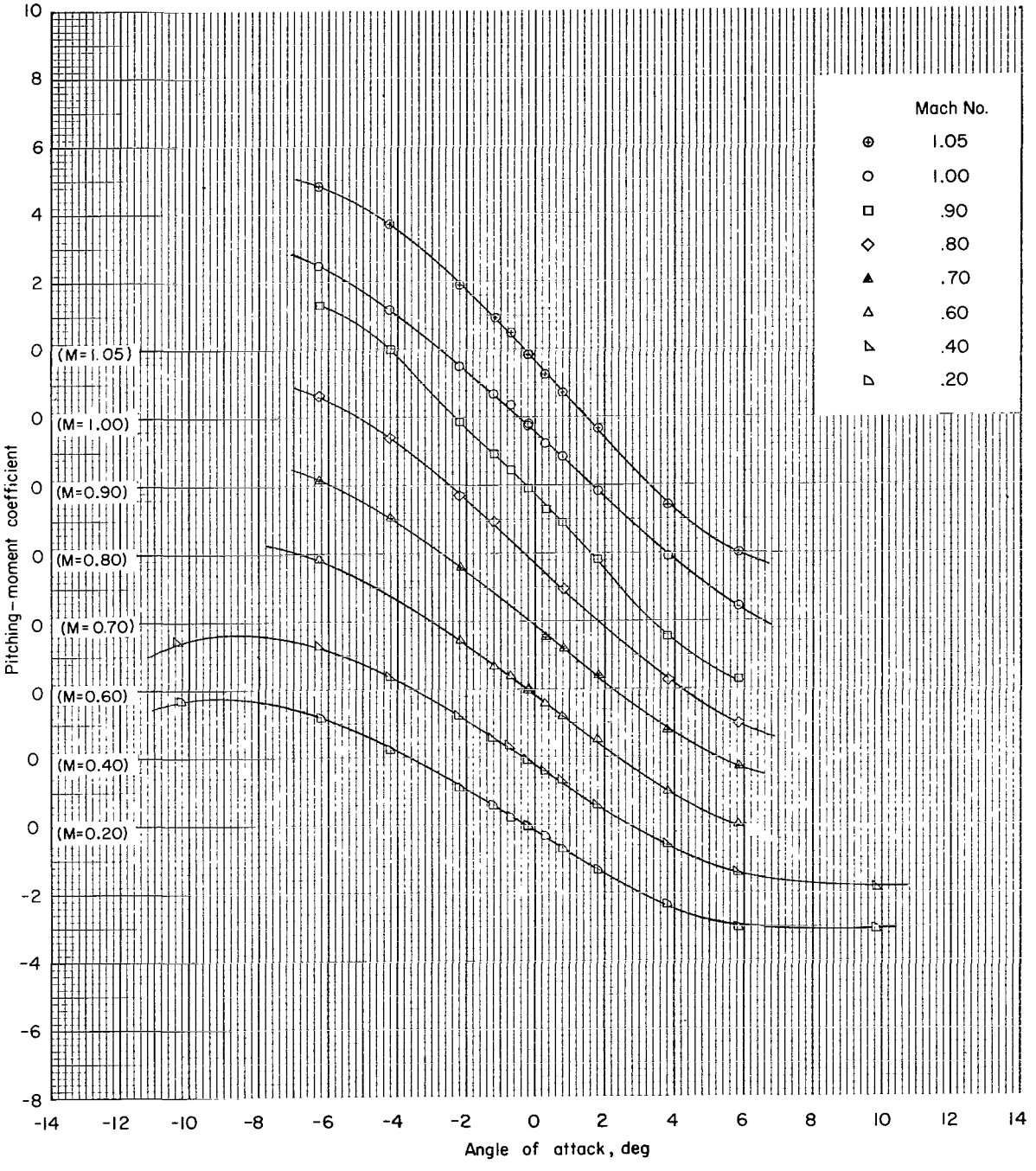

(b-1) Subsonic Mach numbers; configuration 2; $\phi = 0^{o}$.

Figure 8.- Continued.

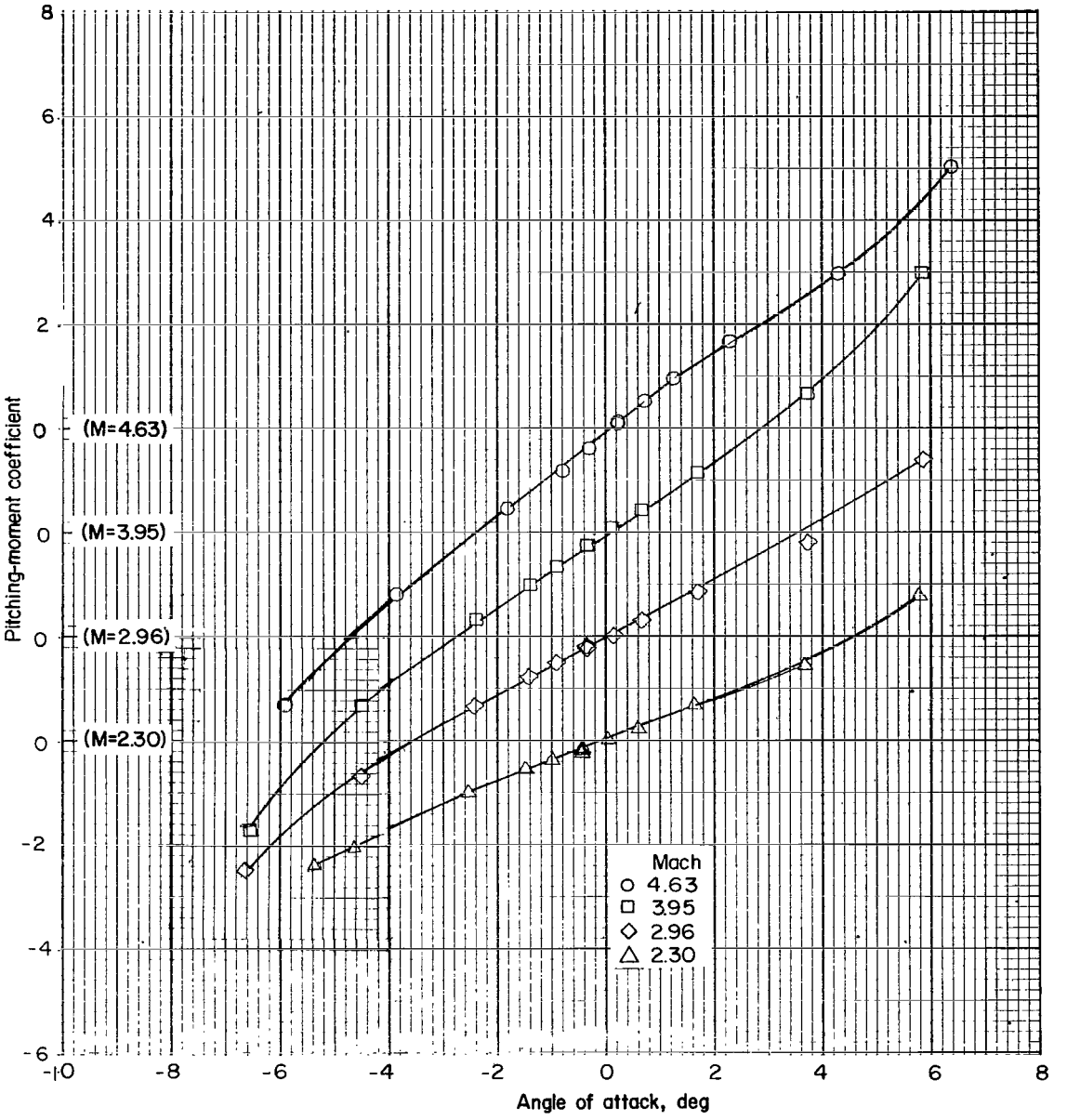

(b-2) Supersonic Mach numbers; configuration 2; $\phi = 0^{o}$.

Figure 8.- Continued.

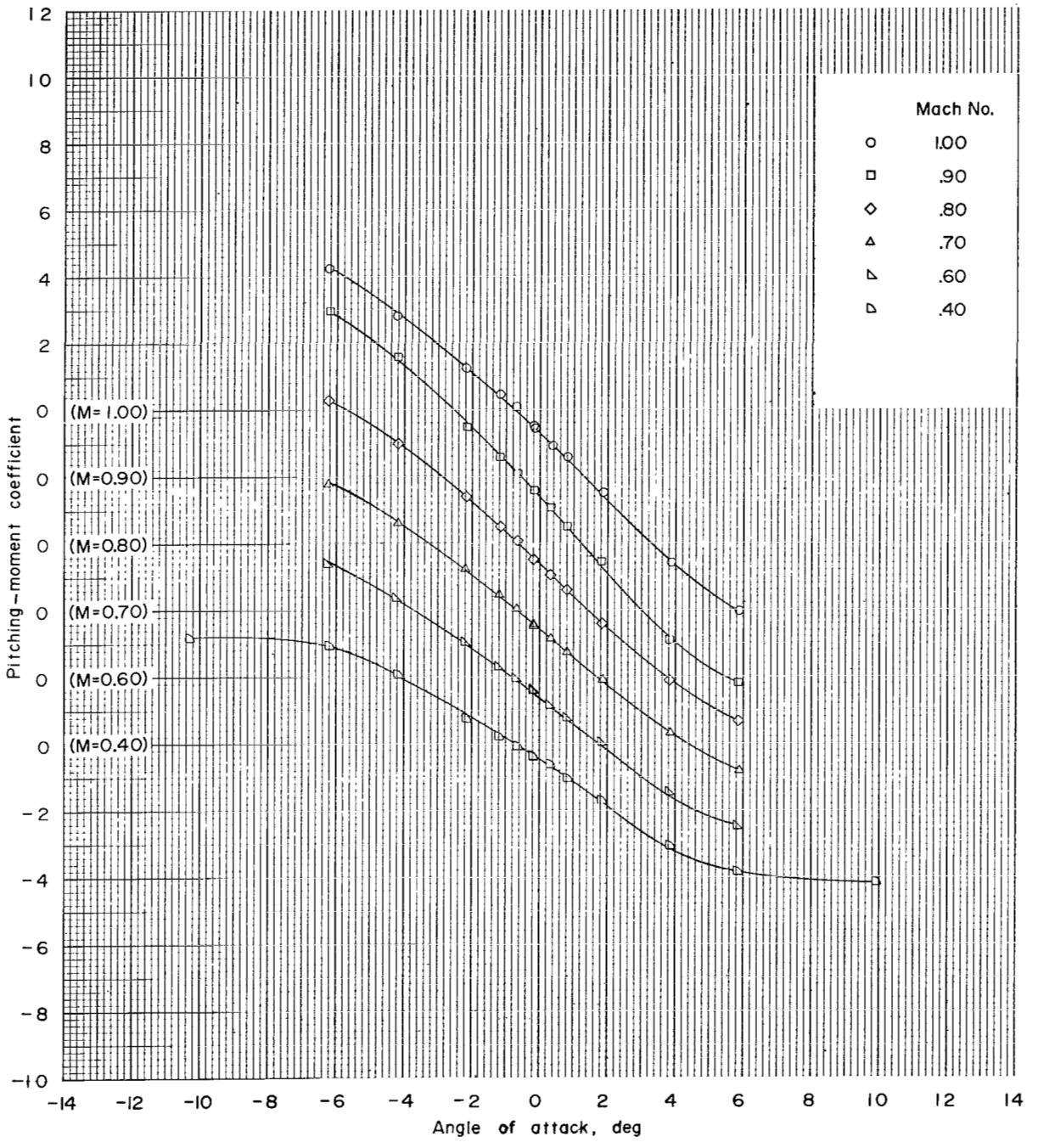

(c-1) Subsonic Mach numbers; configuration 3; $\phi = 0^{o}$.

Figure 8.- Continued.

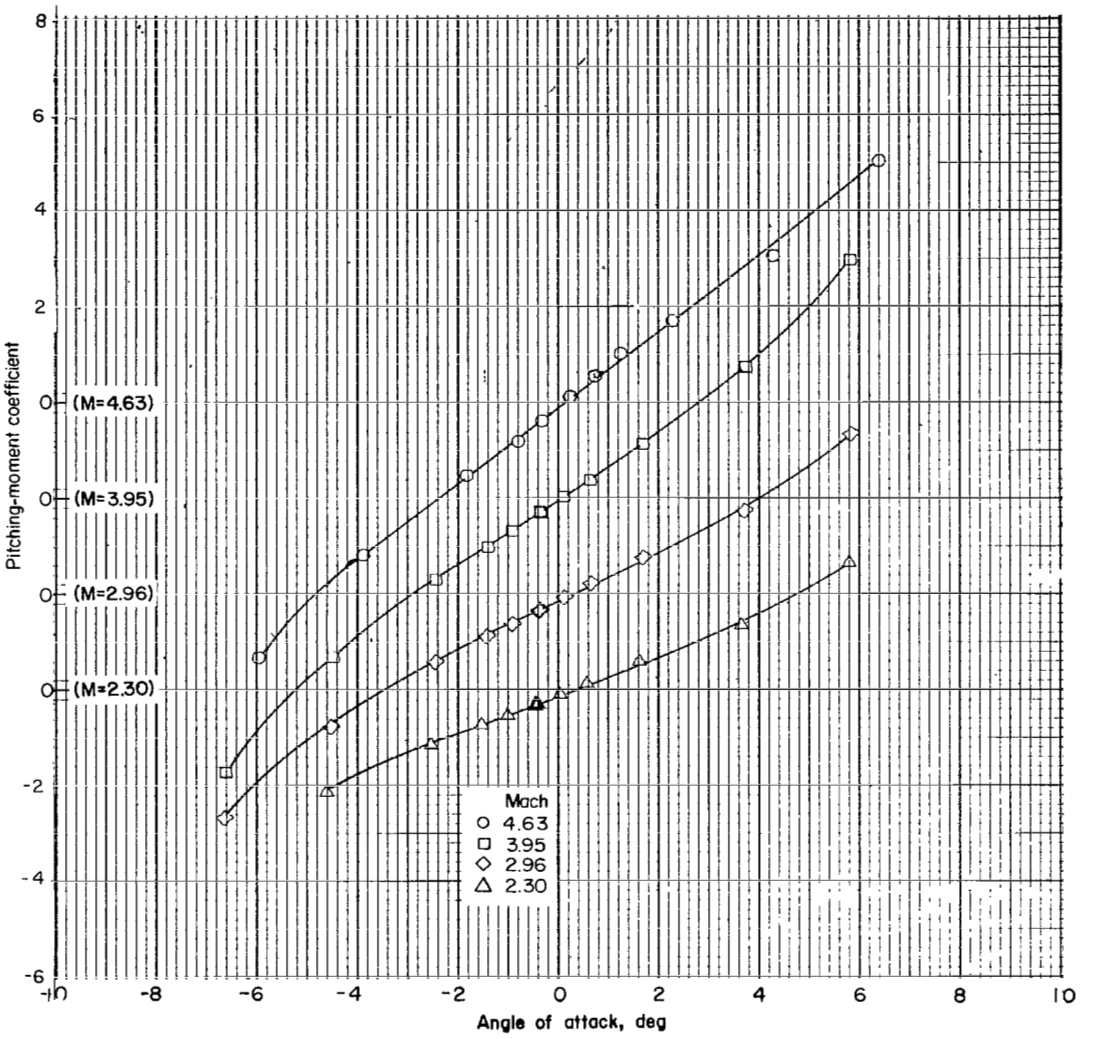

(c-2) Supersonic Mach numbers; configuration 3; $\phi = 0^{o}$.

Figure 8.- Continued.

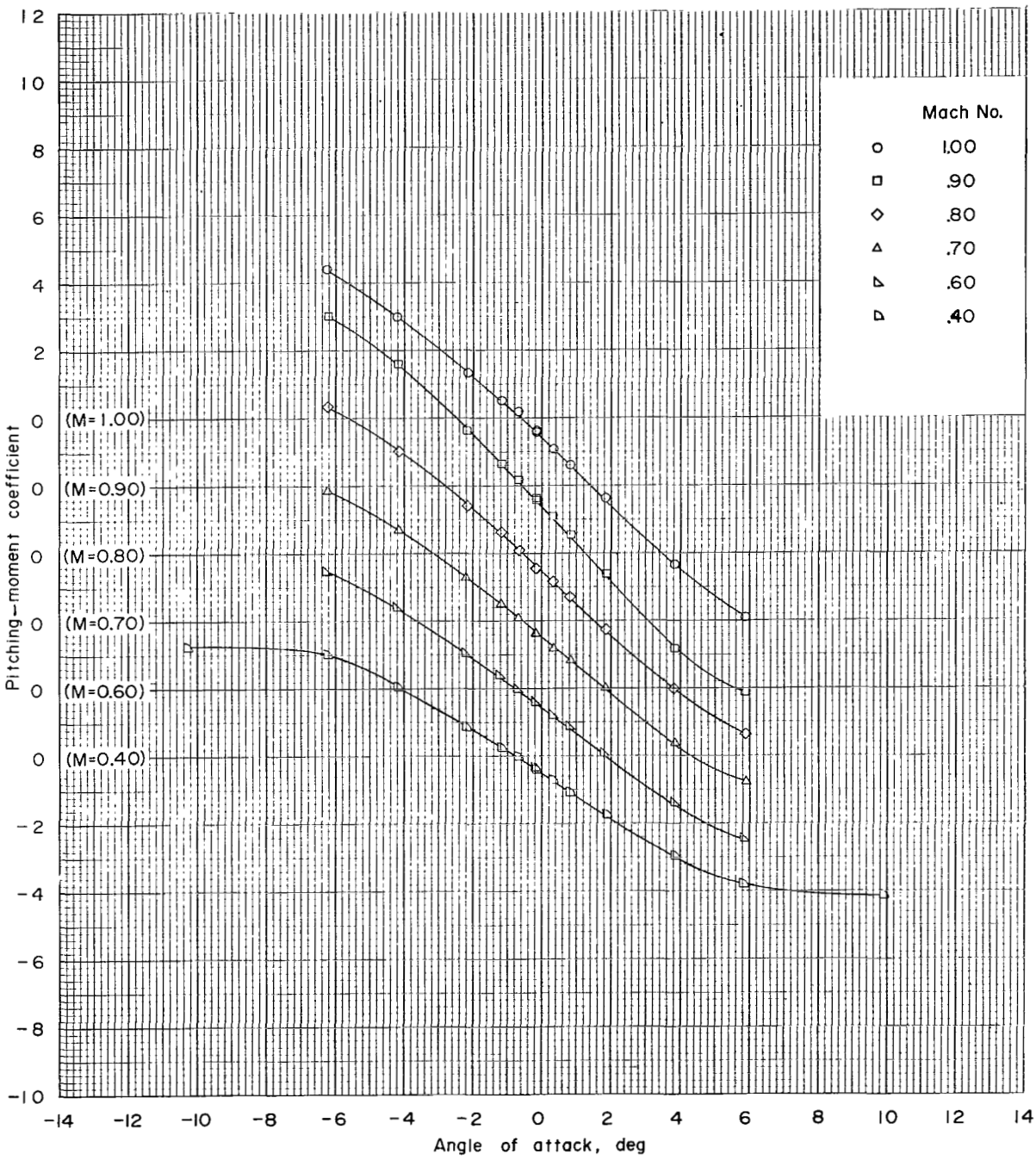

(d-1) Subsonic Mach numbers; configuration 4; $\phi = 0^{o}$.

Figure 8.- Continued.

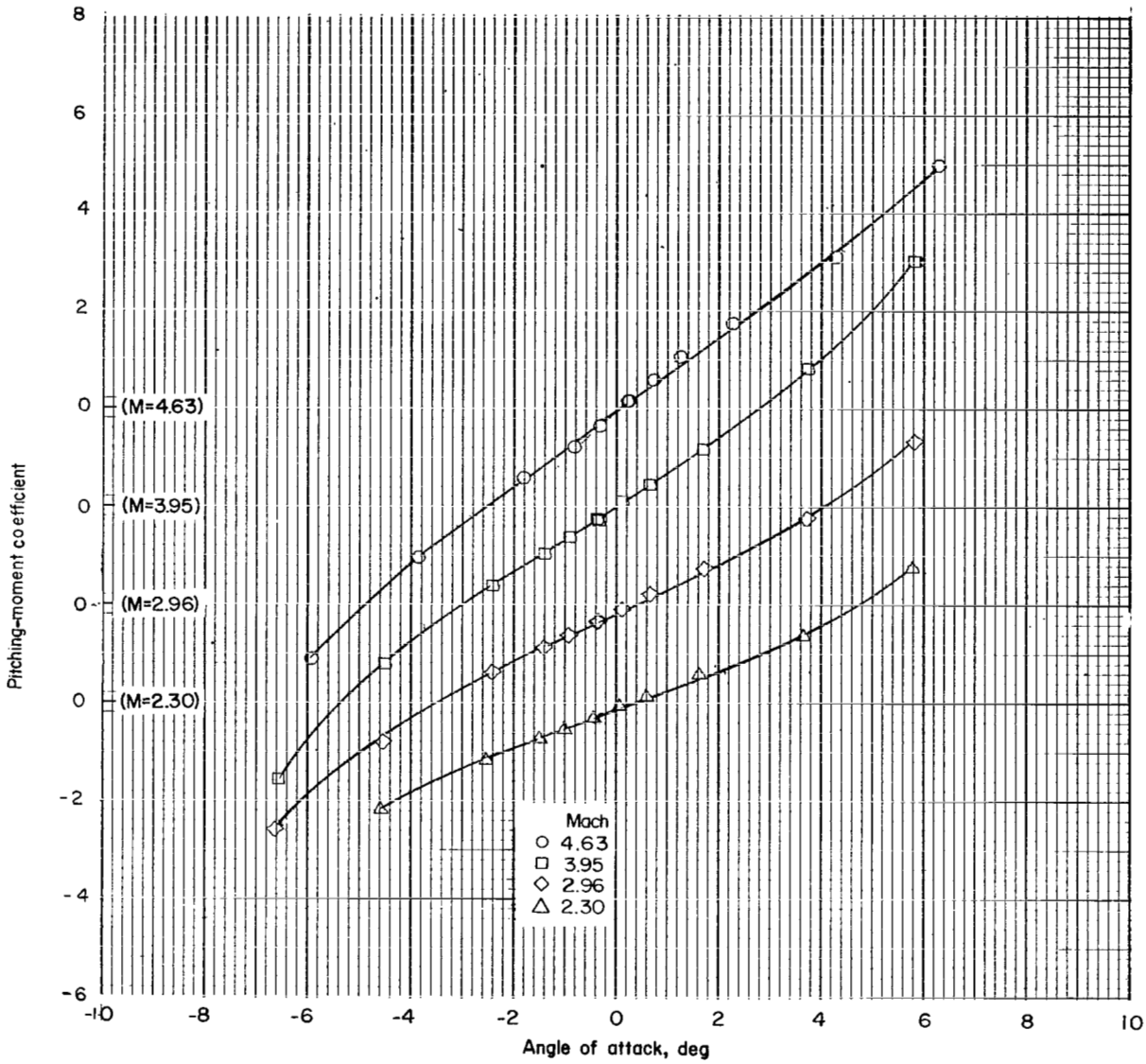

(d-2) Supersonic Mach numbers; configuration 4; $\phi = 0^{o}$.

Figure 8.- Continued.

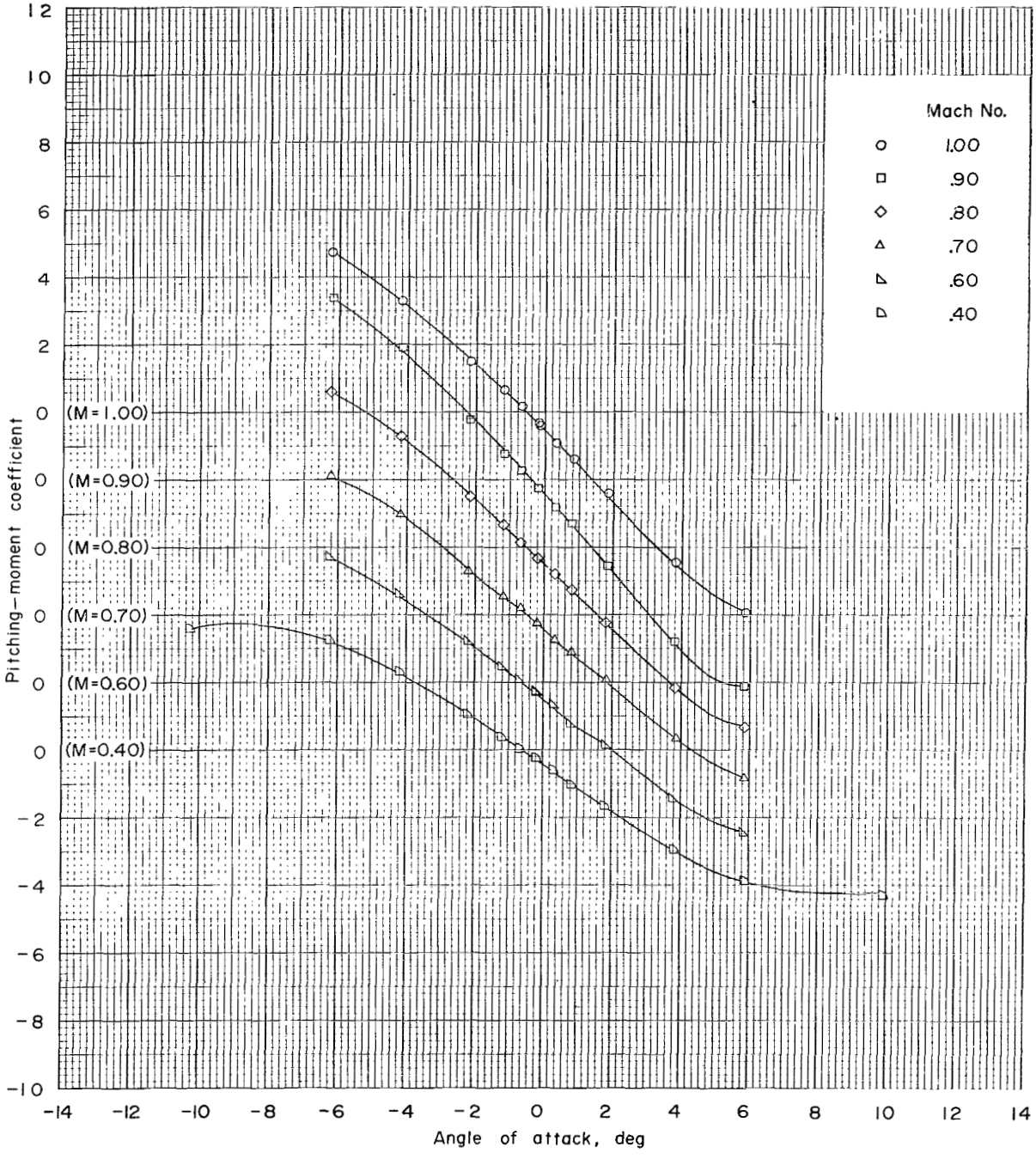

(e-1) Subsonic Mach numbers; configuration 5; $\phi = 0^{o}$.

Figure 8.- Continued.

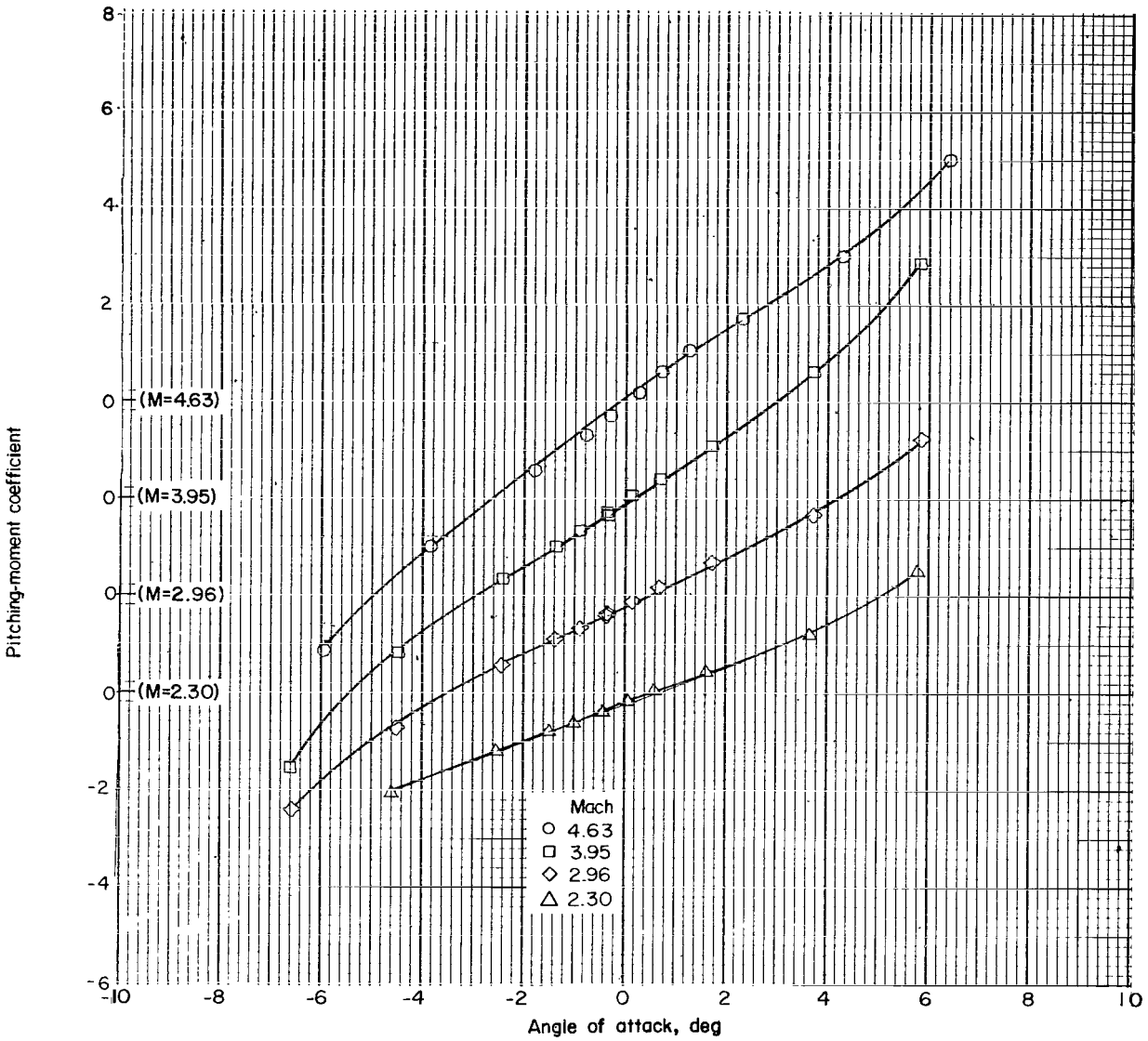

(e-2) Supersonic Mach numbers; configuration 5; $\phi = 0^{o}$.

Figure 8.- Continued.

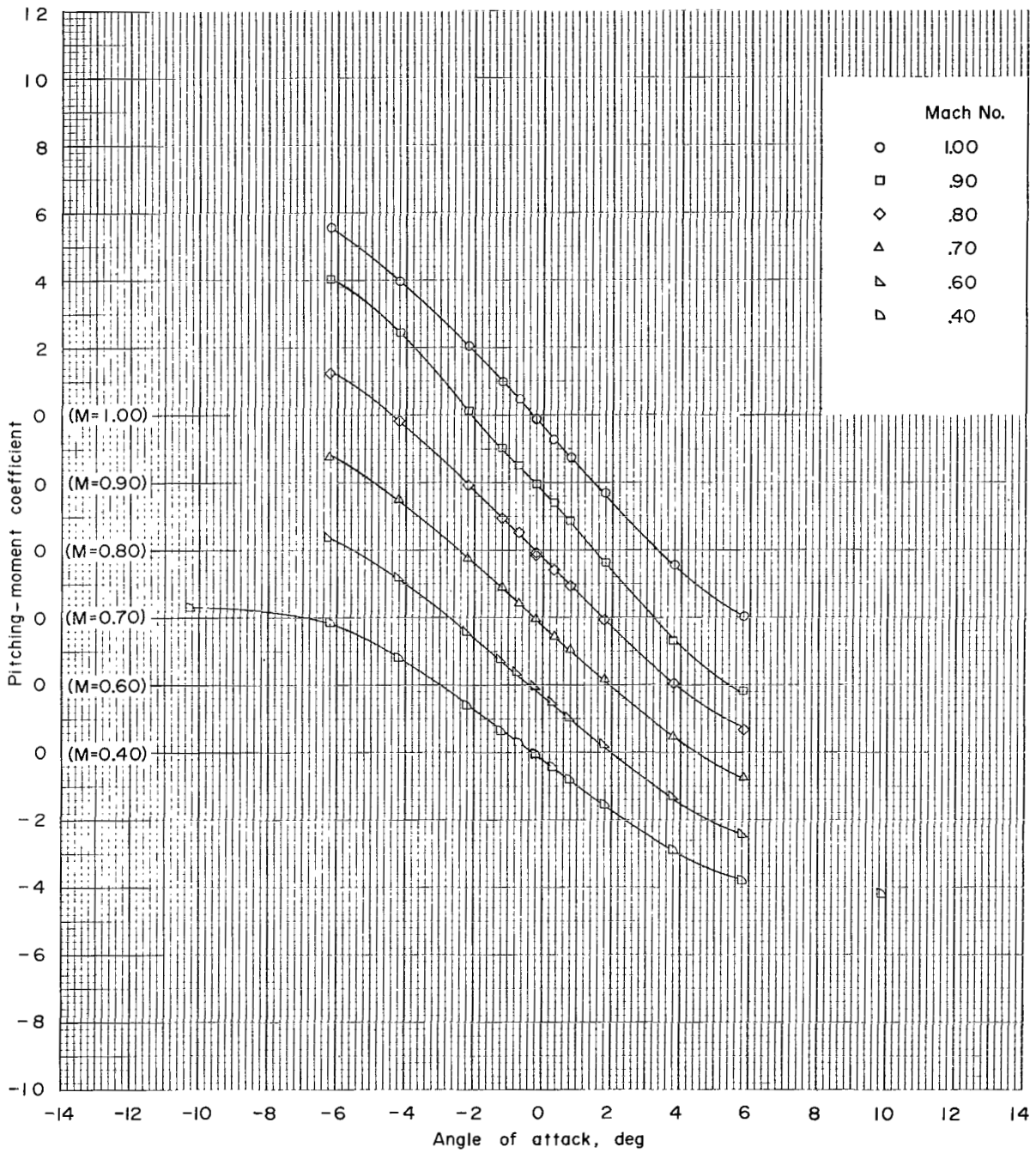

(f-1) Subsonic Mach numbers; configuration 6; $\phi = 0^{o}$.

Figure 8.- Continued.

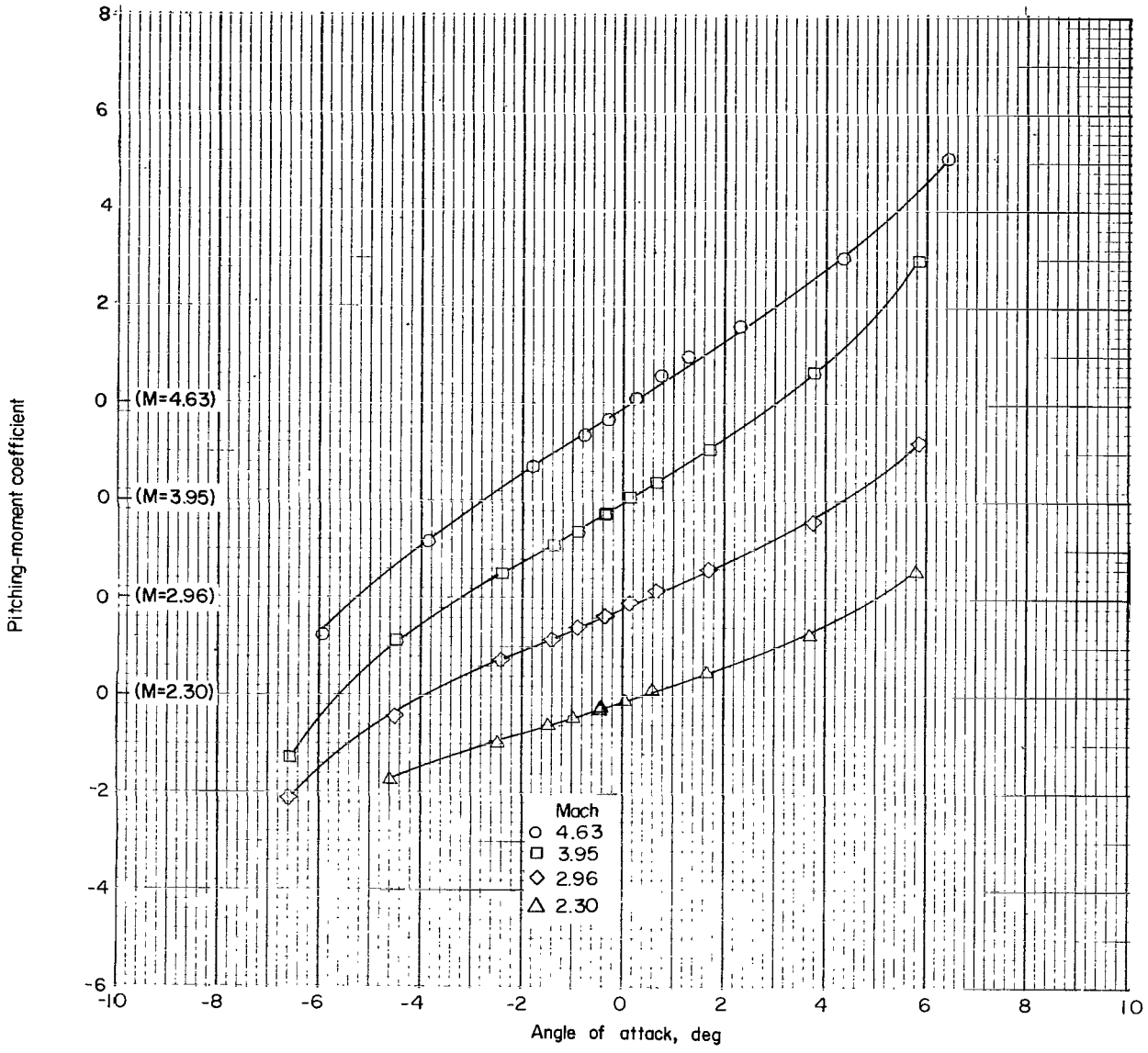

(f-2) Supersonic Mach numbers; configuration 6; $\phi = 0^{o}$.

Figure 8.- Continued.

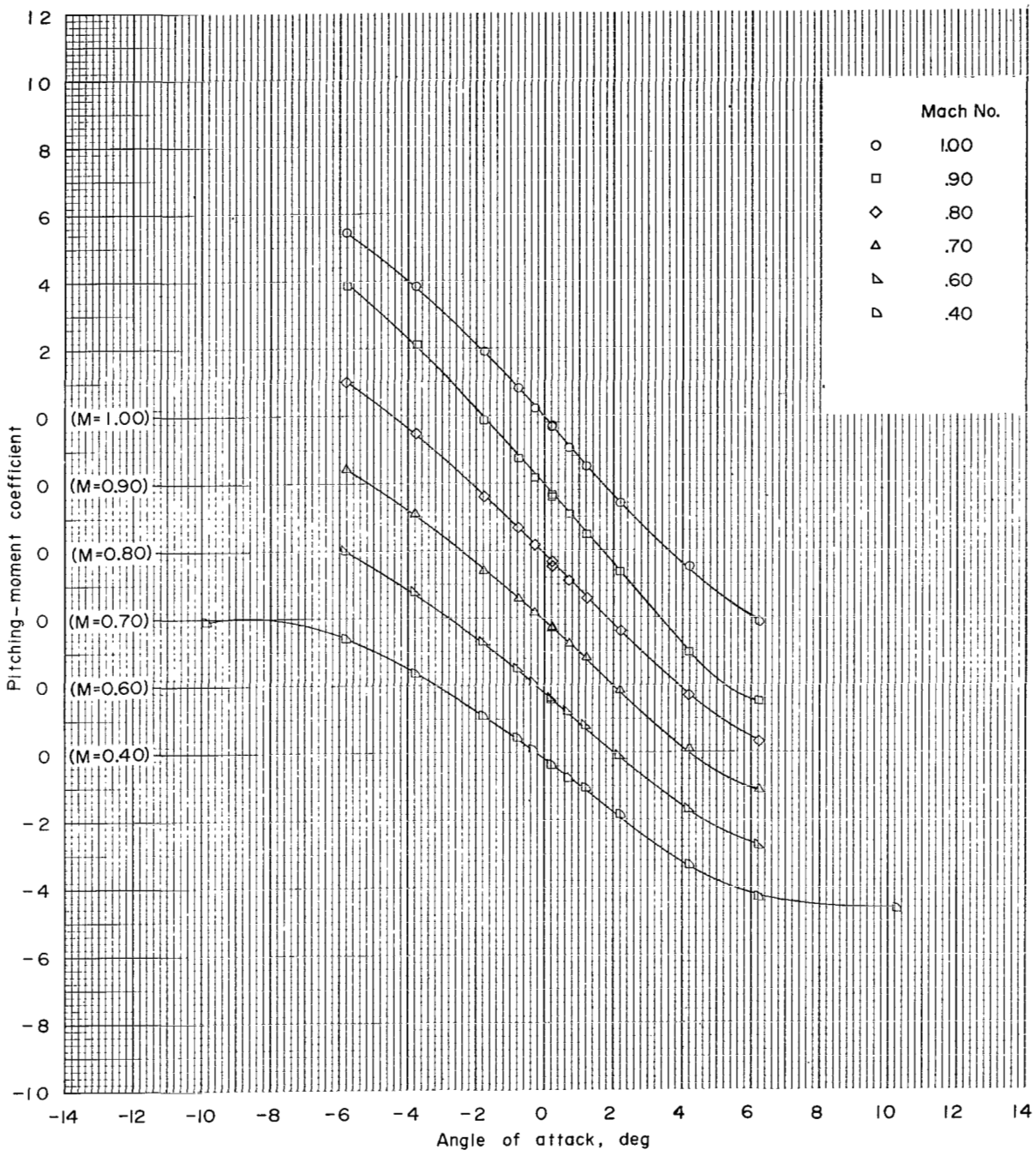

(g-1) Subsonic Mach numbers; configuration 6; $\phi = 180^{o}$.

Figure 8.- Continued.

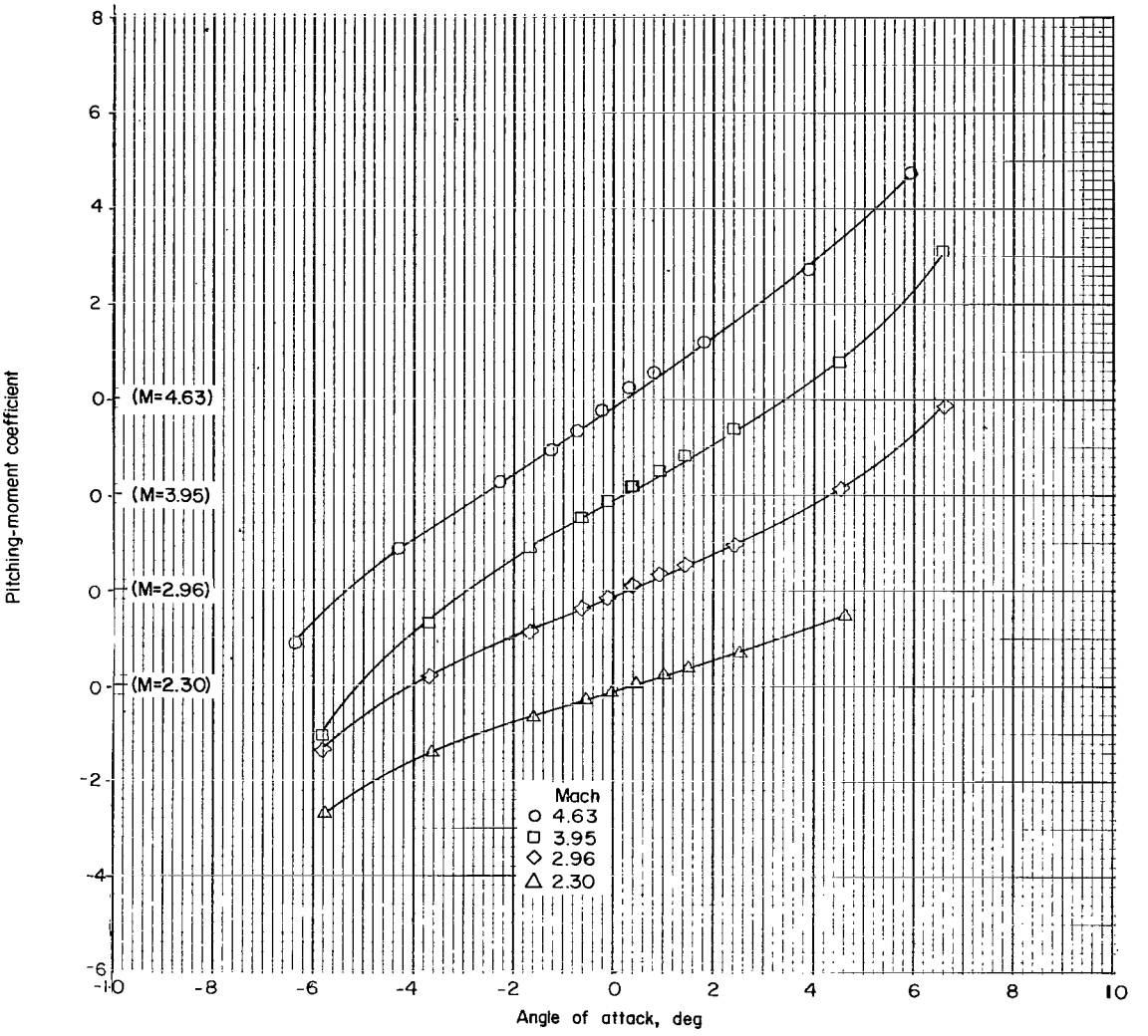

(g-2) Supersonic Mach numbers; configuration 6; $\phi = 180^{o}$.

Figure 8.- Continued.

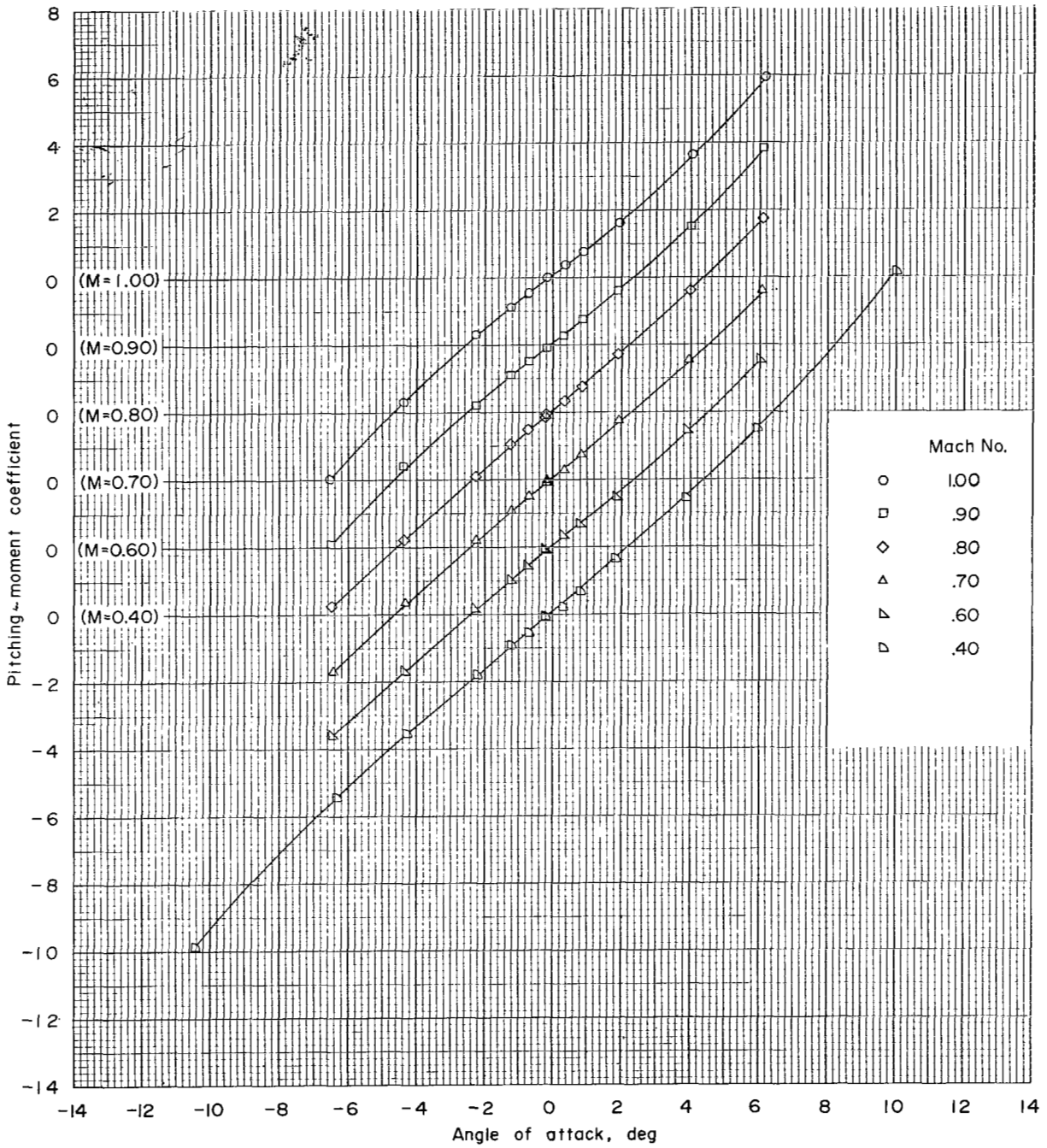

(h-1) Subsonic Mach numbers; configuration 7; $\phi = 0^{o}$.

Figure 8.- Continued.

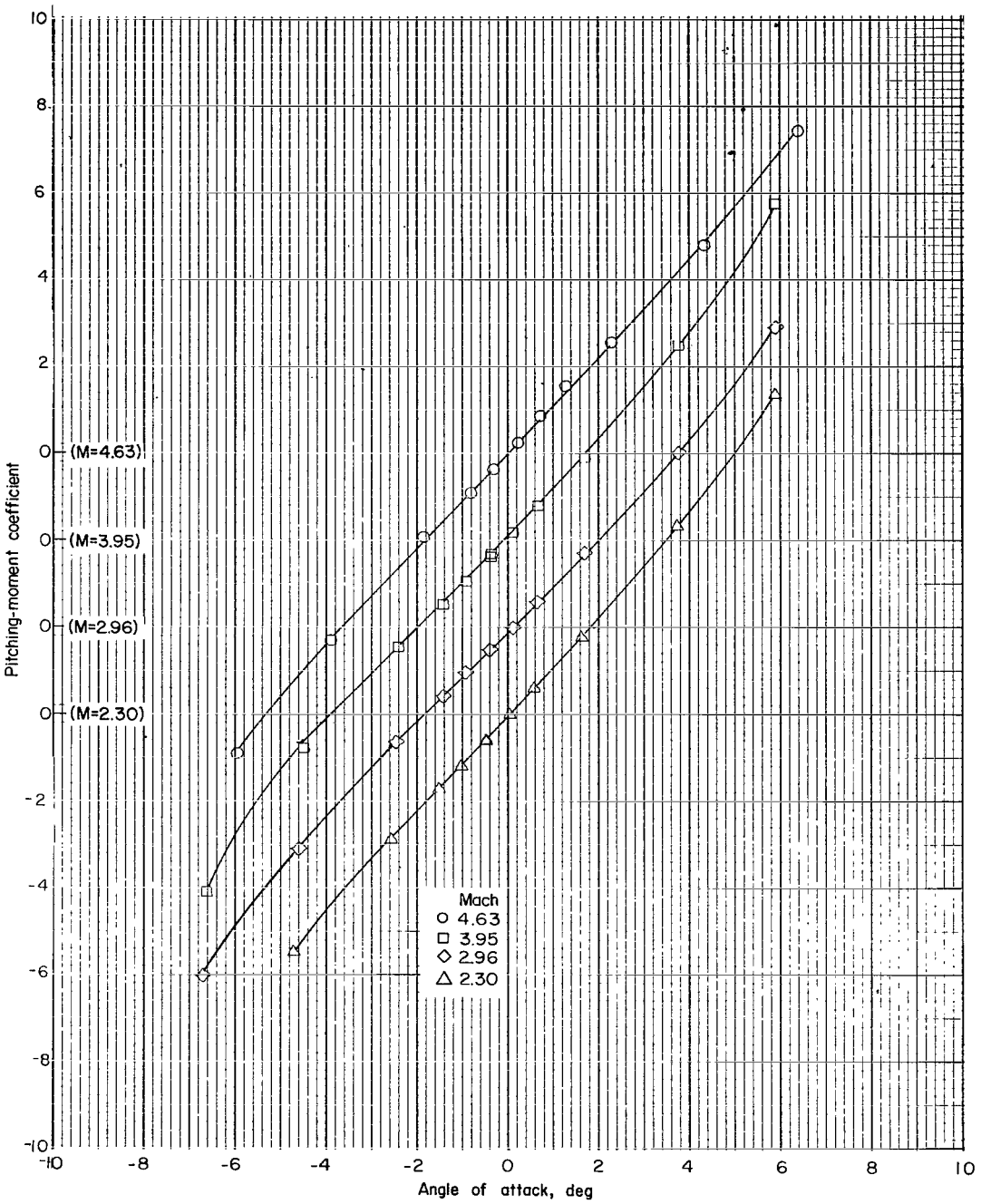

(h-2) Supersonic Mach numbers; configuration 7; $\phi = 0^{o}$.

Figure 8.- Continued.

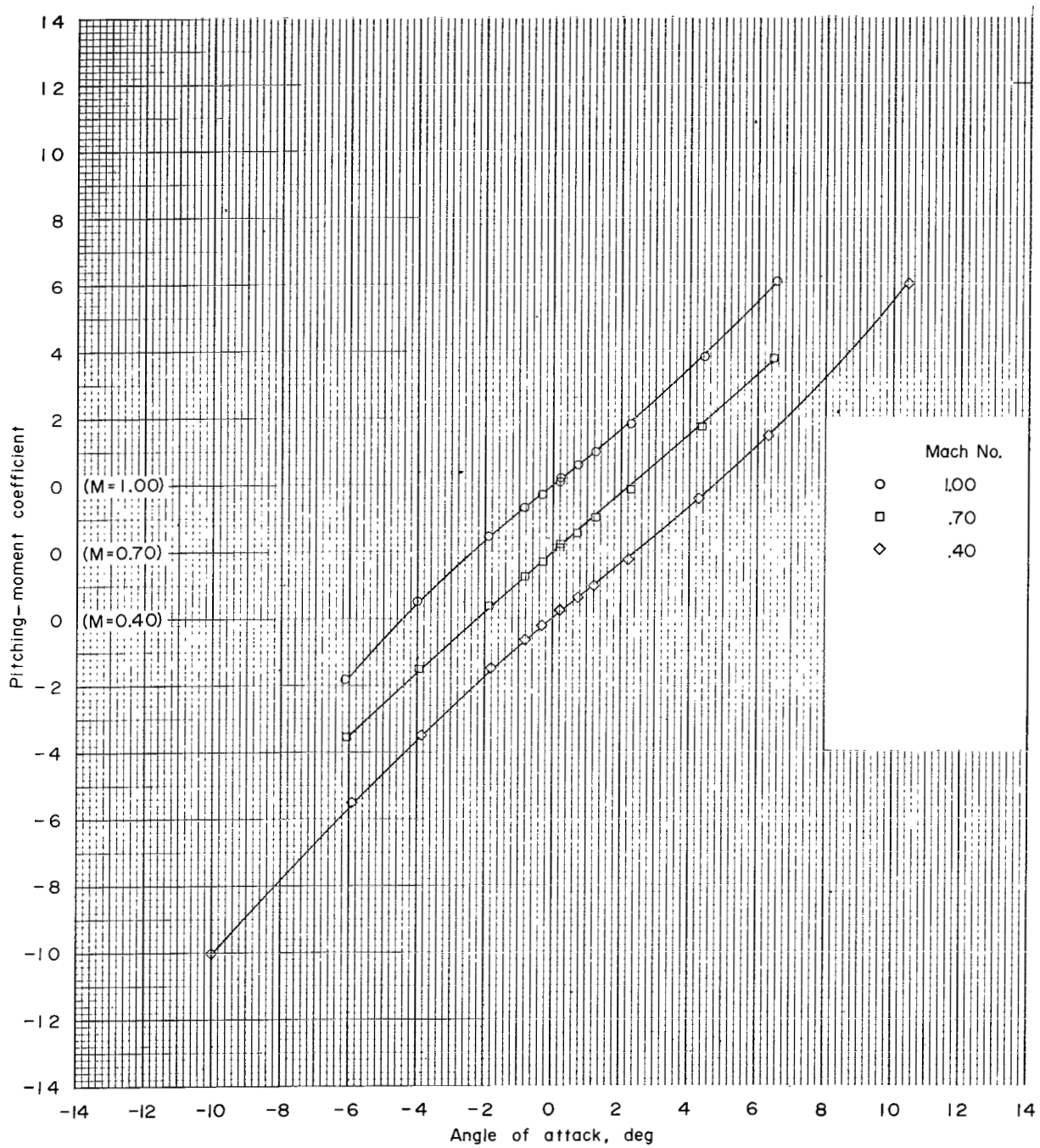

(i-1) Subsonic Mach numbers; configuration 7; $\phi = 180^{o}$.

Figure 8.- Continued.

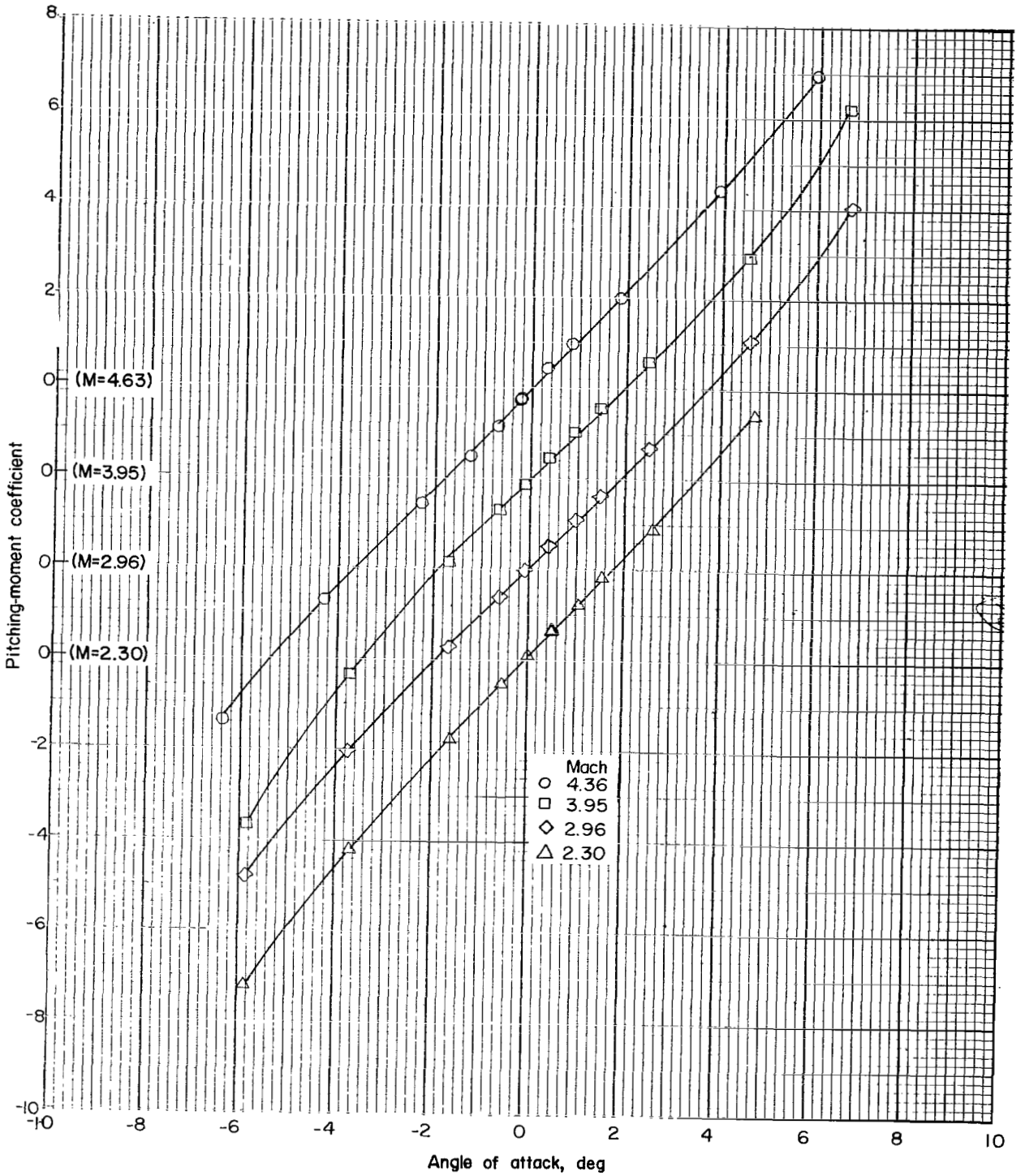

(i-2) Supersonic Mach numbers; configuration 7; $\phi = 180^{o}$.

Figure 8.- Concluded.

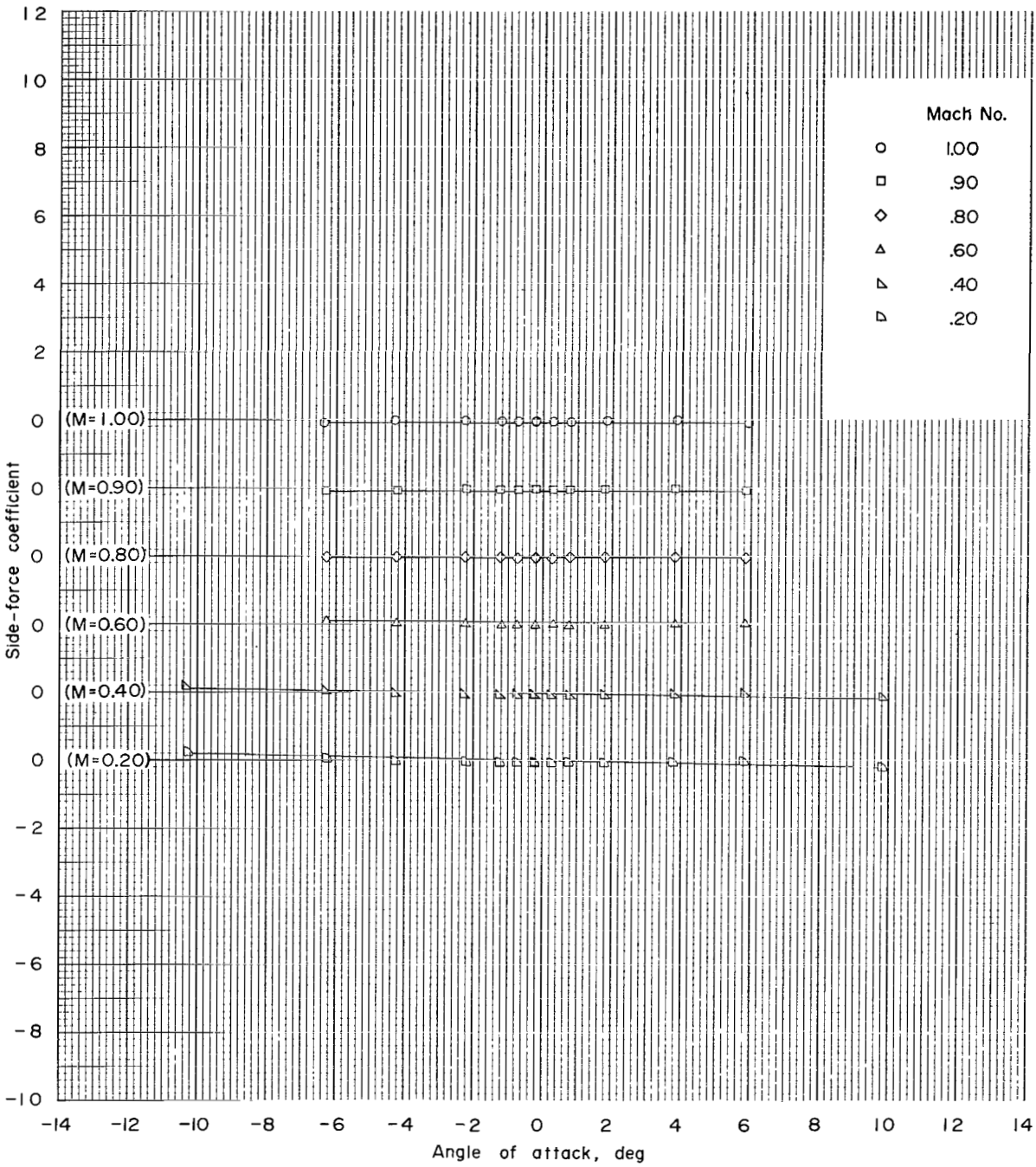

(a-1) Subsonic Mach numbers; configuration 1; $\phi = 0^{o}$.

Figure 9.- Side-force coefficient as function of angle of attack, roll angle, and Mach number.

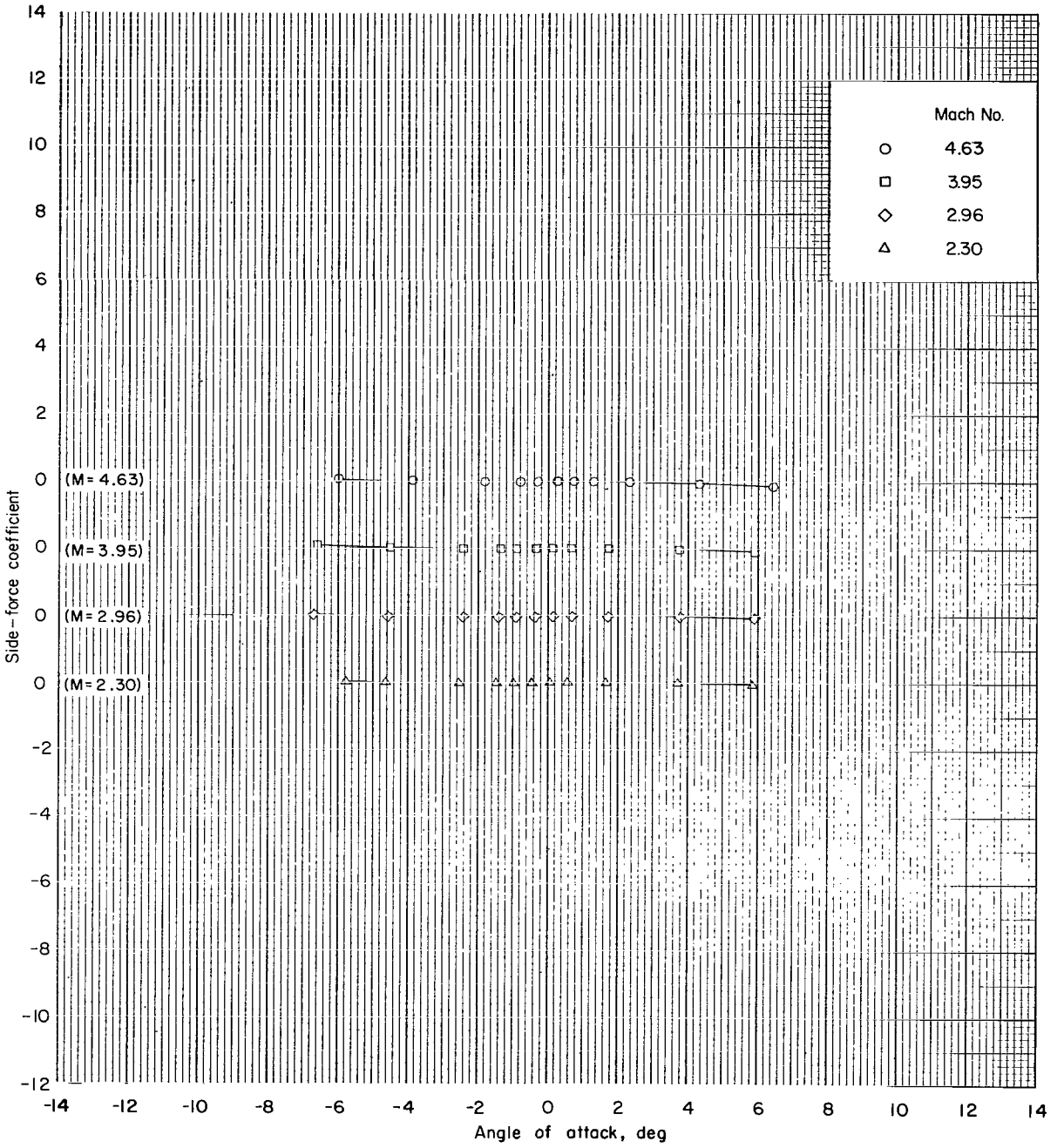

(a-2) Supersonic Mach numbers; configuration 1; $\phi = 0^{o}$.

Figure 9.- Continued.

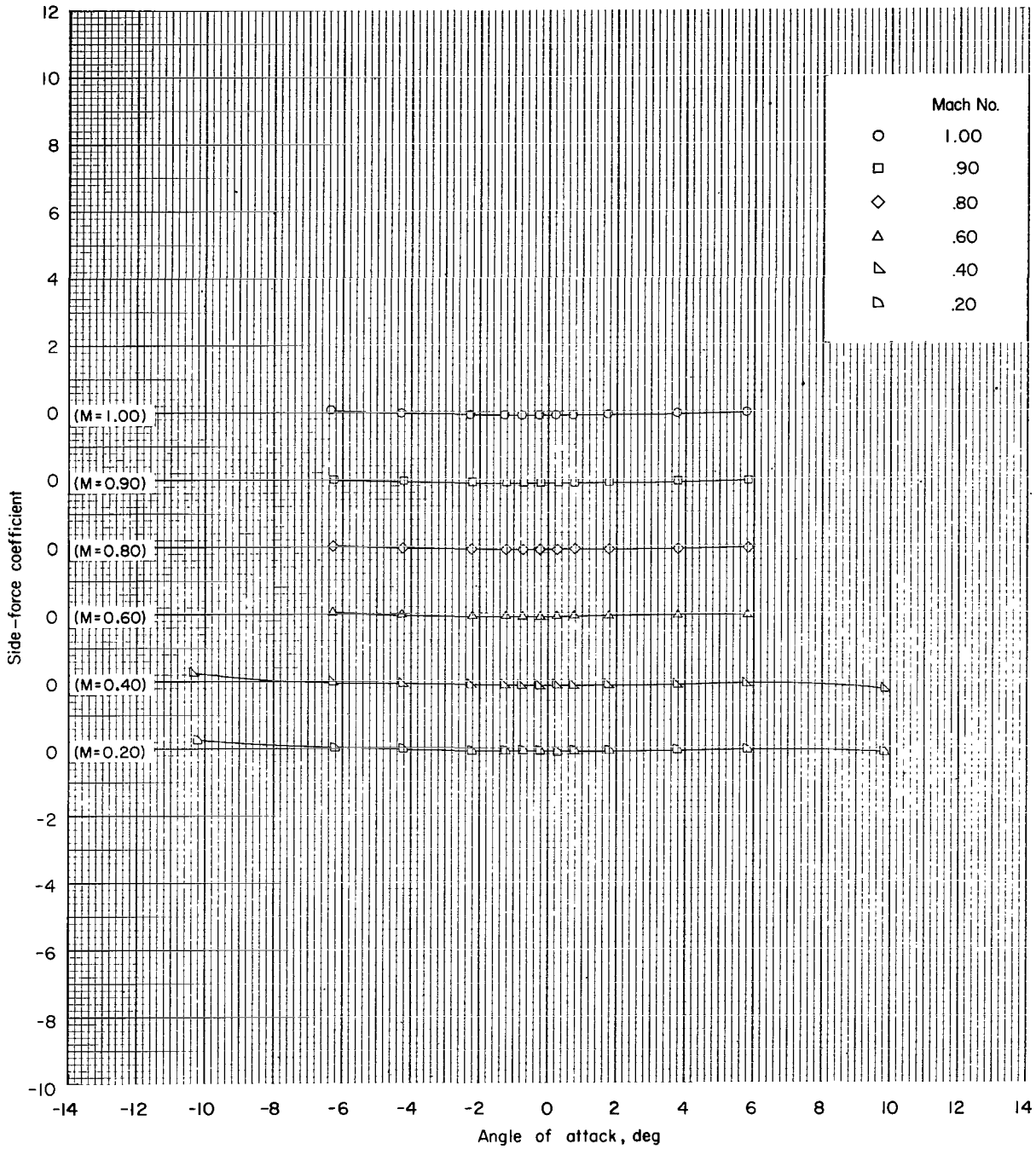

(b-1) Subsonic Mach numbers; configuration 2; $\phi = 0^{o}$.

Figure 9.- Continued.

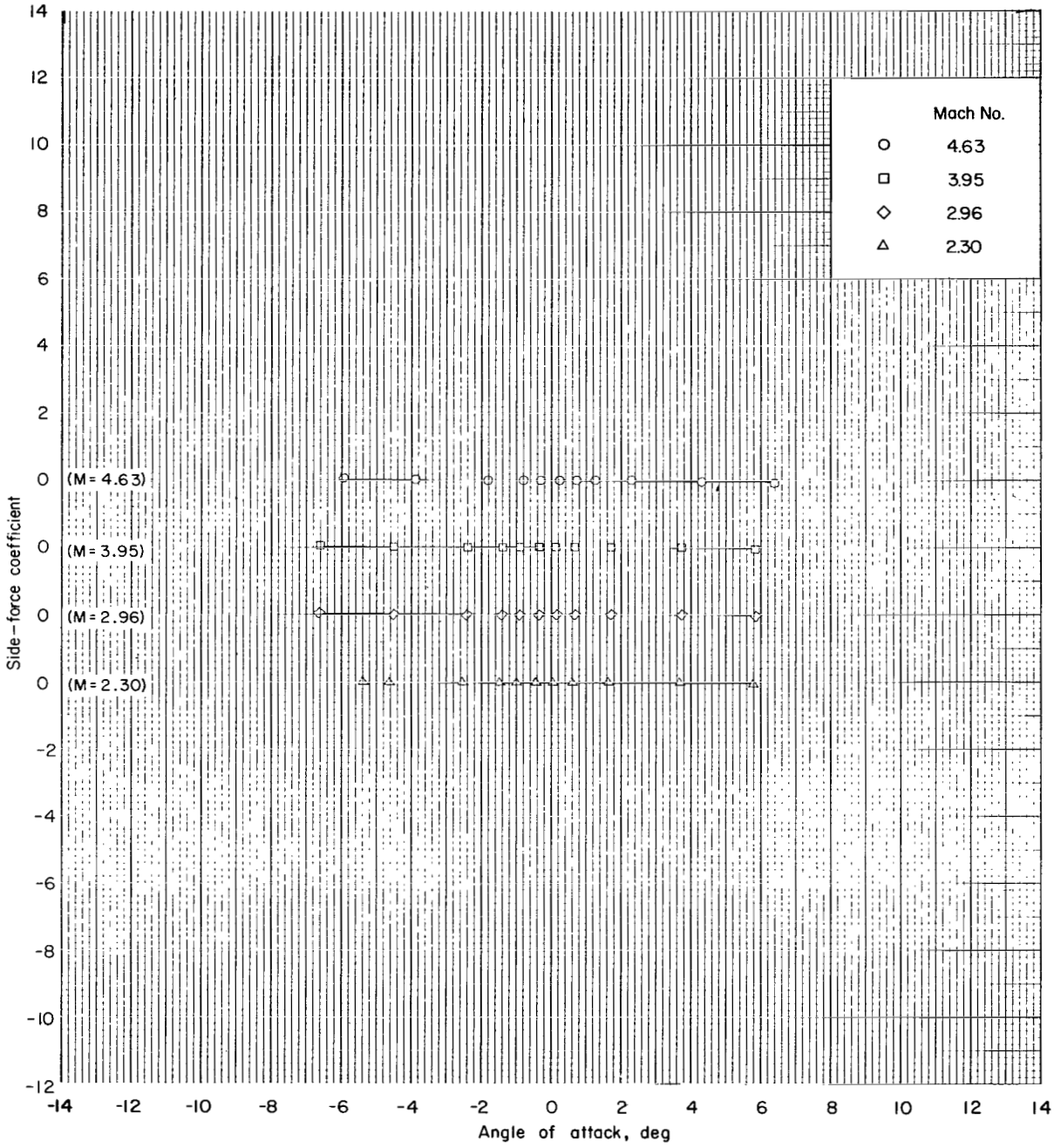

(b-2) Supersonic Mach numbers; configuration 2; $\phi = 0^{o}$.

Figure 9.- Continued.

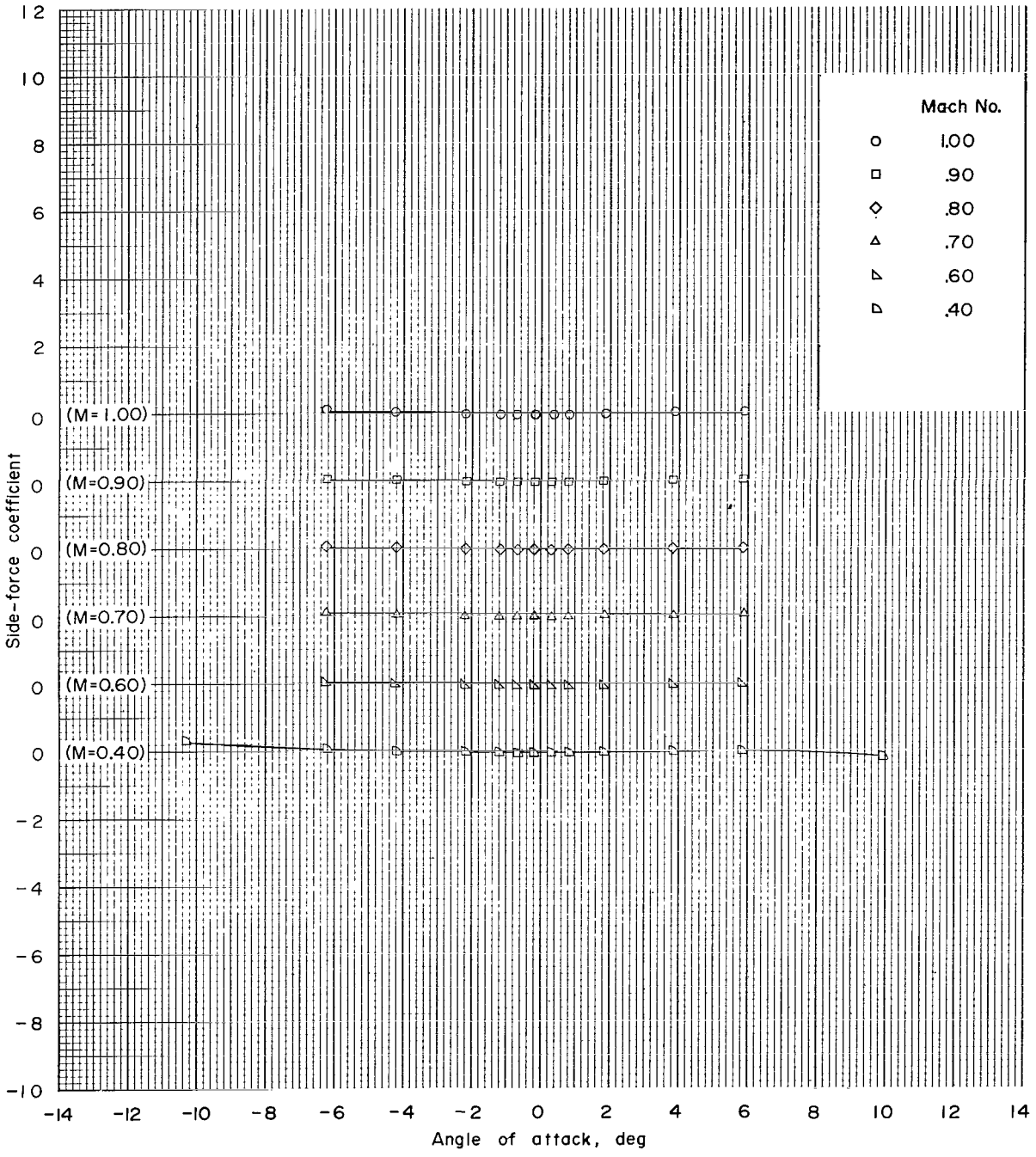

(c-1) Subsonic Mach numbers; configuration 3; $\phi = 0^{o}$.

Figure 9.- Continued.

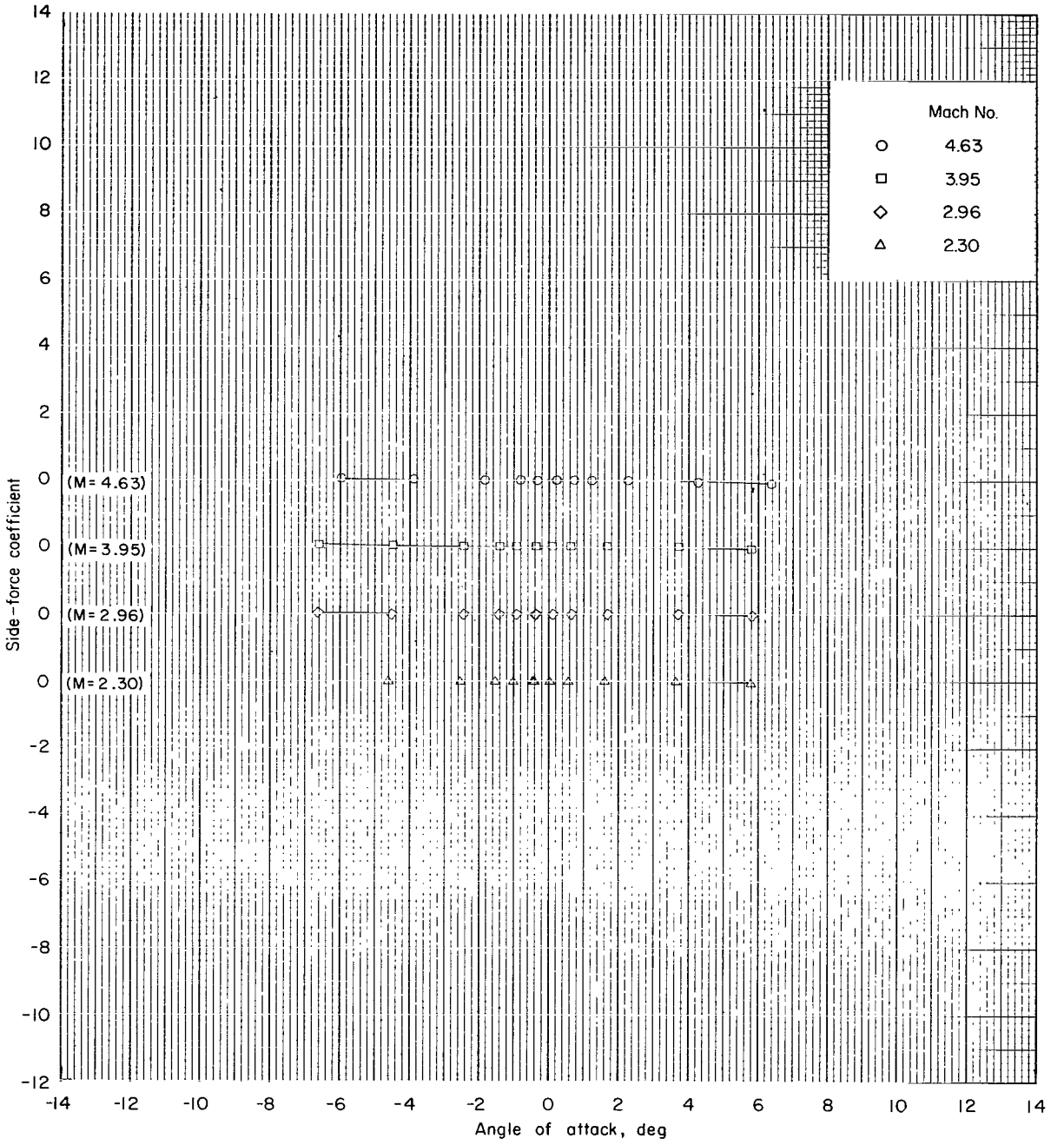

(c-2) Supersonic Mach numbers; configuration 3; $\phi = 0^{o}$.

Figure 9.- Continued.

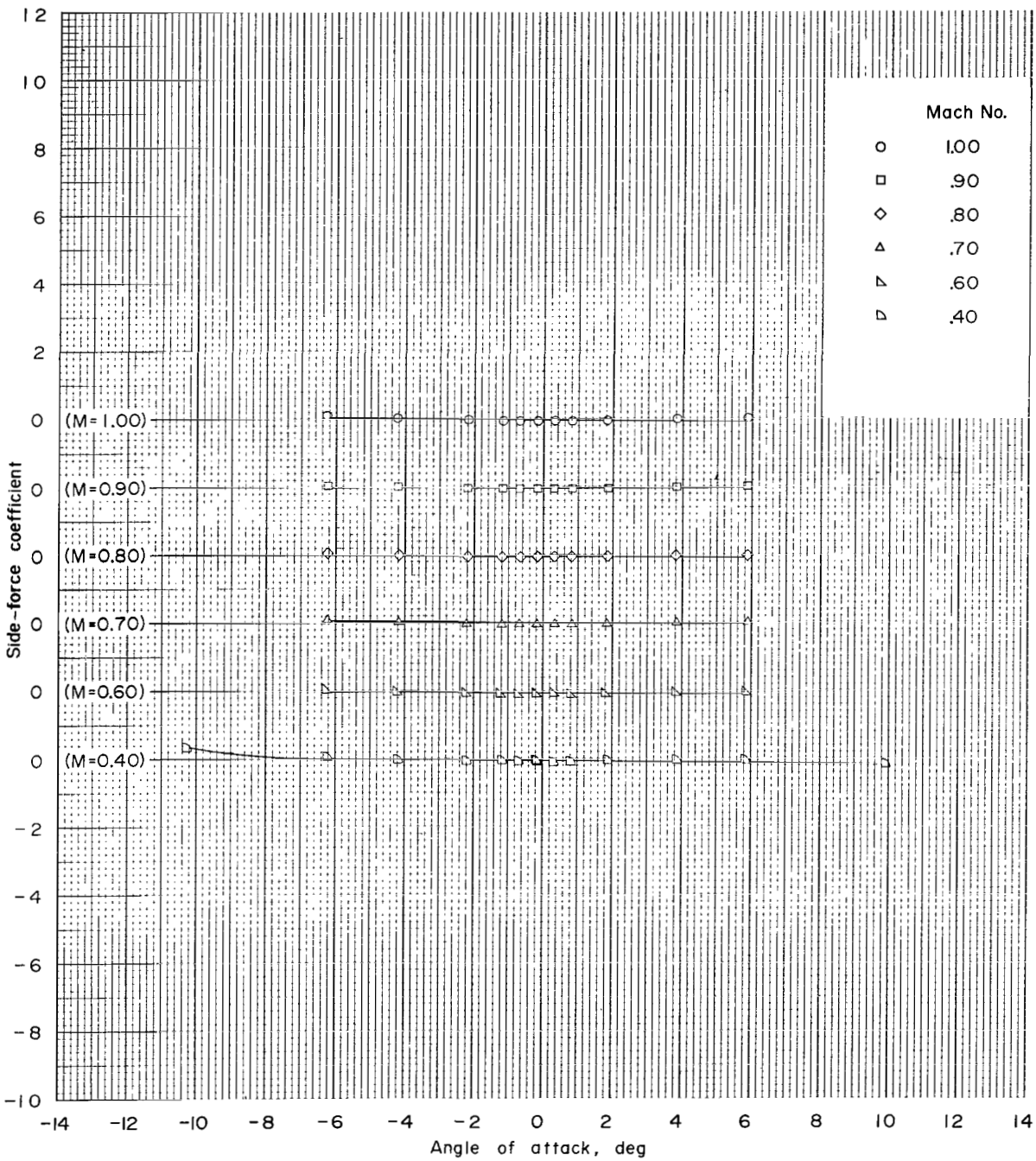

(d-1) Subsonic Mach numbers; configuration 4; $\phi = 0^{o}$.

Figure 9.- Continued.

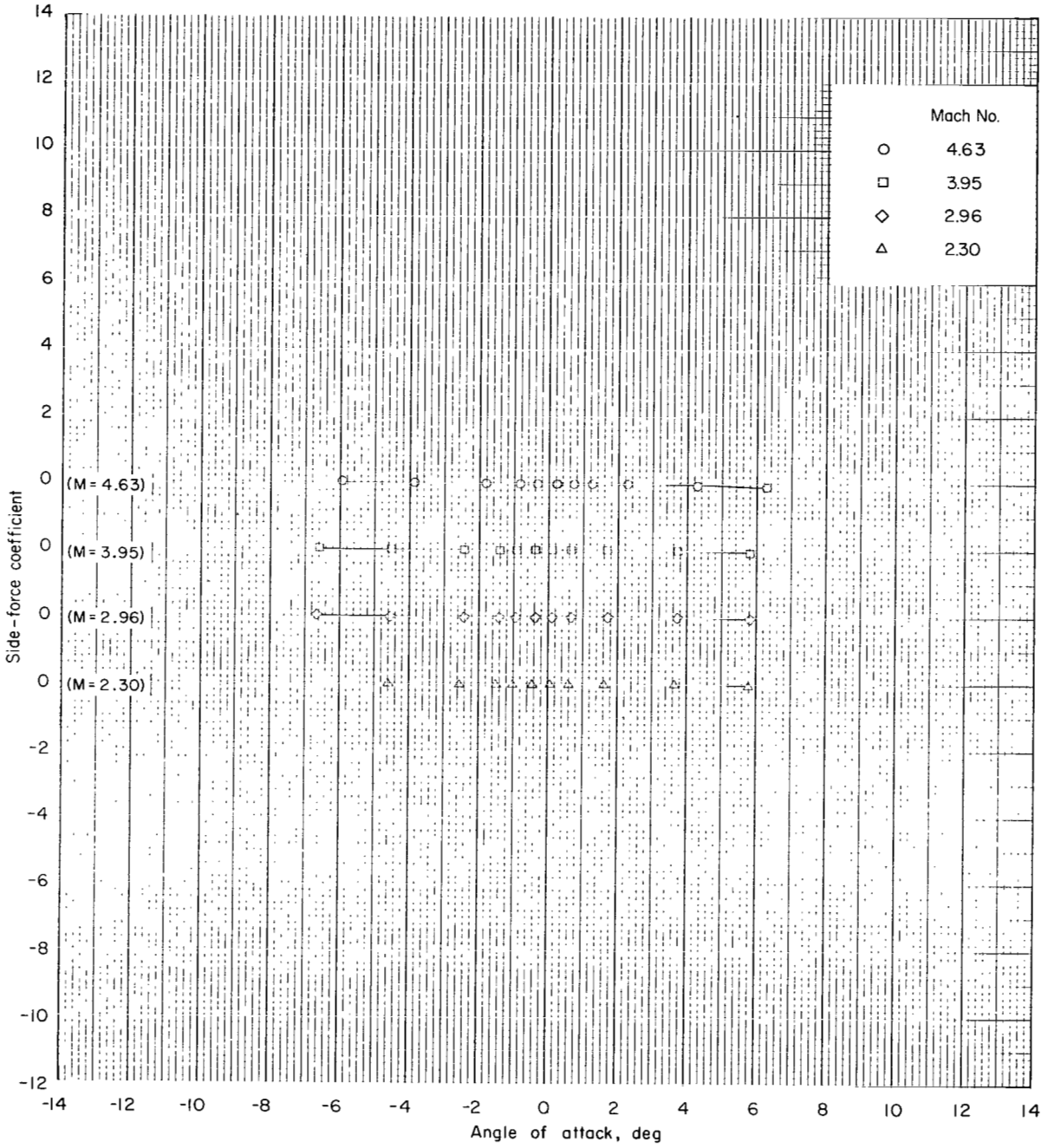

(d-2) Supersonic Mach numbers; configuration 4; $\phi = 0^{o}$.

Figure 9.- Continued.

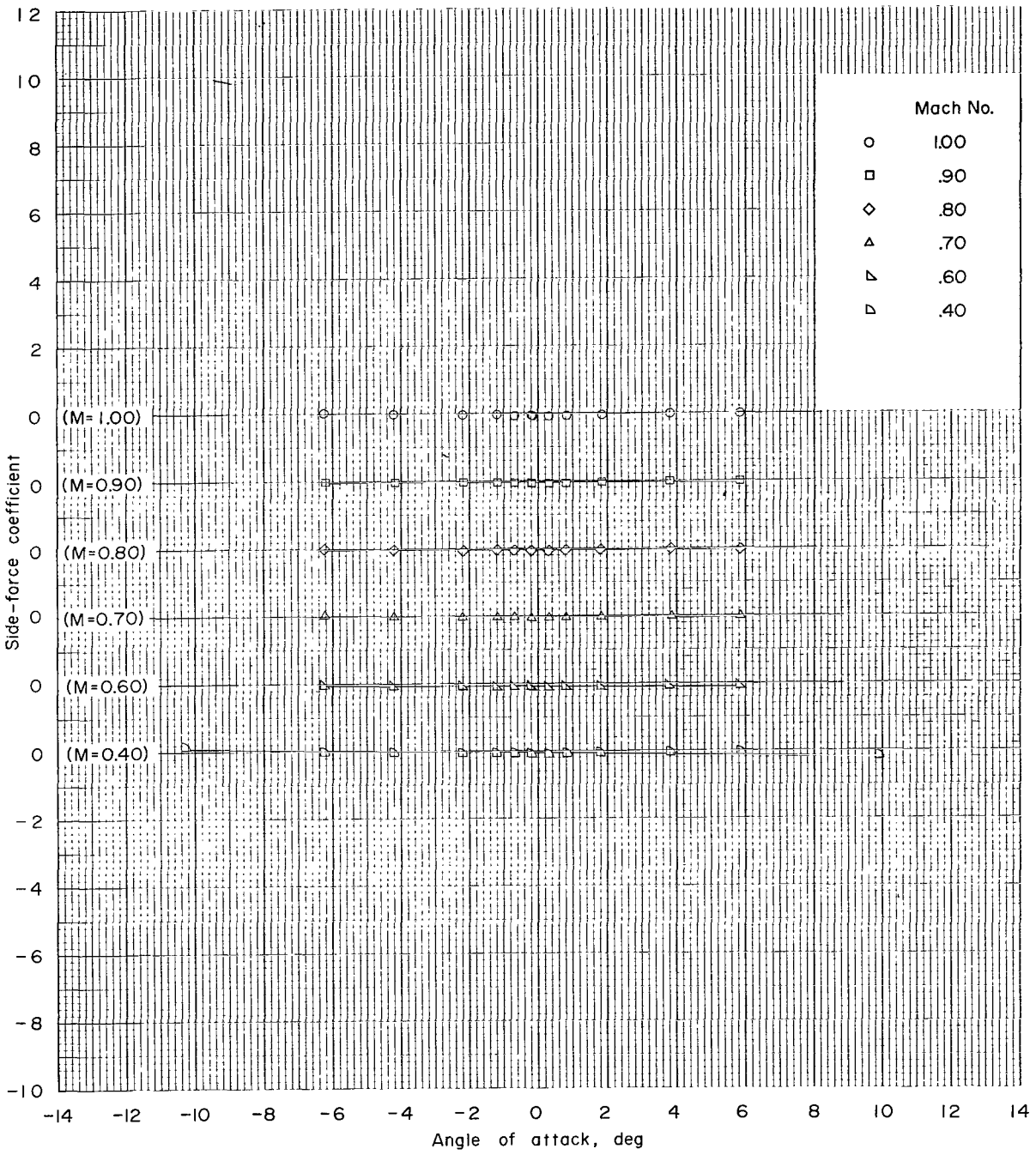

(e-1) Subsonic Mach numbers; configuration 5; $\phi = 0^{o}$.

Figure 9.- Continued.

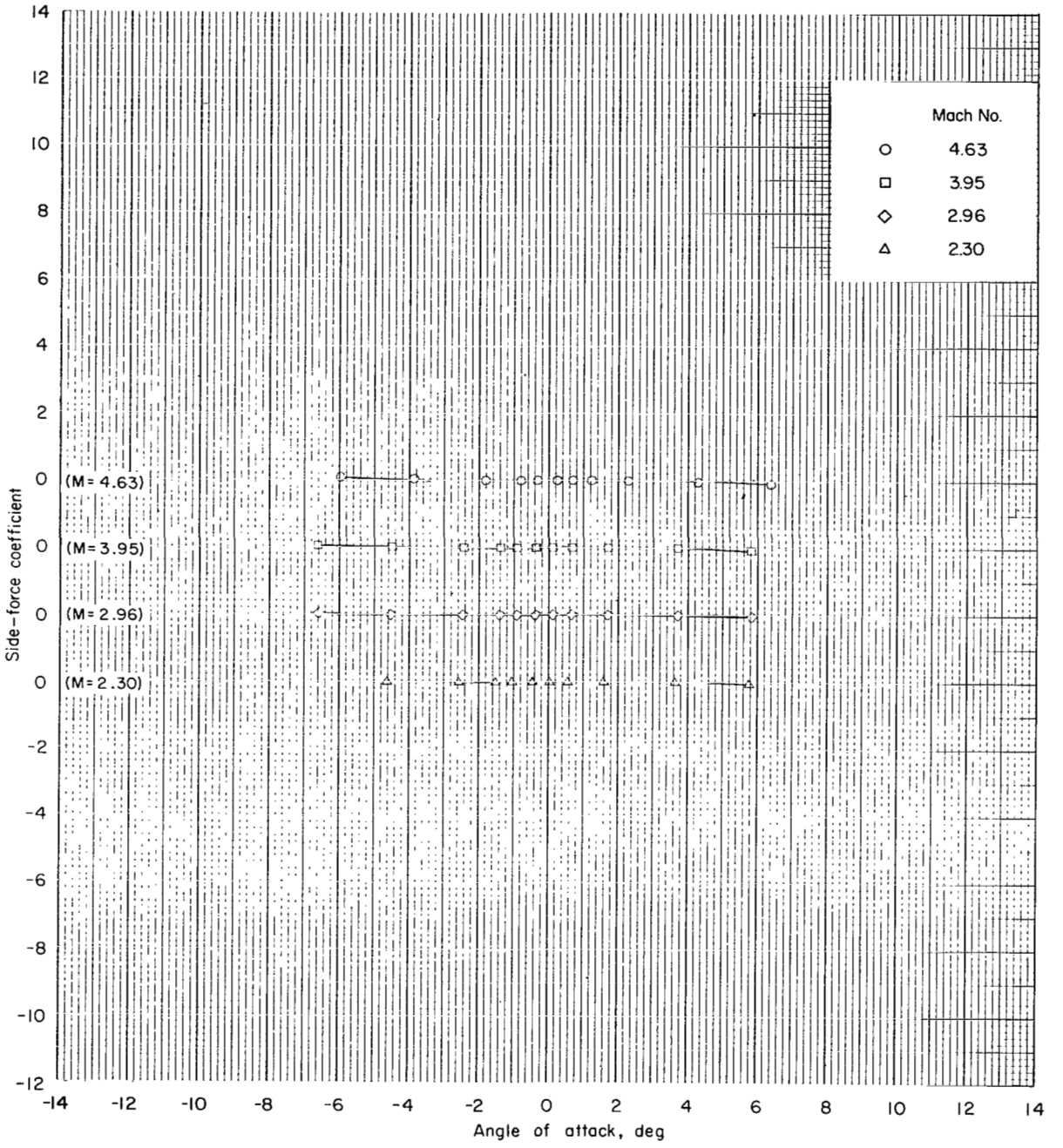

(e-2) Supersonic Mach numbers; configuration 5; $\phi = 0^{o}$.

Figure 9.- Continued.

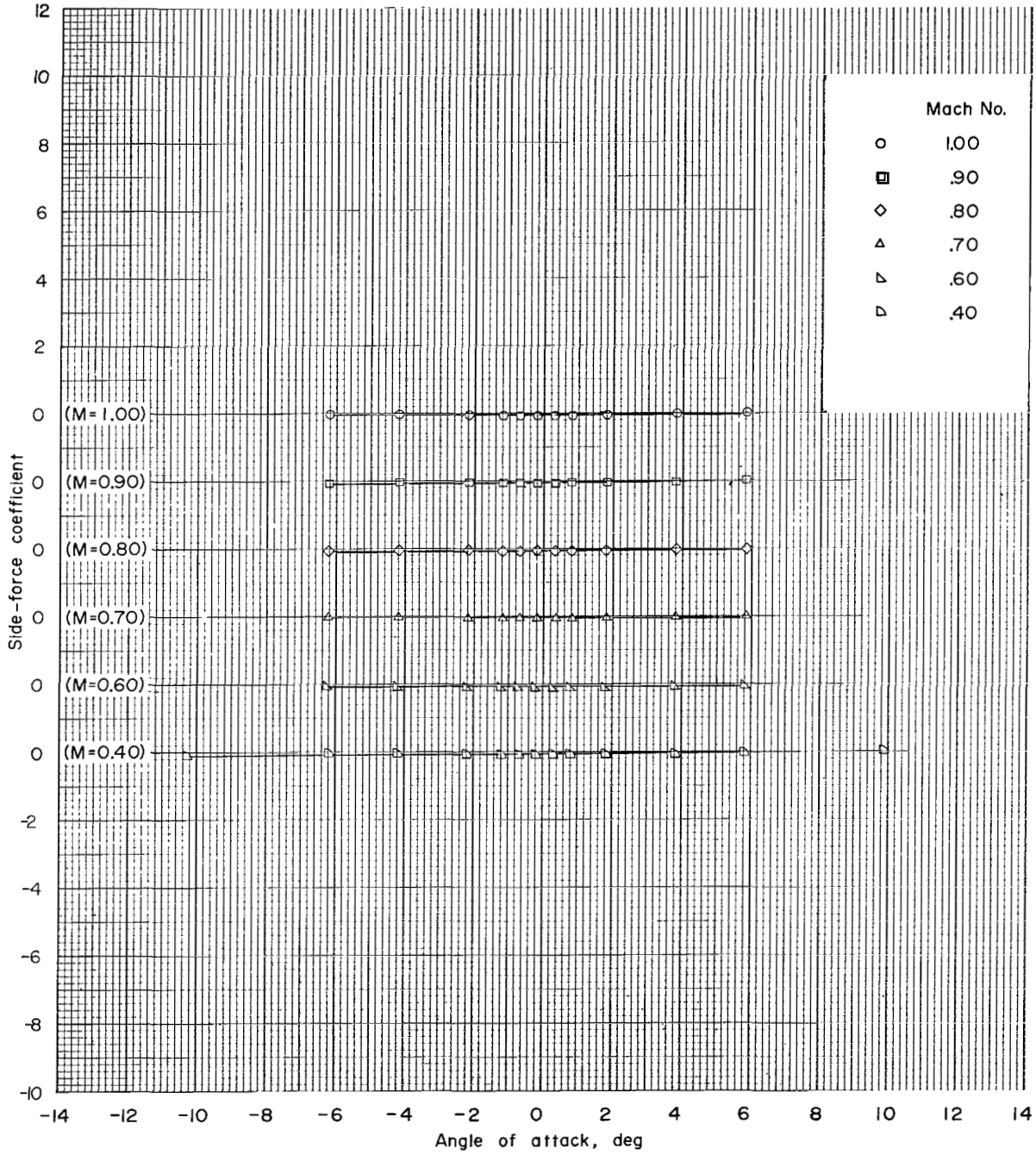

(f-1) Subsonic Mach numbers; configuration 6; $\phi = 0^{o}$.

Figure 9.- Continued.

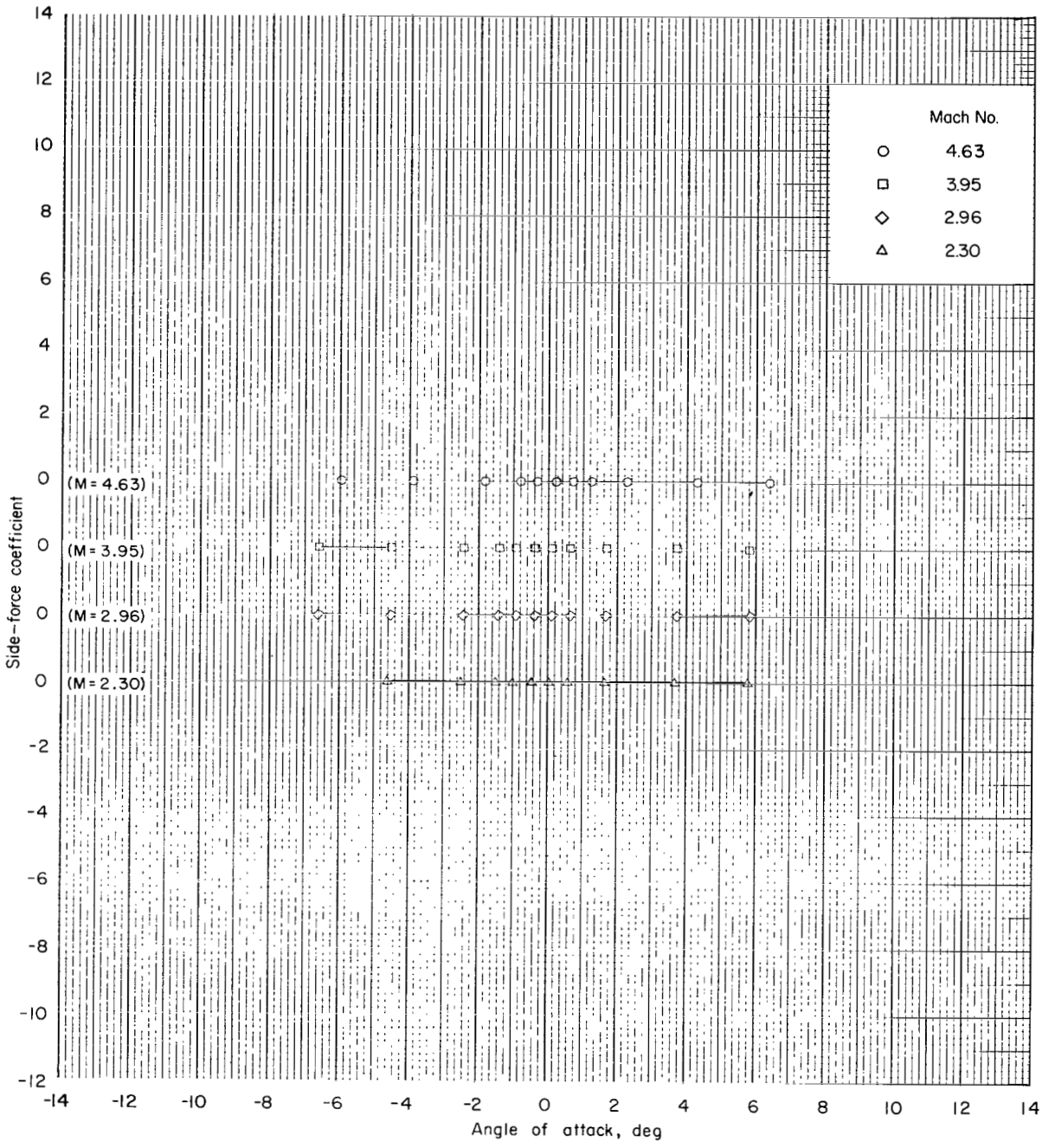

(f-2) Supersonic Mach numbers; configuration 6; $\phi = 0^{o}$.

Figure 9.- Continued.

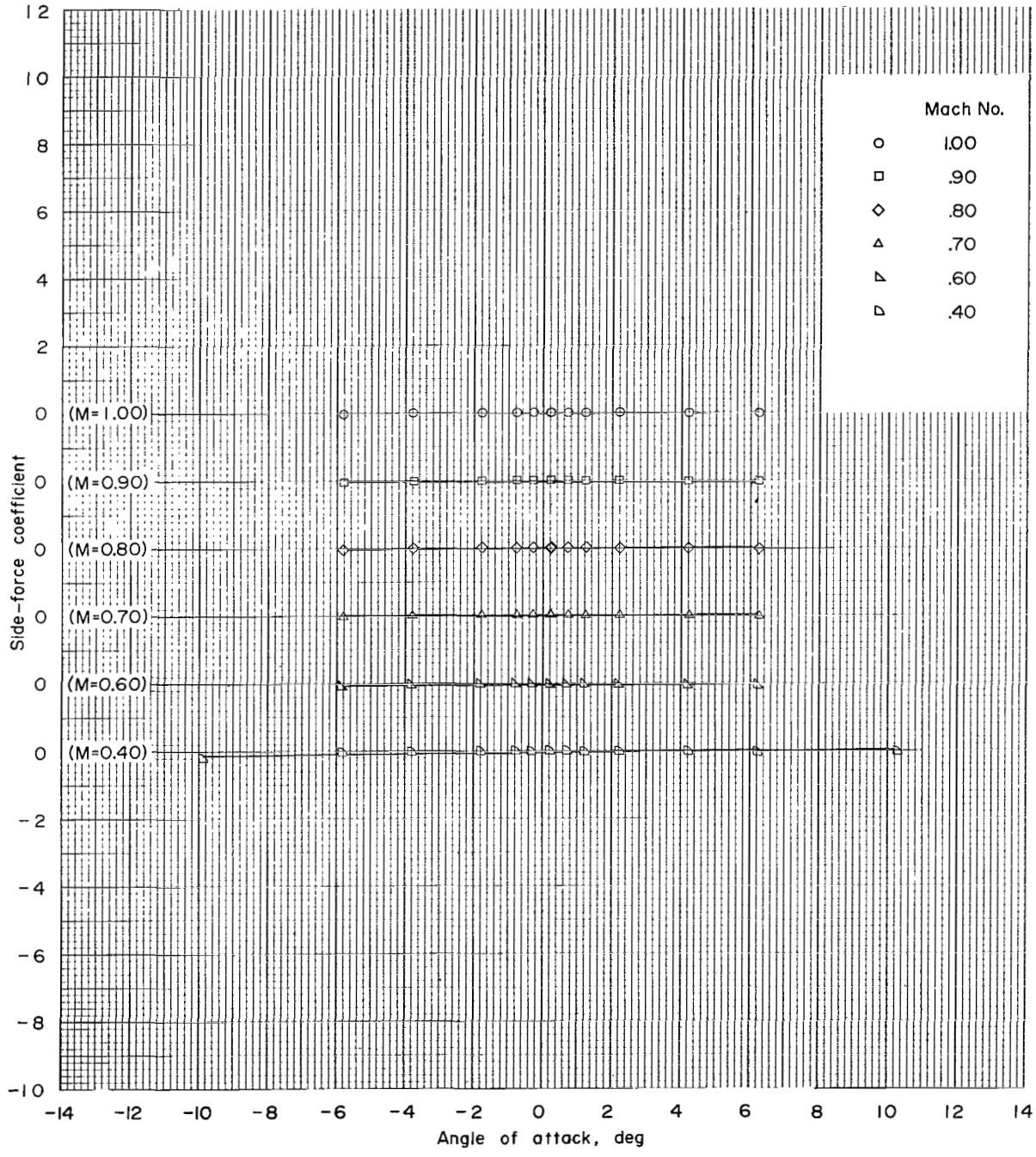

(g-1) Subsonic Mach numbers; configuration 6; $\phi = 180^{o}$.

Figure 9.- Continued.

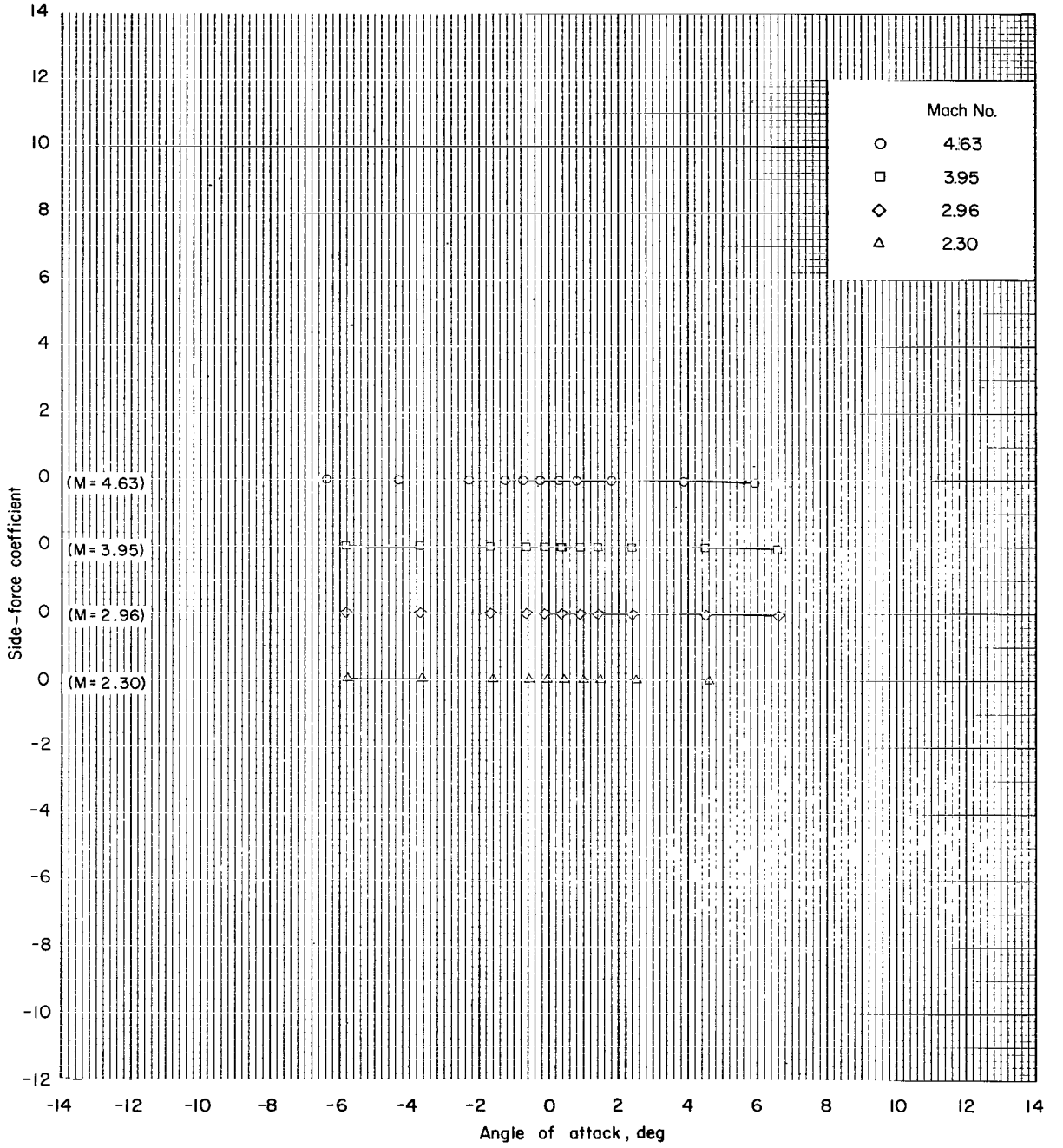

(g-2) Supersonic Mach numbers; configuration 6; $\phi = 180^{o}$.

Figure 9.- Continued.

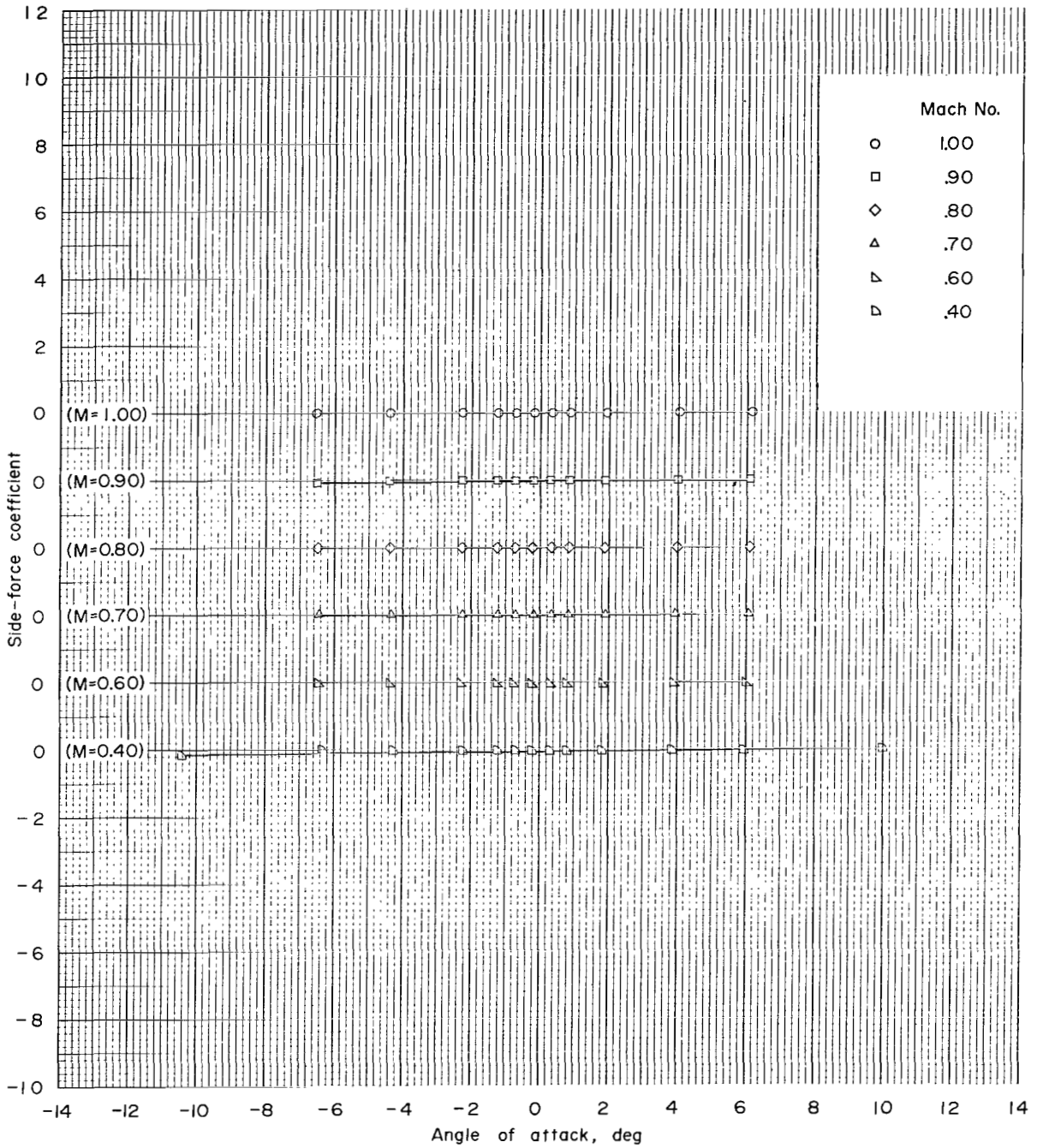

(h-1) Subsonic Mach numbers; configuration 7; $\phi = 0^{o}$.

Figure 9.- Continued.

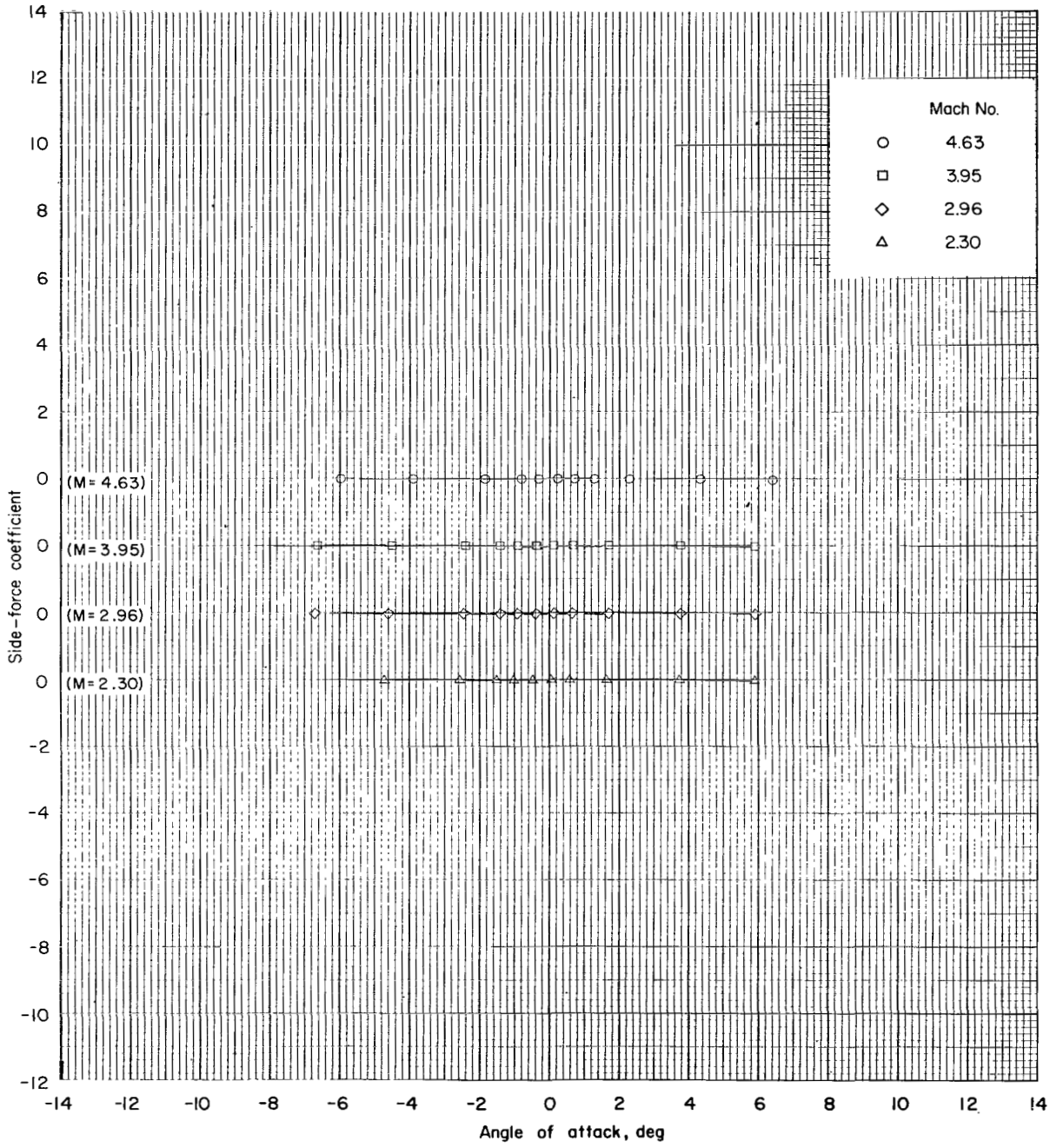

(h-2) Supersonic Mach numbers; configuration 7; $\phi = 0^{o}$.

Figure 9.- Continued.

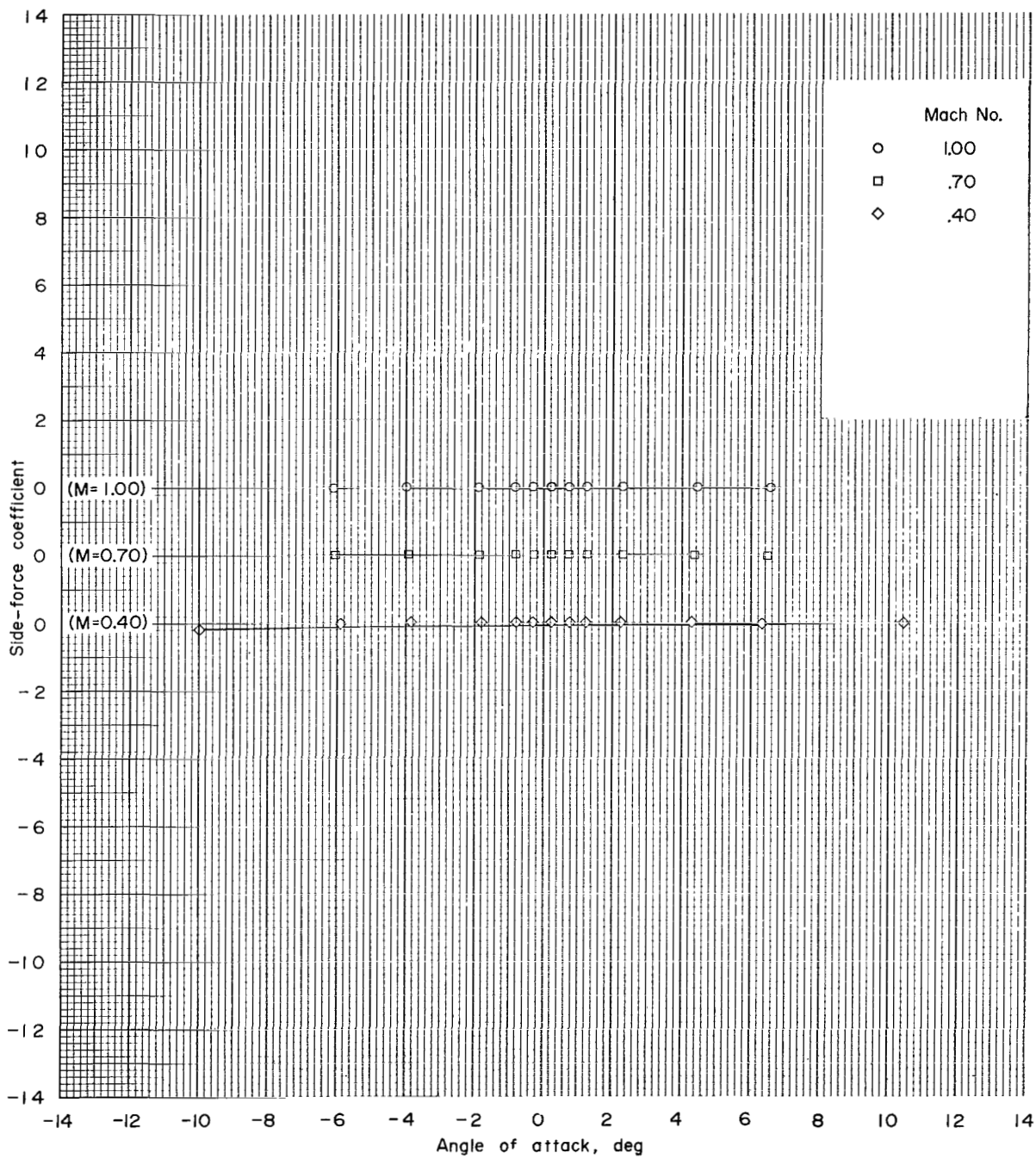

(i-1) Subsonic Mach numbers; configuration 7; $\phi = 180^{o}$.

Figure 9.- Continued.

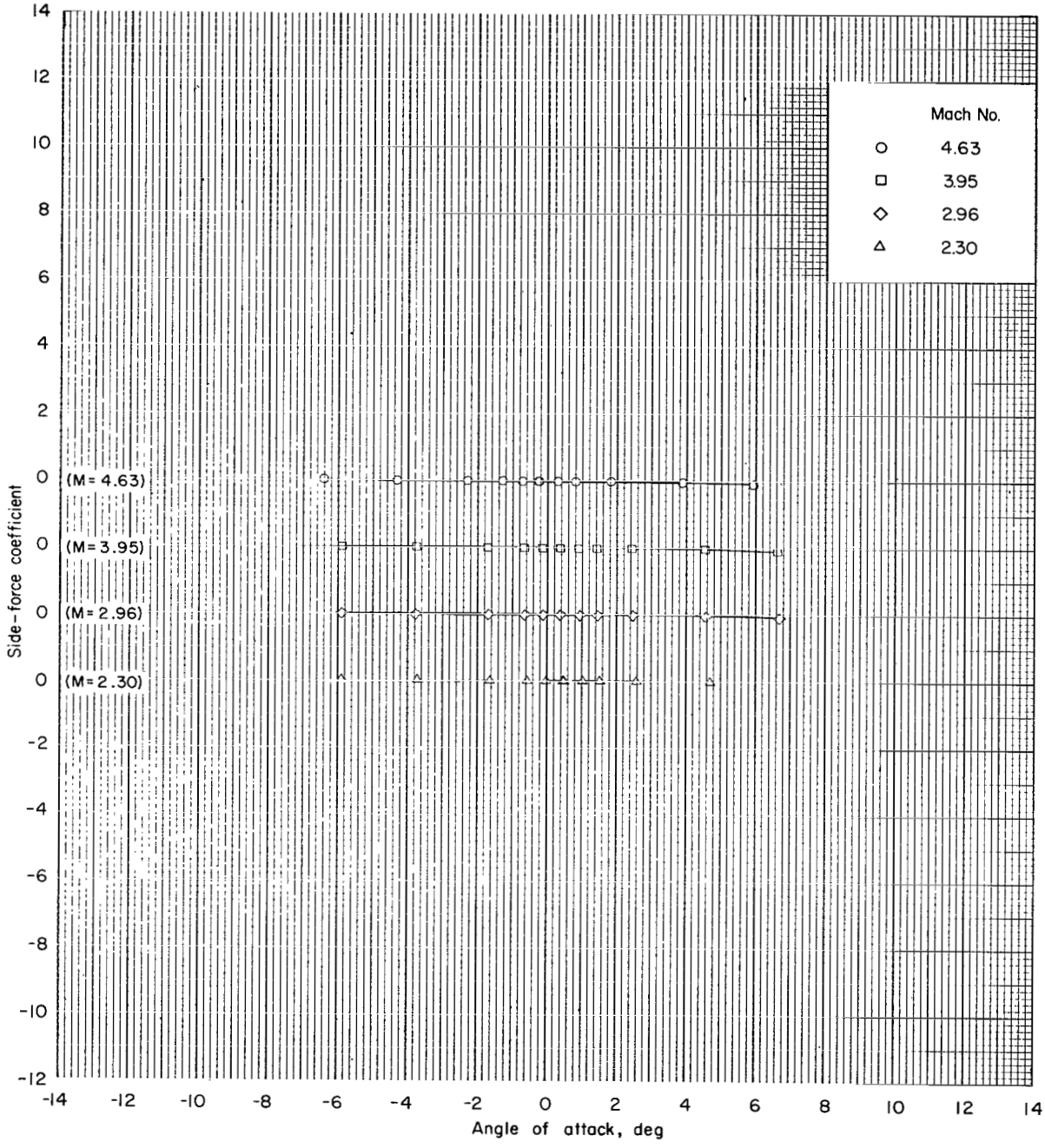

(i-2) Supersonic Mach numbers; configuration 7; $\phi = 180^{o}$.

Figure 9.- Concluded.

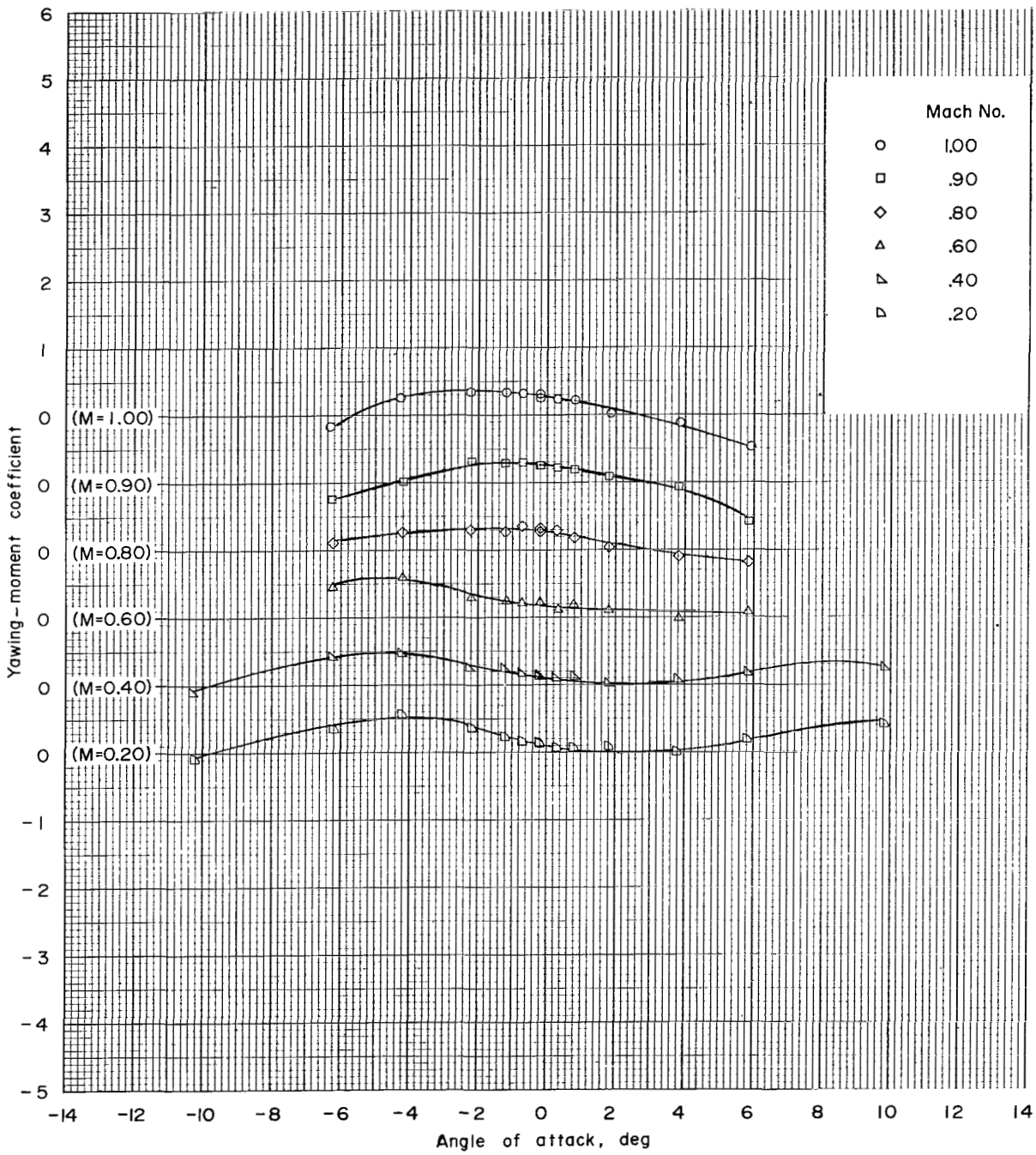

(a-1) Subsonic Mach numbers; configuration 1; $\phi = 0^{o}$.

Figure 10.- Yawing-moment coefficient as function of angle of attack, roll angle, and Mach number.

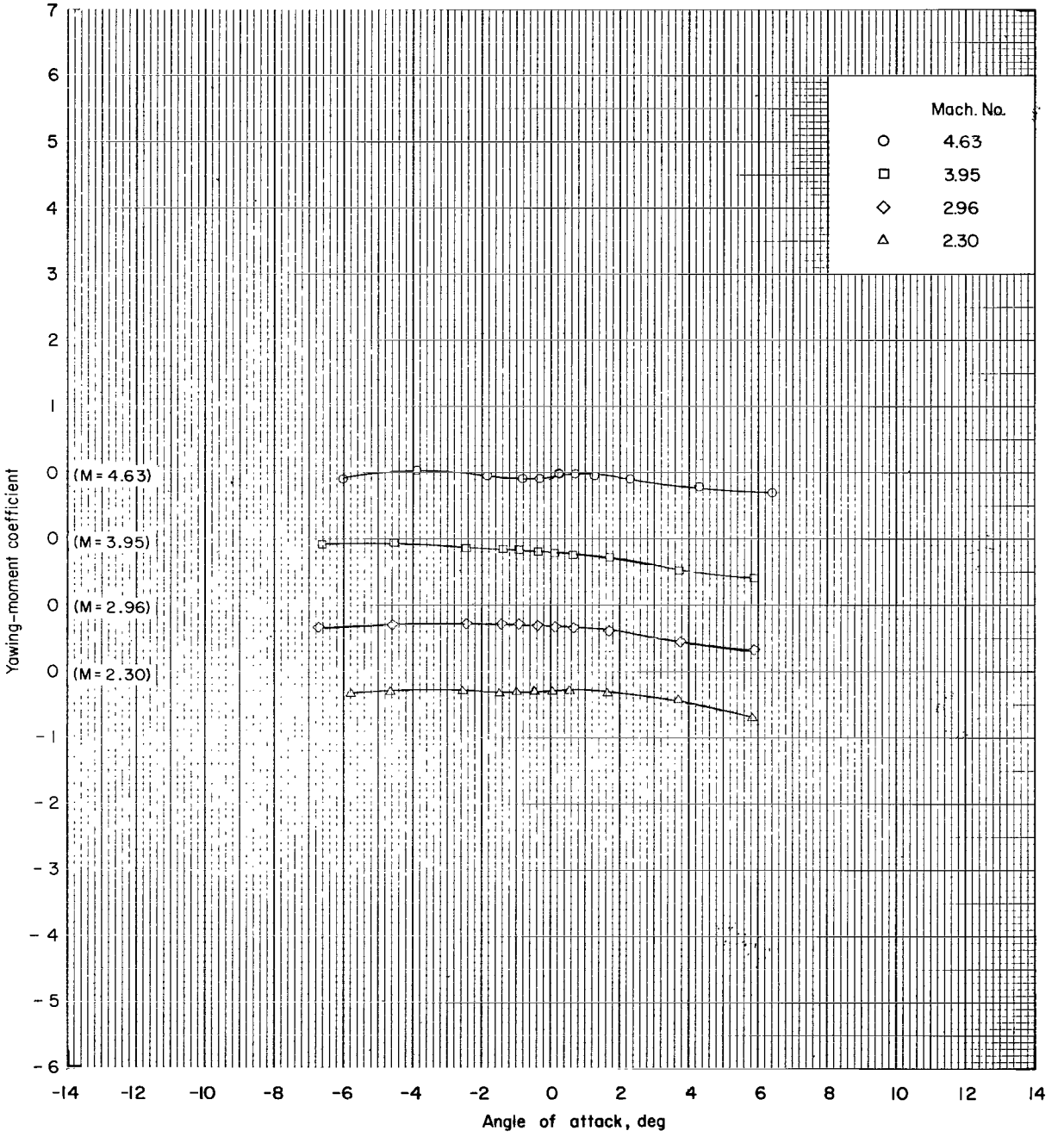

(a-2) Supersonic Mach numbers; configuration 1; $\phi = 0^{o}$.

Figure 10.- Continued.

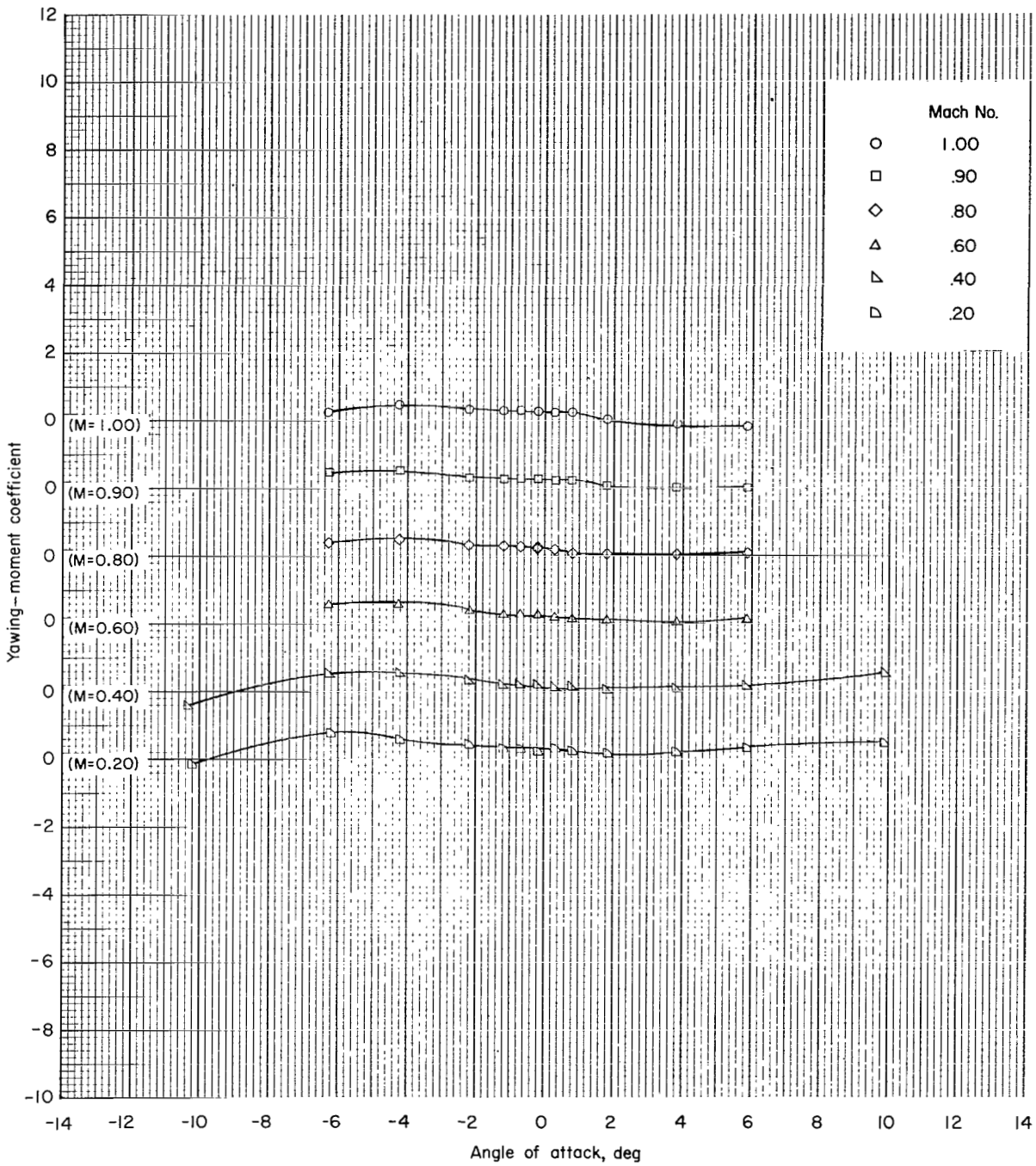

(b-1) Subsonic Mach numbers; configuration 2; $\phi = 0^{o}$.

Figure 10.- Continued.

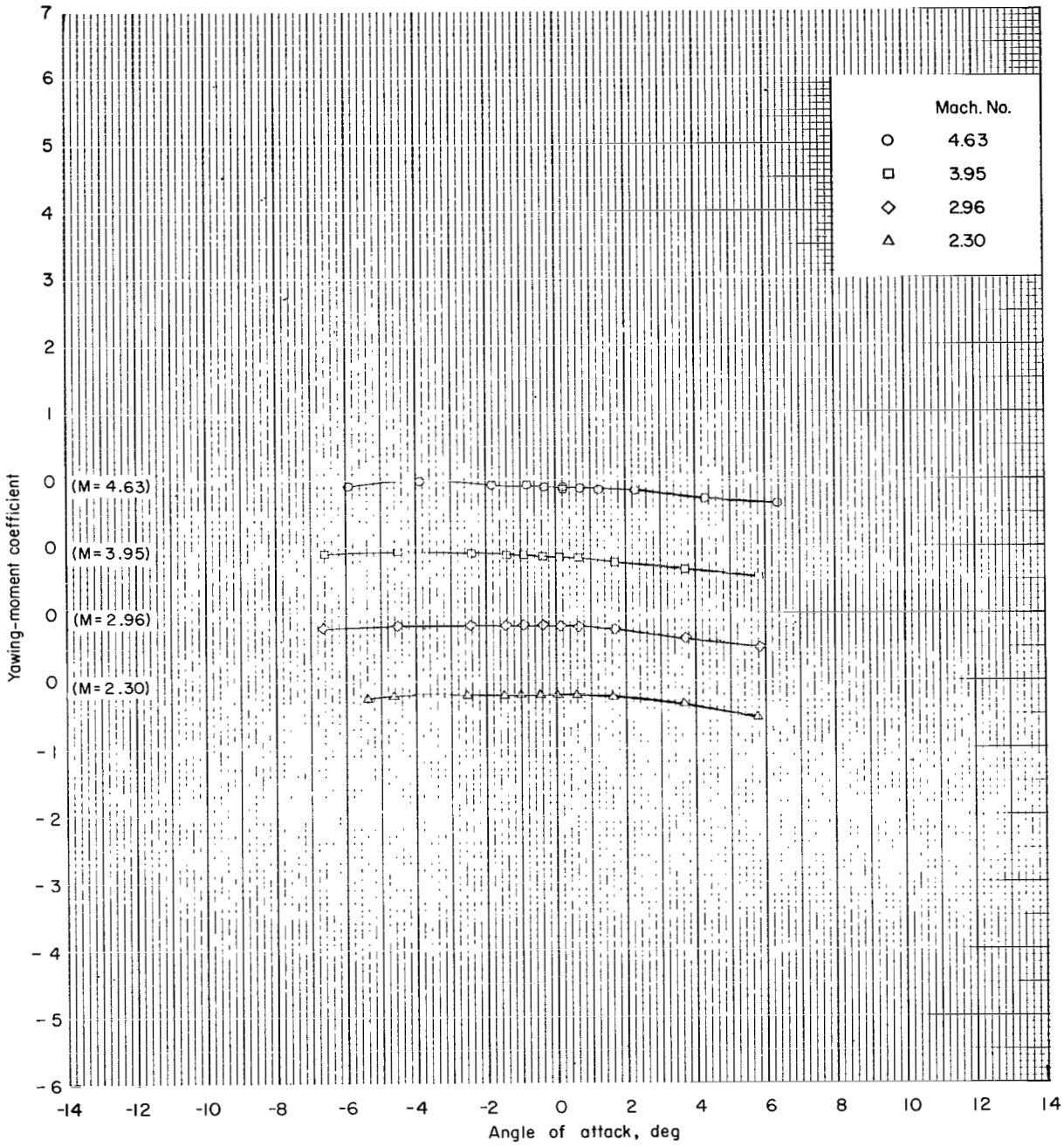

(b-2) Supersonic Mach numbers; configuration 2; $\phi = 0^{o}$.

Figure 10.- Continued.

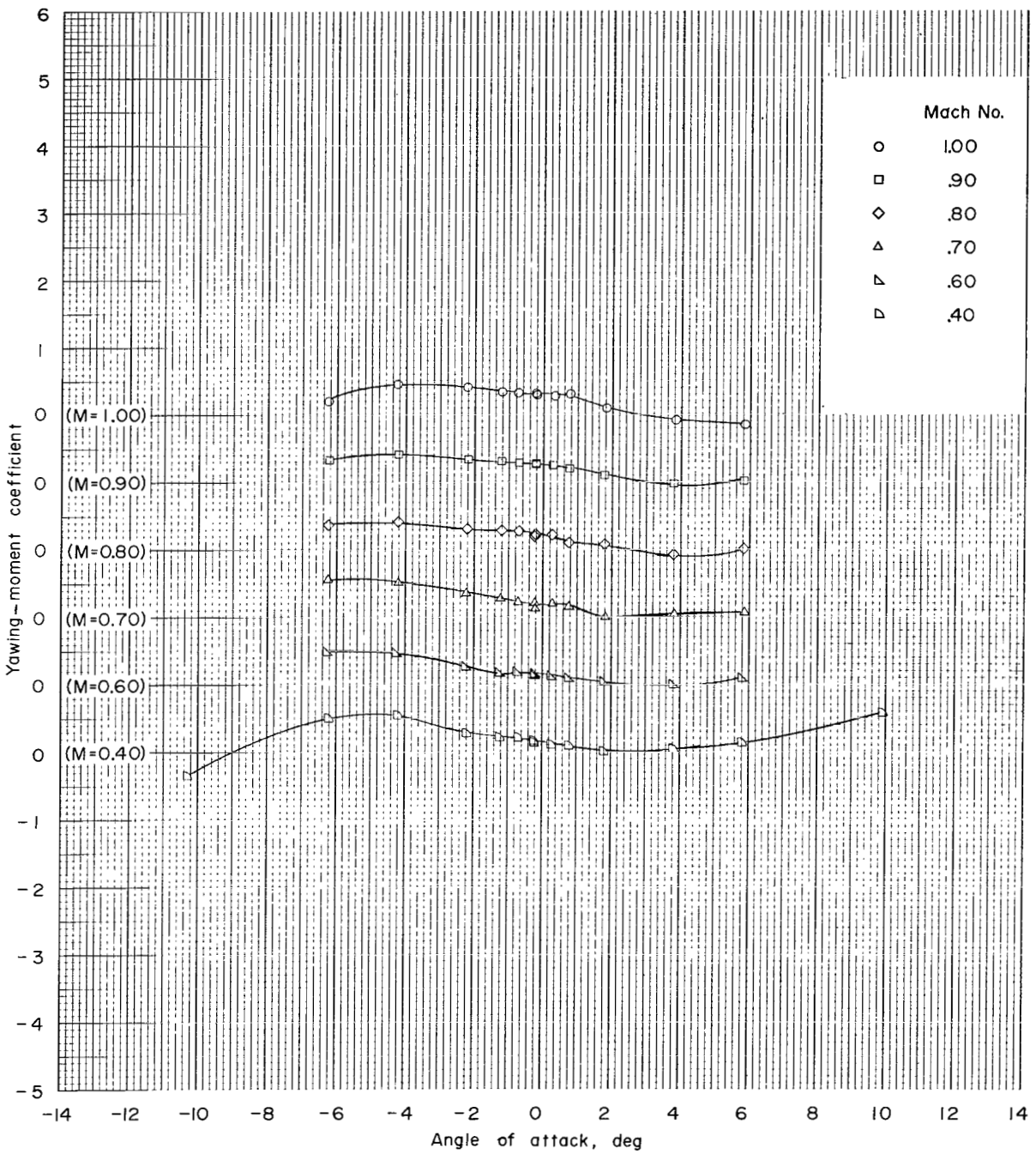

(c-1) Subsonic Mach numbers; configuration 3; $\phi = 0^{o}$.

Figure 10.- Continued.

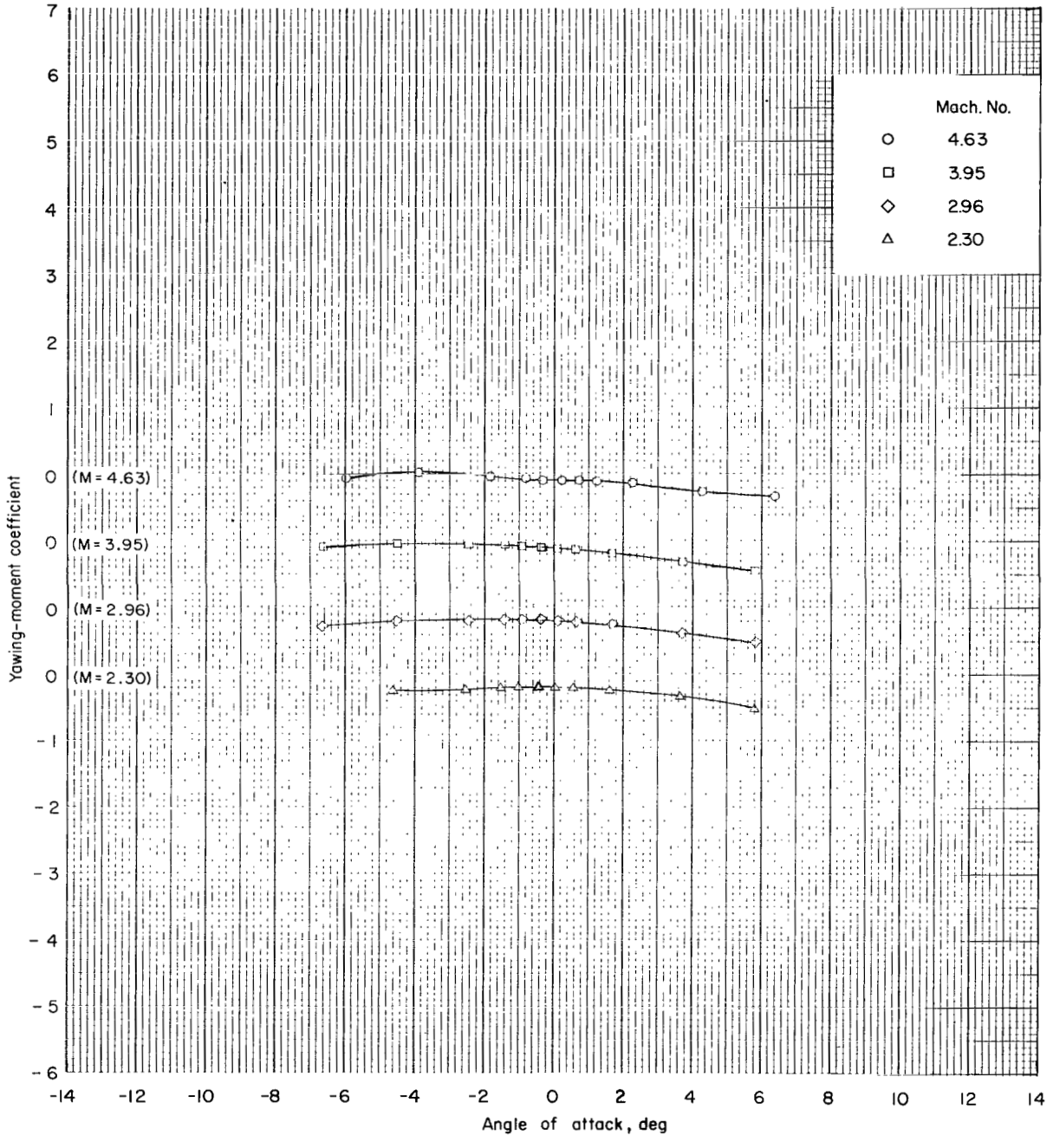

(c-2) Supersonic Mach numbers; configuration 3; $\phi = 0^{o}$.

Figure 10.- Continued.

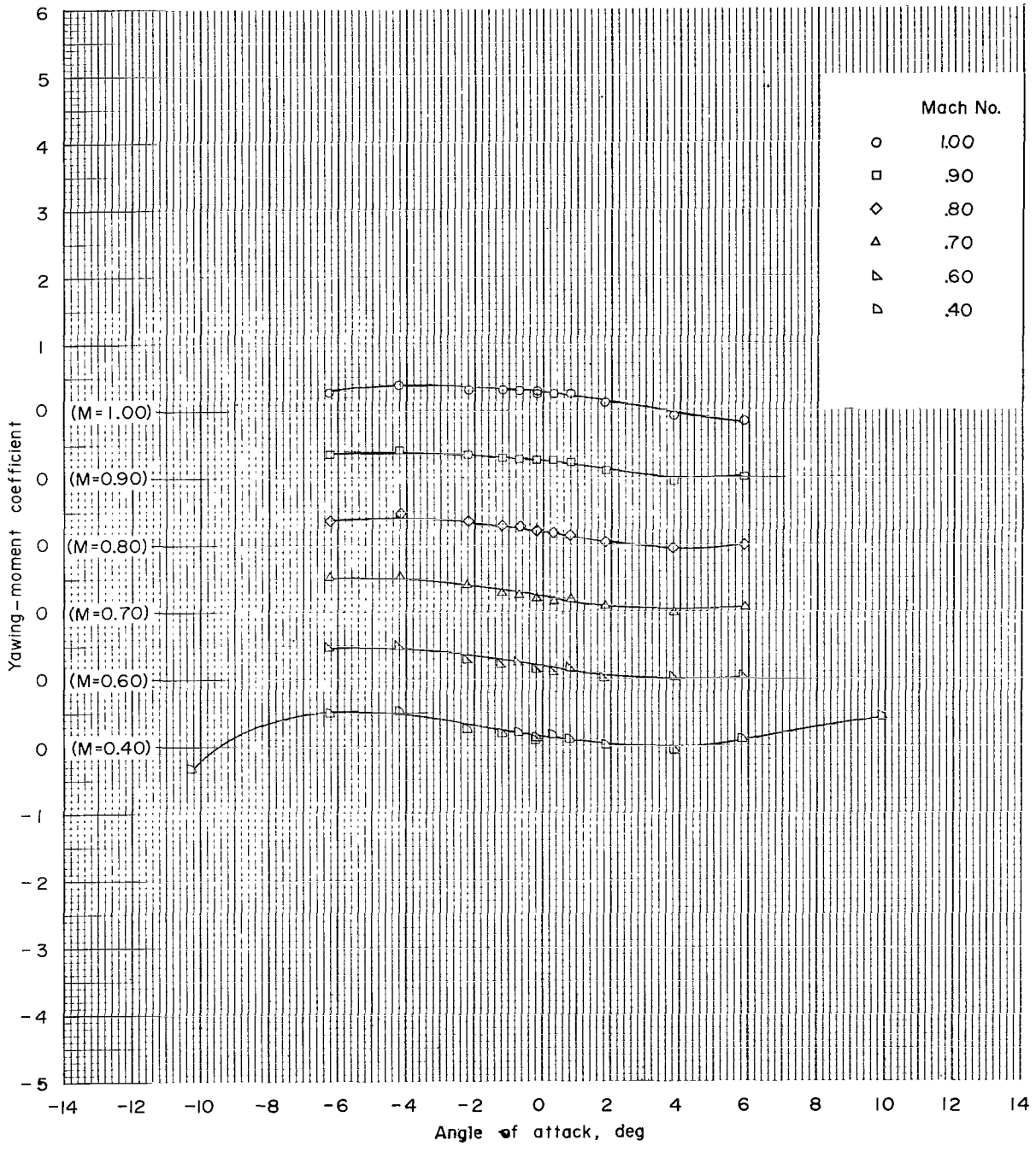

(d-1) Subsonic Mach numbers; configuration 4; $\phi = 0^{o}$.

Figure 10.- Continued.

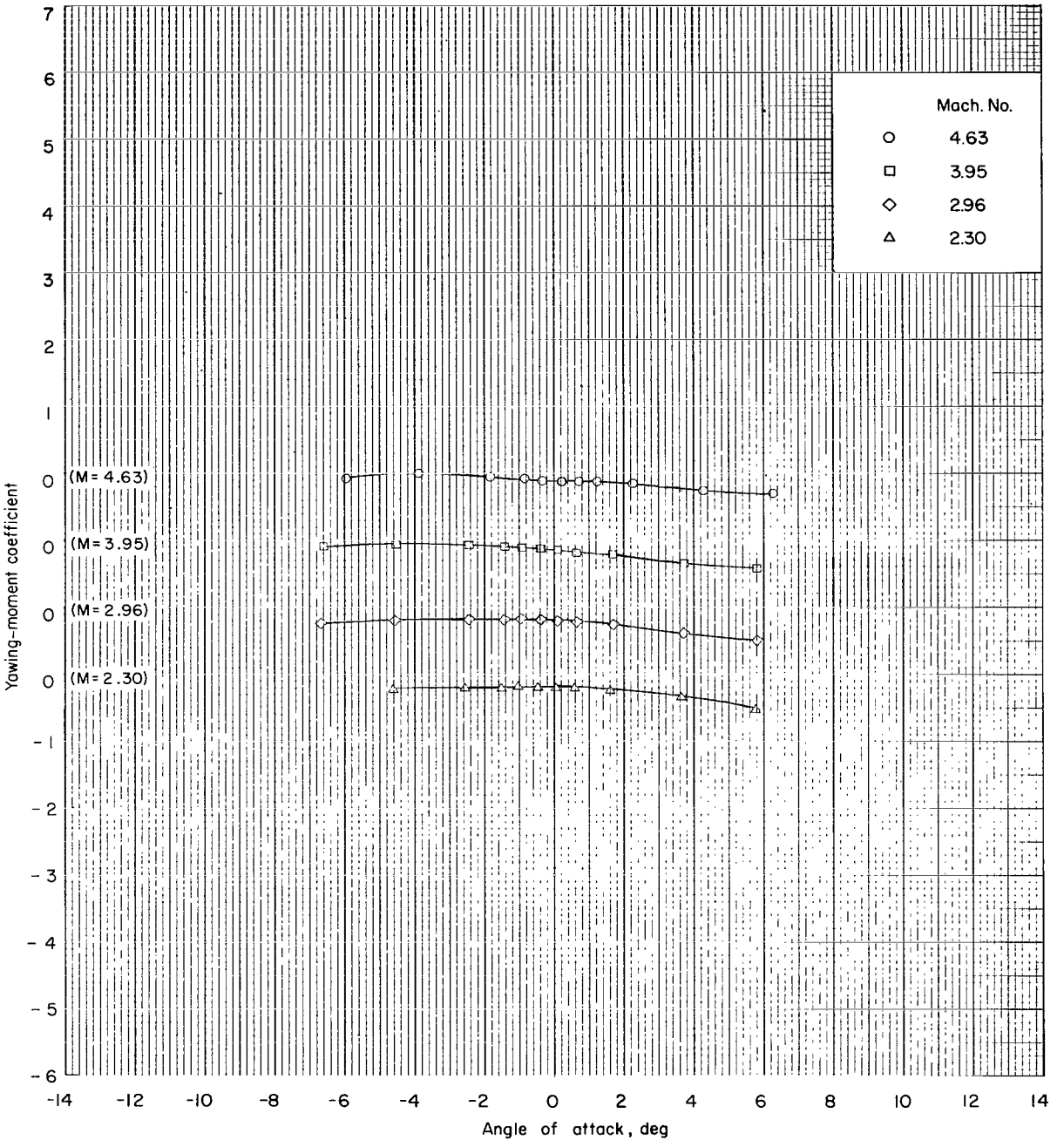

(d-2) Supersonic Mach numbers; configuration 4; $\phi = 0^{o}$.

Figure 10.- Continued.

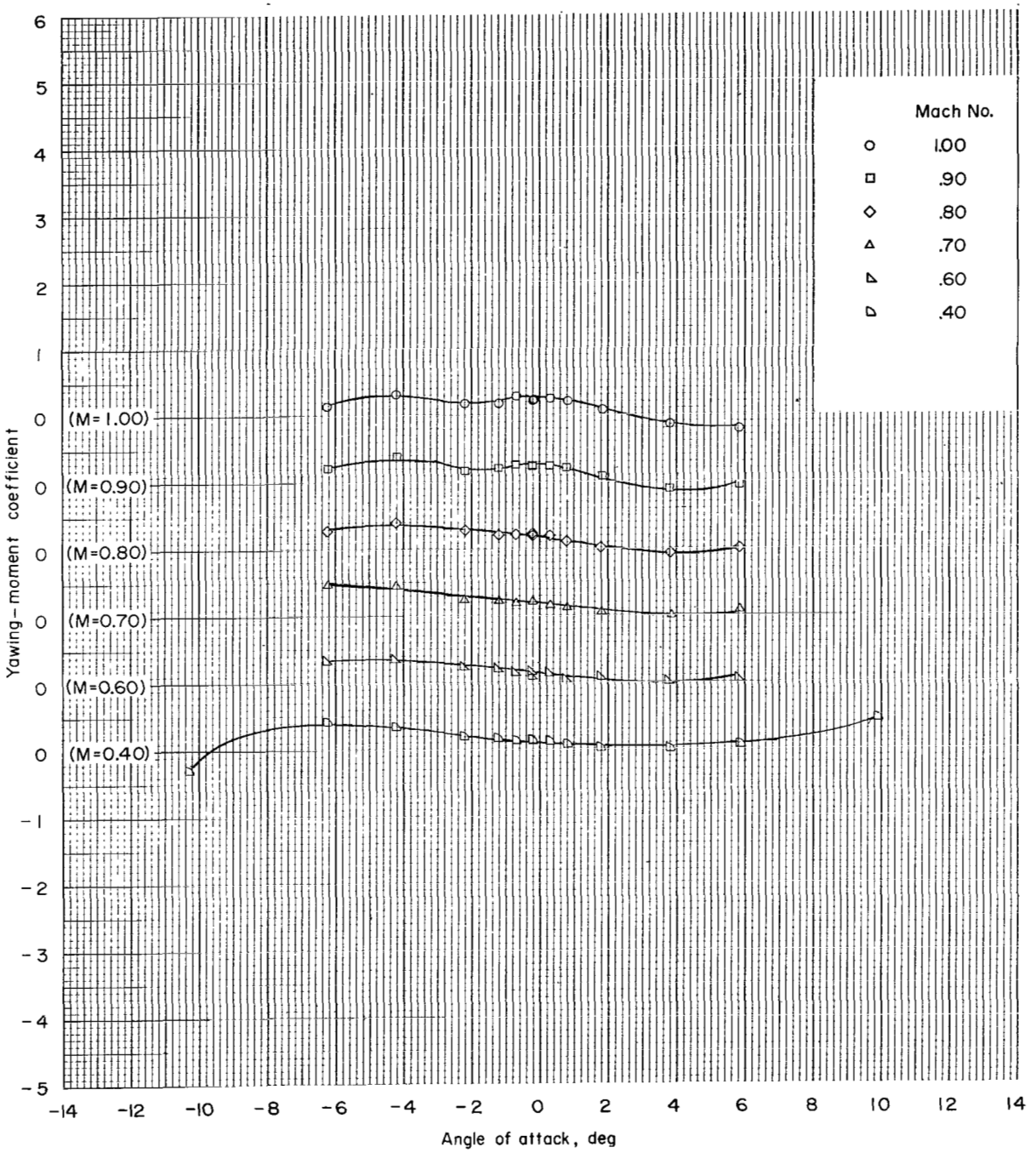

(e-1) Subsonic Mach numbers; configuration 5; $\phi = 0^{o}$.

Figure 10.- Continued.

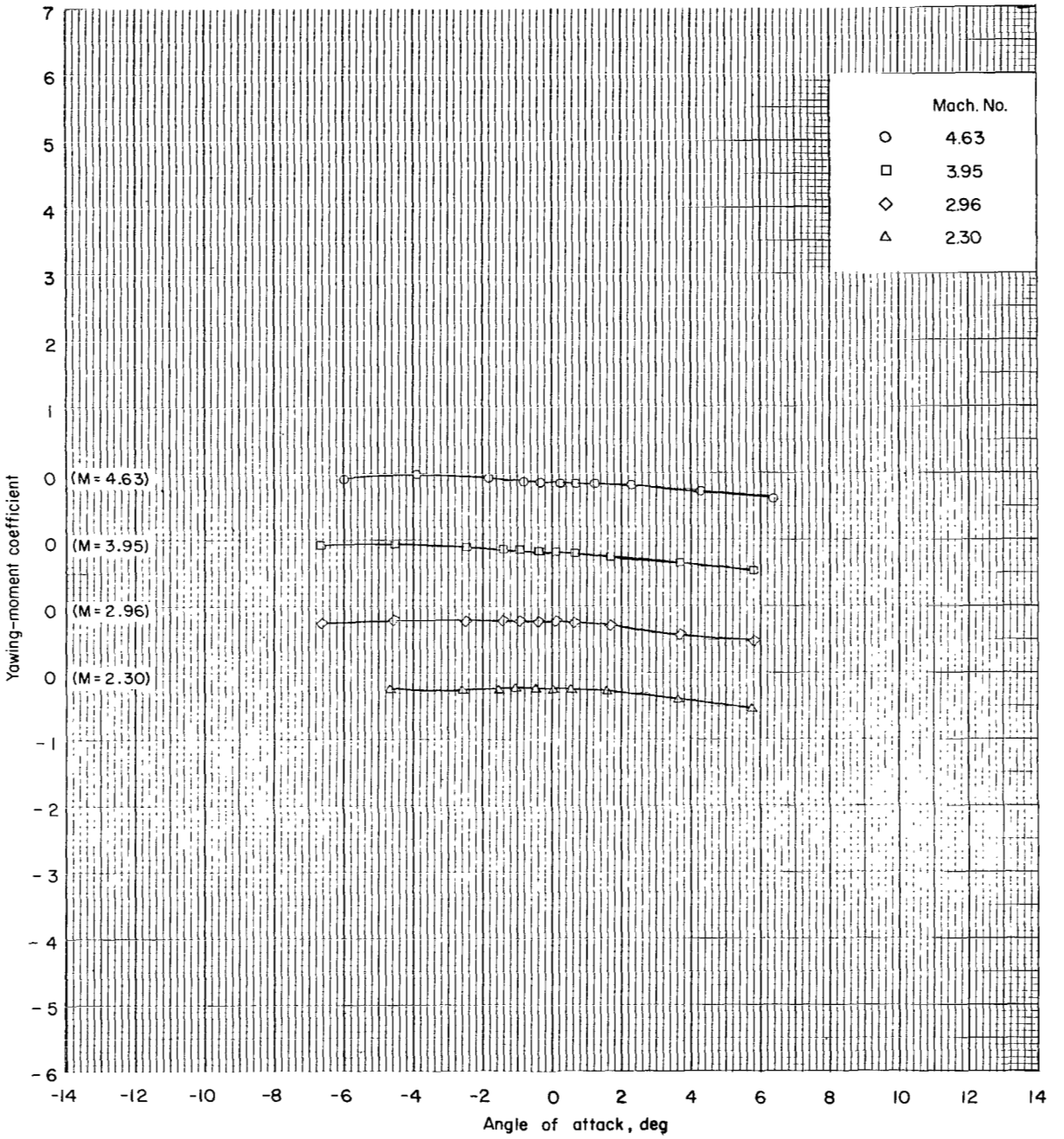

(e-2) Supersonic Mach numbers; configuration 5; $\phi = 0^{o}$.

Figure 10.- Continued.

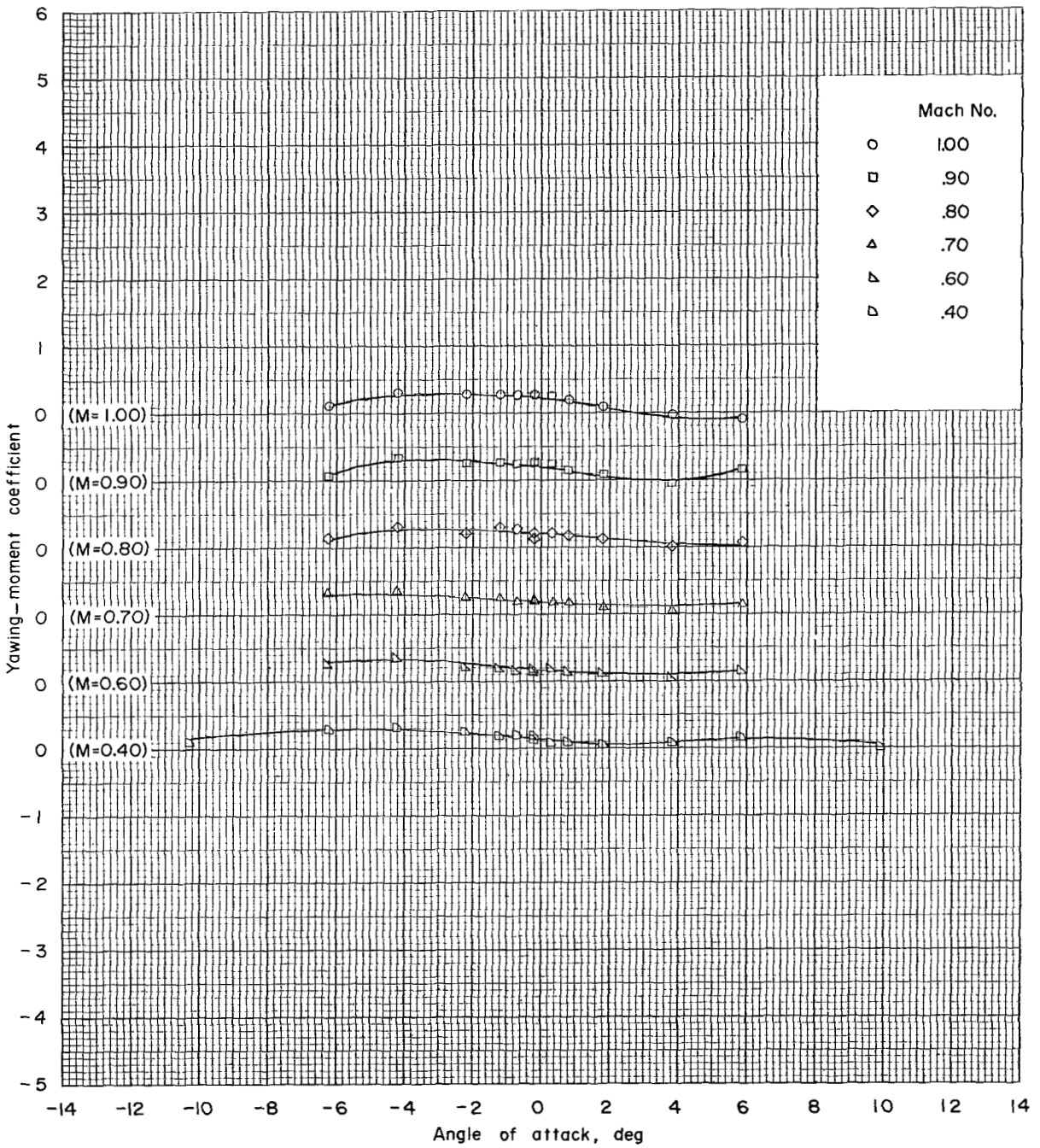

(f-1) Subsonic Mach numbers; configuration 6; $\phi = 0^{o}$.

Figure 10.- Continued.

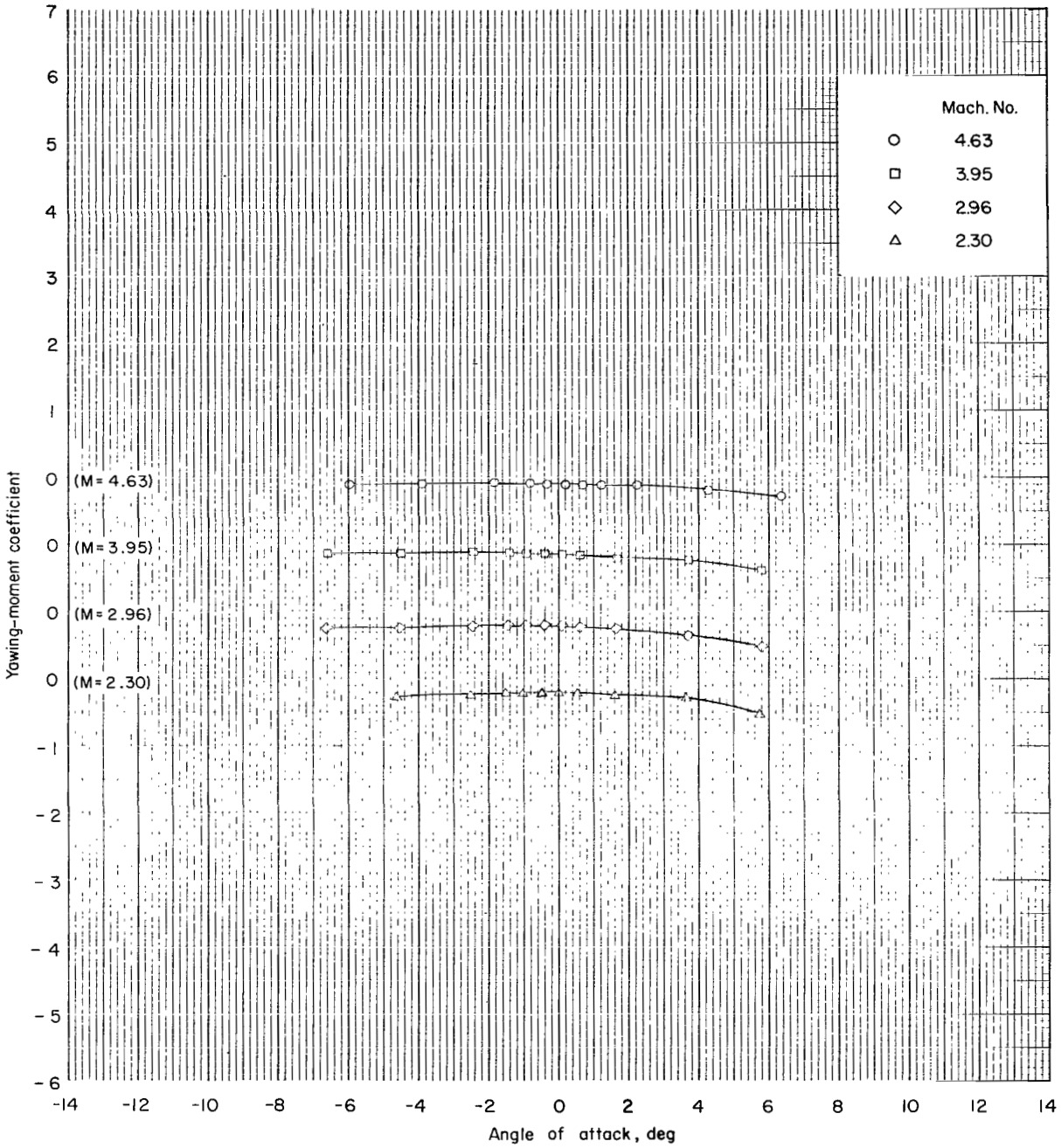

(f-2) Supersonic Mach numbers; configuration 6; $\phi = 0^{o}$.

Figure 10.- Continued.

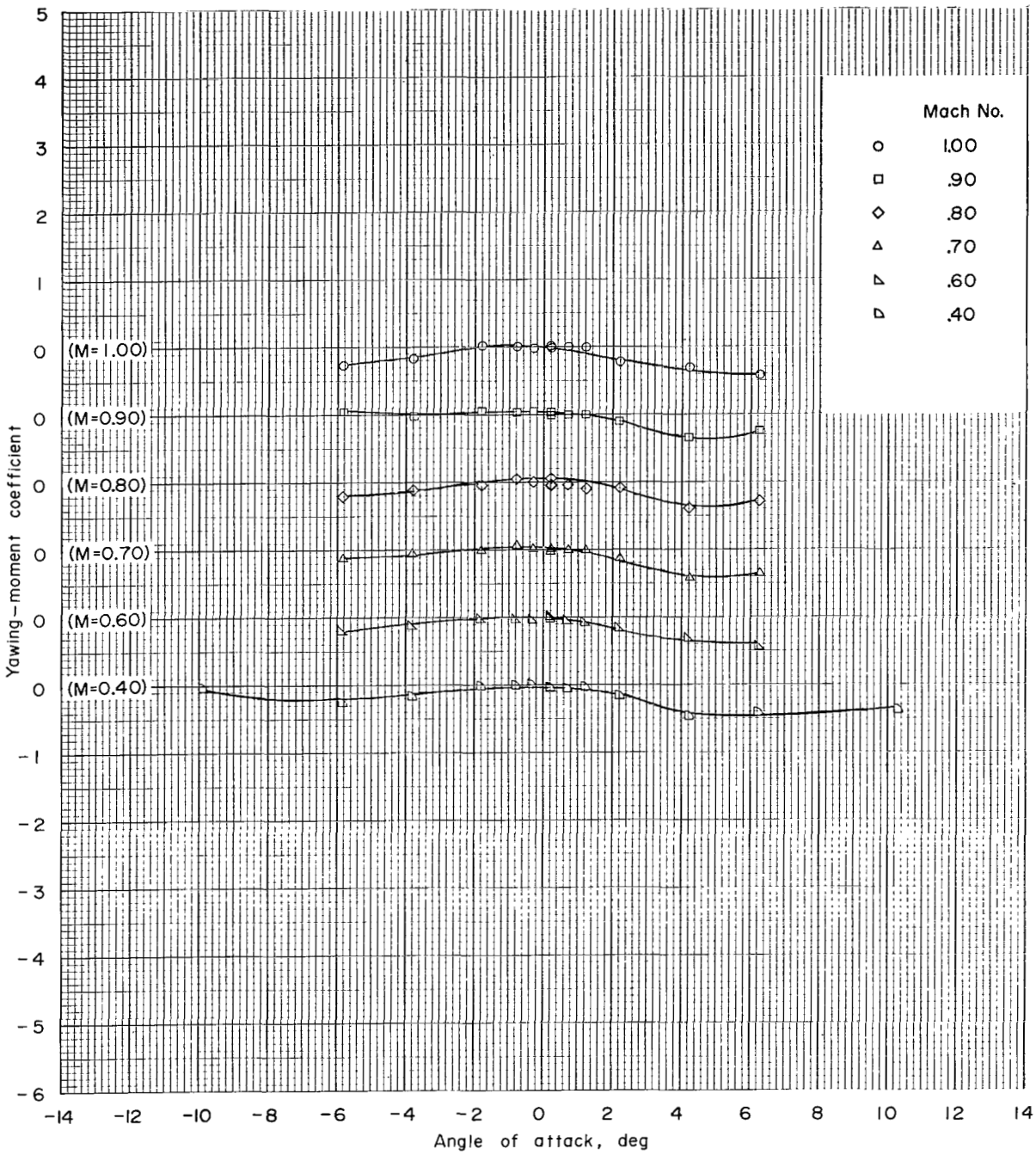

(g-1) Subsonic Mach numbers; configuration 6; $\phi = 180^{o}$.

Figure 10.- Continued.

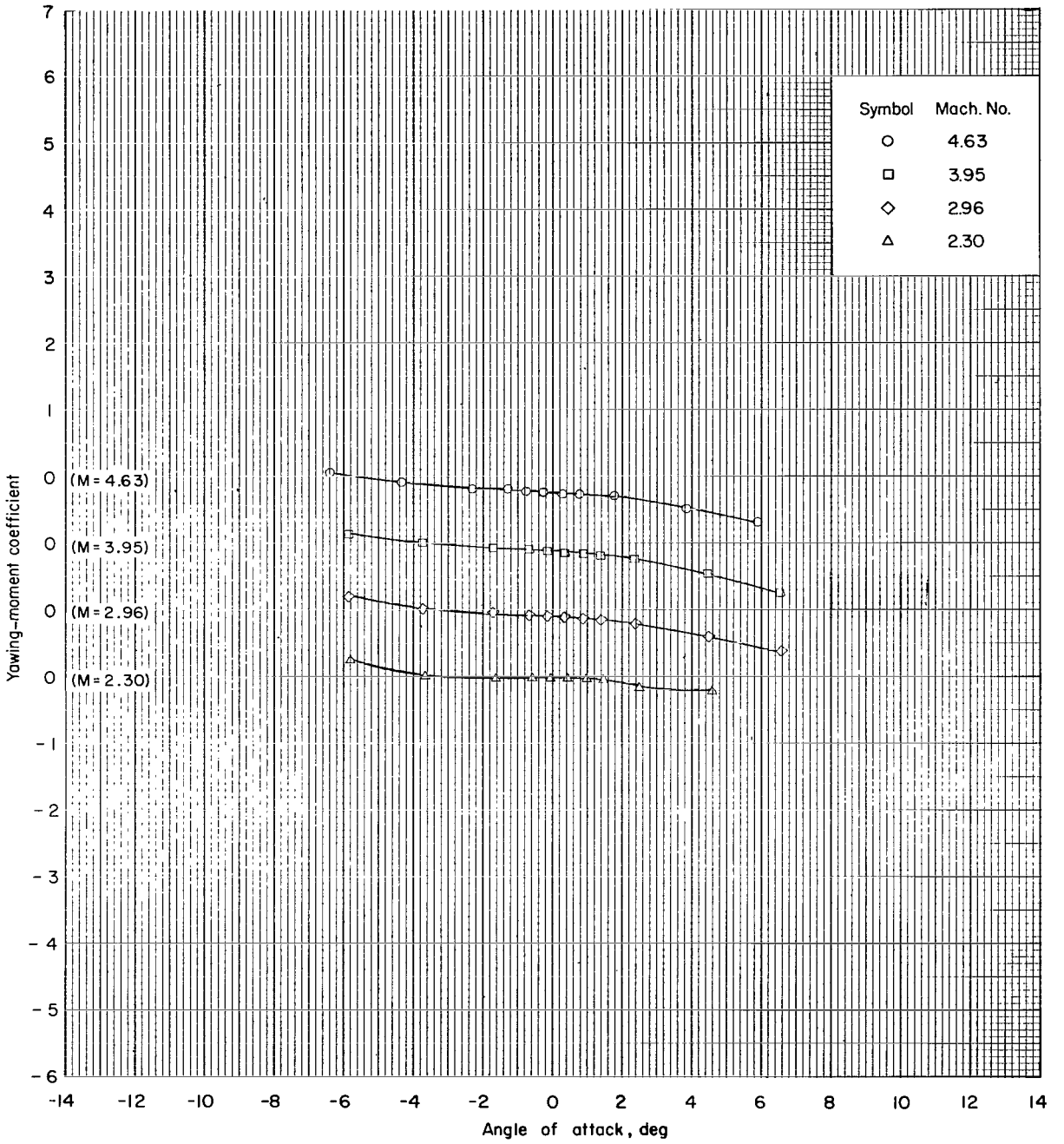

(g-2) Supersonic Mach numbers; configuration 6; $\phi = 180^{o}$.

Figure 10.- Continued.

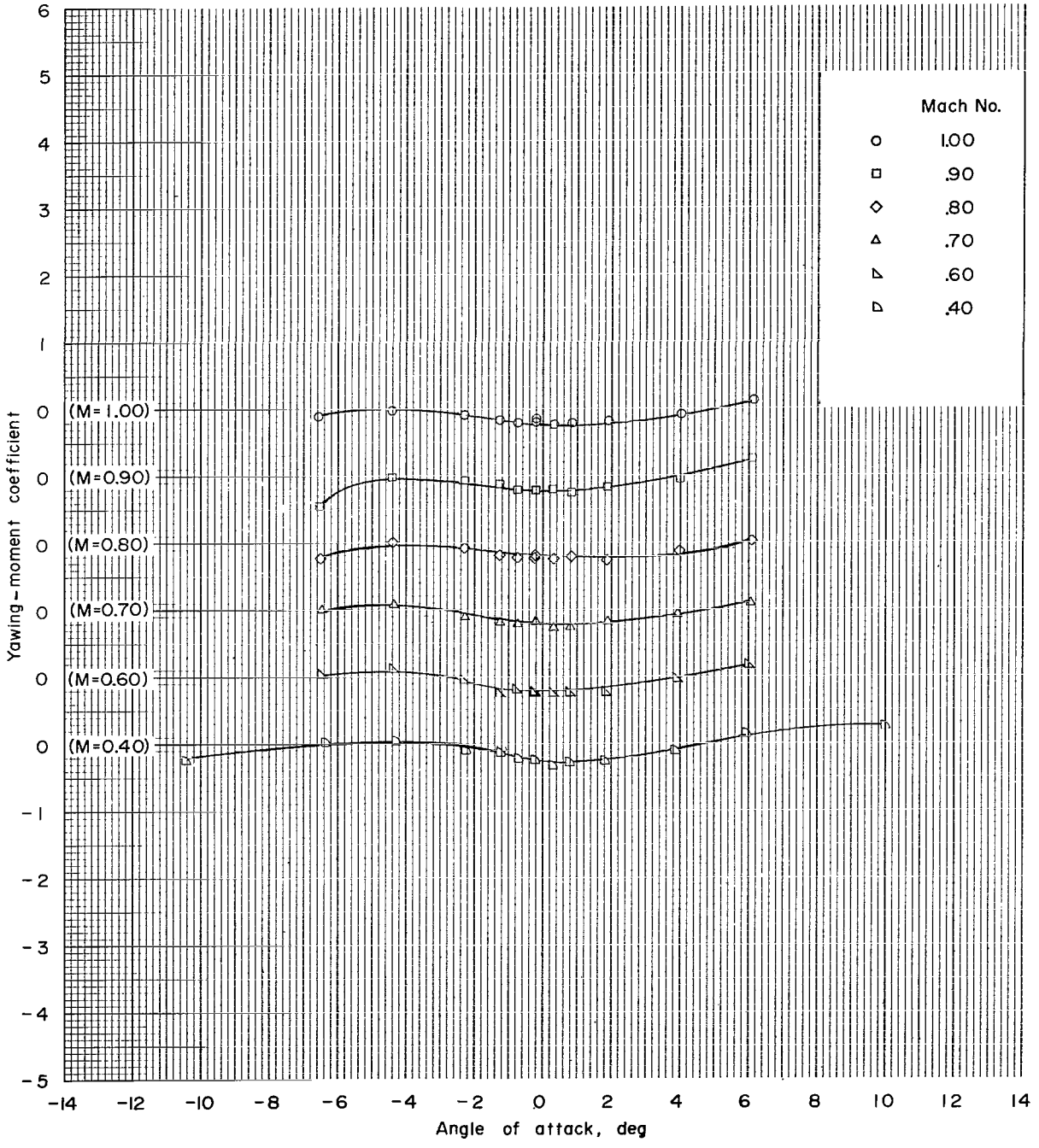

(h-1) Subsonic Mach numbers; configuration 7; $\phi = 0^{o}$.

Figure 10.- Continued.

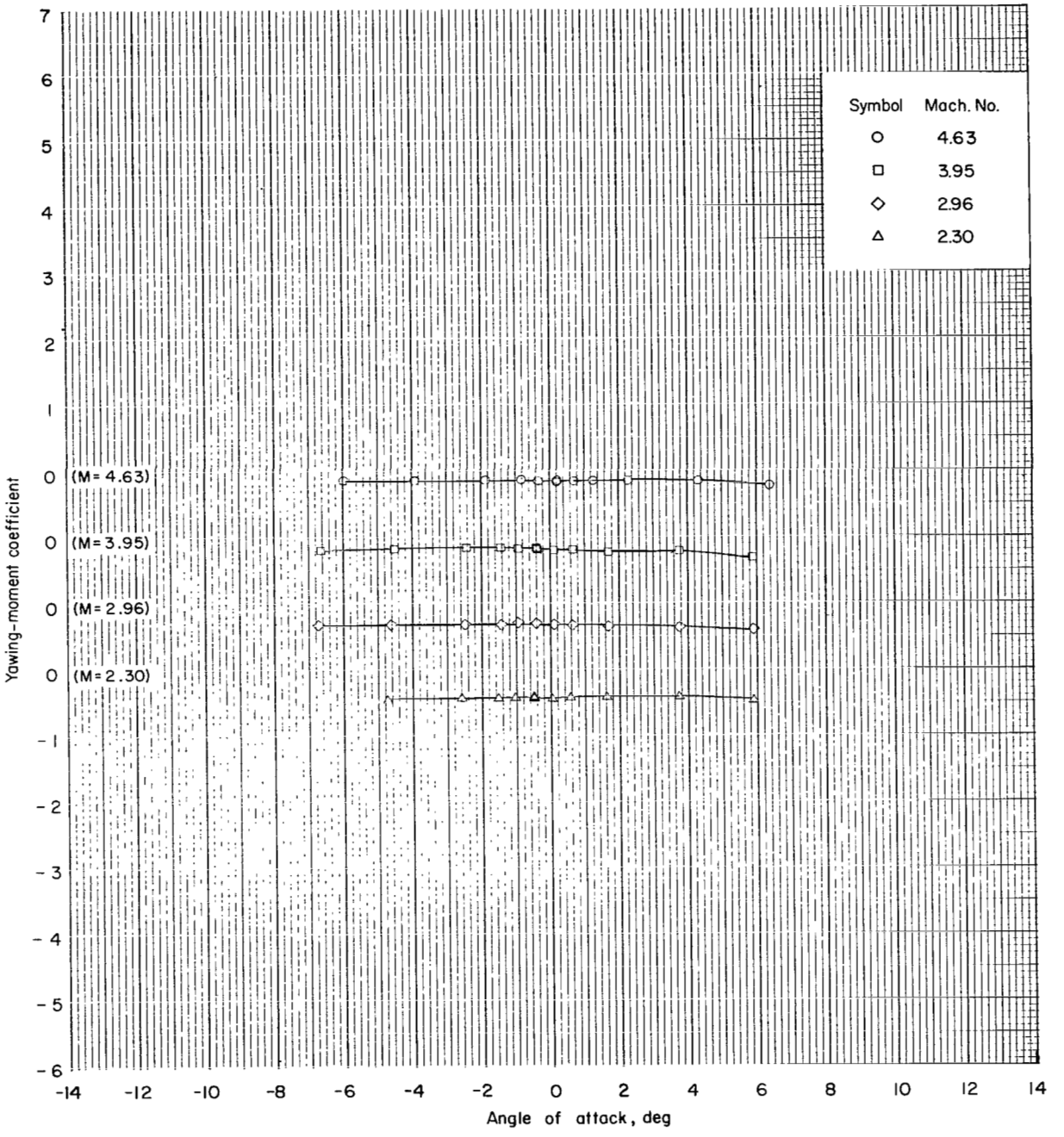

(h-2) Supersonic Mach numbers; configuration 7; $\phi = 0^{o}$.

Figure 10.- Continued.

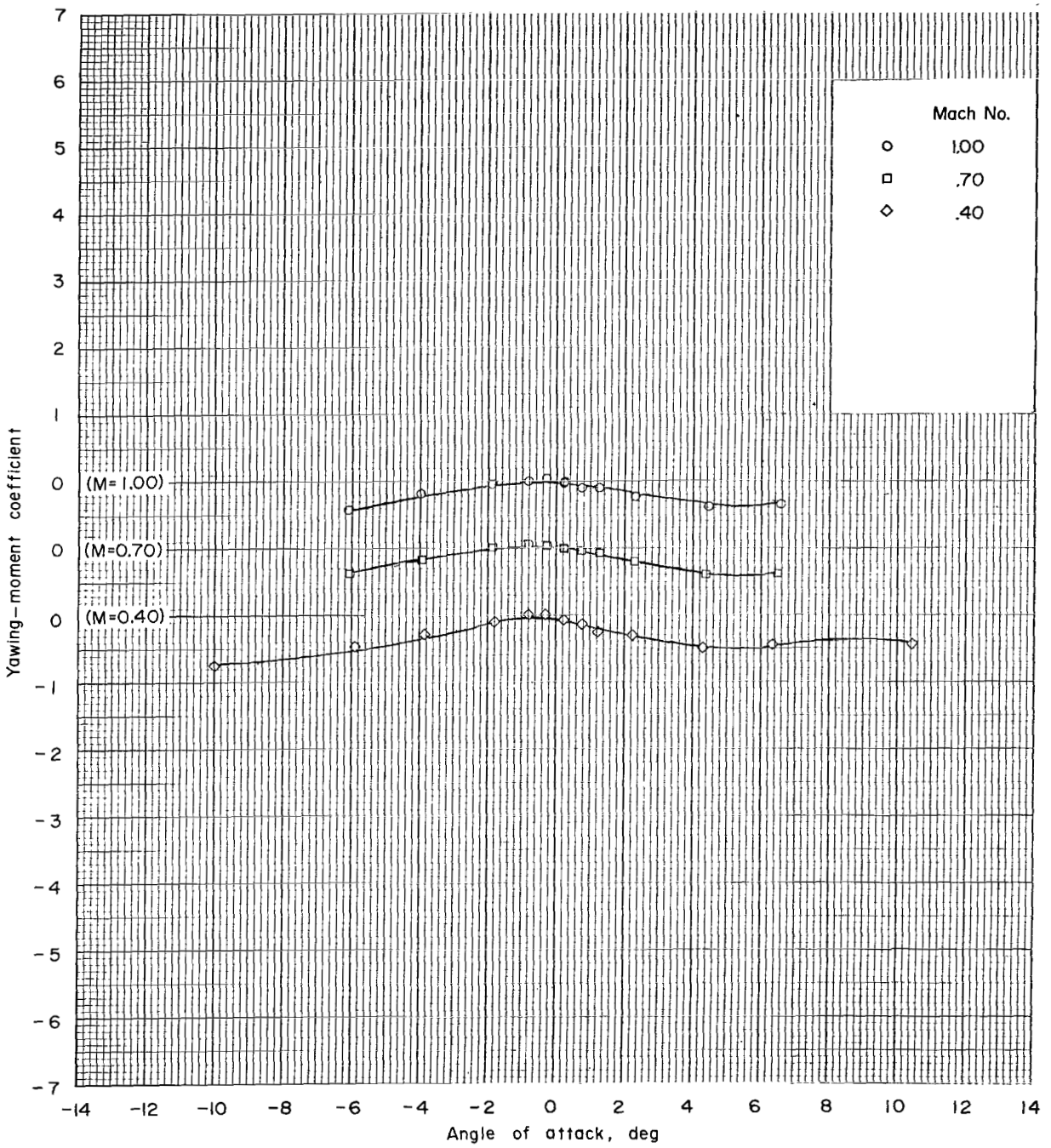

(i-1) Subsonic Mach numbers; configuration 7; $\phi = 180^{o}$.

Figure 10.- Continued.

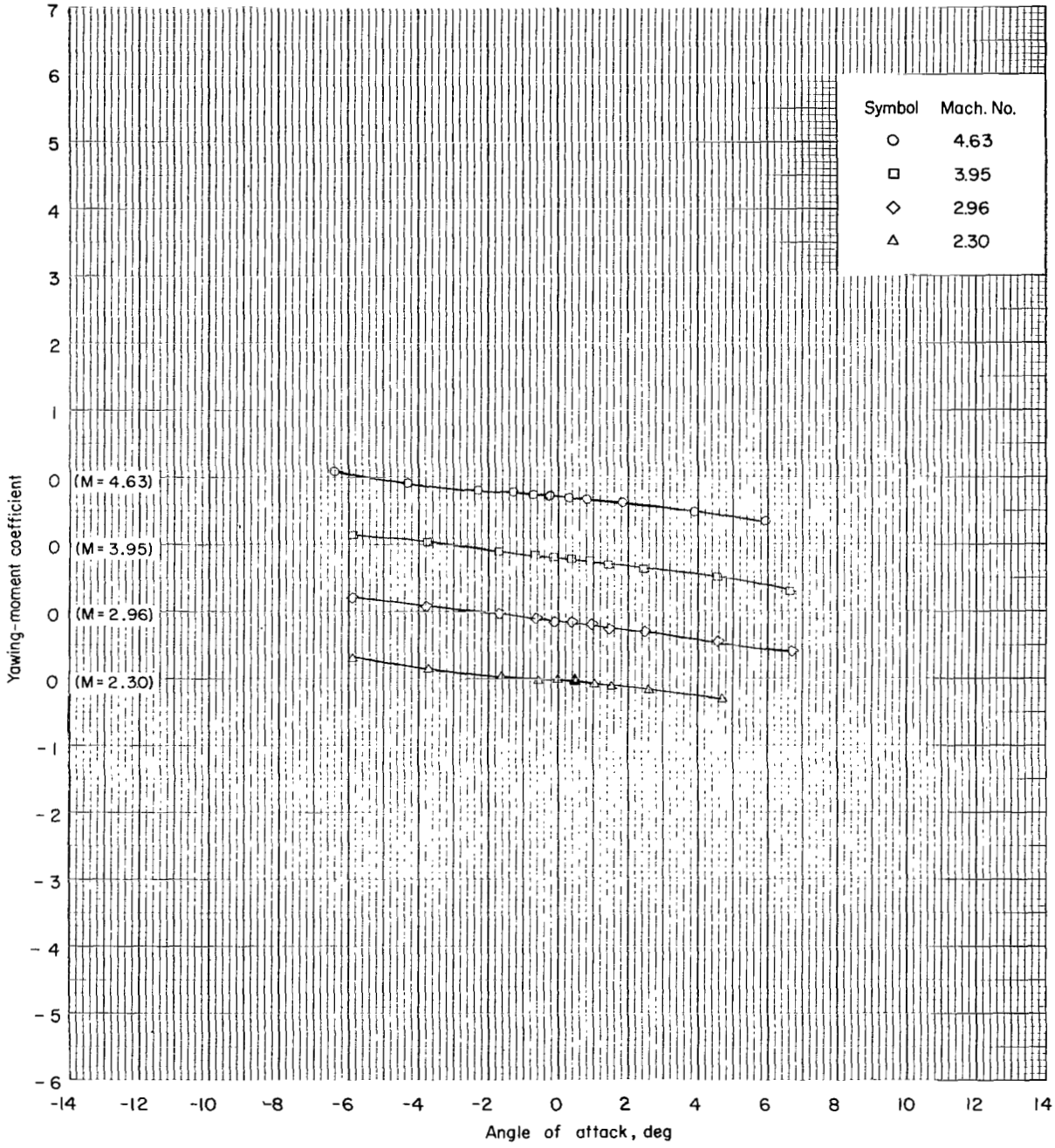

(i-2) Supersonic Mach numbers; configuration 7; $\phi = 180^{o}$.

Figure 10.- Concluded.

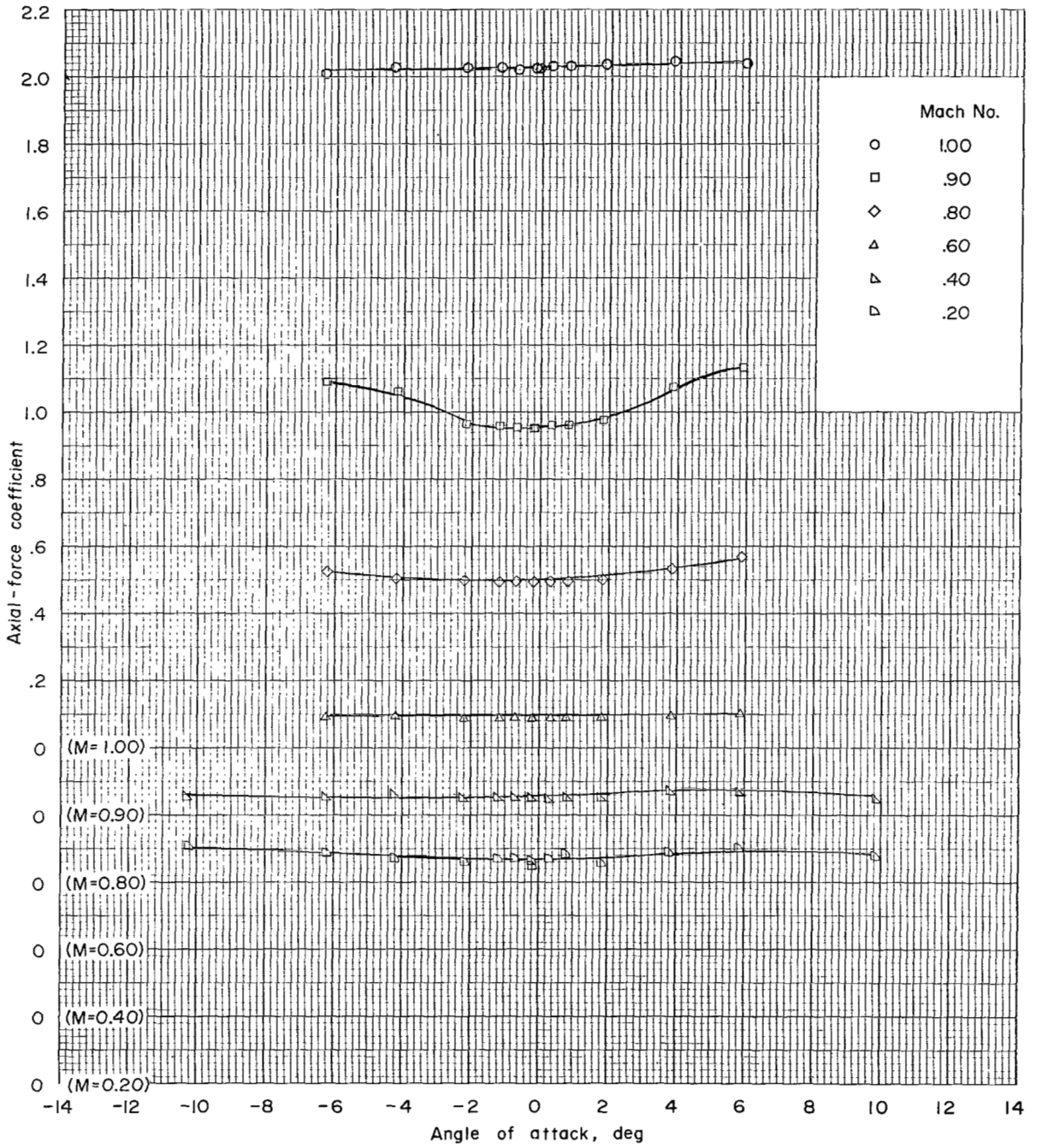

(a-1) Subsonic Mach numbers; configuration 1; $\phi = 0^{o}$.

Figure 11.- Axial force as function of angle of attack, roll angle, and Mach number.

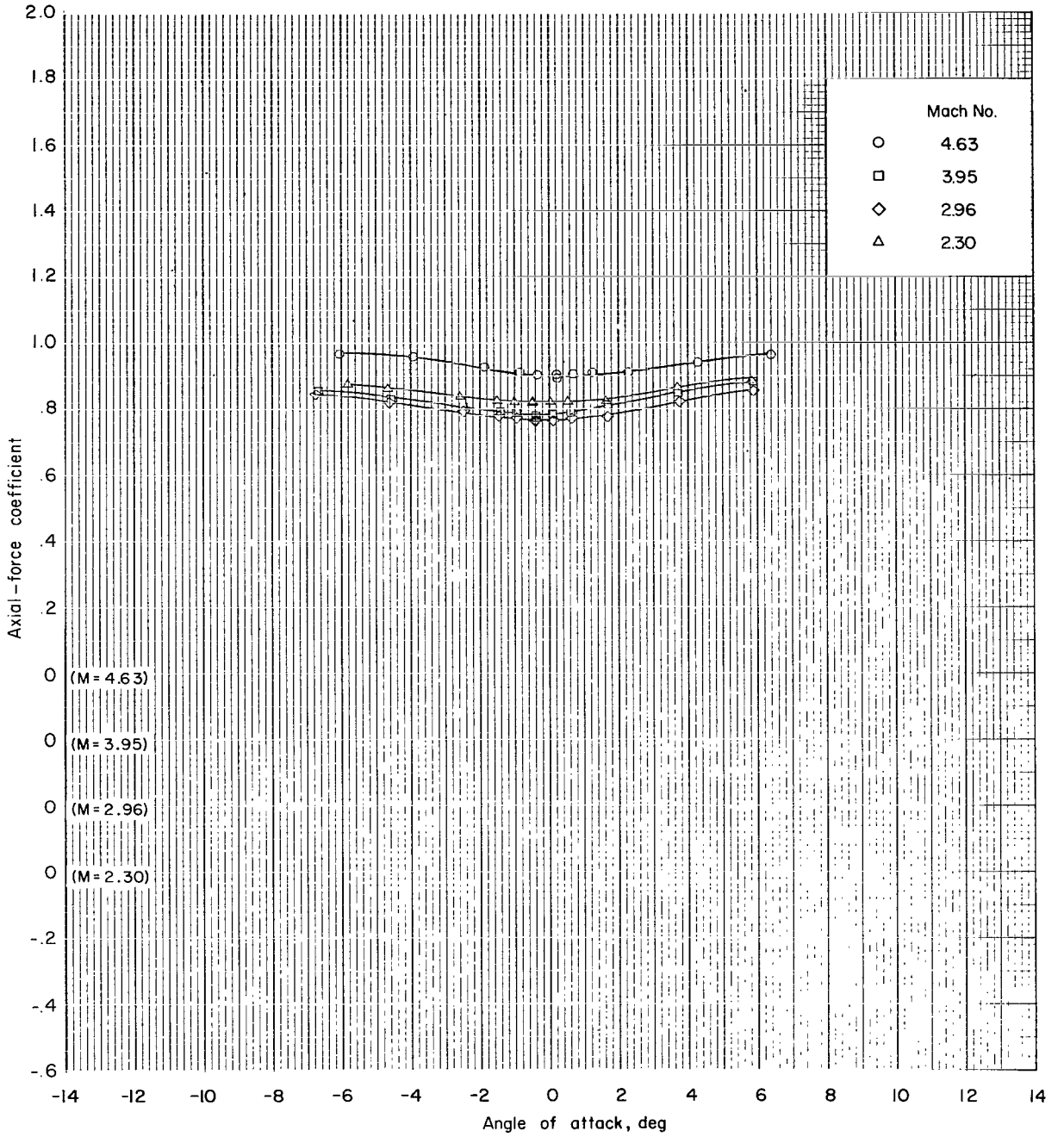

(a-2) Supersonic Mach numbers; configuration 1; $\phi = 0^{o}$.

Figure 11.- Continued.

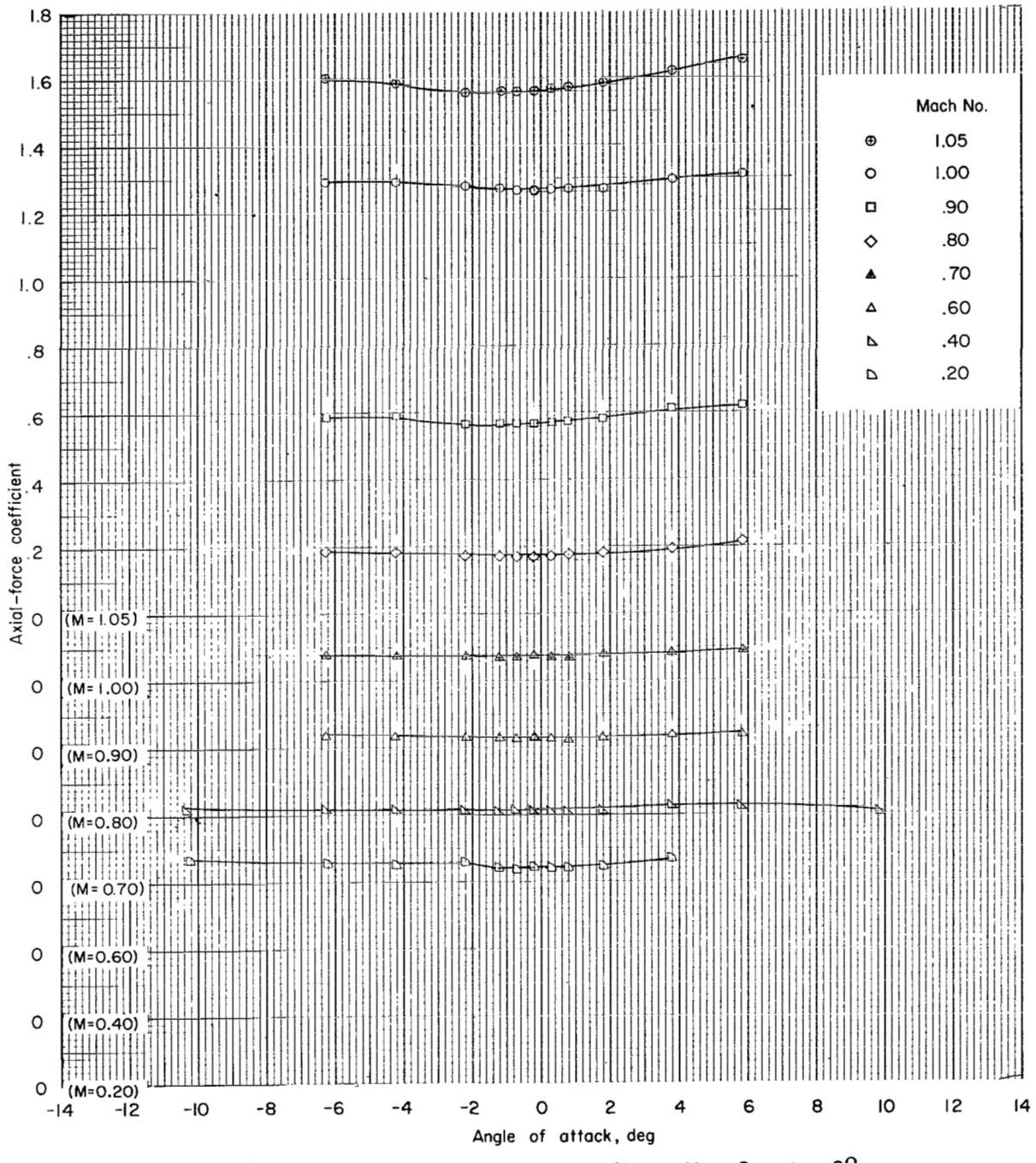

(b-1) Subsonic Mach numbers; configuration 2; $\phi = 0^{o}$.

Figure 11.- Continued.

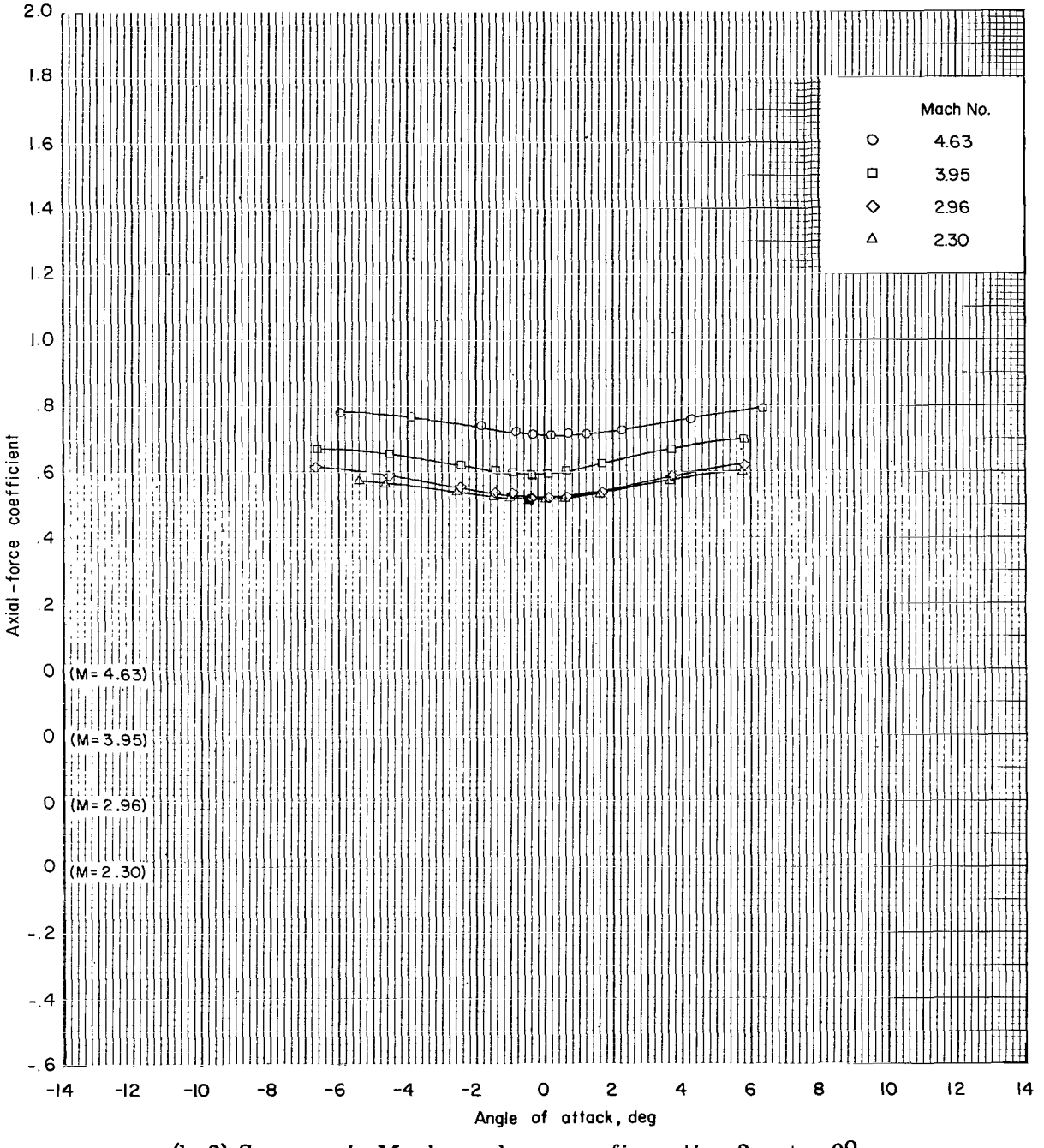

(b-2) Supersonic Mach numbers; configuration 2; $\phi = 0^{o}$.

Figure 11.- Continued.

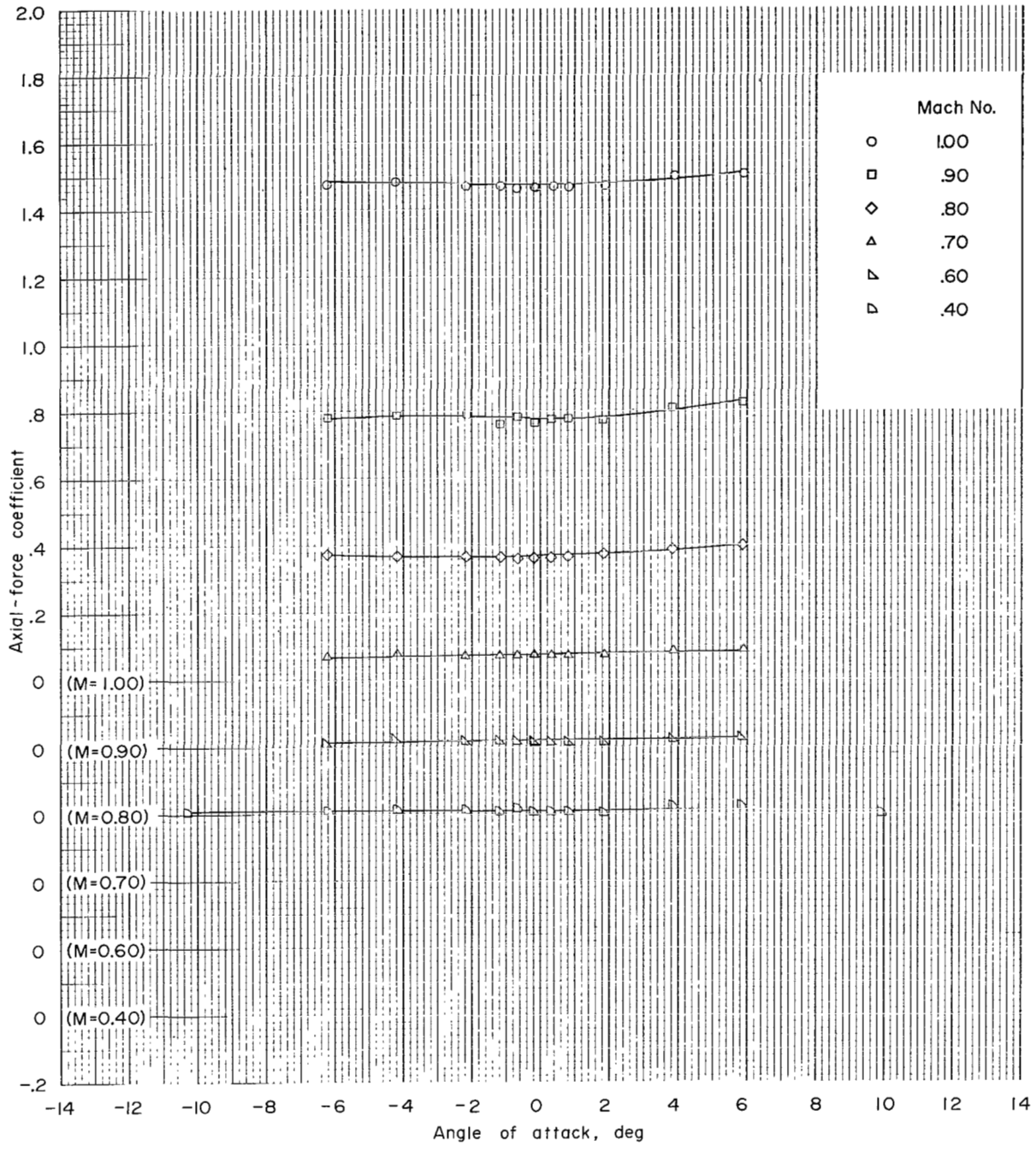

(c-1) Subsonic Mach numbers; configuration 3; $\phi = 0^{o}$.

Figure 11.- Continued.

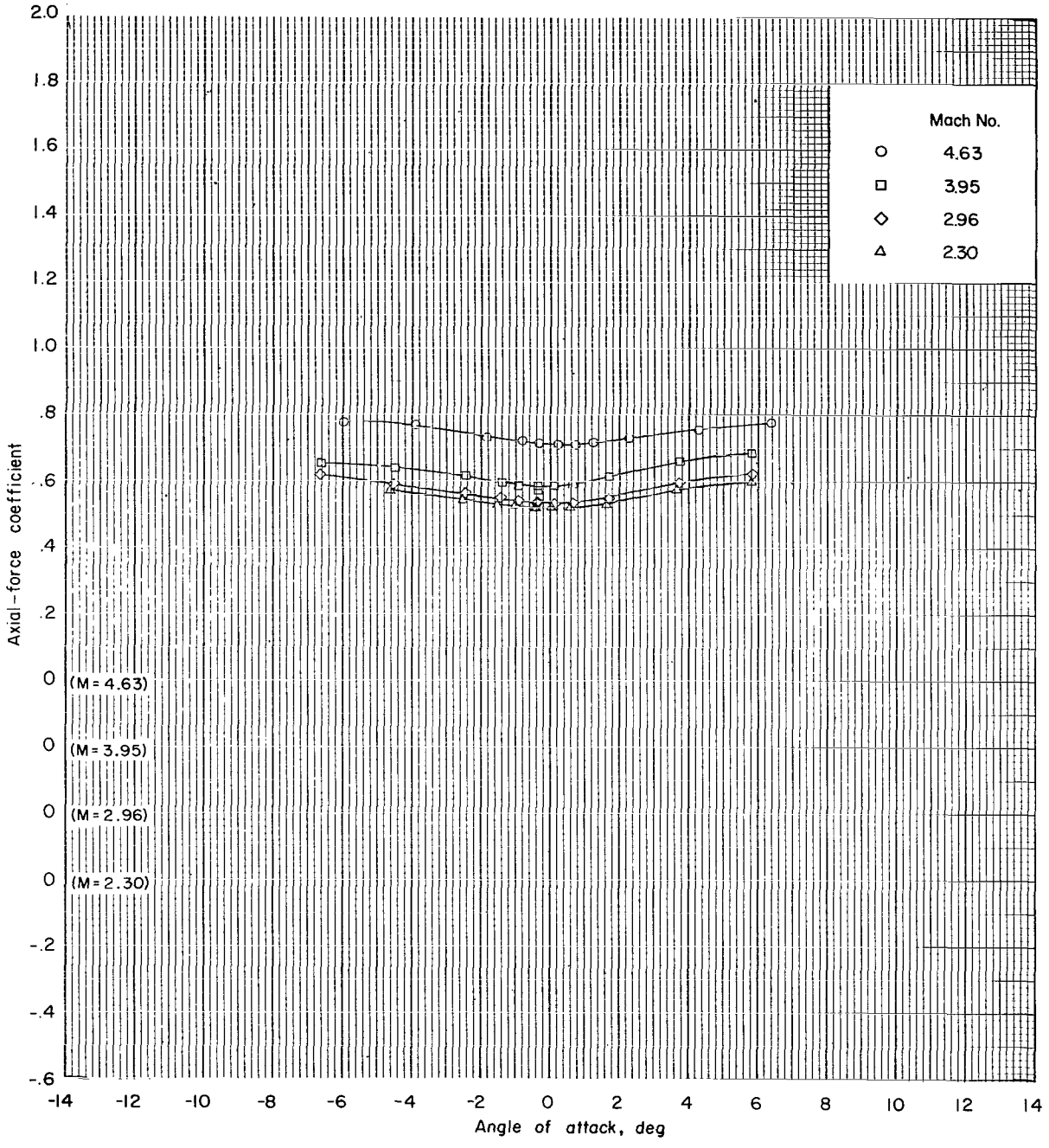

(c-2) Supersonic Mach numbers; configuration 3; $\phi = 0^{o}$.

Figure 11.- Continued.

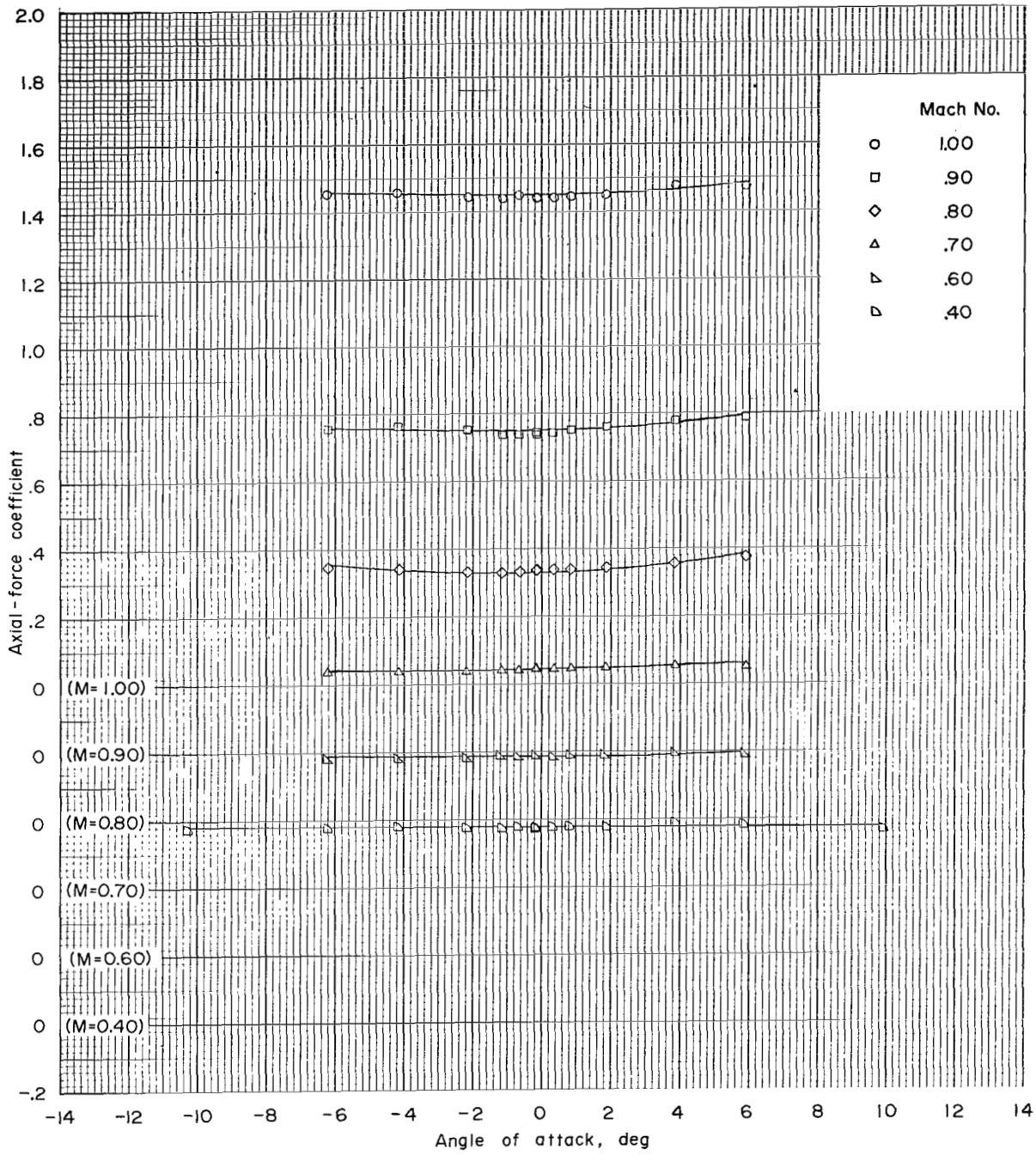

(d-1) Subsonic Mach numbers; configuration 4; $\phi = 0^{o}$.

Figure 11.- Continued.

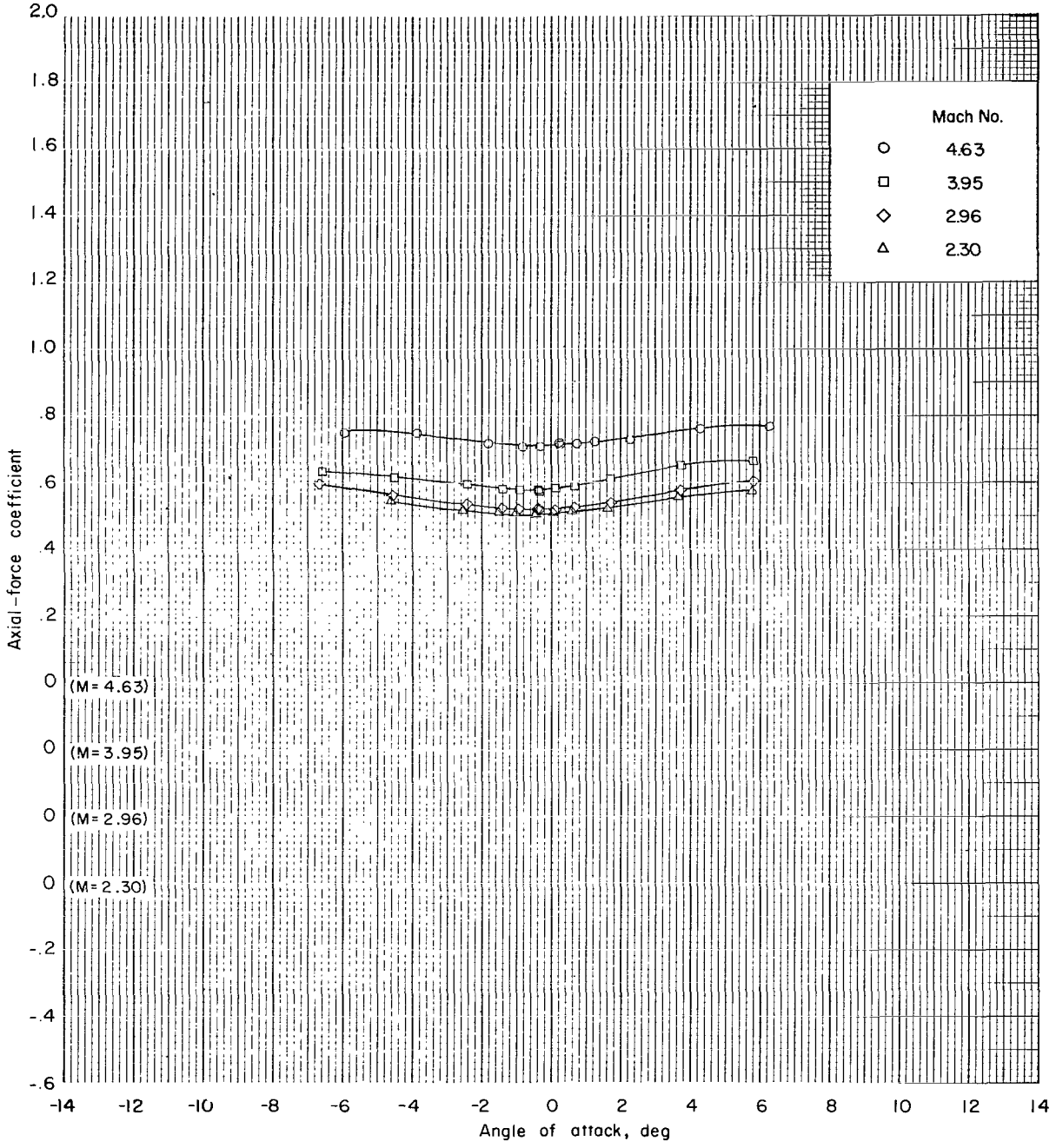

(d-2) Supersonic Mach numbers; configuration 4; $\phi = 0^{o}$.

Figure 11.- Continued.

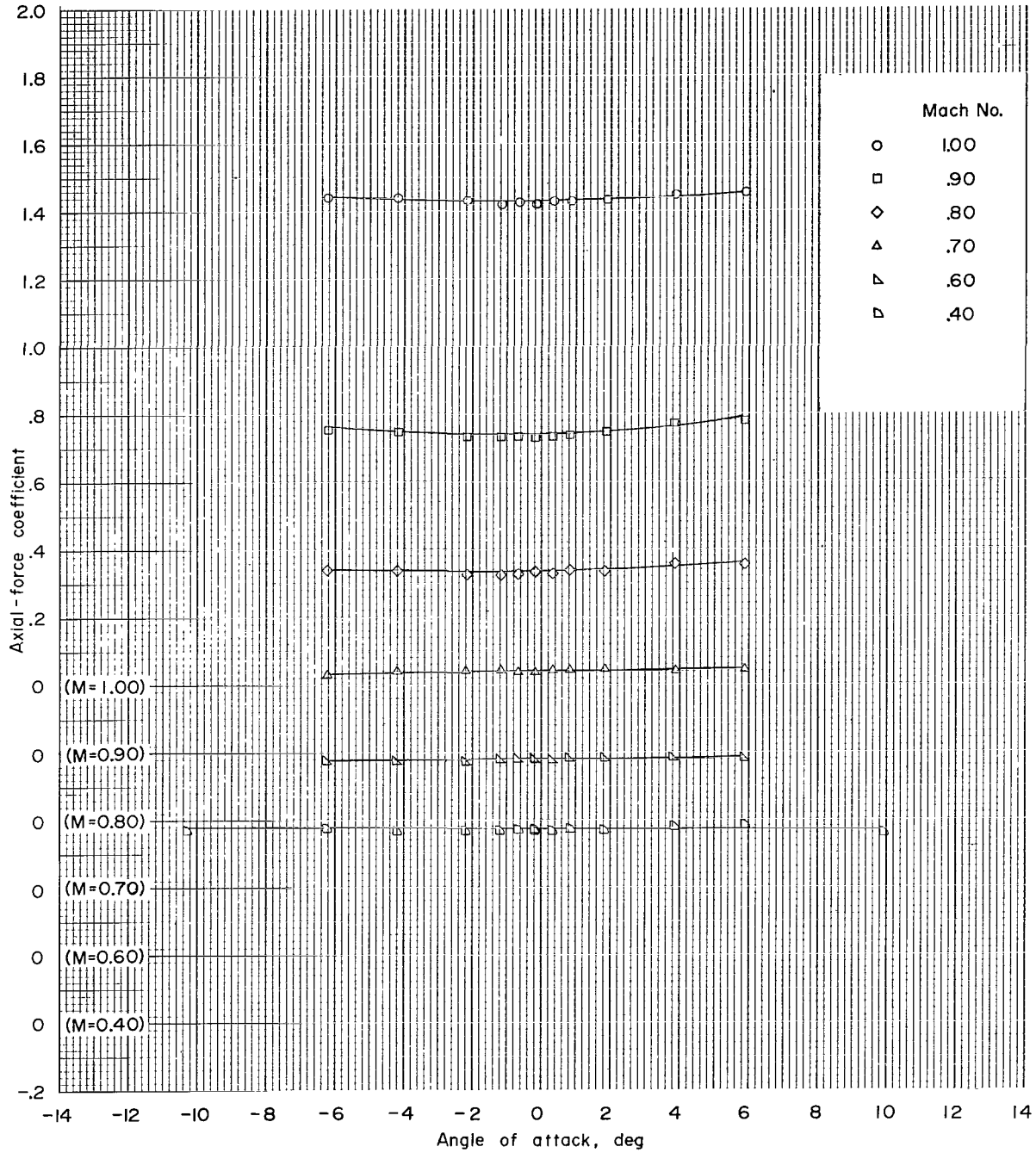

(e-1) Subsonic Mach numbers; configuration 5; $\phi = 0^{o}$.

Figure 11.- Continued.

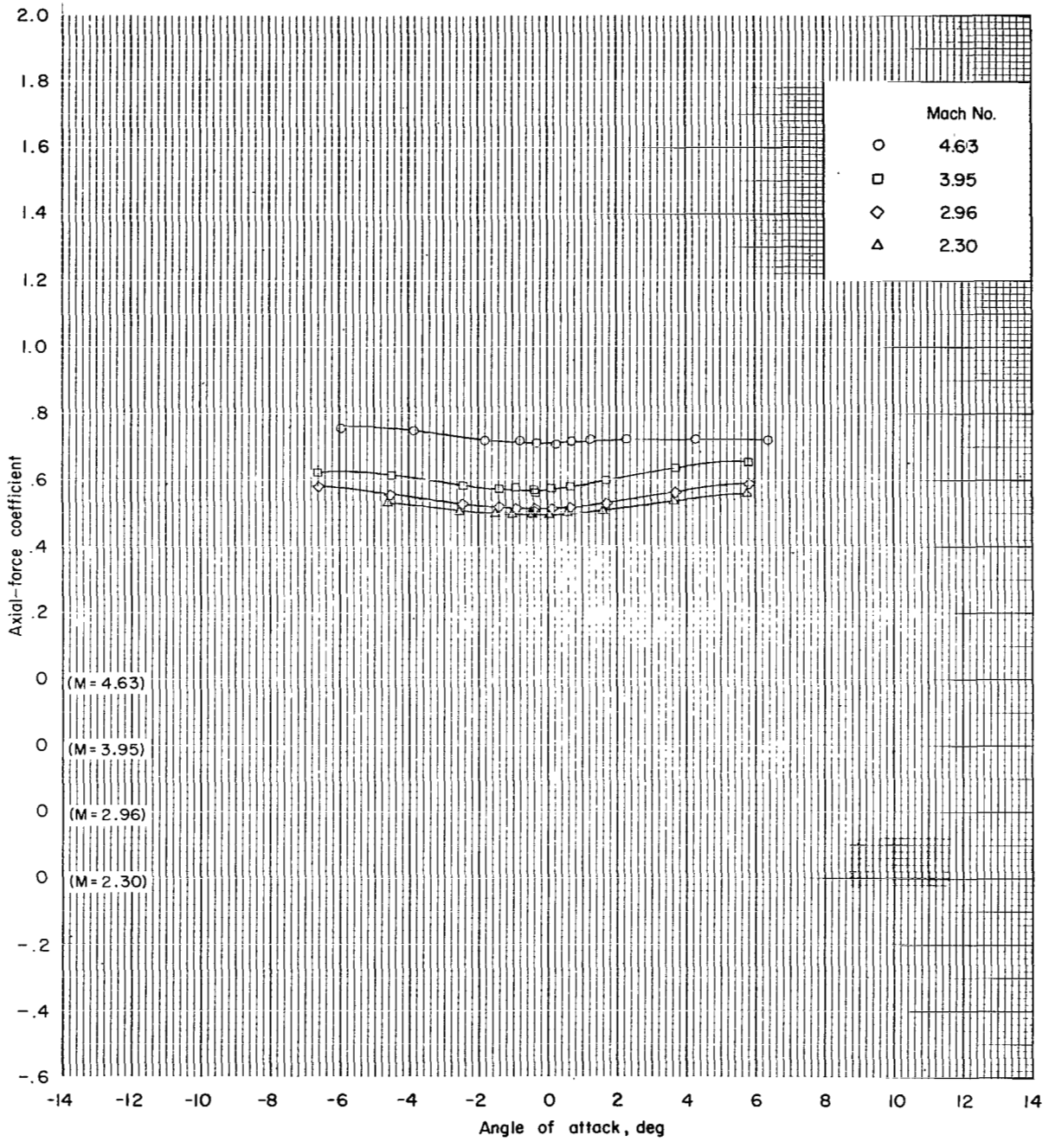

(e-2) Supersonic Mach numbers; configuration 5; $\phi = 0^{o}$.

Figure 11.- Continued.

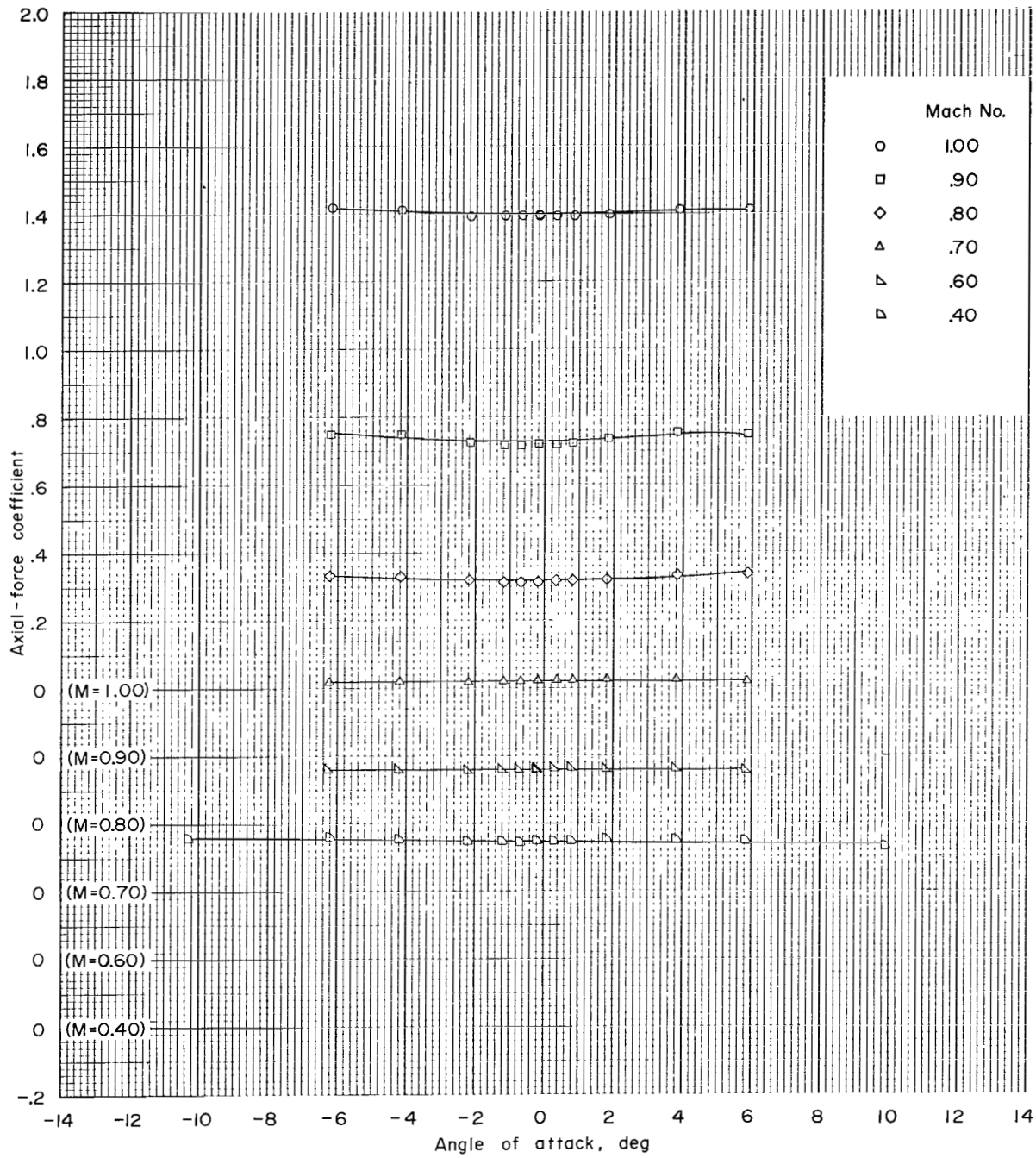

(f-1) Subsonic Mach numbers; configuration 6; $\phi = 0^{o}$.

Figure 11.- Continued.

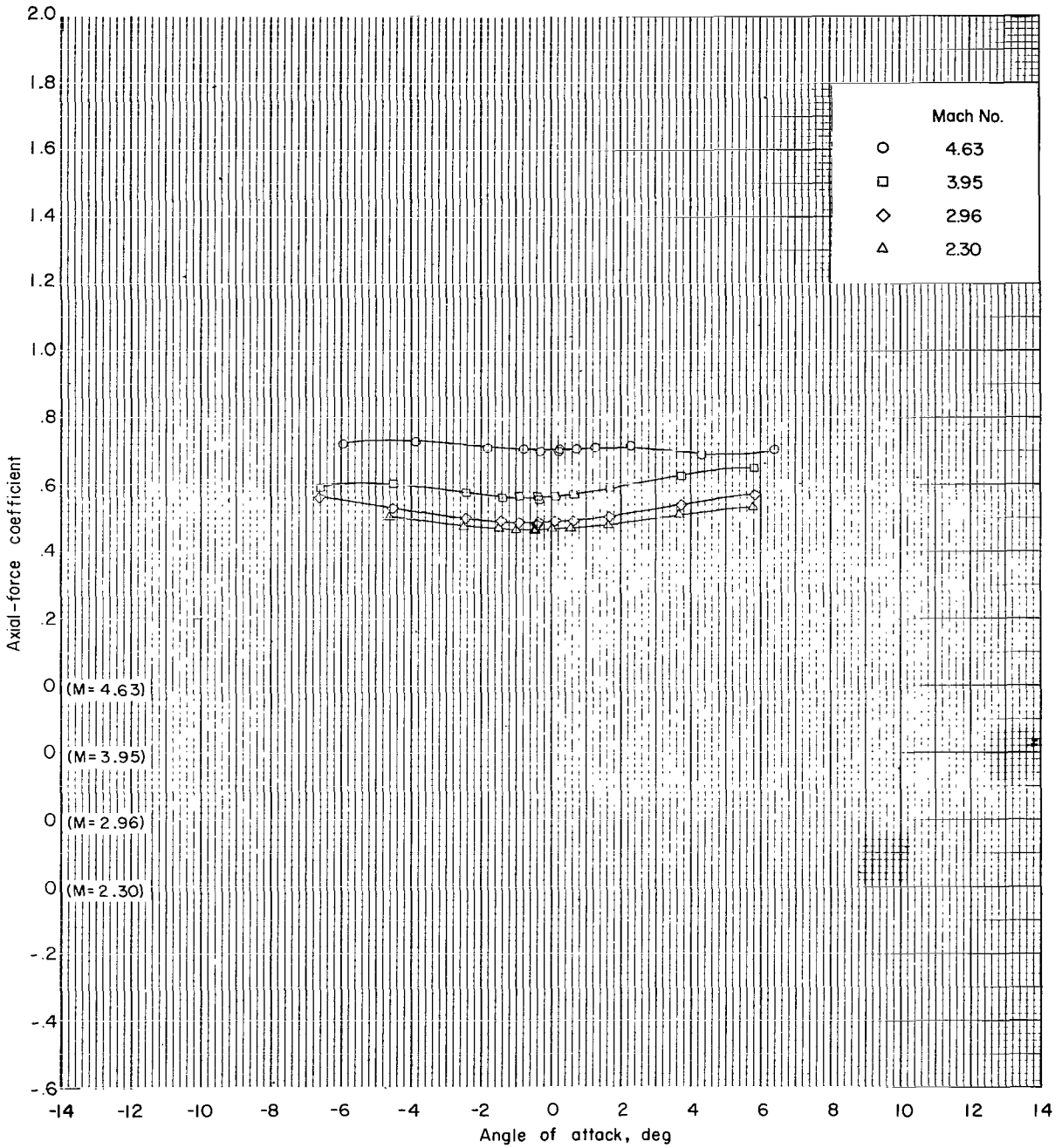

(f-2) Supersonic Mach numbers; configuration 6; $\phi = 0^{o}$.

Figure 11.- Continued.

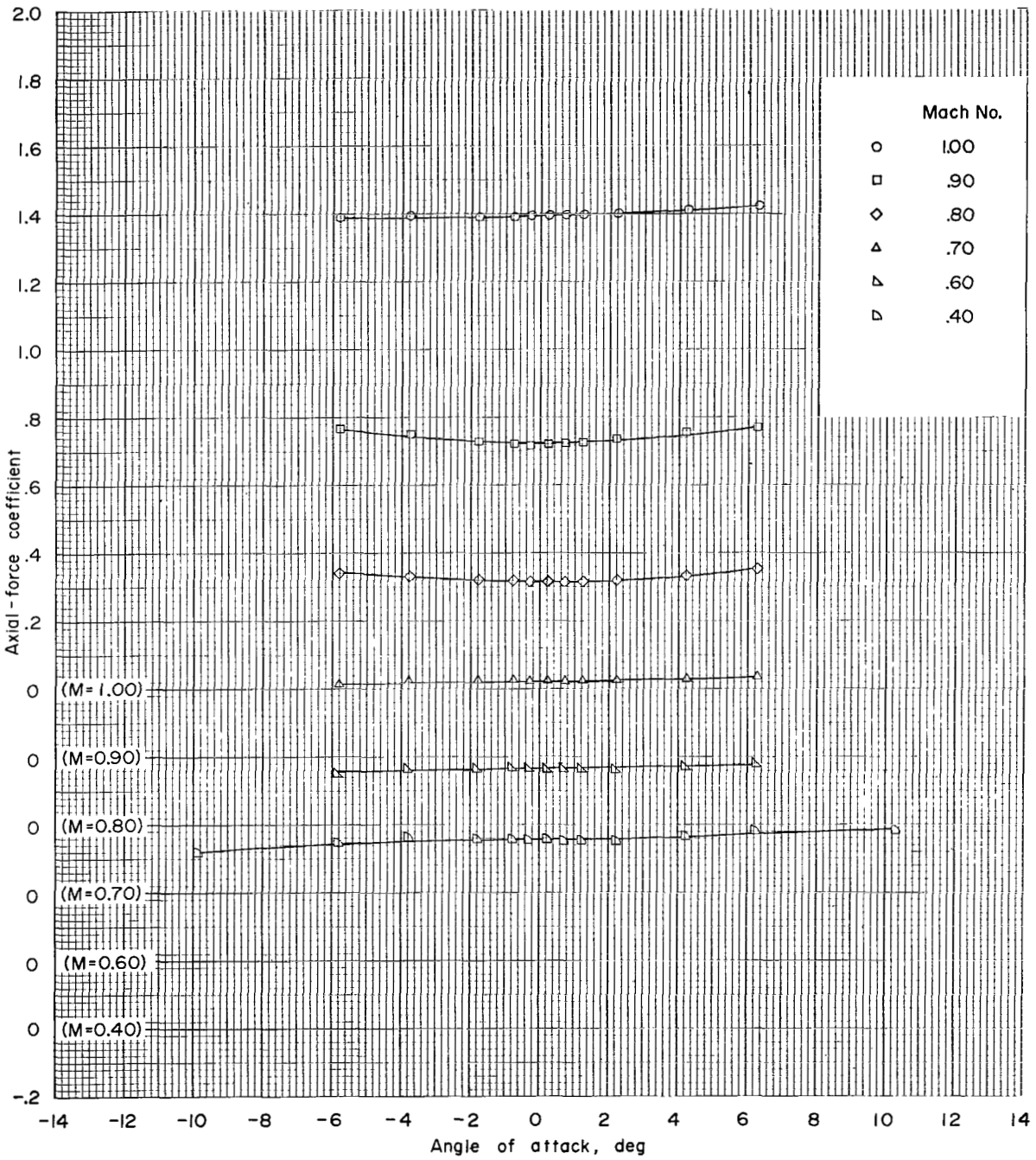

(g-1) Subsonic Mach numbers; configuration 6; $\phi = 180^{o}$.

Figure 11.- Continued.

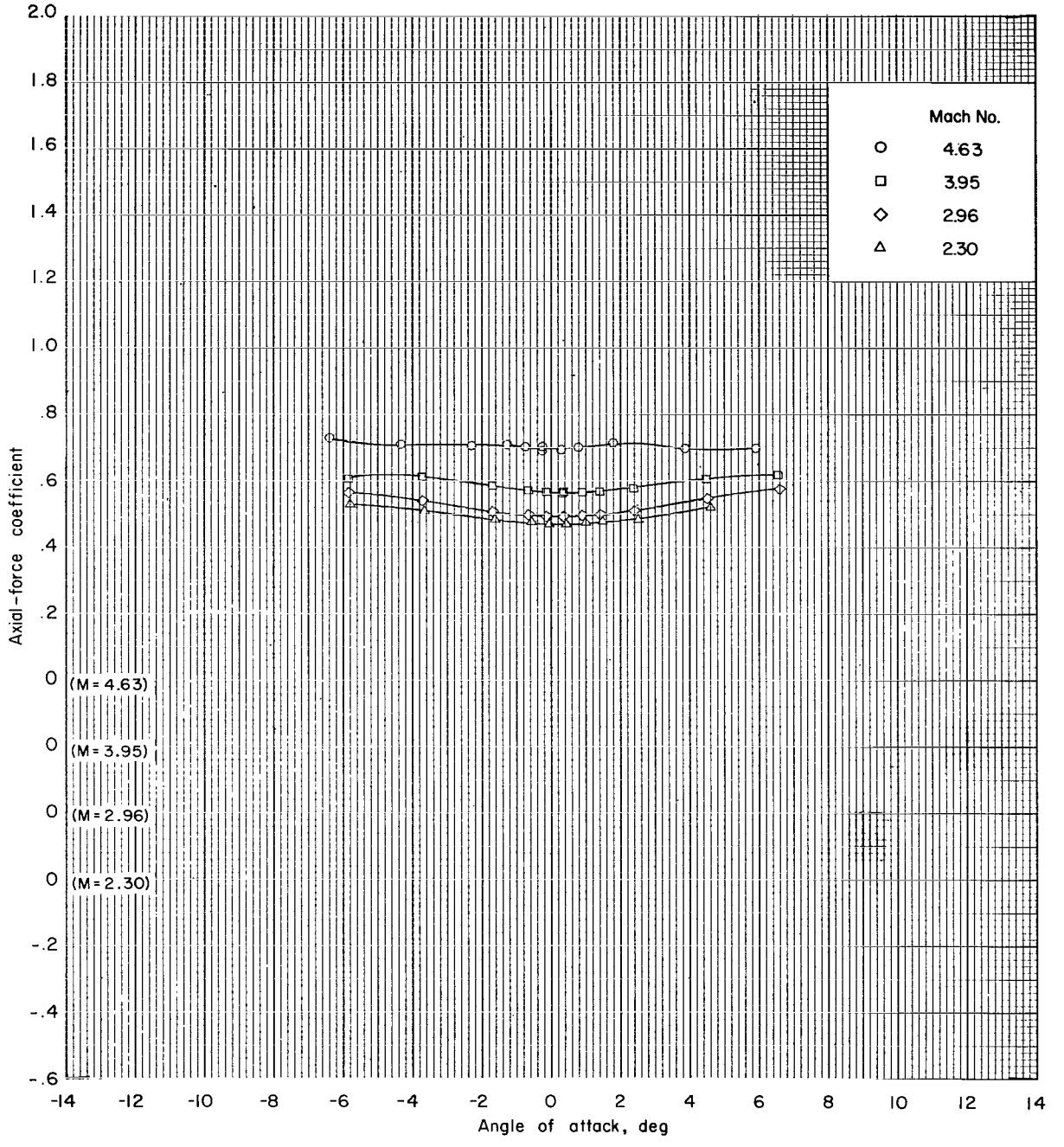

(g-2) Subsonic Mach numbers; configuration 6; $\phi = 180^{o}$.

Figure 11.- Continued.

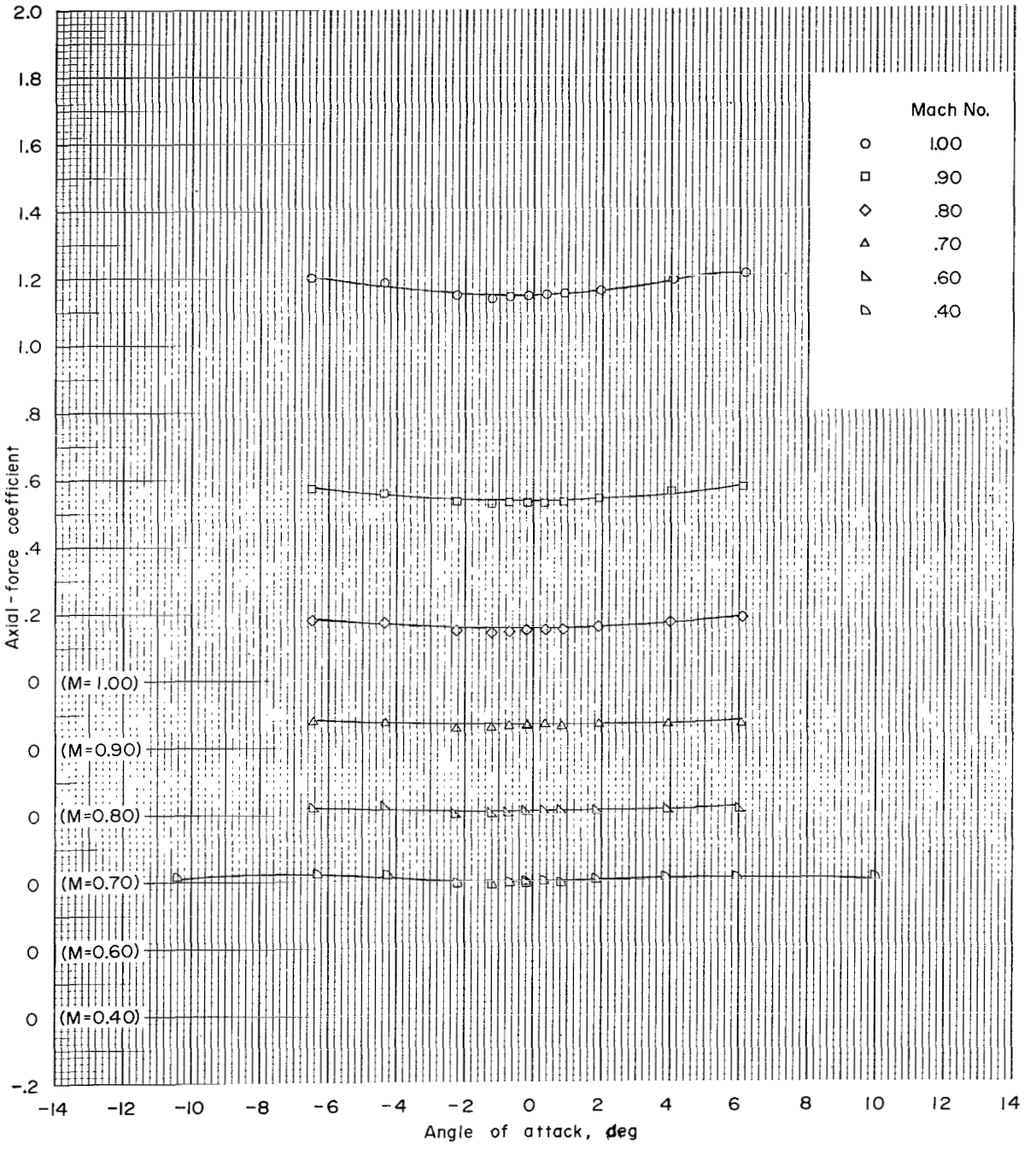

(h-1) Subsonic Mach numbers; configuration 7; $\phi = 0^{o}$.

Figure 11.- Continued.

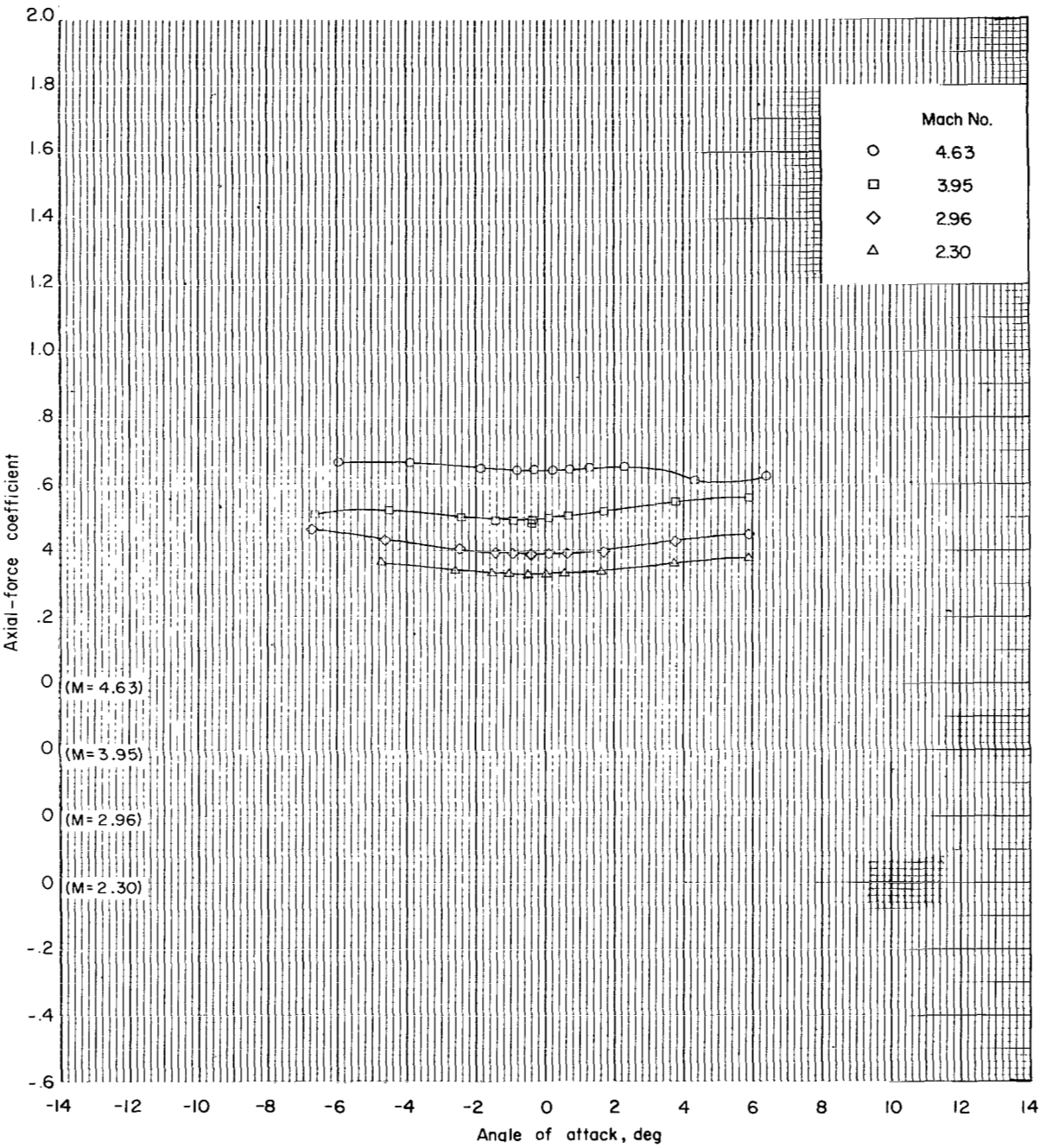

(h-2) Supersonic Mach numbers; configuration 7; $\phi = 0^{o}$.

Figure 11.- Continued.

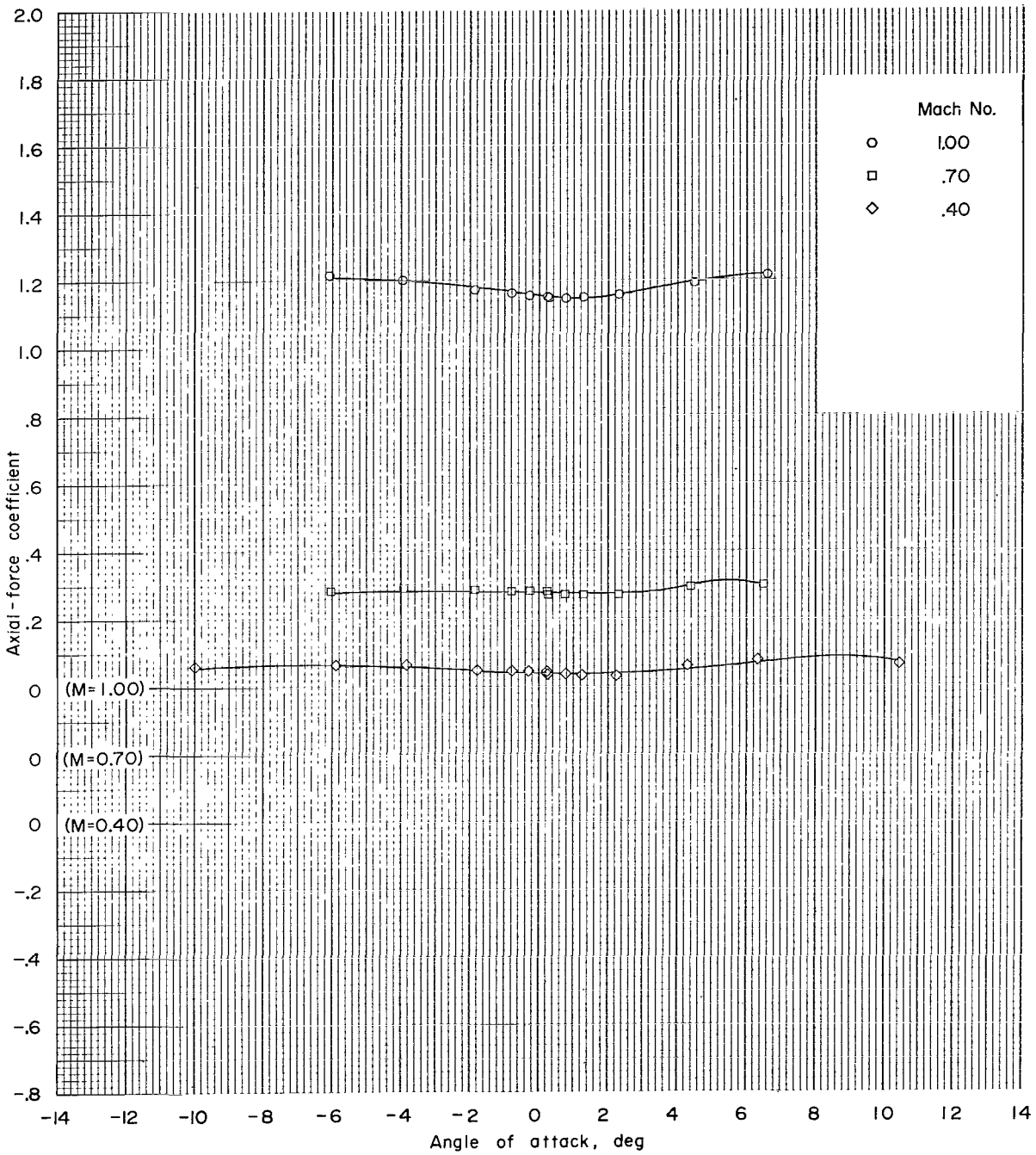

(i-1) Subsonic Mach numbers; configuration 7; $\phi = 180^{o}$.

Figure 11.- Continued.

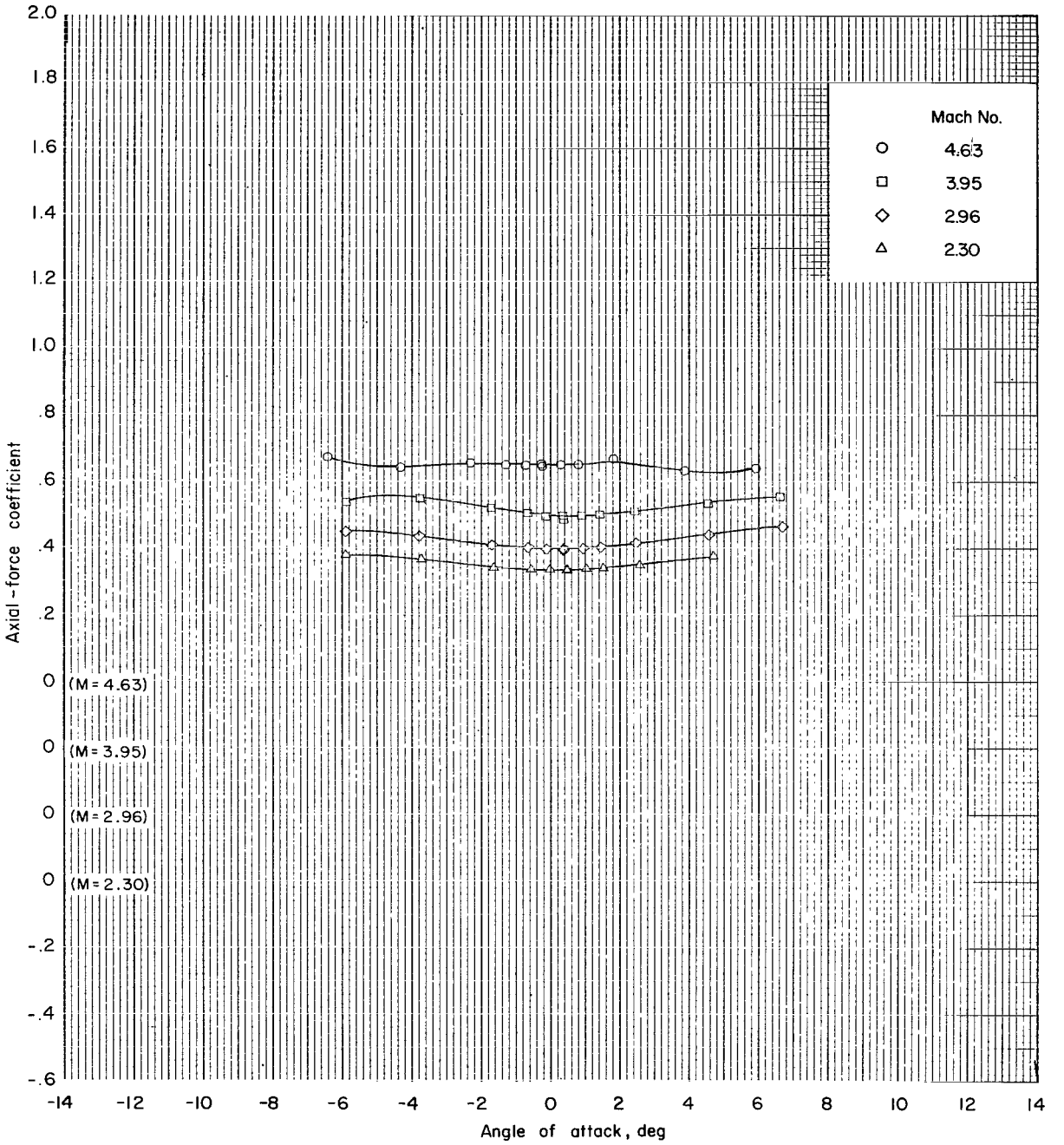

(i-2) Supersonic Mach numbers; configuration 7; $\phi = 180^{o}$.

Figure 11.- Concluded.

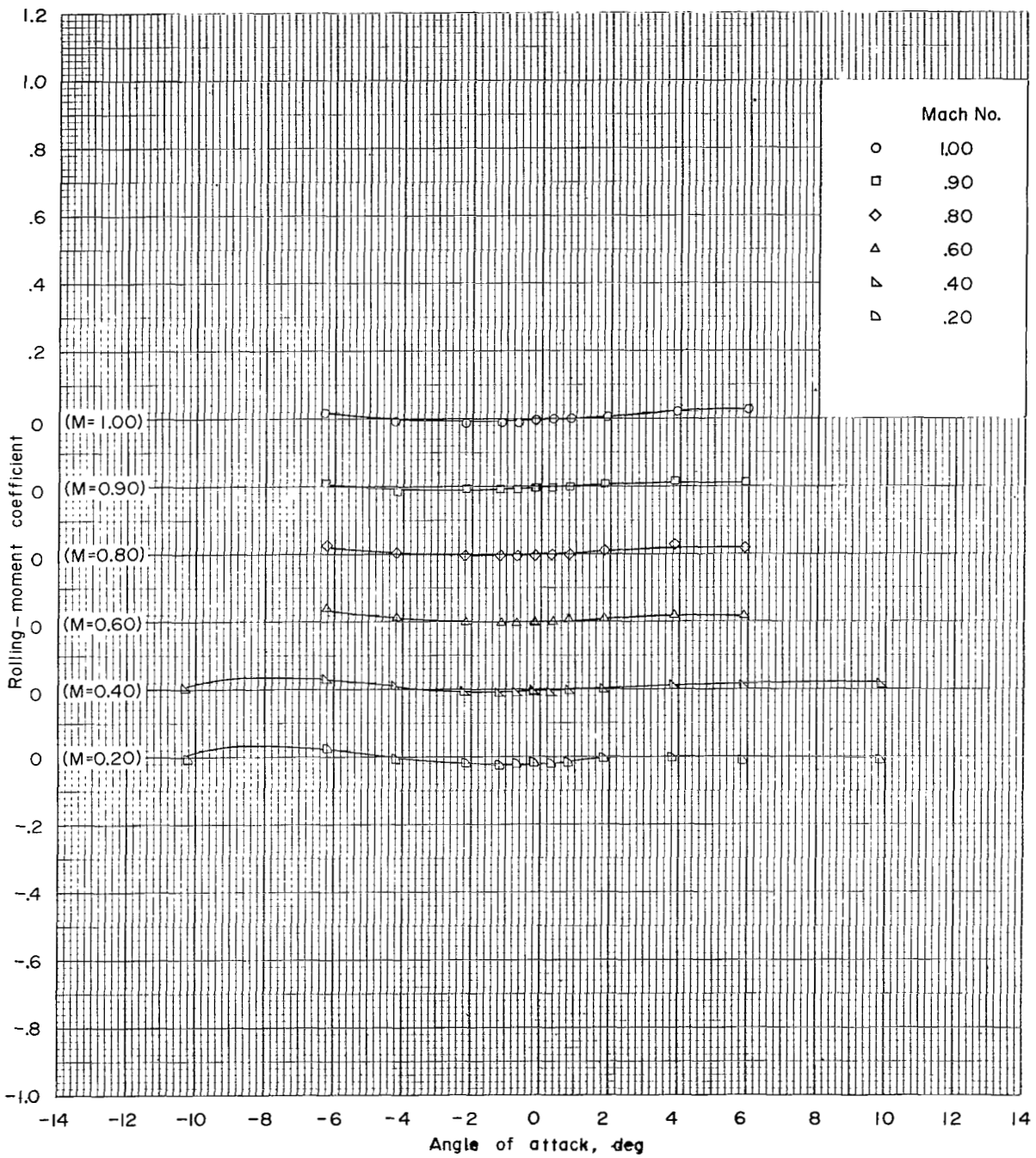

(a-1) Subsonic Mach numbers; configuration 1; $\phi = 0^{o}$.

Figure 12.- Rolling-moment coefficient as function of angle of attack, roll angle, and Mach number.

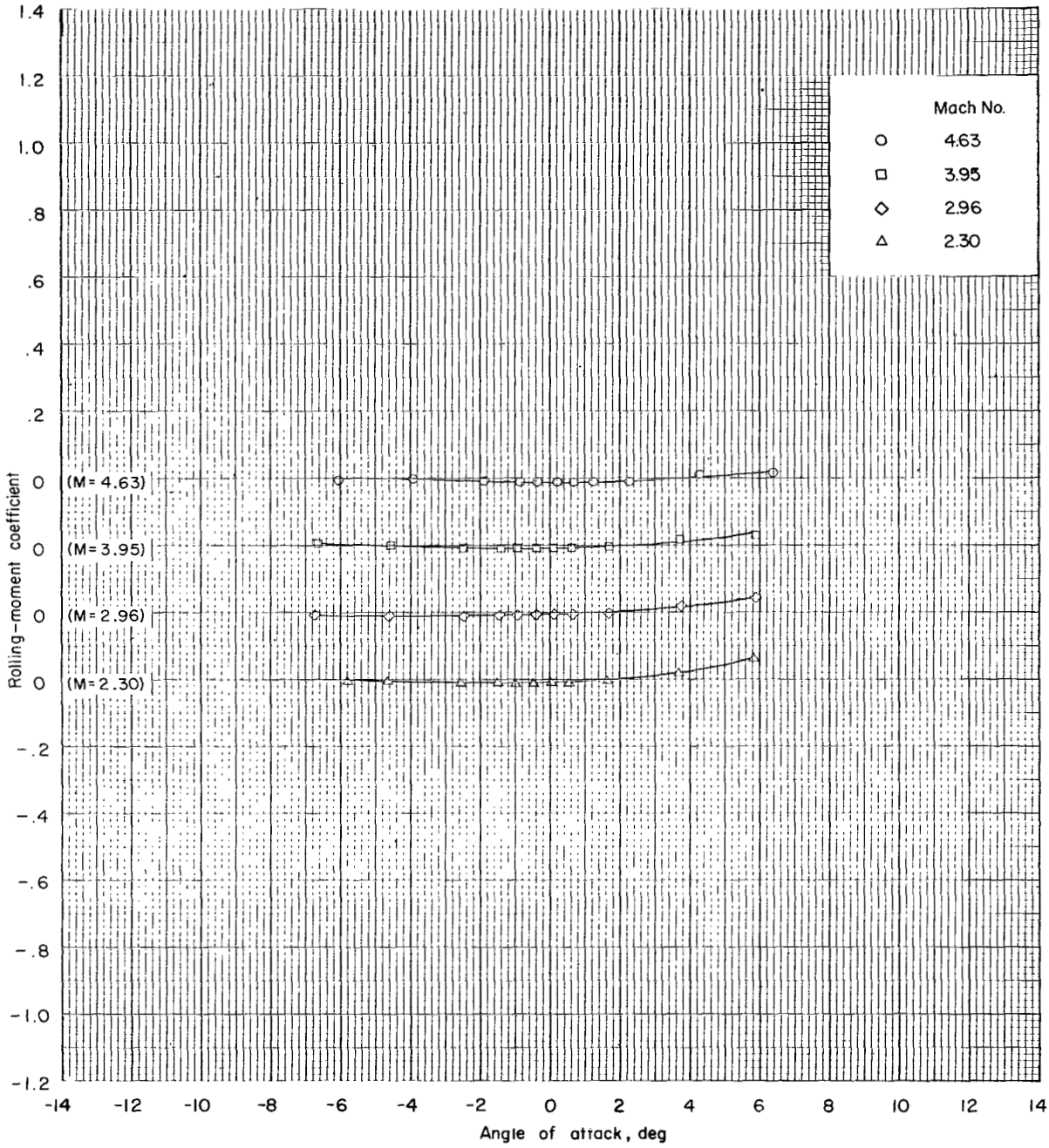

(a-2) Supersonic Mach numbers; configuration 1; $\phi = 0^{o}$.

Figure 12.- Continued.

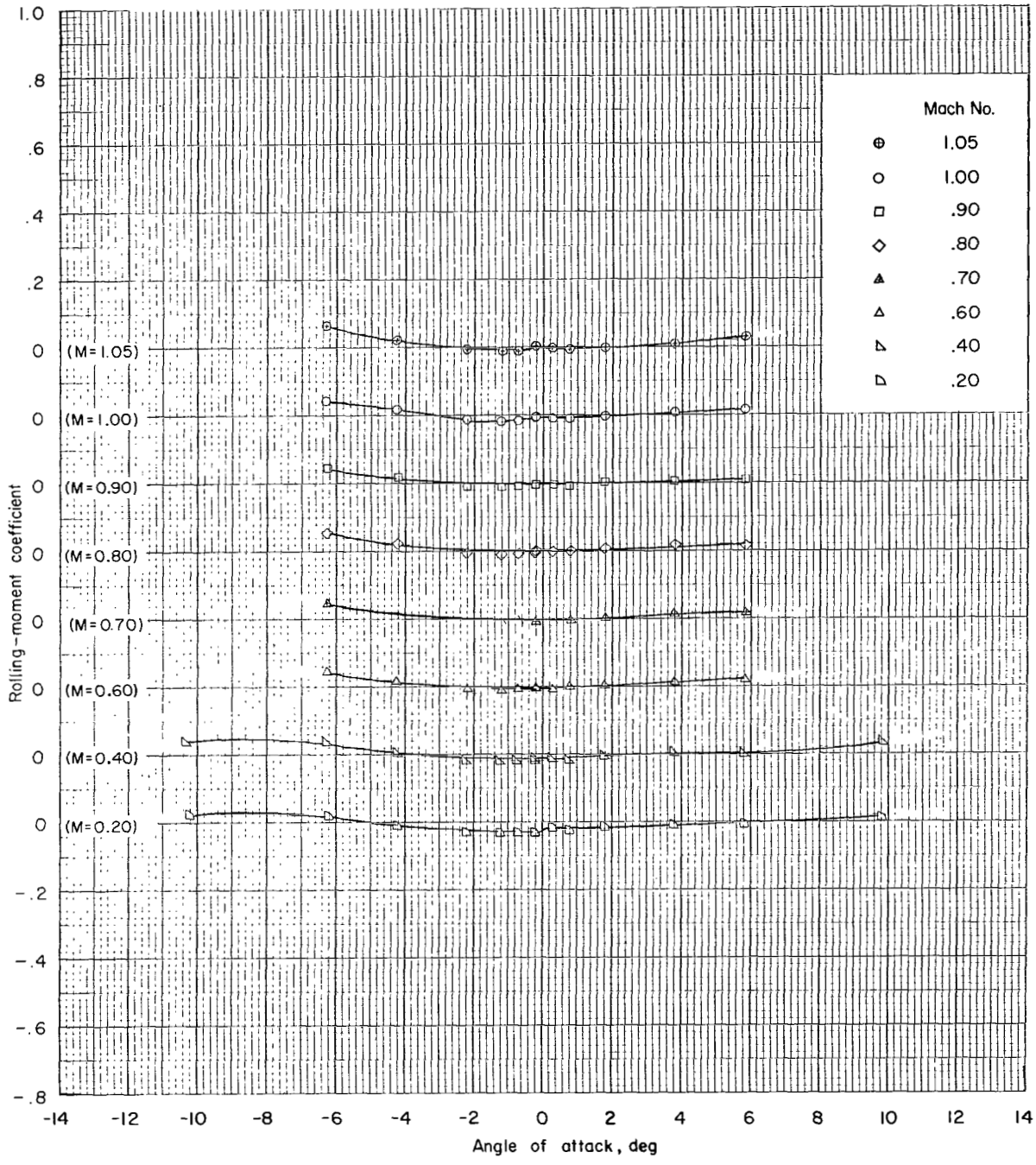

(b-1) Subsonic Mach numbers; configuration 2; $\phi = 0^{o}$.

Figure 12.- Continued.

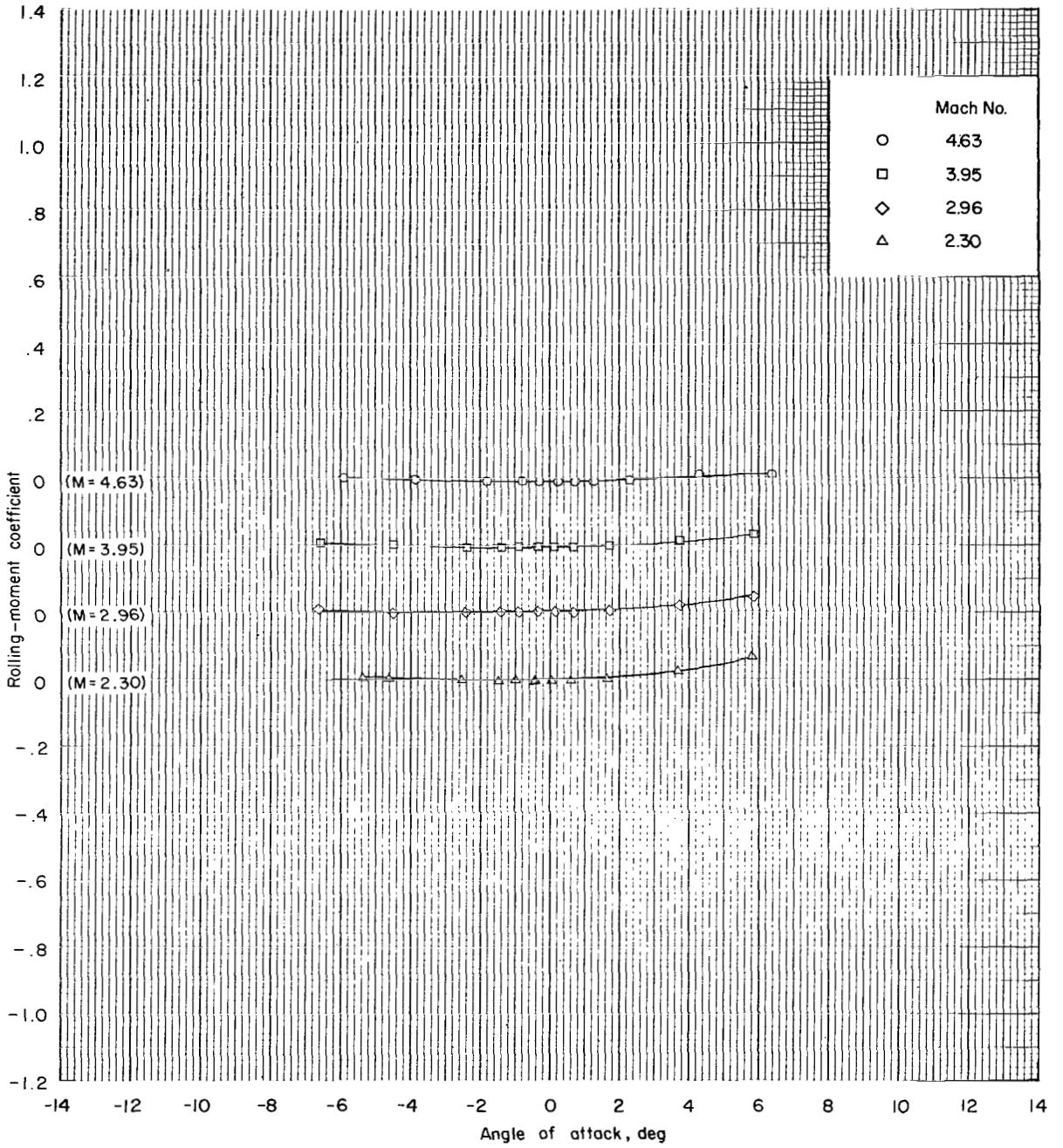

(b-2) Supersonic Mach numbers; configuration 2; $\phi = 0^{o}$.

Figure 12.- Continued.

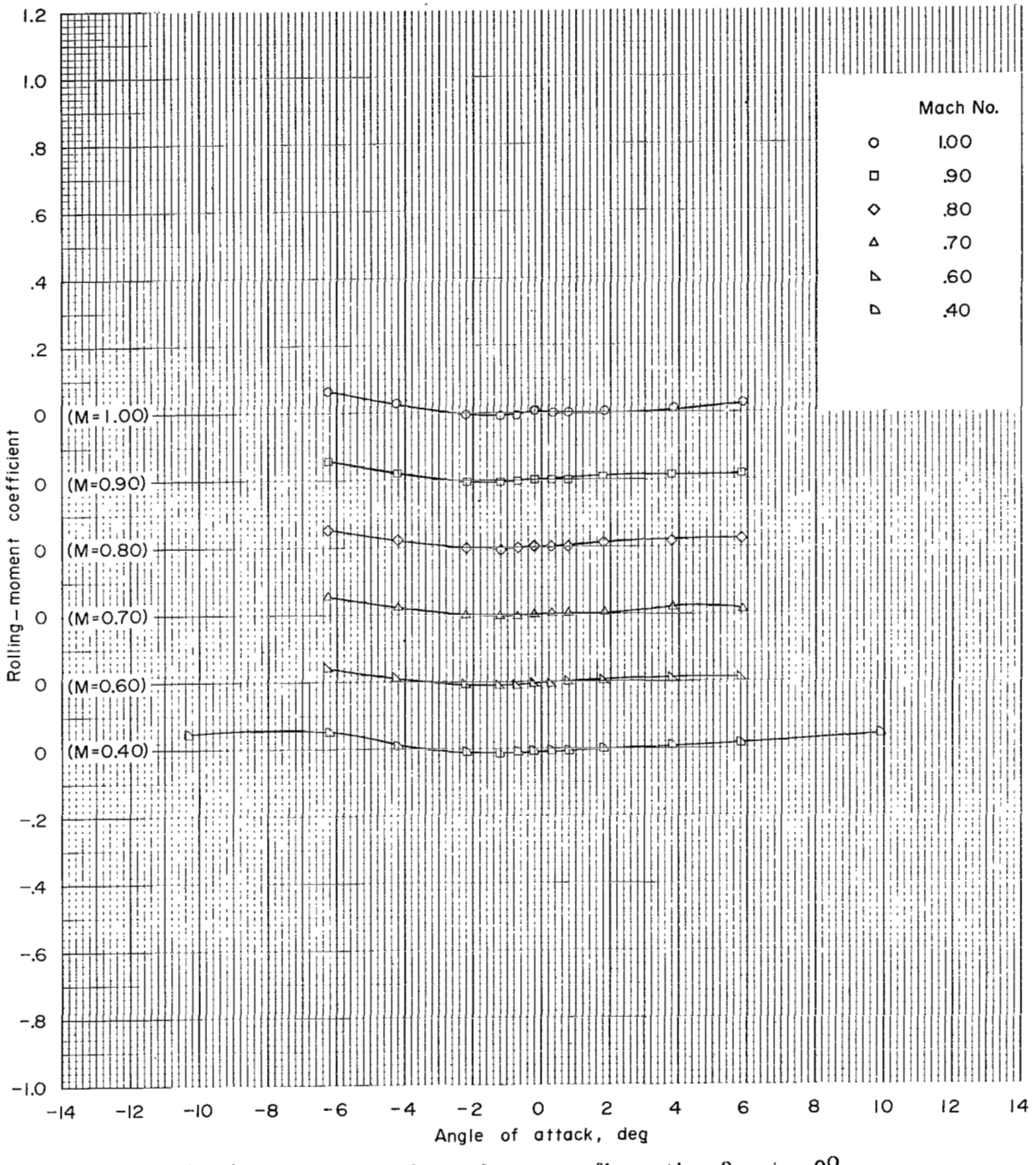

(c-1) Subsonic Mach numbers; configuration 3; $\phi = 0^{o}$.

Figure 12.- Continued.

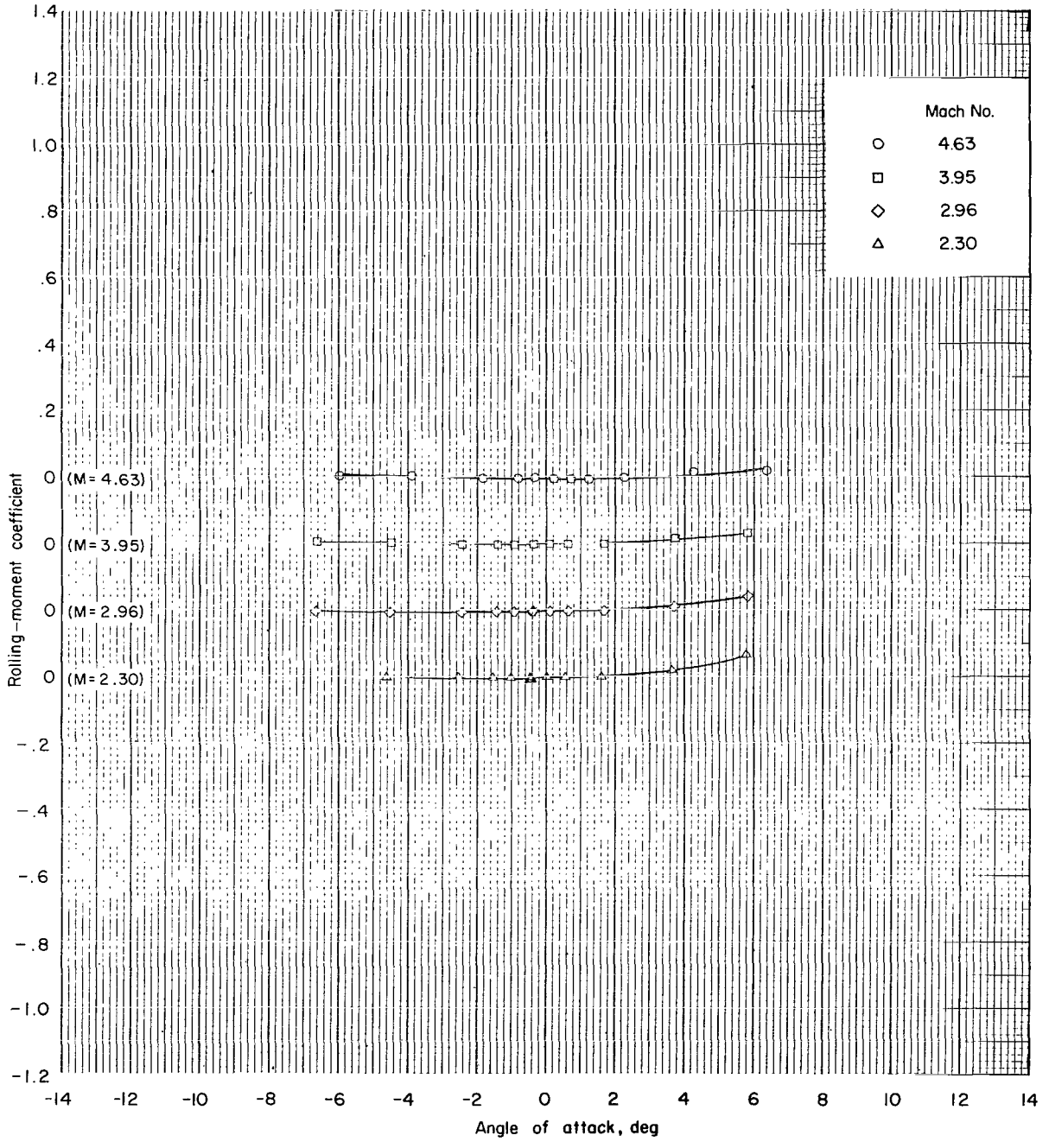

(c-2) Supersonic Mach numbers; configuration 3; $\phi = 0^{o}$.

Figure 12.- Continued.

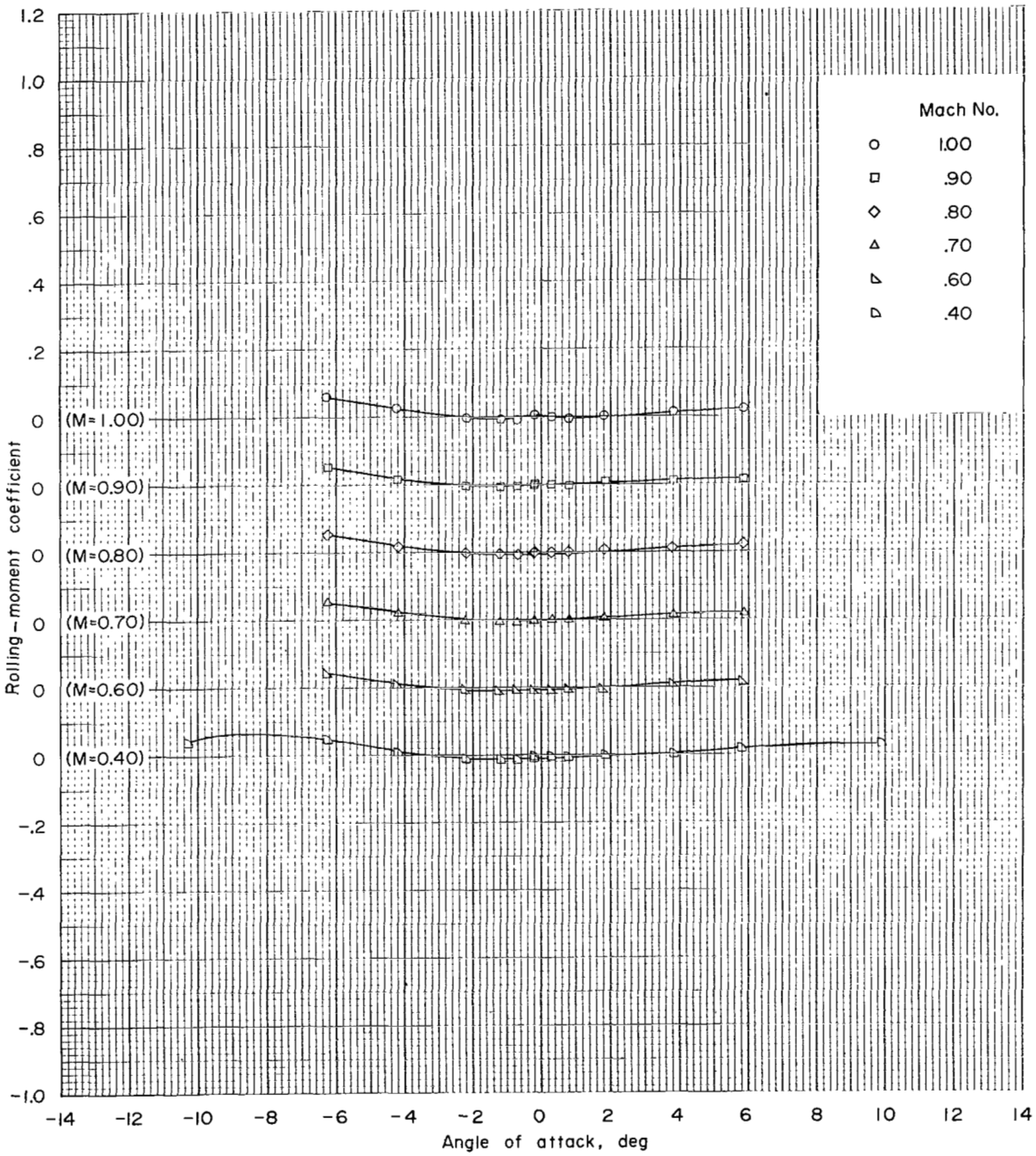

(d-1) Subsonic Mach numbers; configuration 4; $\phi = 0^{o}$.

Figure 12.- Continued.

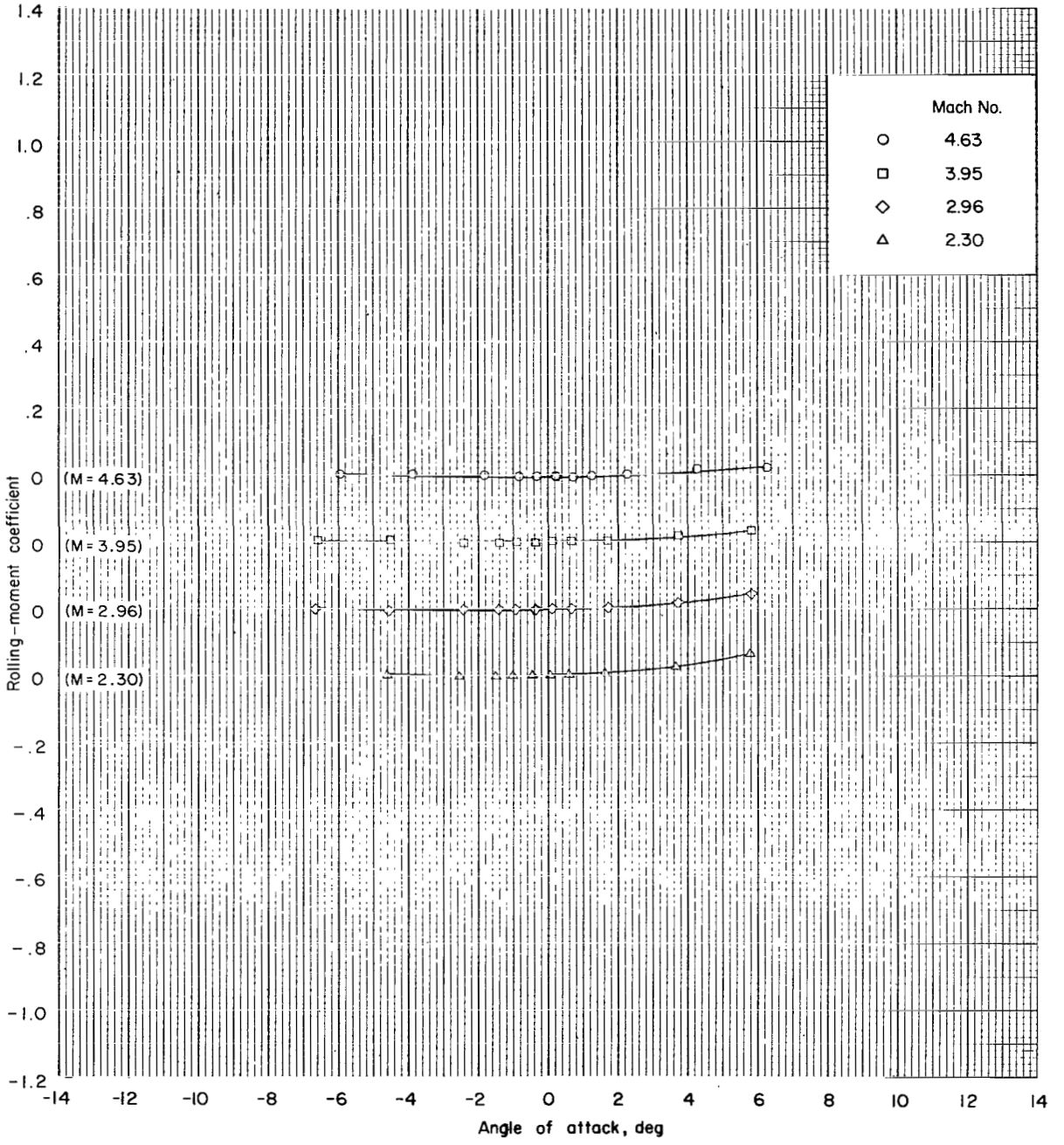

(d-2) Supersonic Mach numbers; configuration 4; $\phi = 0^{o}$.

Figure 12.- Continued.

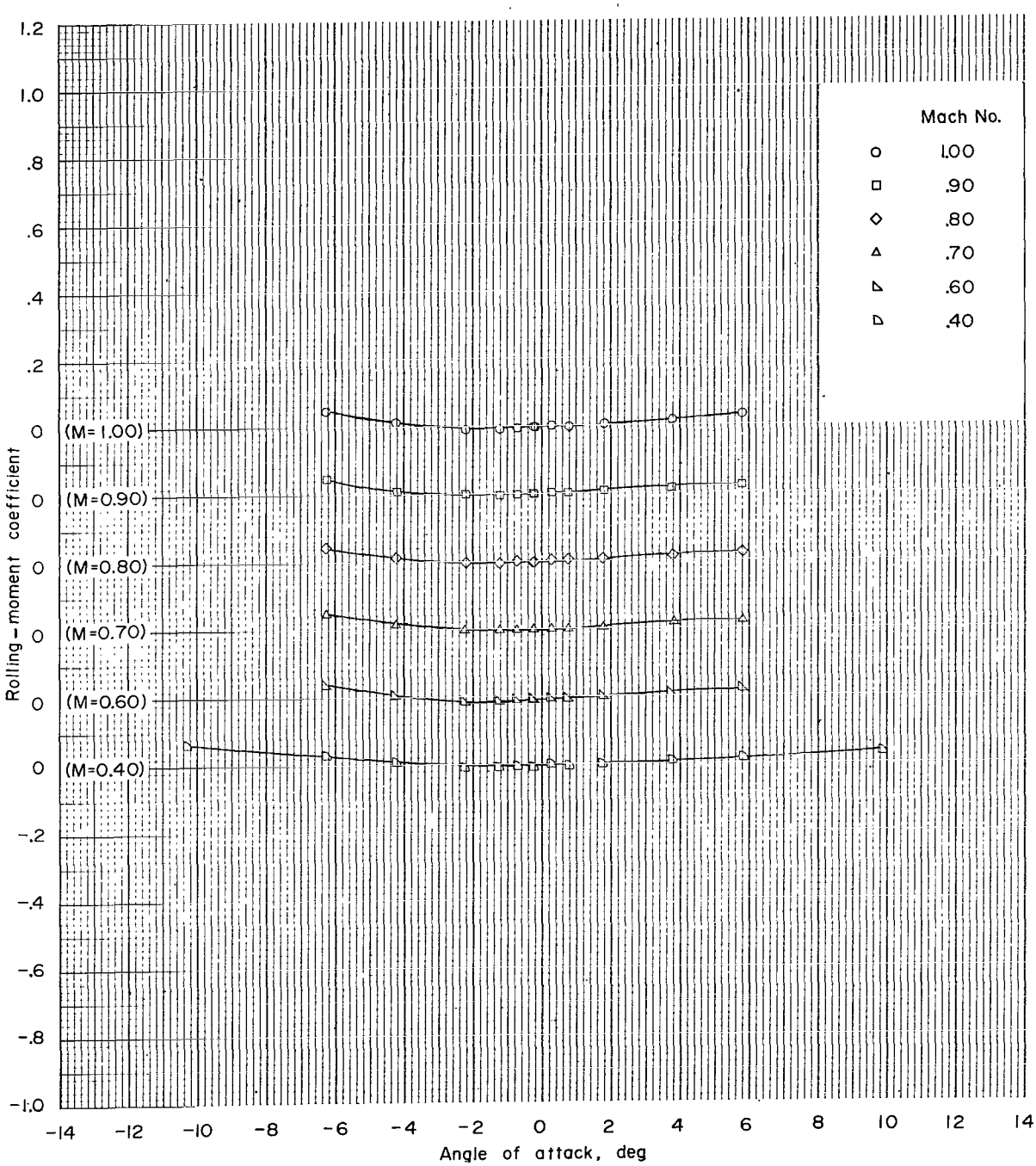

(e-1) Subsonic Mach numbers; configuration 5; $\phi = 0^{o}$.

Figure 12.- Continued.

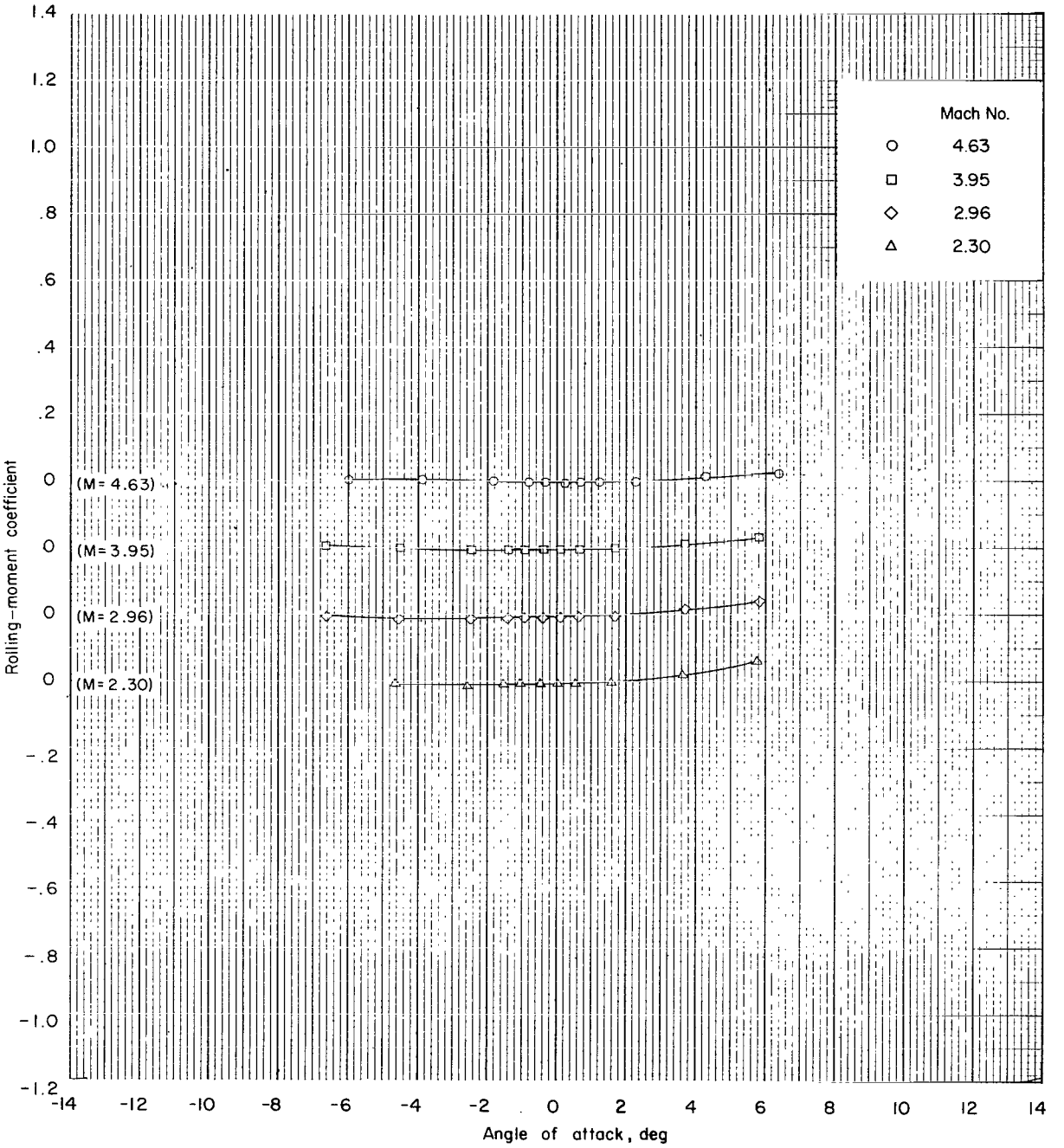

(e-2) Supersonic Mach numbers; configuration 5; $\phi = 0^{o}$.

Figure 12.- Continued.

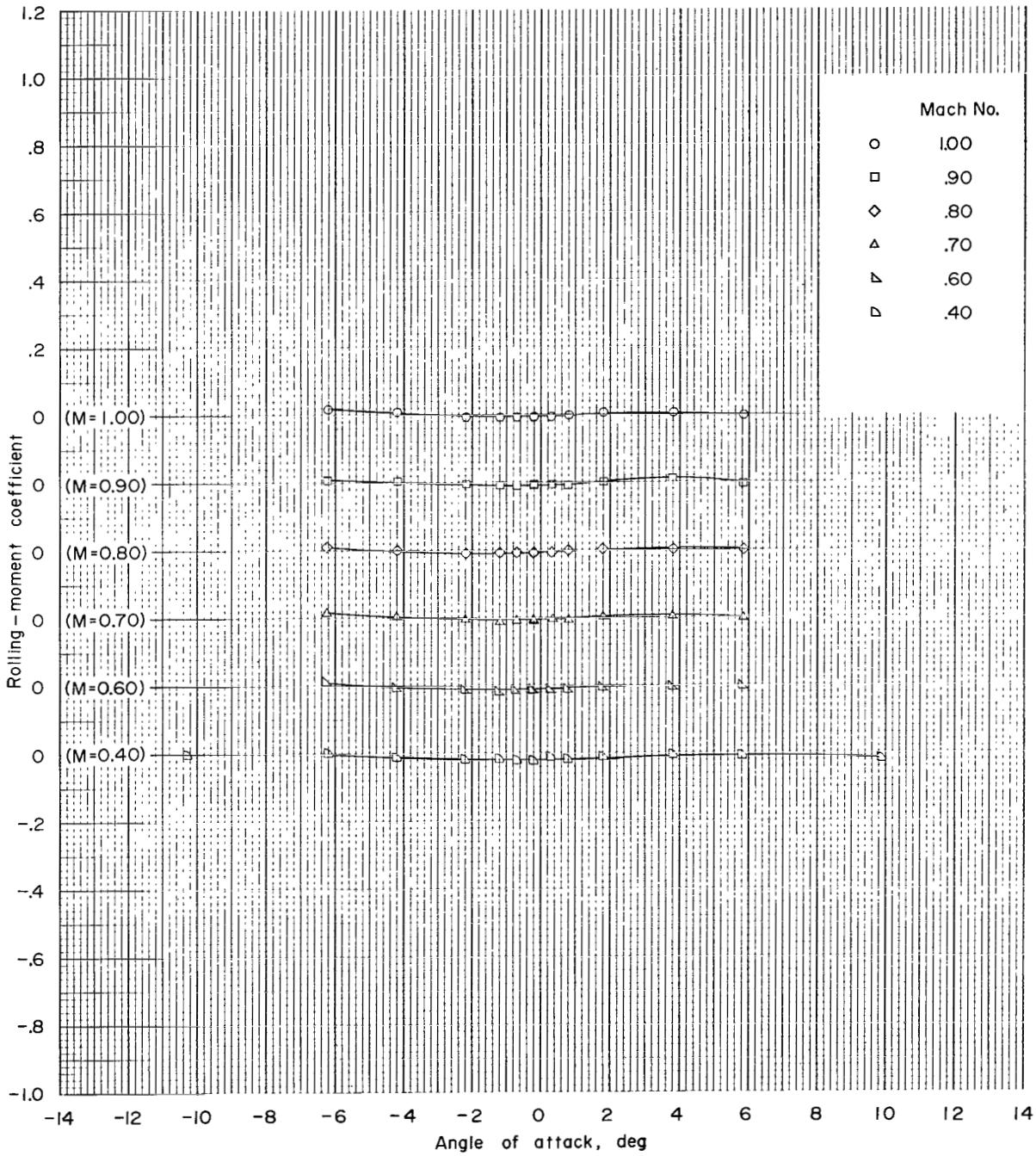

(f-1) Subsonic Mach numbers; configuration 6; $\phi = 0^{o}$.

Figure 12.- Continued.

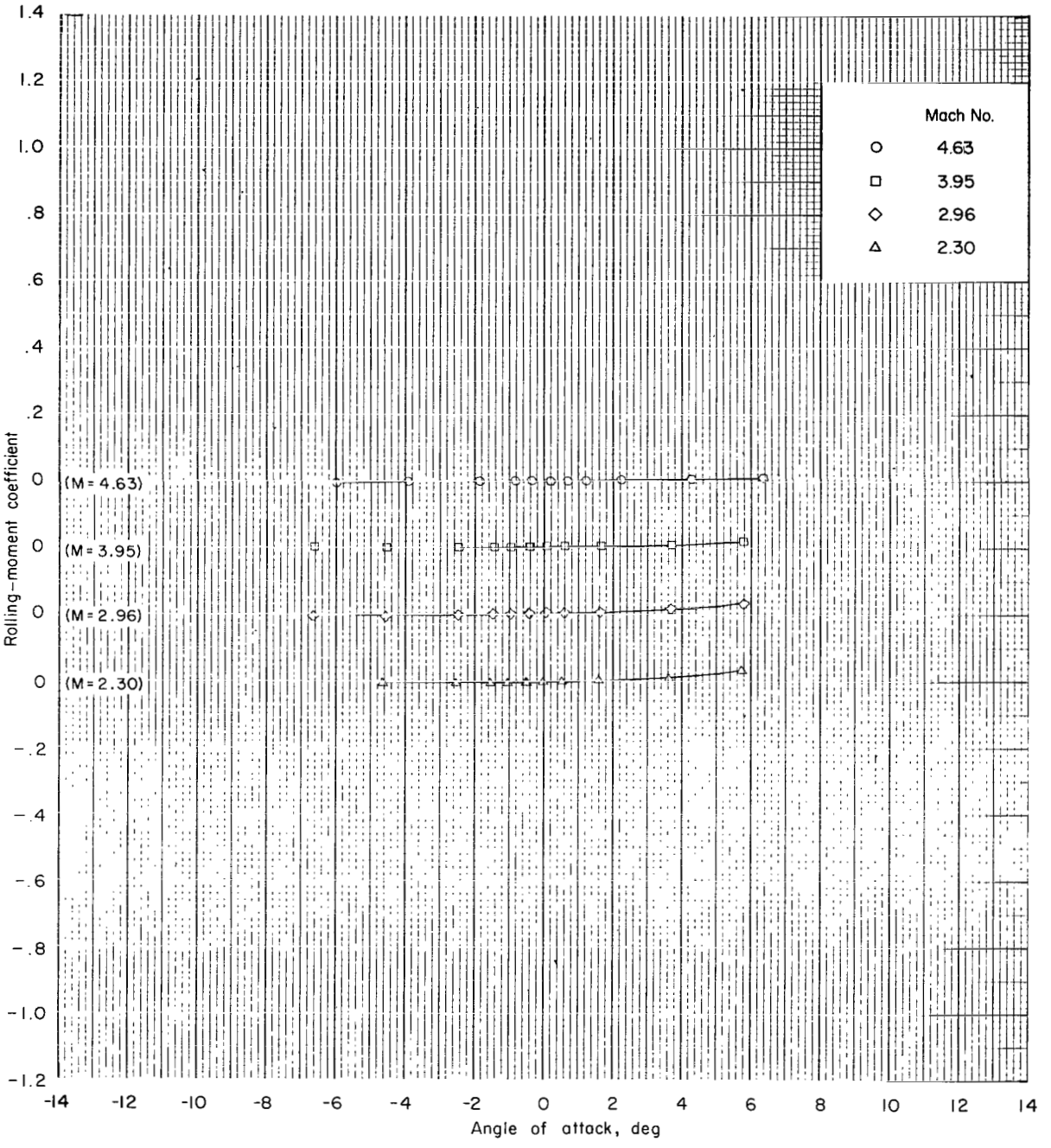

(f-2) Supersonic Mach numbers; configuration 6; $\phi = 0^{o}$.

Figure 12.- Continued.

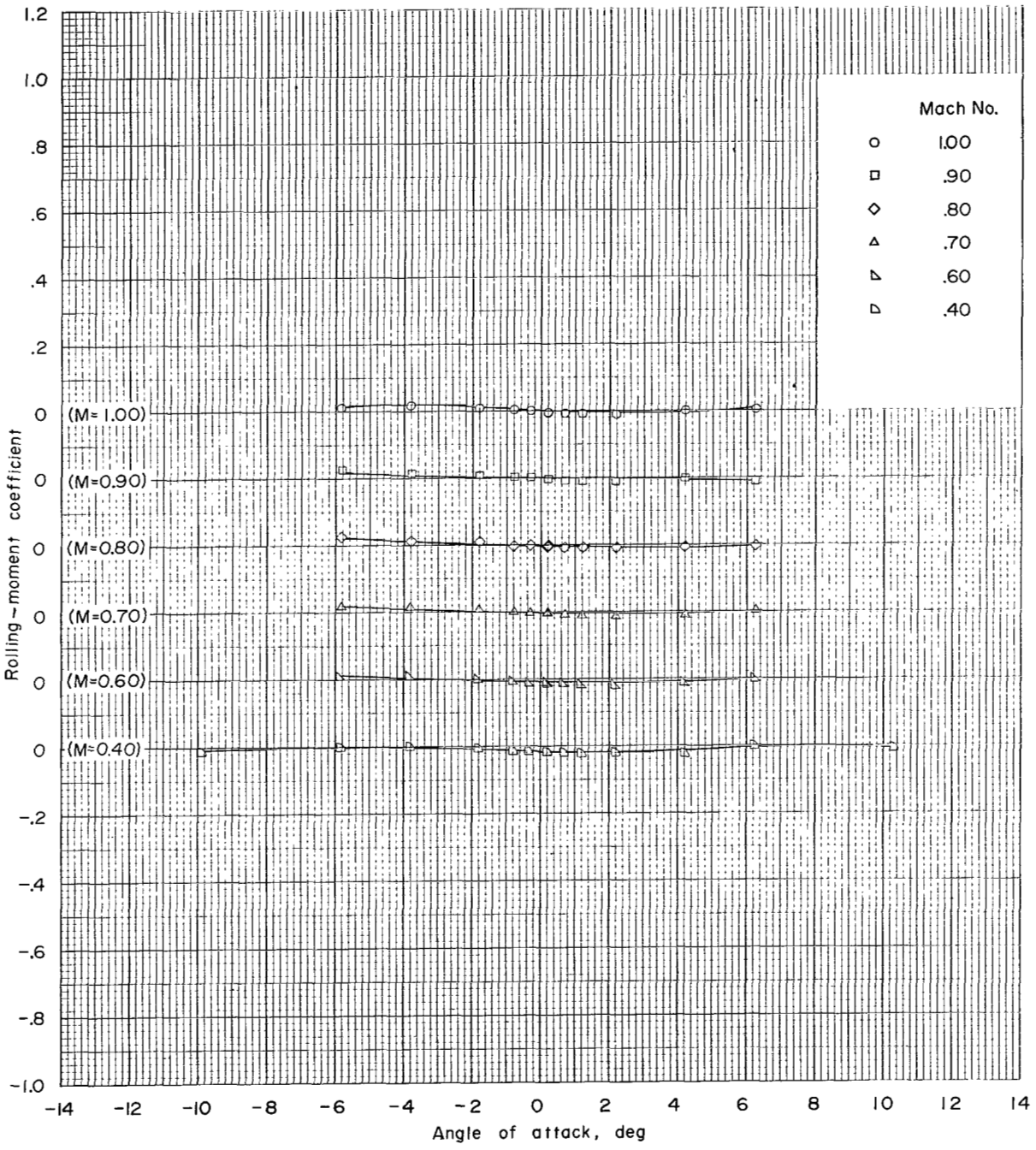

(g-1) Subsonic Mach numbers; configuration 6; $\phi = 180^{o}$.

Figure 12.- Continued.

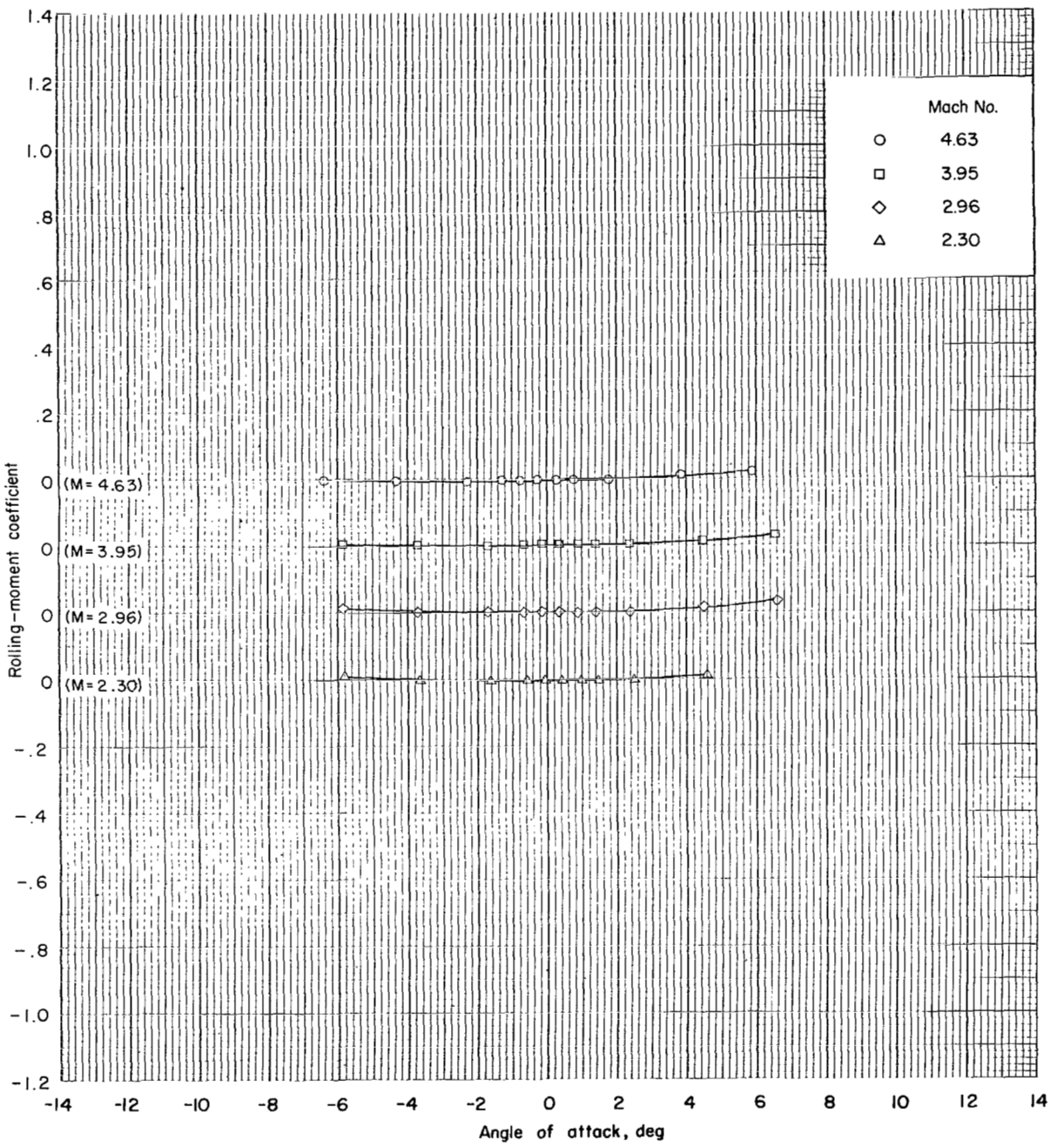

(g-2) Supersonic Mach numbers; configuration 6; $\phi = 180^{o}$.

Figure 12.- Continued.

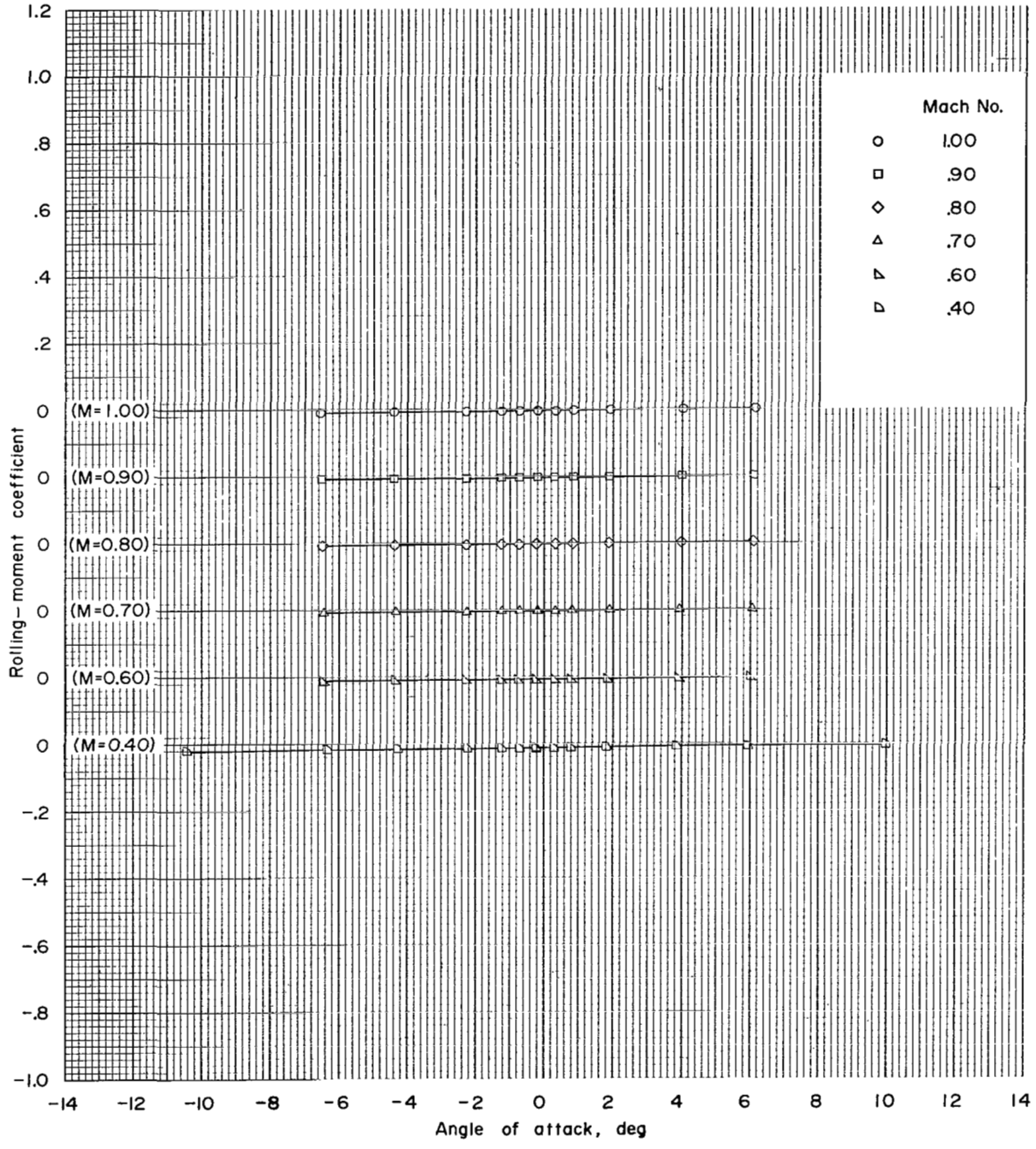

(h-1) Subsonic Mach numbers; configuration 7; $\phi = 0^{o}$.

Figure 12.- Continued.

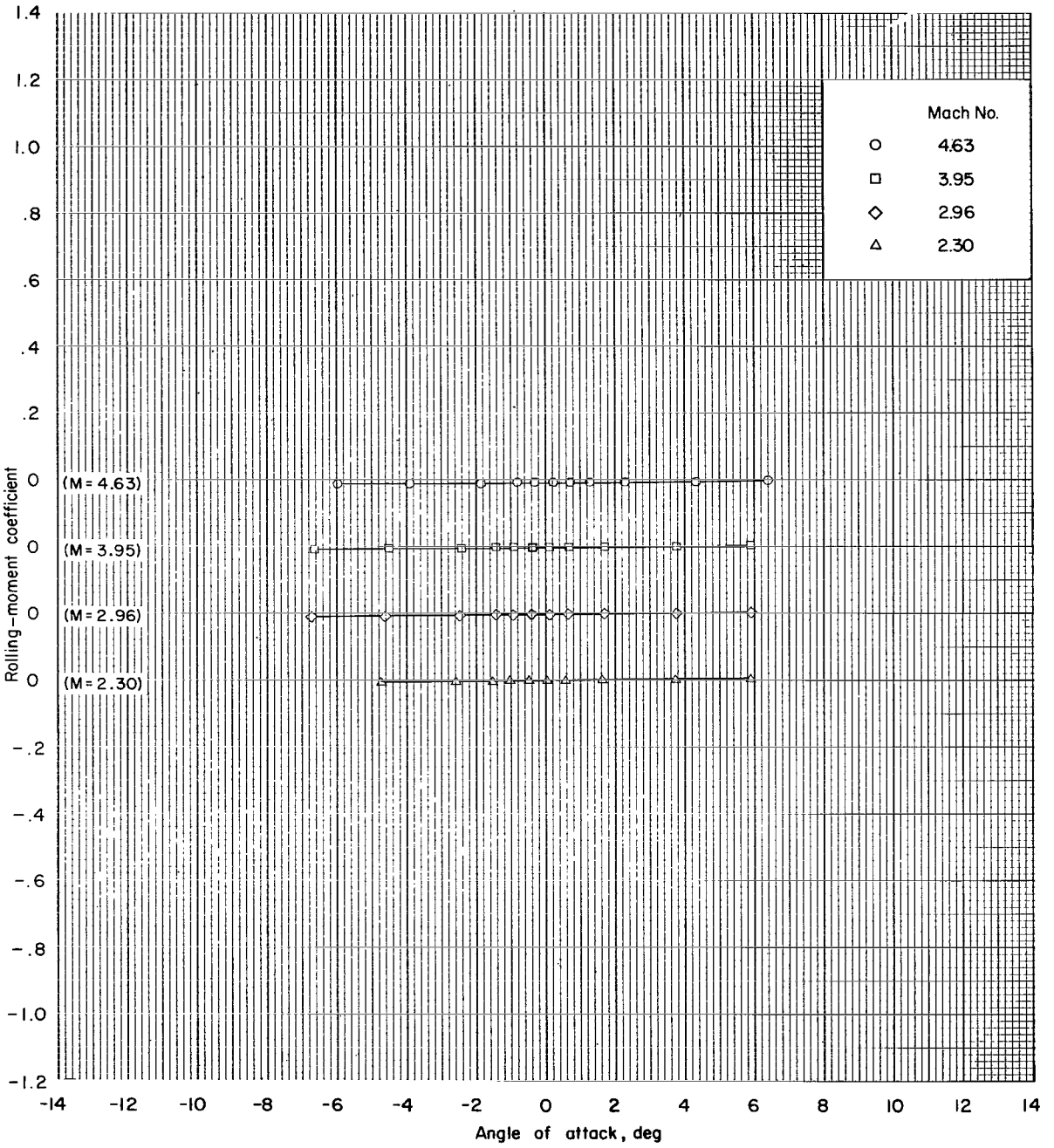

(h-2) Supersonic Mach numbers; configuration 7; $\phi = 0^{o}$.

Figure 12.- Continued.

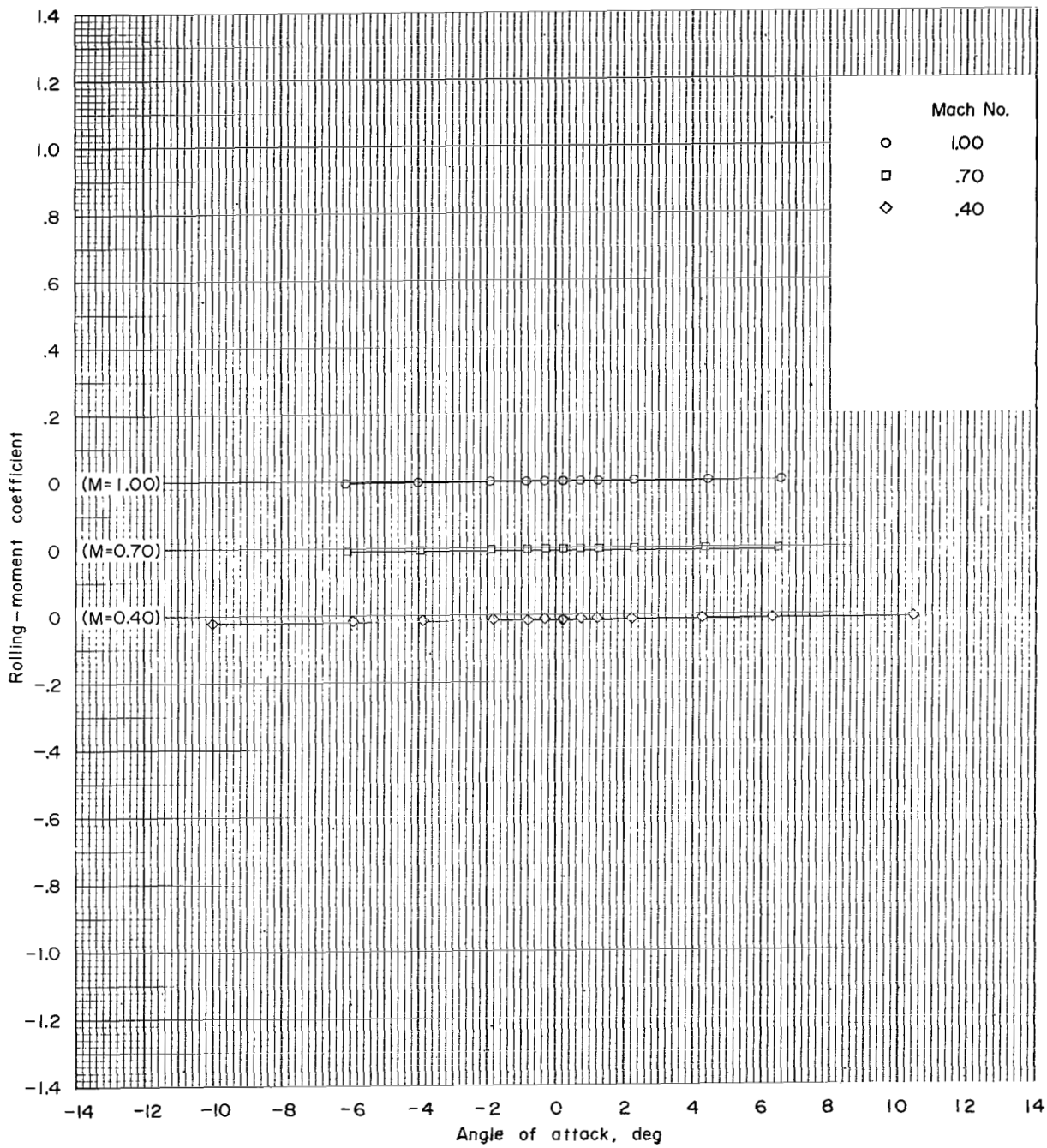

(i-1) Subsonic Mach numbers; configuration 7; $\phi = 180^{o}$.

Figure 12.- Continued.

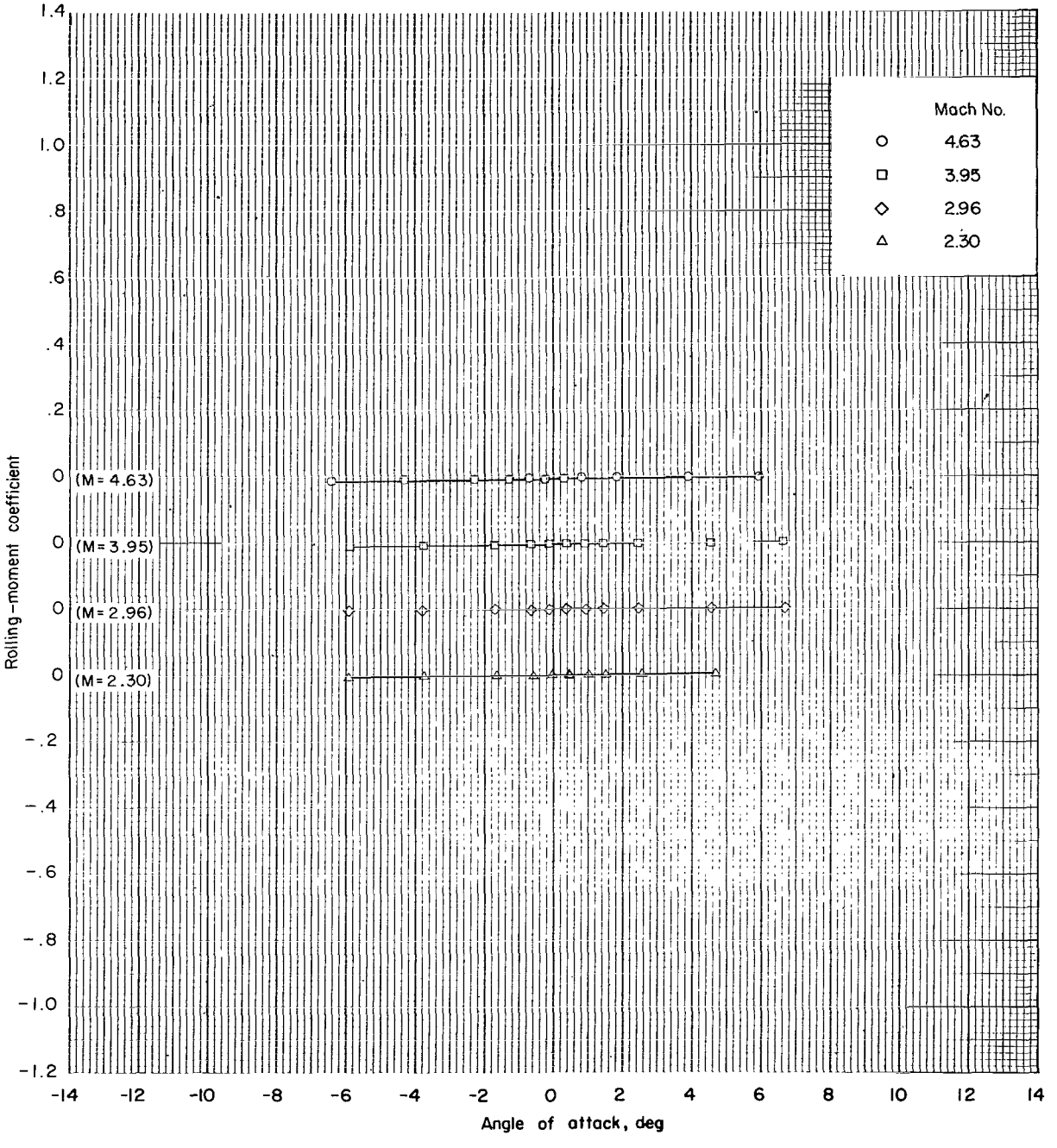

(i-2) Supersonic Mach numbers; configuration 7; $\phi = 180^{o}$.

Figure 12.- Concluded.

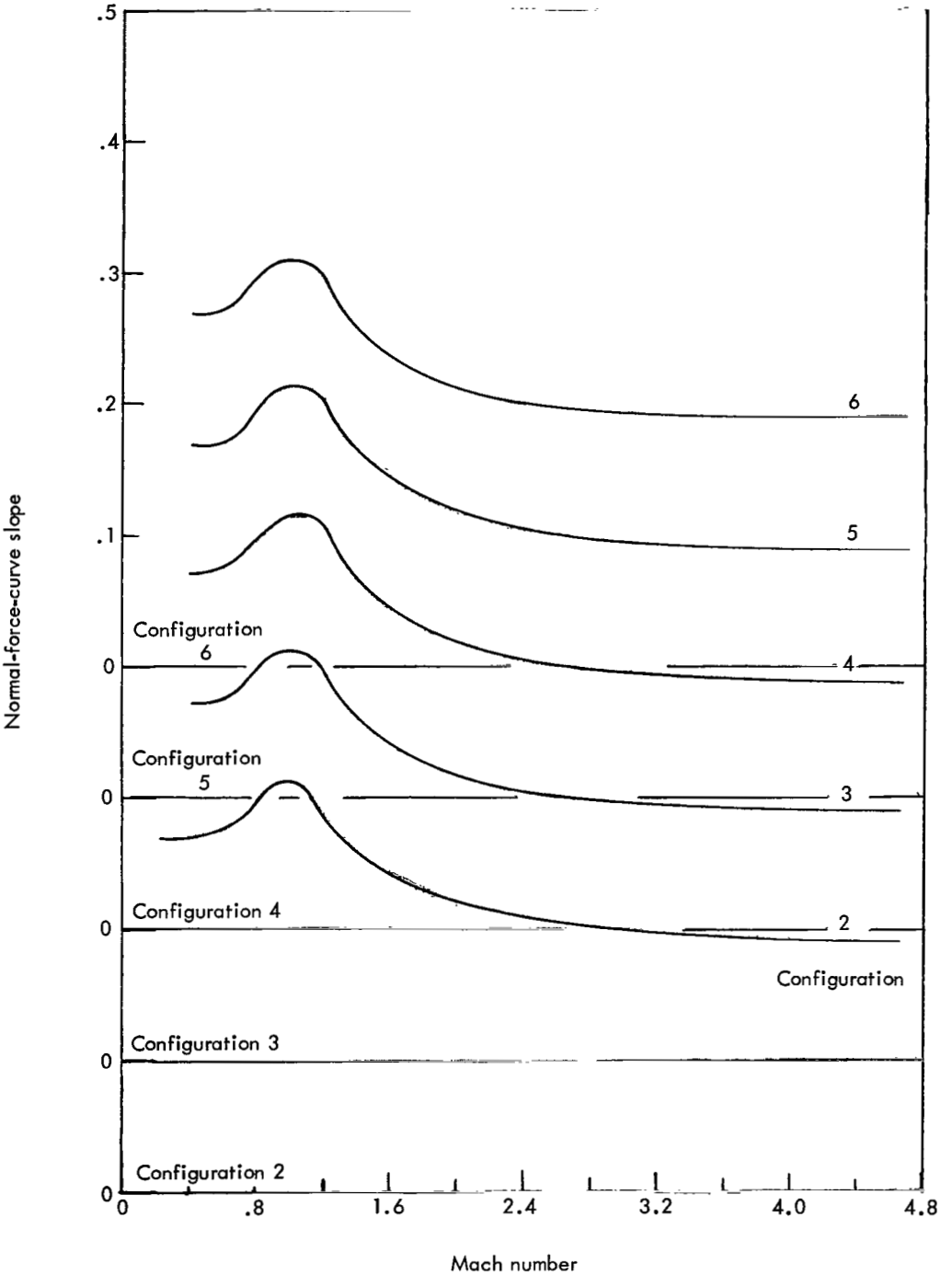

Figure 13.- Effect of protuberances on normal-force-curve slope at $\alpha = 0^{o}$.

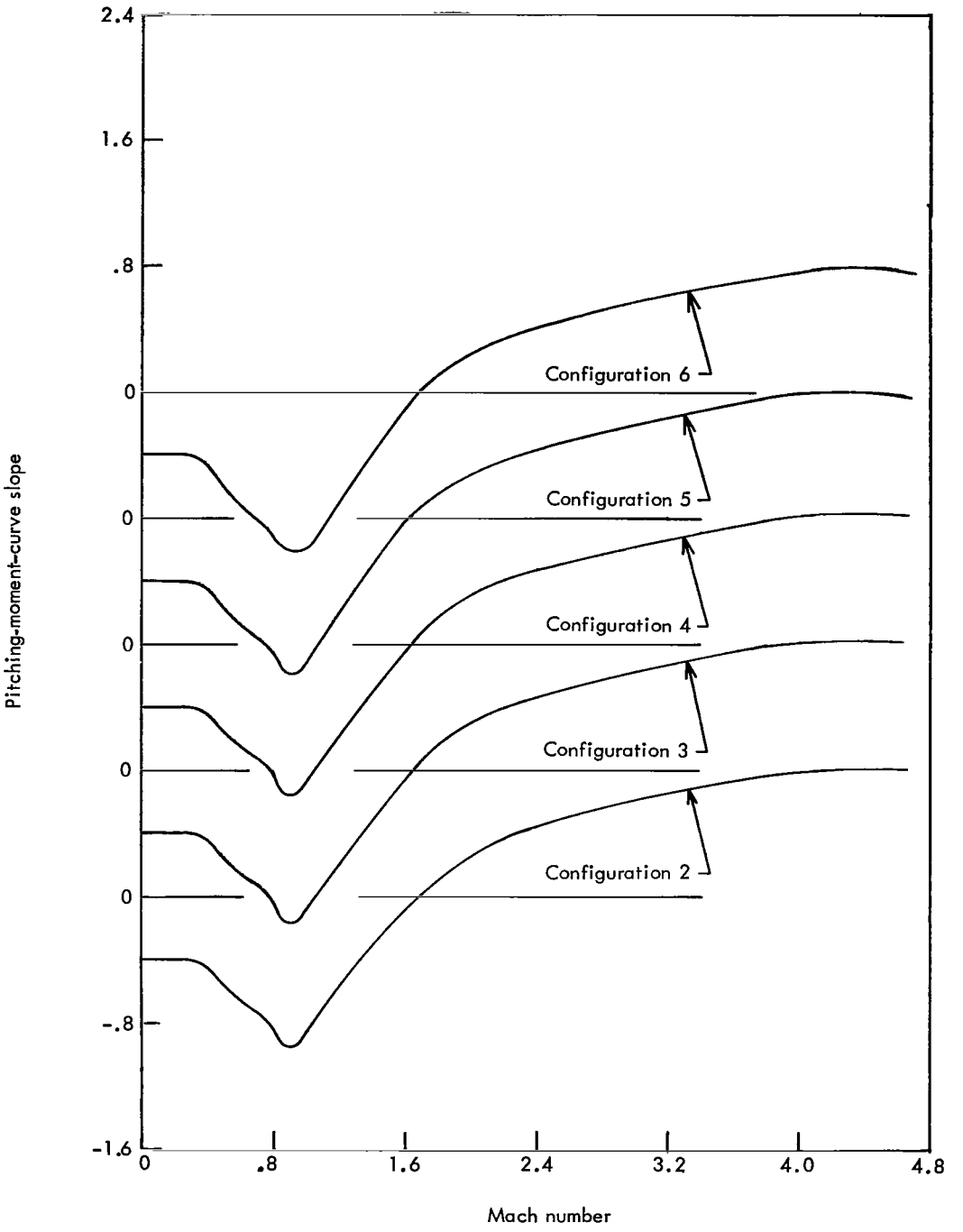

Figure 14.- Effect of protuberances on pitching-moment-curve slope at $\alpha = 0^{o}$.

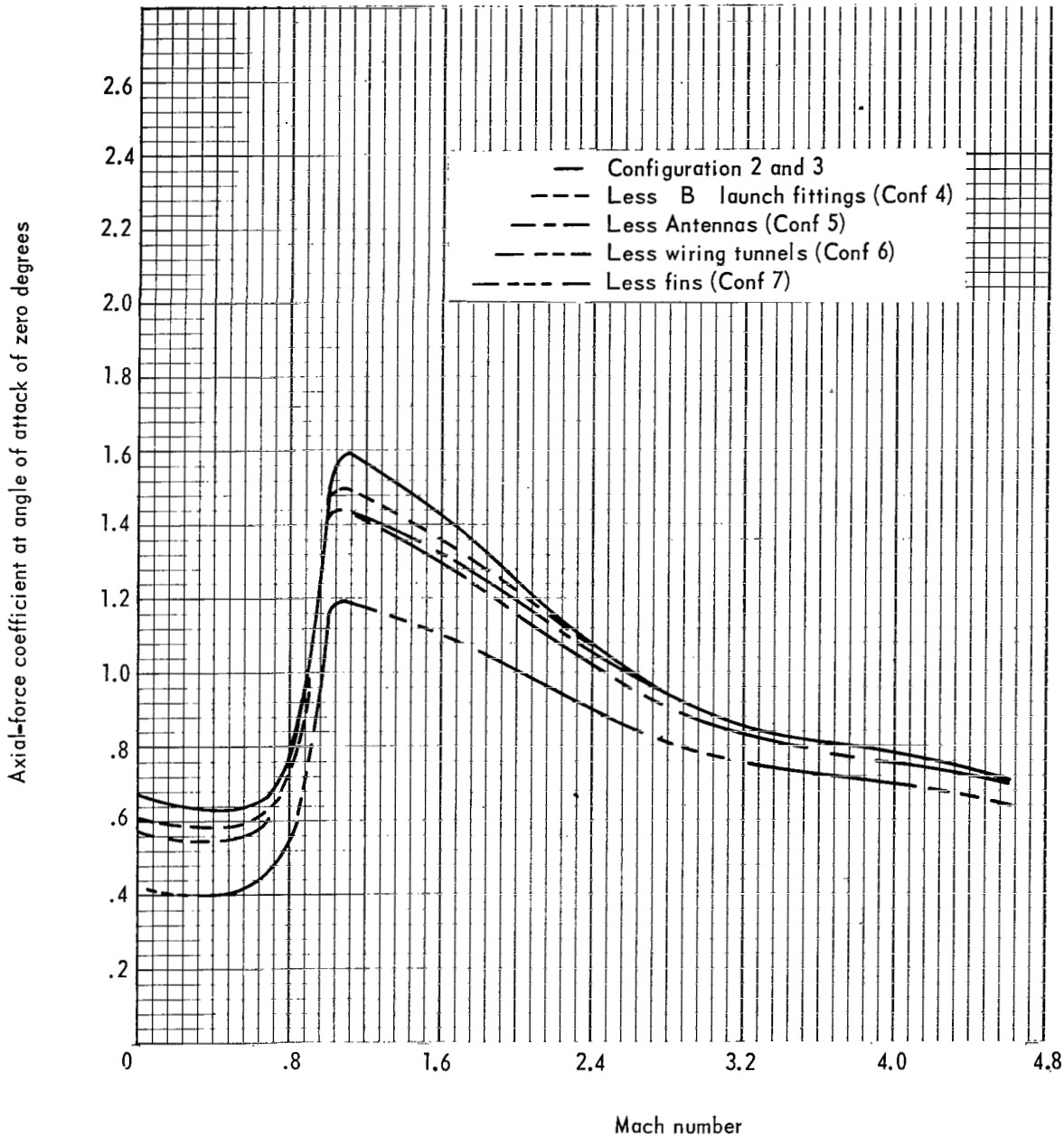

Figure 15.- Effect of protuberances on axial-force coefficient at $\alpha = 0^{o}$.

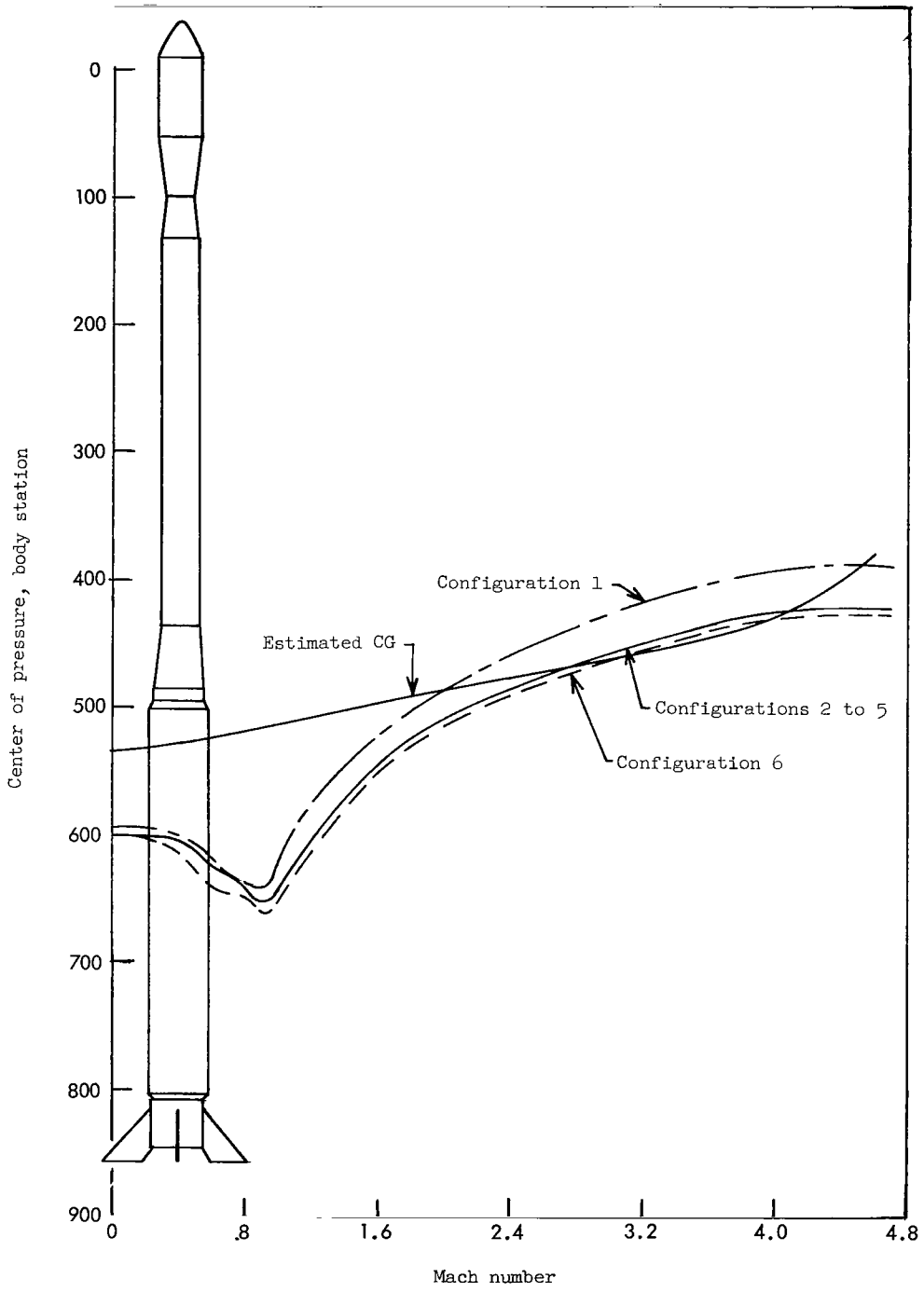

Figure 16.- Effect of protuberances and heat-shield diameter on center of pressure at $\alpha = 0^{o}$. Body station given in inches (1 in. = 2.54 cm).

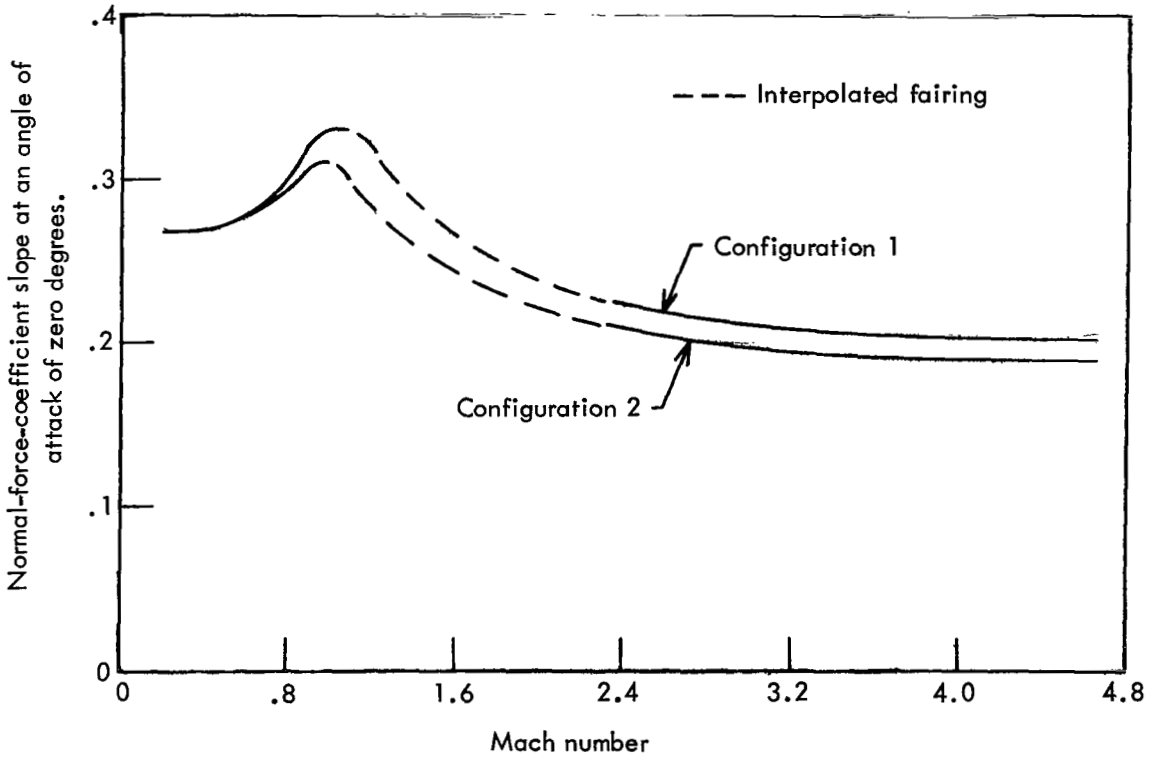

Figure 17.- Effect of heat-shield diameter on normal-force-curve slope at $\alpha = 0^{o}$.

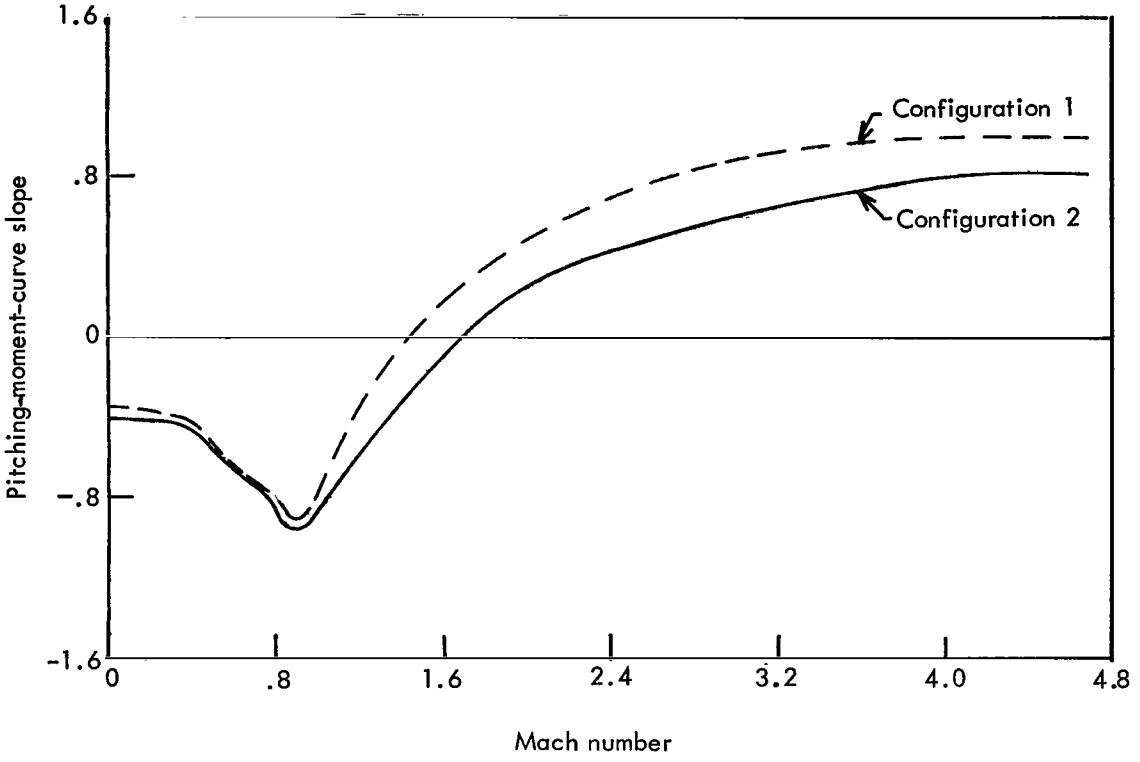

Figure 18.- Effect of heat-shield diameter on pitching-moment-curve slope at $\alpha = 0^{o}$.

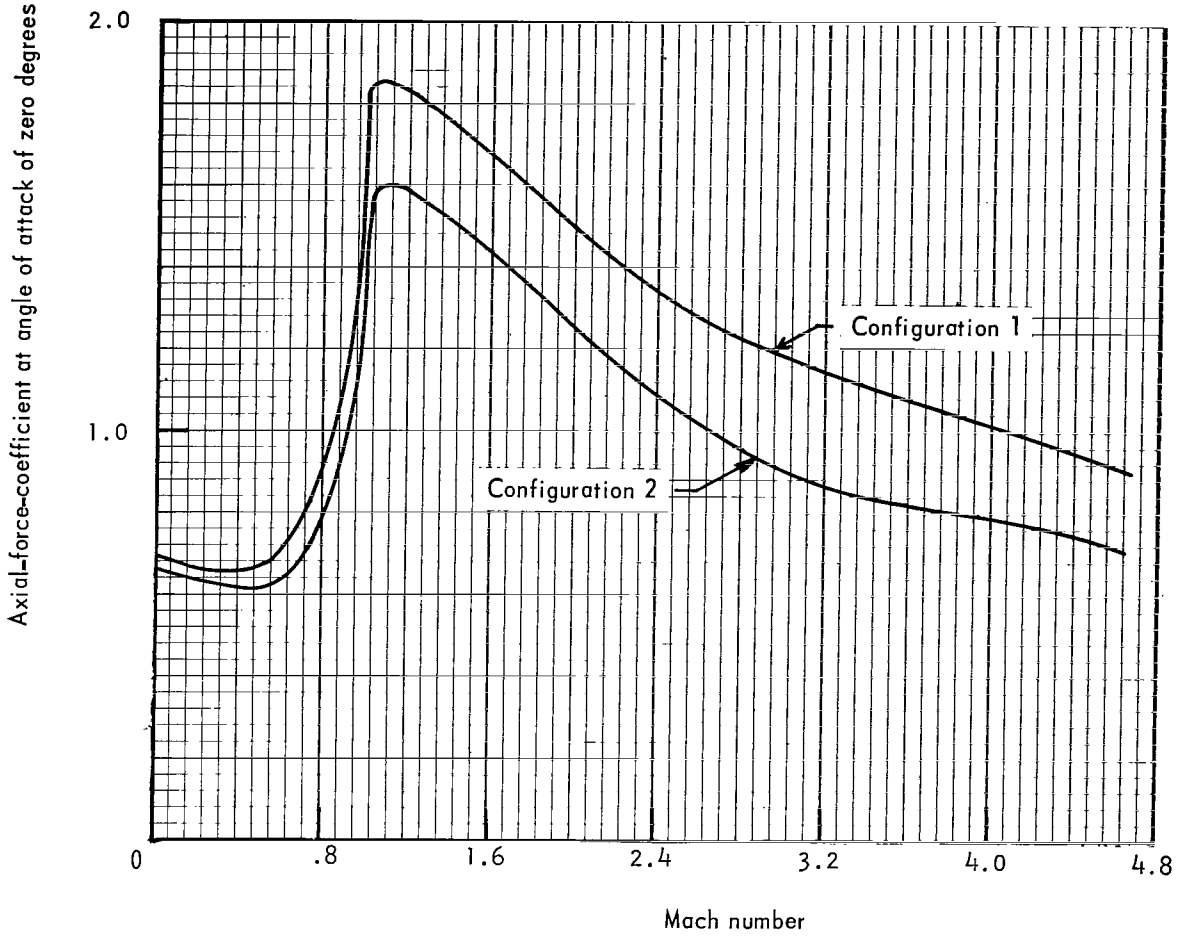

Figure 19.- Effect of heat-shield diameter on axial-force coefficient at $\alpha = 0^{o}$.

NASA-Langley, 1971 —— 31 L-7538

02U 001 26 51 3DS 71118 00903
AIR FORCE WEAPONS LABORATORY /WLOL/
KIRTLAND AFB, NEW MEXICO 87117

ATT E. LOU BOWMAN, CHIEF, TECH. LIBRARY

"The aeronautical and space activities of the United States shall be conducted so as to contribute . . . to the expansion of human knowledge of phenomena in the atmosphere and space. The Administration shall provide for the widest practicable and appropriate dissemination of information concerning its activities and the results thereof."

—NATIONAL AERONAUTICS AND SPACE ACT OF 1958

NASA SCIENTIFIC AND TECHNICAL PUBLICATIONS

TECHNICAL REPORTS: Scientific and technical information considered important, complete, and a lasting contribution to existing knowledge.

TECHNICAL NOTES: Information less broad in scope but nevertheless of importance as a contribution to existing knowledge.

TECHNICAL MEMORANDUMS: Information receiving limited distribution because of preliminary data, security classification, or other reasons.

CONTRACTOR REPORTS: Scientific and technical information generated under a NASA contract or grant and considered an important contribution to existing knowledge.

TECHNICAL TRANSLATIONS: Information published in a foreign language considered to merit NASA distribution in English.

SPECIAL PUBLICATIONS: Information derived from or of value to NASA activities. Publications include conference proceedings, monographs, data compilations, handbooks, sourcebooks, and special bibliographies.

TECHNOLOGY UTILIZATION PUBLICATIONS: Information on technology used by NASA that may be of particular interest in commercial and other non-aerospace applications. Publications include Tech Briefs, Technology Utilization Reports and Technology Surveys.

Details on the availability of these publications may be obtained from:

SCIENTIFIC AND TECHNICAL INFORMATION OFFICE

NATIONAL AERONAUTICS AND SPACE ADMINISTRATION

Washington, D.C. 20546